NTNU
Norwegian University of
Science and Technology

Minimum Time Bilateral Observer Design for 2x2 Systems of Linear Hyperbolic PDEs

With Application to Oil Well Drilling State Estimation for Improved Kick Handling

Nils Christian Aars Wilhelmsen

Master of Science in Cybernetics and Robotics
Submission date: June 2018
Supervisor: Ole Morten Aamo, ITK

Norwegian University of Science and Technology
Department of Engineering Cybernetics

Problem Description

Background

Systems of 2×2 hyperbolic PDEs can be applied to model the dynamics of drilling fluid in the drill string during oil well drilling, and implementing attenuating controllers to stabilize the drilling system during incidences such as kicks requires observers for (efficient) estimation of drill string states. Observers for 2×2 systems, usually normalized to evolve on $[0, 1]$, have previously been designed for sensing at one end, either $x = 0$ or $x = 1$. They provide finite (and minimum time) convergence of the estimates governed by the transport speed of the system equations. The topic of the MSc thesis is to investigate whether an observer with bilateral sensing (sensing at both $x = 0$ and $x = 1$) for 2×2 systems that achieves convergence in minimum time shorter than the minimum time for single boundary sensing can be derived. The following points should be addressed by the student:

Tasks

1. Review relevant literature (a number of recent papers will be provided as a starting point).
2. Consider if a 2×2 system on $[0, 1]$ can be transformed into a $2 + 2$ system on $[0, 1]$ by simply splitting the domain at some x_s in $(0, 1)$, redefining boundary conditions and rescaling of the two sub-domains.
3. Attempt extending the existing non-minimum time collocated observer design for $2 + 2$ systems to achieve convergence in minimum time.
4. Investigate if convergence in minimum time can be achieved for the 2×2 system bilateral observer by applying the $2 + 2$ collocated observer from item 3 together with the coordinate transform from item 2. The splitting location x_s may influence the minimum time, and if so, investigate if there is an optimal location x_s that achieves overall minimum time.
5. Illustrate your findings in simulations.
   (a) Consider first performing toy simulations to verify the 2×2 system bilateral observers converge in minimum time shorter than the minimum time for sensing in one end.
   (b) If time permits, consider applying the 2×2 system bilateral observer to a simulation of oil well drilling, where both topside and downhole measurements are available.
6. If time permits, consider writing a scientific paper based on your findings.
7. Write a report

Assignment given: 6^{th} February 2018
Supervisor: Professor Ole Morten Aamo, ITK

Preface

This Master's Thesis is submitted in partial fulfillment for the degree of MSc in Engineering Cybernetics at the Norwegian University of Science and Technology, and concludes my five-year study in this programme. I would like to thank Professor Ole Morten Aamo for being my thesis supervisor, and also Henrik Anfinsen for sharing his expert knowledge of the field. Their helpful and valuable discussions and comments throughout the semester have been of great importance for this thesis work. Additionally, I want to thank Haavard Holta for some useful comments during the thesis supervision meetings and Benjamin Clement Sebastian for proofreading.

The resources that were made available and form the basis for this thesis are as follows:

1. The papers Vazquez et al. (2011), Hu et al. (2016), Auriol and Di Meglio (2016), Hu et al. (2015), Coron et al. (2017), Anfinsen and Aamo (2017b) were provided as a starting point.
2. MATLAB code written by Henrik Anfinsen that solves kernel equations for $2+1$ systems based on the method described in Anfinsen and Aamo (2017a) was provided as a starting point for the simulations.

Using the aforementioned resources as a starting point, the thesis work has ended up with contributions/results that can be summed up as follows:

1. A minimum time collocated observer for a class of coupled $2+2$ linear hyperbolic PDE systems has been derived.
2. A minimum time bilateral observer for coupled 2×2 linear hyperbolic PDE systems has been derived in a novel way by folding the domain and applying the $2+2$ collocated observer from contribution 1.
3. The MATLAB code for solving kernel equations for $2+1$ systems has been extended to solve kernel equations for the class of $2+2$ systems the collocated observer in contribution 1 was derived for.
4. Applying the code from contribution 3, the observer in contribution 2 was simulated and bench-marked against a previously derived unilateral 2×2 observer.
5. It has been demonstrated in simulations how the bilateral observer from contribution 2 can be applied to an example from oil well drilling.

Trondheim, June 2018
Nils Christian Aars Wilhelmsen

Abstract

We consider state estimation of 1D systems of 2×2 linear first-order coupled hyperbolic PDEs, consisting of two distributed states propagating information in opposite directions but interacting across the spatial domain. These types of systems can be used to model various technical and physical phenomena. In most practical situations only measurements from boundary points are available, and the interior states must from these be deduced. We derive a bilateral boundary observer, utilizing sensing at both boundaries of the spatial domain, to provide state estimates of the 2×2 system which are correct within a finite and theoretically minimal amount of time. This optimal convergence time is smaller than the corresponding lowest possible convergence time for unilateral boundary observers, being observers only using measurements from a single boundary point. As a first step in the derivation of the 2×2 bilateral observer, we derive for a 1D system of $2 + 2$ linear first-order coupled hyperbolic PDEs, consisting of four distributed states coupled point-wise across the domain, of which two transmit information leftwards and the other two information rightwards, a boundary observer which relies on measurements from a single boundary that is collocated with actuation. The design is achieved by using infinite dimensional backstepping through applying a Volterra integral transformation composed with a Fredholm integral transformation. We show that this observer converges within the theoretical lower bound for convergence time of unilateral boundary observers for $2 + 2$ systems. Next, we split the spatial domain of the 2×2 system at an interior point, and transform it to a $2 + 2$ system by re-scaling of the sub-domains and redefining boundary conditions. A bilateral observer for the 2×2 system is subsequently derived from the previously derived minimum time unilateral observer for the $2 + 2$ system. How the splitting point should be chosen to achieve minimum time convergence for the bilateral 2×2 observer is shown. To demonstrate the efficiency of the 2×2 bilateral observer, we implement 2×2 systems and their corresponding minimum time bilateral observers in simulations. These are bench-marked against 2×2 unilateral boundary observers only sensing a single boundary point, and it is found that the bilateral observers have superior performance to the unilateral observers. As an application of the theory derived, it is next shown how the 2×2 system can be used to model the pressure and flow dynamics of drilling fluid during oil well drilling. A scenario where the observers are used for state estimation during kick handling is considered. The scenario is simulated and it is shown that an observer using both topside and downhole measurements during drilling has a more efficient response with respect to correctly estimating the states of the drilling fluid than an observer only utilizing topside measurements, something that can contribute to safer kick handling.

Sammendrag

Vi betrakter tilstandsestimering av 1D systemer av 2×2 lineære førsteordens koblede hyperbolske PDEer, som består av to distribuerte tilstander som forplanter informasjon i motsatt retninger og vekselvirker over det romlige domenet. Slike typer systemer kan brukes til å modellere diverse tekniske og fysiske fenomener. I fleste praktiske tilfeller så er kun målinger fra randpunkter tilgjengelige, og tilstandene over de interiøre punktene må fra disse deduseres. Vi utleder en bilateral randestimator, som bruker målinger fra begge randene av det romlige domenet for å produsere tilstandsestimater av 2×2 systemet som er riktig innen en endelig og teoretisk minimal lengde av tid. Denne optimale konvergenstiden er mindre enn den tilsvarende lavest mulige konvergenstiden for unilaterale randestimatorer, som er estimatorer som kun benytter seg av målinger fra et randpunkt. Som et første steg i utledningen av 2×2 bilaterale estimatorer, så utleder vi ved hjelp av uendelig dimensjonal backstepping, ved å anvende en komposisjon av en Volterra og Fredholm integral transformasjon, en unilateral randestimator som benytter seg av randmålinger ko-lokalisert med aktuering for et 1D system av $2 + 2$ lineære førsteordens koblede hyperbolske PDEer. Denne typen system består av fire distribuerte tilstander koblet punktvis over domenen, hvorav to sender informasjon i positiv retning og de to andre informasjon i negativ retning. Vi viser at denne estimatoren konvergerer innen den teoretisk nedre grensen for konvergenstid av unilaterale estimatorer for $2 + 2$ systemer. Deretter deler vi den spatialle domenen for 2×2 systemet på et indre punkt, og transformerer den til et $2 + 2$ system ved å reskalere sub-domenene og redefinere randbetingelsene. En bilateral estimator for 2×2 systemet er deretter utledet fra den tidligere utledete minimumstid konvergente unilaterale estimatoren for $2 + 2$ systemet. Hvordan splittepunktet burde blir valgt for å oppnå konvergens innen minimal tid for den bilaterale 2×2 estimatoren er vist. For å demonstrere ytelsen av den 2×2 bilaterale estimatoren så implementerer vi 2×2 systemer og deres tilsvarende minimumstid bilaterale estimatorer i simuleringer. Disse er sammenliknet opp mot 2×2 unilaterale randestimatorer som kun bruker målinger fra høyre rand, og man finner at de bilaterale estimatorene har raskere konvergenstid enn de unilaterale estimatorene. Som en anvendelse av teorien som har blitt utledet, blir 2×2 systemet transformert for å modellere trykk og flyt av borrefluidet i en borrestreng. En situasjon hvor estimatorene blir brukt for tilstandsestimering under håndtering av brønnspark er undersøkt. Det blir vist at en estimator som bruker målinger fra riggen i tillegg til nedhullsmålinger har en mer effektiv respons med tanke på riktig estimering av tilstandene til borrefluidet enn en estimator som kun baserer seg på toppsidemålinger, noe som kan bidra til tryggere håndtering av brønnspark.

Contents

List of Figures

List of Symbols

Sets & variables

Symbol	Explanation
$\mathbb{R}$	Set of real numbers.
$\mathbb{R}^p$	Set of vectors with p real components, $p \in \{1, 2, \dots\}$
$C^0(\mathbb{D})$	Set of continuous functions defined over the domain $\mathbb{D}$.
$C^1(\mathbb{D})$	Set of differentiable functions over the domain $\mathbb{D}$.
$L^2(\mathbb{D})$	Set of square integrable functions over the domain $\mathbb{D}$.
$\mathcal{T}_u$	Upper triangular domain defined as $\{(x, \xi) \mid 0 \leq x \leq \xi \leq 1\}$.
$\mathcal{T}_l$	Lower triangular domain defined as $\{(z, \zeta) \mid 0 \leq \zeta \leq z \leq 1\}$.
$\mathcal{S}_0$	Square domain defined as $\{(x, \xi) \mid 0 \leq x, \xi \leq 1\}$.
t	Temporal variable satisfying $t \in [0, \infty) \subset \mathbb{R}$.
x, ξ	Spatial variables satisfying $x, \xi \in [0, 1] \subset \mathbb{R}$.
z, ζ	Auxiliary spatial variables for lower triangular kernel used for numerical solution method satisfying $z, \zeta \in [0, 1] \subset \mathbb{R}$.
s	Dummy variable.

$n + m$ systems

Symbol	Explanation
n, m	Number of states with respectively positive and negative transport speeds, $n, m \in \mathbb{Z}^+$.
$\bar{u}(x,t), \bar{v}(x,t)$	Distributed state vectors with respectively n components with positive transport speeds and m components with negative transport speeds.
$u_i(x,t), v_j(x,t)$	i^{th} and j^{th} scalar component of $\bar{u}(x,t)$ and $\bar{v}(x,t)$, respectively, $i \in \{1, \dots, n\}, j \in \{1, \dots, m\}$.
$\bar{u}_0(x), \bar{v}_0(x)$	Initial conditions for respective distributed state vectors $u(x,t)$ and $v(x,t)$.

$u_{i,0}(x), v_{i,0}(x)$	i^{th} and j^{th} component of $\bar{u}_0(x)$ and $\bar{v}_0(x)$, respectively, $i \in \{1,\dots,n\}, j \in \{1,\dots,m\}$.
$\Lambda^+(x), \Lambda^-(x)$	Respectively $n \times n$ and $m \times m$ diagonal matrices of positive and negative transport speeds.
$\lambda_i(x), \mu_j(x)$	Respectively scalar entry in i^{th} row and column of $\Lambda^+(x)$ and j^{th} row and column of $\Lambda^-(x)$, $i \in \{1,\dots,n\}, j \in \{1,\dots,m\}$.
$\Sigma^{++}(x), \Sigma^{+-}(x)$	Respectively $n \times n$ and $n \times m$ coupling coefficient matrices appearing in PDE for $\bar{u}(x,t)$.
$\sigma^{++}_{ij}(x), \sigma^{+-}_{kl}(x)$	Respectively entry in i^{th} row and j^{th} column of $\Sigma^{++}(x)$, k^{th} row and l^{th} column of $\Sigma^{+-}(x)$, $i,j,k \in \{1,\dots,n\}, l \in \{1,\dots,m\}$.
$\Sigma^{-+}(x), \Sigma^{--}(x)$	Respectively $m \times n$ and $m \times m$ coupling coefficient matrices appearing in PDE for $\bar{v}(x,t)$.
$\sigma^{-+}_{ij}(x), \sigma^{--}_{kl}(x)$	Respectively entry in i^{th} row and j^{th} column of $\Sigma^{-+}(x)$, k^{th} row and l^{th} column of $\Sigma^{--}(x)$, $i,k,l \in \{1,\dots,m\}, j \in \{1,\dots,n\}$.
Q_0, R_1	Respectively $n \times m$ and $m \times n$ reflection coefficient matrices appearing in boundary conditions for $x = 0$ and $x = 1$.
Q_{ij}, R_{kl}	Respectively entries in the i^{th} row and j^{th} column of Q_0 and k^{th} row and l^{th} column of R_1, $i,l \in \{1,\dots,n\}, j,k \in \{1,\dots,m\}$.
$U(t)$	m-dimensional vector of boundary control inputs entering at $\bar{v}(1,t)$.
$\bar{U}_j(t)$	j^{th} scalar component of $U(t)$, $j \in \{1,\dots,m\}$.
$y(t)$	n-dimensional vector of boundary measurements collocated with $U(t)$.
$\bar{y}_i(t)$	i^{th} scalar component of $y(t)$, $i \in \{1,\dots,n\}$.

$n+m$ collocated observers and backstepping transformations

Symbol	**Explanation**
$\mathcal{V}$	Volterra integral transformation.
$\mathcal{F}$	Fredholm integral transformation.
$\check{u}(x,t), \check{v}(x,t)$	Vectors of observer estimates for distributed state vector $\bar{u}(x,t)$ and $\bar{v}(x,t)$, respectively.
$\check{u}_i(x,t), \check{v}_j(x,t)$	Respectively i^{th} component of $\check{u}(x,t)$ and j^{th} component of $\check{v}(x,t)$, $i \in \{1,\dots,n\}, j \in \{1,\dots,m\}$.
$\tilde{u}(x,t), \tilde{v}(x,t)$	Vectors of observer estimation errors for distributed state vectors $\bar{u}(x,t)$ and $\bar{v}(x,t)$, respetively.
$\tilde{u}_i(x,t), \tilde{v}_j(x,t)$	Respetively i^{th} component of $\tilde{u}(x,t)$ and j^{th} component of $\tilde{v}(x,t)$, $i \in \{1,\dots,n\}, j \in \{1,\dots,m\}$.

$P^+(x), P^-(x)$	Collocated observer gains for $\check{u}(x,t)$ and $\check{v}(x,t)$ respectively.
$P^+_{ij}(x), P^-_{kl}(x)$	Respectively entry in i^{th} row and j^{th} column of $P^+(x)$, k^{th} row and l^{th} column of $P^-(x)$, $i,j,l \in \{1,\ldots,n\}, k \in \{1,\ldots,m\}$.
$M(x,\xi), N(x,\xi)$	Observer kernels used in calculating $P^+(x)$ and $P^-(x)$, respectively.
$M_{ij}(x,\xi), N_{kl}(x,\xi)$	Respectively entry in i^{th} row and j^{th} column of $M(x,\xi)$, k^{th} row and l^{th} column of $N(x,\xi)$, $i,j,l \in \{1,\ldots,n\}, k \in \{1,\ldots,m\}$.
$H(x)$	$n \times n$ strictly lower triangular matrix appearing in boundary condition of PDE system for $M(x,\xi)$ and $N(x,\xi)$.
$h_{ij}(x)$	Non-zero scalar of $H(x)$ in the ith column and jth row, where $i \in \{2,\ldots,n\}$ and $j \in \{1,\ldots,i-1\}$.
$\tilde{\alpha}(x,t), \tilde{\beta}(x,t)$	Distributed state vectors in intermediate target error system.
$\tilde{\alpha}_i(x,t), \tilde{\beta}_j(x,t)$	Respectively i^{th} component of $\tilde{\alpha}(x,t)$ and j^{th} component of $\tilde{\beta}(x,t)$, $i \in \{1,\ldots,n\}, j \in \{1,\ldots,m\}$.
$\alpha(x,t), \beta(x,t)$	Vectors of mathematically constructed states in intermediate target system.
$\alpha_i(x,t), \beta_j(x,t)$	Respectively i^{th} component of $\alpha(x,t)$ and j^{th} component of $\beta(x,t)$, $i \in \{1,\ldots,n\}, j \in \{1,\ldots,m\}$.
$\alpha_0(x), \beta_0(x)$	Vectors of initial conditions for $\alpha(x,t)$ and $\beta(x,t)$, respectively.
$\alpha_{i,0}(x), \beta_{j,0}(x)$	Respectively i^{th} component of $\alpha_0(x)$ and j^{th} component of $\beta_0(x)$, $i \in \{1,\ldots,n\}, j \in \{1,\ldots,m\}$.
$\hat{\alpha}(x,t), \hat{\beta}(x,t)$	Artificial observer estimates of mathematically constructed distributed state vector $\alpha(x,t)$ and $\beta(x,t)$, respectively.
$\hat{\alpha}_i(x,t), \hat{\beta}_j(x,t)$	Respectively i^{th} component of $\hat{\alpha}(x,t)$ and j^{th} component of $\hat{\beta}(x,t)$, $i \in \{1,\ldots,n\}, j \in \{1,\ldots,m\}$.
$D^+(x,\xi), D^-(x,\xi)$	Terms appearing in target system definitions, defined respectively as $M(x,\xi)\Sigma^{+-}(\xi) - \int_\xi^x M(\xi,s)D^+(s,\xi)ds$ and $N(x,\xi)\Sigma^{+-}(\xi) - \int_\xi^x N(\xi,s)D^+(s,\xi)ds$.
$d^+_{ij}(x,\xi), d^-_{kl}(x,\xi)$	Respectively entry in the i^{th} row and j^{th} column of $D^+(x,\xi)$, k^{th} row and l^{th} column of $D^-(x)$, $i \in \{1,\ldots,n\}, j,k,l \in \{1,\ldots,m\}$.
$V(t)$	m-dimensional vector of mathematically constructed boundary control inputs in intermediate target system actuating $\alpha(1,t)$.
$V_j(t)$	jth component of $V(t)$, $j \in \{1,\ldots,m\}$.
$\eta(t)$	n-dimensional vector of measurement collocated with control in mathematically constructed inetermediate error system, defined as $\alpha(1,t)$.
$\eta_i(t)$	ith component of $\eta(t)$.

$T^+(x)$	Strictly lower triangular 2×2 matrix of artificial observer gains added to observer for mathematically constructed intermediate $2+2$ system to produce 2-dimensional state vector estimates $\hat{\alpha}(x,t)$ and $\hat{\beta}(x,t)$.
$T^+_{ij}(x)$	Component in the ith row and jth column of $T^+(x)$, $i \in \{1,\ldots,2\}$.
$K_1(x,\xi)$	Strictly lower triangular 2×2 matrix observer kernel used to calculate $T^+(x)$.
$k_{21}(x,\xi)$	Non-zero term of $K_1(x,\xi)$ in 2^{nd} row and 1^{st} column.
$K(x,\xi)$	4×4 matrix defined as $diag\{K_1(x,\xi),0\}$.
$\tilde{\gamma}(x,t), \tilde{\nu}(x,t)$	Distributed error state vectors from minimum time convergent target error system.
$\tilde{\gamma}_i(x,t), \tilde{\nu}_j(x,t)$	Respectively i^{th} and j^{th} scalar components of $\tilde{\gamma}(x,t)$ and $\tilde{\nu}(x,t)$, $i,j \in \{1,2\}$.
$\breve{K}_1(x,\xi)$	Term appearing in minimum time convergent $2+2$ target error system defined as $\left[\begin{smallmatrix} 0 & 0 \\ 0 & k_{21}(x,\xi) \end{smallmatrix}\right]$.
$\breve{\Sigma}^{+-}(x)$	Term appearing in minimum time convergent $2+2$ target error system defined as $\left[\begin{smallmatrix} 0 & 0 \\ \sigma^+_{11}(x) & \sigma^+_{12}(x,\xi) \end{smallmatrix}\right]$.
$\breve{D}^+(x,\xi)$	Term appearing in minimum time convergent $2+2$ target error system defined as $\left[\begin{smallmatrix} 0 & 0 \\ d^+_{11}(x) & d^+_{12}(x,\xi) \end{smallmatrix}\right]$.
$\tilde{\delta}(x,t)$	Defined as $[\tilde{\alpha}^T(x,t), \tilde{\beta}^T(x,t)]$, where $n=m=2$.
$\tilde{\omega}(x,t)$	Defined as $[\tilde{\gamma}^T(x,t), \tilde{\nu}^T(x,t)]^T$.
t_F	General finite non-minimum convergence time.
$t_{1,min}$	Theoretical minimal convergence time of observer using sensing at a single boundary(unilateral observer).
$t_{2,min}$	Theoretical minimal convergence time of observer using sensing at both boundaries(bilateral observer).

2×2 system and bilateral observer

Symbol	**Explanation**
$u(x,t), v(x,t)$	Scalar distributed states of 2×2 system.
$\lambda(x), \mu(x)$	Scalar transport speeds for 2×2 system.
$\sigma^+(x), \sigma^-(x)$	Scalar coupling coefficient for 2×2 system.
Q, R	Reflection coefficients for 2×2 system appearing for boundary at $x=0$ and $x=1$, respectively.
$u_0(x), v_0(x)$	Initial conditions for $u(x,t)$ and $v(x,t)$, respectively.
$U_1(t), U_2(t)$	Boundary control inputs actuating $u(0,t)$ and $v(1,t)$, respectively.
$y_1(t), y_2(t)$	Boundary measurements respectively collocated with $U_2(t)$ and $U(1,t)$, and defined as $u(1,t)$ and $v(0,t)$.
x_s	Splitting point in 2×2 system domain when transforming to $2+2$ system, where $x_s \in (0,1)$.

$r_{x_s}(x), r_{x_s}^{-1}(x)$	Mapping from right sub-domain $[x_s, 1]$ of 2×2 system to spatial domain $[0, 1]$ of $2 + 2$ system, and its inverse.
$l_{x_s}(x), l_{x_s}^{-1}(x)$	Mapping from left sub-domain $[0, x_s]$ of 2×2 system to spatial domain $[0, 1]$ of $2 + 2$ system, and its inverse.
$\mathscr{T}_{x_s,i}[u, v], \mathscr{T}_{x_s,i}^{-1}[\bar{u}, \bar{v}]$	Coordinate transform mapping 2×2 system into $2+2$ system based on relationship between λ, μ, x_s, $i \in \{1, \ldots, 4\}$, and its corresponding inverse.
$\mathscr{T}[u, v], \mathscr{T}^{-1}[\bar{u}, \bar{v}]$	Defined as $\mathscr{T}_{x_s,i}$ for $x_s = \frac{1}{2}$ and $i = 3$, and its inverse.
$\hat{u}(x, t), \hat{v}(x, t)$	Observer estimates of $u(x, t)$ and $v(x, t)$, respectively.
$P^{++}(x), P^{+-}(x)$	Bilateral observer gain for $\hat{u}(x, t)$.
$P^{-+}(x), P^{--}(x)$	Bilateral observer gain for $\hat{v}(x, t)$.
$f(x), f^{-1}(x)$	Function defined as $\int_x^1 \frac{ds}{\lambda(s)} - \int_0^x \frac{ds}{\mu(s)}$, and its inverse.
$g(x), g^{-1}(x)$	Function defined as $\int_0^x \frac{ds}{\lambda(s)} - \int_x^1 \frac{ds}{\mu(s)}$, and its inverse.
F, G	Range of $f(x)$ and $g(x)$, respectively, satisfying $F, G \subset \mathbb{R}$.

Simulation specific

Symbol	**Explanation**
$\bar{P}^{+}(x), \bar{P}^{-}(x)$	Unilateral 2×2 observer gains.
$\bar{M}(x, \xi), \bar{N}(x, \xi)$	Scalar kernel for calculating $\bar{P}^{+}(x)$ and $\bar{P}^{-}(x)$, respectively.
$K(z, \zeta), L(z, \zeta)$	States of $2 + 2$ kernel system with two positive transport velocities, defined over $\mathcal{T}_l$.
$P(z, \zeta), R(z, \zeta)$	States of $2 + 2$ kernel system with with one positive and one negative transport velocity, defined over $\mathcal{T}_l$.
$\varepsilon_i(z)$	Transport velocities parallel z axis, $i \in \{1, \ldots, 4\}$.
$\eta_i(\zeta)$	Transport velocities parallel ζ axis, $i \in \{1, \ldots, 4\}$.
$a_i(z, \zeta)$	Coupling coefficients in $2 + 2$ system for $K(z, \zeta)$, $i \in \{1, \ldots, 4\}$.
$b_i(z, \zeta)$	Coupling coefficients in $2 + 2$ system for $L(z, \zeta)$, $i \in \{1, \ldots, 4\}$.
$c_i(z, \zeta)$	Coupling coefficients in $2 + 2$ system for $P(z, \zeta)$, $i \in \{1, \ldots, 4\}$.
$d_i(z, \zeta)$	Coupling coefficients in $2 + 2$ system for $R(z, \zeta)$, $i \in \{1, \ldots, 4\}$.
$f_i(z)$	Boundary condition functions for boundaries over (z, z), $i \in \{1, 2\}$.
ϱ_i	Boundary condition coupling coefficients for boundary conditions along $(z, 0)$, $i \in \{1, \ldots, 4\}$.
$\hat{N}$	Number of spatial grid points in simulation.
Δ	Grid dimension in solvers and simulation.
h	Time step used on simulation.

Oil well drilling

Symbol	Explanation
l	Depth of well.
z	Spatial variable representing position in drill string satisfying $z \in [0, l]$.
$p(z,t)$	Pressure of drilling mud.
$q(z,t)$	Volumetric flow of drilling mud.
$p_l(t)$	Topside pressure actuating signal.
$q_{bit}(t)$	Downhole flow actuating signal.
$\iota_1(t)$	Topside pressure measurement.
$\iota_2(t)$	Topside flow measurement.
$\iota_3(t)$	Downhole pressure measurement.
$\iota_4(t)$	Downhole flow measurement.
β	Bulk modulus of drilling mud.
ρ	Density of drilling mud.
A_1	Cross-sectional area of drill string annulus.
F_1	Friction factor in drill string.
g	Acceleration of gravity.
J	Production index of the well.
t_K	Time of kick.
t_D	Delay time for estimating reservoir pressure.
$p_r(t)$	Reservoir pressure.

Part I

Background

Chapter 1

Introduction

1.1 Motivation

Systems of linear first-order coupled 2×2 hyperbolic partial differential equations(PDEs), which consist of two time varying distributed states defined continuously over a one-dimensional finite spatial interval, with each state convecting information in opposite directions and interacting with each other at both interior and boundary points, have received an increasing amount of attention within estimation and control circles the past decade. These types of systems can be used to describe a wide range of physical phenomena, such as traffic flow (see f.ex. Colombo (2002) or Goatin (2006)), gas pipelines (see f.ex. Gugat et al. (2011) or Canuto and Quarteroni (1987)), heat exchangers (see f.ex. Xu and Sallet (2002) or Bartecki (2015)), oil drilling (see f.ex. Di Meglio and Aarsnes (2015) or Krstic and Bekiaris-Liberis (2013)), open channel flow (see f.ex. Coron et al. (1999) or Bastin and Coron (2011)), and transmission lines (see f.ex. Curro et al. (2011) or Clarke (1983)), to name a few.

In most practical situations only one or both boundaries of the spatial domain are available for measurement, despite information pertaining to the state of interior locations often being of interest. To solve this problem, state estimation algorithms known as *observers* have been developed both for hyperbolic(see f.ex Li and Liu (2012)) and other types(parabolic in Smyshlyaev and Krstic (2005)) of PDEs. Observers for PDE systems are infinite dimensional generalizations of observers for ordinary differential equations(ODEs)(see f.ex. Chen (1998)), which estimate the states of the ODE system, of which there are a finite number.

Particularly for linear PDE systems, one common motivation for being interested in the system states at interior points, rather than just the states which are trivially available via boundary measurements, is that often full state information is required to implement control algorithms to achieve objectives such as stabilization or trajectory tracking. The *separation principle* for linear systems allows observer design to be performed separately from controller design, thus allowing usage of state estimates from the observer in place of full state information in the controller implementation. Hence, in addition to being of interest in itself, the problem of observer design is also interesting as a stepping stone in the implementation of systems applying full state feedback control algorithms for linear PDE systems.

When implementing a full state feedback control algorithm with an observer relying on boundary measurements in the loop, since the control algorithm is dependent on correct state information to function properly (the *garbage in - garbage out* principle), a bottleneck affecting the time the controller uses to stabilize or steer the system to its control objective is the time the observer needs to come up with correct state estimates. This motivates the need for observers producing state estimates converging to the actual system state values quickly, contributing to the efficiency of the overall boundary feedback setup.

Most observer algorithms for hyperbolic PDE systems defined over a one-dimensional spatial interval, which have been focused on previously, have used a single, rather than both boundaries of the domain in their design. In some practical situations only a single boundary is available for measurement, and in these cases the implementation of an algorithm relying on both boundaries is clearly infeasible. However, it is possible to make observers for the systems of hyperbolic PDEs we are concerned with in this dissertation that converge in finite time, but an observer relying on only a single boundary measurement has its minimal theoretical convergence time bounded from below by the sum of the propagation times of the slowest characteristics in both directions, whereas the lower theoretical bound for convergence time of an observer relying on both boundary measurements is only limited by the slowest overall characteristic, rather than both(Li and Rao (2010)). This implies that if designed correctly, an observer for a first-order linear hyperbolic PDE system using both rather than a single boundary measurement will be able to produce state estimates which are correct sooner than an observer only using a single boundary measurement. For situations when one does have access to measurements from both sides of the domain, it would thus be preferable to implement an algorithm exploiting both of these measurements to make an overall more efficient system.

As stated earlier, oil drilling is one of multiple different technical applications systems of 2×2 coupled hyperbolic PDEs can be used to describe. During oil drilling operations, a water based liquid referred to as *mud* is pumped down the drill pipe and into the well. It flows through the drilling bit at the bottom of the drill string, lubricating and cooling the bit down before collecting cuttings left over from drilling and bringing them upwards towards the surface through the annulus between the drill string and the outside casing (Pavlov et al. (2010)). In addition to this the mud acts as a pressure barrier against the pressure from the well, implying that ideally the pressure of the mud at the bottom of the drill string should equal the pressure from the well.

Managed pressure drilling(MPD) systems aim at actively controlling the pressure of the mud in the drill string with the help of sensors and actuators placed on the rig and drill string to achieve goals such as balancing the mud and well pressure. Traditionally the sensing and actuation equipment has been limited to be topside on the rig; with the advent of *wired drill pipe(WDP)* technology, it is also possible to place sensing and actuation equipment downhole(Sui et al. (2017)), thereby exploiting the possibility of collecting downhole data and sending downhole actuation signals to make safer MPD systems with quicker and more accurate responses. A situation which can occur during drilling which requires a quick response from the system in order to guarantee the safety of the personnel and equipment involved is when a sudden increase or decrease of the well pressure occurs, known as a *kick* or *loss*, respectively(Aamo (2013)). The mud acts as a first line of defence

against incidences such as these, and the quicker the destabilizing effects of the occurrence can be brought under control, the better. Often the drilling pipe is several kilometers long, and therefore it often takes some time before disturbances which occur downhole can be observed through topside measurements. By utilizing downhole WDP measurements, state estimators and controllers which correctly predict the drill string states and start attenuating the disturbance before it has reached the rig can be implemented.

In addition to being an interesting theoretical problem in itself, the possible increases in safety and efficiency of drilling operations along with resultant reductions in both materialistic and human costs should motivate the design of the bilateral observer for 2×2 linear hyperbolic PDEs described above. In the thesis the general theory will be developed first and then subsequently demonstrated on a model of an oil drilling system.

1.2 Previous Work

Design of deterministic observers(state estimators where possible random noise in the process of interest is disregarded, which is the type considered in this thesis) was originally developed for linear ODE systems, with the seminal paper Luenberger (1966) setting the stage in terms of structure and design method for observers found today by presenting the so-called *Luenberger observer*. This type of observer works by replicating the model of the system one is estimating but adding an *output error injection* term consisting of the measurement error multiplied by an *observer gain*, and is the pattern used in all observers considered in this thesis. According to Radke and Gao (2006), early state estimators which had been considered before the Luenberger observer include but are not limited to the Alpha-Beta-Gamma filter, the Proportional Integral observer and the Plant Output Based estimator.

With respect to observer design for PDEs, early approaches usually based their design on discretizing the domain to approximate the system as a set of ODEs, using for example the Galerkin method(Balas (1983)). Designs based on spectral theory(see f.ex. Fujii (1980) or Nambu (1984)) and frequency domain methods(Logemann (1993)) have also been considered. An increasingly used design approach for both observer and controller design, due to its power and elegance, is the *infinite dimensional backstepping* technique, developed first for solving PDE control problems and later extended to PDE observer problems, observation being the mathematical dual of control.

The backstepping technique in its finite dimensional form was initially developed around 1990 as a version of feedback linearization for nonlinear ODEs, with the added ability of being able to handle uncertainties in the system(Krstic and Smyshlyaev (2008b)), something which almost always occurs in practice. It can be applied on systems which have a cascaded structure where the innermost subsystem can be stabilized first, and then the outer subsystems stabilized recursively until the outermost control input is reached, at which point the necessary control law will have been built. As described in Khalil (2002), the design procedure involves finding an asymptotically stable target system and then applying a diffeomorphism mapping the system to be controlled to the target system through a change of coordinates, and the necessary control law can then subsequently be discovered. PDE systems with boundary control inputs can intuitively be seen as infinite dimensional analogues

of cascaded ODE systems on which backstepping can be applied, with the interior states of the PDE being analogous to the inner ODE subsystems which are "stepped back" from when designing the control law. It was this structural analogue that inspired the development of infinite dimensional backstepping, with research on this commencing around a decade later in 2000.

Infinite dimensional backstepping in its current form, building on the contributions given in Boskovic et al. (2001), Balogh and Krstic (2001) and Balogh and Krstic (2002), was first seen in the paper Liu (2003), where it was applied to the control problem of stabilizing a naturally unstable heat equation. Applying the technique to an observation rather than control problem was firstly done slightly later in Smyshlyaev and Krstic (2005) by generalizing the finite dimensional backstepping observer design for nonlinear ODEs given in Krener and Kang (2003) to the infinite dimensional case, in a similar way to the approach which had worked successfully for control problems previously.

The aforementioned contributions all dealt with parabolic PDEs, and the first time the infinite dimensional backstepping technique was applied to open loop unstable hyperbolic PDEs was in Krstic et al. (2008) where the hyperbolic PDE considered was of second-order, and then subsequently in Krstic and Smyshlyaev (2008a) the technique was applied to first-order hyperbolic PDEs for the first time.

The extension to systems of 2×2 linear hyperbolic first-order PDEs was initiated by Vazquez et al. (2011), where both a single boundary controller and an observer with measurements collocated with the actuated boundary, being referred to as a *collocated* observer, was derived. Generalization to systems of first-order hyperbolic PDEs with an arbitrary number n rightwards convecting distributed states, but only a single leftwards convecting distributed state, so-called $n+1$ systems, can for the case of sensing anti-collocated with control, referred to as an *anti-collocated* observer, be found in Di Meglio et al. (2013). Building on this, the fully general $n+m$ case, where also m distributed leftwards convecting states are permitted, was first solved in Hu et al. (2016) for the anti-collocated case. One disadvantage of the solution presented there was that both the controller and observer converged in a time larger than the lower theoretical bound for single-sided actuation and sensing, so to improve on this Auriol and Di Meglio (2016) presented a solution guaranteeing minimum time convergence for both controller and observer. Later the same minimum time control problem was solved in Coron et al. (2017), building on results from Hu et al. (2015), but using a different design method based on composing a Volterra integral transformation with a Fredholm integral transformation. With the previous $n+1$ observer result being for anti-collocated observers, a collocated $n+1$ observer was presented in Anfinsen and Aamo (2016), being designed to solve the disturbance rejection problem. Subsequently in Anfinsen and Aamo (2017b) this observer was generalized to a fully general $n+m$ collocated observer, also in conjunction with solving disturbance rejection. The $n+m$ collocated observer presented there was however non-minimum time convergent.

The paper Auriol and Di Meglio (in press), which has not yet been published but accepted for publication in *IEEE Transactions on Automatic Control*(IEEE TAC), derives both a minimum time controller and observer for systems of general $n+m$ first-order linear hyperbolic PDEs relying on actuation and sensing at both boundaries of the one-dimensional spatial domain, respectively. The bilateral observer is derived there by exploiting the duality of observation and control and is thus solved as a control problem, with the solution thereafter transformed back to

calculate the observer gains. This is different from the method used to derive the bilateral observer in this thesis, where we solve the observation problem for 2×2 systems using a trick that involves folding of the spatial domain.

With respect to the oil drilling application considered in this thesis, much of the early work on automatic detection and attenuation of kick and loss incidences using MPD considered lumped rather than distributed models, as in for example Zhou et al. (2010), which derives an adaptive observer for estimating bottomhole pressure(BHP), and in Zhou et al. (2011), which presents a switched control scheme for regulation of annular pressure during drilling together with related observers for estimating flow rate through the drilling bit. A PDE observer for a drill string relying on topside measurements designed for application to kick detection and attenuation is derived in Hauge et al. (2013), whereas in Landet et al. (2013) a continuous PDE model of an MPD system was developed for application to the *heave problem* in MPD. This model was modified in Holta et al. (2017) to model problems involving kicks and losses during drilling, with the reservoir pressure being incorporated as a term in the bottomhole boundary condition. That paper, in addition to deriving an adaptive control law, incorporated an adaptive collocated observer for estimation of the system states and unknown boundary conditions.

1.3 Scope and Assumptions

We will in this thesis only be focusing on the linear case, so semilinear or nonlinear PDEs are not considered. Also, all the systems considered can be described by hyperbolic PDEs, and all the PDEs are of first order. The transport velocities of the PDEs are assumed spatially varying in the theoretical derivations, whereas the simulations are performed only for the special case of constant transport velocities. The coupling coefficients are spatially varying in both the theoretical derivations and simulations.

A minimum-time collocated observer for a class of linear hyperbolic first order PDE systems with certain structural assumptions relevant to the objective of the thesis, consisting of four coupled equations of which two have positive transport speeds and the other two have negative transport speeds, is first derived. We will here refer to this type of PDE system as a $2 + 2$ system. Next, these results are used to derive a minimum-time bilateral observer for a system of linear hyperbolic first-order coupled PDE systems consisting of two coupled equations transporting information in opposite directions, which will be referred to as 2×2 systems. Notice that 2×2 systems and $1+1$ systems are the same, although we will use the term 2×2 system. To visually and numerically demonstrate the improvement in convergence time a bilateral compared to a unilateral observer for 2×2 systems brings, the observers are firstly implemented in toy simulations.

Next, to demonstrate the practical applicability of the theoretical results derived, it is demonstrated how the general 2×2 model can be transformed to a simple linearized model of a drill pipe, with pressure and volumetric flow in the annulus being the physical parameters emphasized. In the oil drilling model it is assumed that the transport velocities involved, which are functions of the physical quantities *bulk modulus* and *density* of the mud as well as the cross sectional area of the annulus, are constant. The friction factor in the drill pipe is also assumed constant. Since a WDP is used, it is assumed that we have access to bottomhole measurements

of pressure and volumetric flow, as well as being able to sense the corresponding topside quantities using sensors on the rig. The flow through the drilling bit and the topside pressure are the possible points of actuation in the setup.

Using this model, the performance of a bilateral observer using both topside and downhole measurements is compared to that of a unilateral observer, only being able to capitalize on the topside measurements, in the event of a sudden kick whilst drilling. Since in a practical situation the new reservoir pressure after the kick is unknown, an online parameter estimation algorithm can in practice be implemented to obtain the new reservoir pressure. In the simulation this algorithm is instead, for simplicity, "implemented" by allowing the observers access to the correct new reservoir pressure after a short time delay. The effect of this is that the observer state estimates are pushed away from their correct values after the kick, and when the reservoir pressure is made available, one can observe the difference in recovery time to correct state estimates between the bilateral and unilateral observer.

1.4 Contributions

The main theoretical contributions this thesis offers are twofold. Firstly, a minimum-time collocated observer for a class of $2+2$ systems is designed. To the best of the authors knowledge this is a theoretical problem which has not previously been solved. This collocated observer builds on the non-minimum time collocated observer for general $n+m$ first-order linear hyperbolic systems which can be found in Anfinsen and Aamo (2017b). The way this minimum time collocated observer was obtained was through applying the Volterra transformation used in the previously mentioned paper, and composing it with a Fredholm transformation which removes the cascade terms in the target system causing the non-minimum time convergence. This approach is analogous to and inspired from the approach used in Coron et al. (2017) for designing a minimum time stabilizing controller.

Secondly, a minimum-time bilateral observer for a 2×2 system is designed. The approach taken to design this observer is to show that the 2×2 system can be "folded" into a $2+2$ system by using an invertible coordinate transformation, and the 2×2 bilateral observer gains can then be derived in terms of the $2+2$ collocated observer gains.

During the course of this dissertation work, it was discovered that a minimum-time bilateral observer has already been designed for $n+m$ systems in Auriol and Di Meglio (in press), which is accepted for publication in IEEE TAC and available electronically as an early access paper. They take an entirely different approach, however, based on solving a dual control problem.

In addition to purely theoretical contributions, this thesis also offers some simulation and application related contributions. A numerical PDE solver based on the method described in Anfinsen and Aamo (2017a) and written by Henrik Anfinsen in the programming language `MATLAB` for solving kernel PDEs related to observers for $2+1$ systems, which are coupled hyperbolic PDE systems with three coupled states, of which one of the equations transports information in the opposite direction to the two other equations, is extended to solve observer kernel PDEs for the $2+2$ systems considered in this thesis. A simulator for simulating the 2×2 system is built around this PDE solver, and both the bilateral observer derived in this dissertation and the previously derived unilateral observer from Vazquez

et al. (2011) is implemented. Simulations are performed to compare the relative performance of the old unilateral observer to the novel bilateral observer in terms of their efficiency in estimating 2×2 system states.

Lastly, the 2×2 bilateral observer is demonstrated to have applications within oil well drilling. A drilling simulator based on the drill string fluid model originally presented in Landet et al. (2013) is implemented and the bilateral 2×2 observer is applied to estimate the pressure and flow of drilling fluid in a drill string through receiving both topside and downhole pressure and flow measurements. It is demonstrated that it is advantageous to use the bilateral observer, which capitalizes on having access to measurements from both ends of the drill string, rather than a unilateral observer which is only able to utilize topside measurements, during a kick handling scenario.

The contributions and their relative localization in this thesis is summed up as follows.

- In Chapter 3 the derivation of the minimum-time collocated observer for a $2 + 2$ system with certain structural assumptions is presented.
- The derivation of the minimum-time bilateral observer for a 2×2 system is shown in Chapter 4.
- The kernel solvers and simulator which was implemented is described in Chapter 5.
- Chapter 6 presents simulations comparing the performance of the 2×2 bilateral observer to a 2×2 unilateral observer.
- The drilling related contributions find place in Chapters 7 and 8.

1.5 Notation and outline

The most important notational conventions used are summarized here. When a vector quantity is presented, it is unless otherwise stated a column vector. Both scalar, vector and matrix quantities are shown in normal font, but it should be clear from the context which is implied. For example, $f(x,t)$ could be a scalar or a vector, depending on the context.

When a circumflex/caron is shown above a function, as in $\hat{f}(x,t)/\check{f}(x,t)$ this denotes the estimate of the function value. A tilde is used to denote estimation error, so $\tilde{f}(x,t)$ is the estimation error of $f(x,t)$. In the simulation related chapters, when norm signs are shown around the variable, such as $||f(t)||$, the Euclidean norm, also commonly referred to as the L_2 norm, over the spatial variable is implied. For a function $f(x,t)$, with $x \in [a,b]$, the Euclidean norm over the spatial domain as function of time will be defined as

$$||f(t)|| = \sqrt{\frac{1}{b-a}\int_a^b f^2(x,t)dx}. \tag{1.1}$$

With regards to differentiation, $f'(x)$ or $\frac{df(x)}{dx}$ both denote ordinary differentiation with respect to spatial variables. The notation $\dot{f}(t)$ is sometimes used if the

underlying variable is temporal. The notation $f_x(x,t)$ and $\frac{\partial f(x,t)}{\partial x}$ both denote partial differentiation of $f(x,t)$ with respect to x. When a function f is invertible, we use f^{-1} to denote this functions inverse.

The sequence of contributions mentioned in the previous section guides the core structure of the thesis. Macroscopically, the thesis is split into four parts, each part consisting of one or more chapters. Part I is composed of Chapter 1 and Chapter 2 and consists of background material relevant to the thesis. Here Chapter 2 consists of necessary background theory on boundary state estimation of PDEs. Readers familiar with this material from before can skip this chapter. In Part II one finds the main theoretical contributions, with Chapter 3 being devoted to deriving the minimum time $2+2$ collocated observer. Chapter 4 builds on this by applying these results to derive a minimum time 2×2 bilateral observer. To see the observers in action one must turn to Part III, where everything related to the simulations performed is presented. Here in Chapter 5 the numerical solution method which was used is presented and how the solvers used in the simulator work is explained. Thereafter in Chapter 6 results from some toy simulations to demonstrate the capabilities of the designed observer can be found. A presentation of the oil drilling application and how to define the coordinate transformation to place the drilling model in the general 2×2 framework is in Chapter 7 and then the drilling case with the kick is simulated in Chapter 8. The final part, Part IV, is devoted to conclusions and ideas for further work, and consists of Chapter 9 only. After the main body of the thesis one finds the appendices. In Appendix A the various possible coefficient assignments resulting from transforming 2×2 systems into the $2+2$ system framework is listed, whilst Appendix B contains additional material that is relevant to the thesis but did not find its place in the dissertation proper. The folder structure of the `MATLAB` code used to generate the simulations shown in the thesis that was handed in together with this report is in Appendix C, whereas Appendix D contains a conference paper written based on results from this thesis. The Bibliography, which lists the references used, can be found at the end.

Chapter 2

PDE Boundary State Estimation

2.1 Introduction to PDEs

A *partial differential equation*, commonly referred to by the abbreviation *PDE*, is any equation defined over multiple underlying independent variables which expresses the relationship between the value of an unknown function, its partial derivatives of arbitrary order with respect to some or all of the underlying variables, and possibly also the underlying variables themselves. PDEs are natural artifacts from calculus and have been extensively studied due to their ubiquity in modelling various processes and phenomena.

The order of a PDE is defined as the order of highest-order derivative featured in the relationship(Borthwick (2016)). In equation form, a general PDE for a function $u(x_1, \ldots, x_n)$ over n underlying variables of order 2 can be expressed as

$$f(x_1, x_2, \ldots, x_n, u, u_{x_1}, u_{x_2}, \ldots, u_{x_n}, u_{x_1x_1}, u_{x_1x_2}, \ldots, u_{x_nx_n}) = 0, \tag{2.1}$$

where f is some arbitrary function defining the relationship. For linear a linear function, f, the PDE is referred to as *linear*, being the type of f defining PDEs focused on here.

PDEs can be contrasted with *ordinary differential equations*, commonly known as *ODE*s, which are equations which express the relationship between the value of an unknown function over a single variable, its derivatives with respect to the underlying variable and possibly also the underlying variable. For the function $u(x)$ a general ODE of order m can be given by

$$f(x, u(x), u'(x), u''(x), \ldots, u^{(m)}(x)) = 0. \tag{2.2}$$

All the PDEs encountered in this thesis will be defined over two underlying variables, either one dimension of space x and one of time t, or two dimensions of space (x, ξ). Two representative PDEs defined over one dimension of space and one of time, (x, t), commonly encountered in the literature(see f.ex. Kreyszig (2010))

are the *wave equation*, given by

$$u_{tt}(x,t) = \gamma^2 u_{xx}(x,t) \tag{2.3}$$

and the *heat equation*, given in 1D form as

$$u_t(x,t) = \gamma^2 u_{xx}(x,t), \tag{2.4}$$

where γ is any real number. A representative equation defined over two variables of space is the *Laplace equation* given by

$$u_{xx}(x,\xi) + u_{\xi\xi}(x,\xi) = 0. \tag{2.5}$$

Despite the nuanced difference between (2.3) and (2.4), they describe highly different phenomena, with (2.3) being a representative *hyperbolic* PDE and (2.4) being a representative *parabolic* PDE. The equation (2.5) is an example of an *elliptic* PDE. A general linear second-order PDE in two independent variables (x_1, x_2), with $u = u(x_1, x_2)$ being the unknown function, can be written as

$$au_{x_1x_1} + bu_{x_1x_2} + cu_{x_2x_2} + du_{x_1} + eu_{x_2} + fu + g = 0, \tag{2.6}$$

with a, b, c, d, e, f, g in general also being functions of (x_1, x_2). Defining the discriminant as

$$\Delta = b^2 - 4ac, \tag{2.7}$$

then all second order linear PDEs over two independent variables can be classified as(Otto (2011), Ch. 3):

- Elliptic if $\Delta < 0$.
- Parabolic if $\Delta = 0$.
- Hyperbolic if $\Delta > 0$.

In Kreyszig (2010) it is mentioned that it is in general possible for the type of the PDE to vary over the domain, where an example of this is the Tricomi equation, given by

$$x_2 u_{x_1x_1} + u_{x_2x_2} = 0. \tag{2.8}$$

Observing the definition of the discriminant Δ in (2.7), the only terms from (2.6) involved are coefficients of the second order derivatives. Consider the first-order PDE for the unknown function $u(x,t)$

$$\alpha(x,t)u_t + \beta(x,t)u_x = \gamma(x,t), \tag{2.9}$$

which is of the same form as the PDEs considered in this text. Differentiating (2.9) with respect to time t, the following is obtained:

$$\alpha_t u_t + \alpha u_{tt} + \beta_t u_x + \beta u_{xt} = \gamma_t. \tag{2.10}$$

Observe also from (2.9) that

$$u_{xt} = u_{tx} = \frac{1}{\alpha}[\gamma_x - \beta_x u_x - \beta u_{xx} - \alpha_x u_t] \tag{2.11}$$

which implies

$$\alpha u_{tt} - \frac{\beta^2}{\alpha} u_{xx} + [\alpha_t - \frac{\alpha_x \beta}{\alpha}]u_t + [\beta_t - \frac{\beta_x \beta}{\alpha}]u_x + \frac{\beta}{\alpha}\gamma_x - \gamma_t = 0. \tag{2.12}$$

Using the definition of the discriminant in (2.7), we calculate $\Delta = 4\beta^2 > 0$ for real β, and therefore (2.9) is a hyperbolic PDE (Komarla (2016)). Consider now defining multiple states $u_1(x,t)$, $u_2(x,t)$, $u_3(x,t)$, ... over a 1D spatial domain, and using equations of the form (2.9) to describe each of their dynamics, with coupling between the different states possible. This would then define a system of coupled linear hyperbolic PDEs. In Anfinsen (2018), systems of linear hyperbolic PDEs are classified into four classes, referred to as *scalar systems*, 2×2 *systems*, $n + 1$ *systems* and $n + m$ *systems*. For this thesis we are primarily interested in 2×2 and $n + m$ systems. The name 2×2 comes from the fact that this type of system can be expressed as a matrix PDE with 2×2 matrices (Anfinsen (2013)), and can in general be expressed as

$$A(x,t)u_t(x,t) + B(x,t)u_x(x,t) = C(x,t)u(x,t) + D(x,t), \tag{2.13}$$

with $u(x,t) = [u_1(x,t), u_2(x,t)]^T$ and A, B, C, D being 2×2 matrices. On the other hand, the name $n + m$ comes from the fact that systems of this type have n states propagating information in a given direction, call it the positive direction, over the spatial domain, and m states convecting information in the opposite direction from this, which resultantly is the negative direction. The exact definitions of the 2×2 and $n + m$ systems we are interested in will be stated later in the text when it is appropriate to do so.

2.2 Common PDE Solution Methods

Sometimes it is of interest to solve PDEs, that is to find the underlying unknown function over which the PDE is based, as this can provide explicit insight into the phenomenon the PDE is modelling and also allow for the computation of relevant quantities. Some PDEs allow for the solution to be expressed in terms of elementary functions, that is, they can be solved *analytically*. If an analytic solution can not be found, which is the case for most PDEs, one must resort to *numerical* methods. This section will briefly cover some common analytical and numerical techniques to obtain solutions for PDEs. Due to the large variation within PDEs, a whole host of techniques for solving them exist, see f.ex. Ch. 1 of Farlow (1993) for a more comprehensive list of general techniques as only the very most common ones are considered here.

In general, a given PDE can have an infinite number of solutions. To pin down a specific solution we must specify *boundary* and possibly also *initial* conditions. This is in contrast to an ODE which only requires the specification of initial conditions. An example of an initial condition for the PDE (2.9) is

$$u(x,0) = u_0(x), \tag{2.14}$$

where we have specified the value each point x in the spatial domain takes at the instant of time $t = 0$. For a PDE defined over the domain D, the boundary is conventionally denoted as $\partial\mathcal{D}$. Taking the 1D equation (2.9) as an example, if we define the spatial domain as being the continuous interval $D = [0,1] \ni x$, we see the boundary consists of the discrete set $\partial D = \{0,1\}$. The *interior* points are found to be $D\backslash\partial D = (0,1)$. Boundary conditions can then be specified for the left($x = 0$) and/or right($x = 1$) boundary of the domain. Consider a function $g_1(t)$ with $t \in [0,\infty)$. As presented in Griffiths et al. (2015), three common types of boundary conditions can be stated:

- For *Dirichlet* boundary conditions the value at the boundary is explicitly defined. An example is $u(1,t) = g_1(t)$.

- For *Neumann* boundary conditions the spatial derivative of the value at the boundary is defined. An example is $u_x(1,t) = g_1(t)$.

- *Robin* boundary conditions mix the Dirichlet and Neumann cases. An example is $u(1,t) + u_x(1,t) = g_1(t)$.

For the case of PDEs defined over two independent spatial variables, for example one with the domain $D = [0,1] \times [0,1] \ni (x,\xi)$, the boundary ∂D will in general not consist of discrete points as in the case of the 1D spatial domain but instead the curve or line segments surrounding the domain. For higher dimensions this generalizes to surfaces and then hypersurfaces.

When boundary and/or initial conditions have been specified, combined with the PDE of interest we have a *Boundary Value Problem* and/or an *Initial & Boundary Value Problem*, respectively. An important concept when solving PDEs is that of *well-posedness*. A PDE together with its auxilliary conditions is according to Strauss (1992) well-posed if the following three conditions are met :

- *Existence*: At least one solution satisfying all initial and boundary conditions exists.

- *Uniqueness*: Maximum one solution exists.

- *Stability*: The solution depends continuously on the initial and boundary conditions.

A classical way of proving well-posedness of PDEs is to transform them into integral equations, and then applying the *Method of Successive Approximations* to solve the resulting integral equation(see f.ex. Whitham (2011)).

2.2.1 Analytical Solution Methods

Given that we have a well-posed PDE, implying that we have a problem which allows a unique, "well behaved" solution, we want to have a way of finding that solution. We consider here briefly two important analytical methods, namely *Separation of Variables*, and the *Method of Characteristics*.

2.2.1.1 Separation of Variables

The seperation of variables method, described in detail in Kreyszig (2010), starts by assuming the solution can be expressed in the form

$$u(x,t) = F(x)G(t). \tag{2.15}$$

Hence it only works for PDEs where this assumption is true. It will briefly be demonstrated on the heat equation (2.4) defined over the spatial domain $[0,1] \ni x$ and evolving for time $t \in [0,\infty)$. Assume the boundary conditions

$$u(0,t) = 0 \tag{2.16a}$$
$$u(1,t) = 0 \tag{2.16b}$$

and initial condition

$$u(x,0) = u_0(x). \tag{2.17}$$

Plugging (2.15) into (2.4), and rearranging we find

$$\frac{\dot{G}(t)}{G(t)} = c^2 \frac{F''(x)}{F(x)}. \tag{2.18}$$

This equation must be equal to a constant, say $-\phi^2$, where $\phi \in \mathbb{R}$, since the two sides depend on different independent variables. It has now been reduced to two ODEs and these have respective solutions

$$G(t) = G_0 e^{-\phi^2 t}, \tag{2.19a}$$
$$F(x) = A\sin(\frac{1}{c}\phi x) + B\cos(\frac{1}{c}\phi x), \tag{2.19b}$$

where $G_0 = G(0)$ is the initial condition of the ODE $\dot{G} = -\phi^2 G$. Applying the boundary conditions we calculate $B = 0$ and $\phi = \sqrt{n^2c^2\pi^2}, n \in \{0,1,2,\dots\}$. Combining the solutions according to (2.15) we obtain the solution

$$u_n(x,t) = G_0 A_n \sin(n\pi x) e^{-n^2c^2\pi^2 t} \tag{2.20}$$

where the subscript n reflects the fact that the solution depends on the non-negative integer n, which is arbitrary, implying there are an infinite number of possible solutions (2.20). Due to the system being linear the *superposition principle*, telling us that the linear combination of multiple solutions is also a solution, can be applied. Using this and denoting $G_0 A_n = C_n$ we find

$$u(x,t) = \sum_{n=1}^{\infty} C_n \sin(n\pi x) e^{-n^2 c^2 \pi^2 t}. \tag{2.21}$$

Finally applying the initial condition, $u_0(x)$ can be identified as being represented by a Fourier sine series(Kreyszig (2010)), allowing us to identify C_n by the Fourier sine coefficients $C_n = 2\int_0^1 u_0(x)\sin(n\pi x)dx$.

2.2.1.2 Method of Characteristics

The method of characteristics bases itself on expressing curves in the PDE domain along which the solution evolves, parametrized by some external artificial parameter. The PDE reduces to ODEs along these *characteristic* curves, and the solution can subsequently be found by integrating along the curves with respect to the parametrization variable. For a more in depth treatment of this method see f.ex. Griffiths et al. (2015) or Myint-U and Debnath (2007). We will briefly demonstrate the essence of the method on the rudimentary example of finding the solution $u(x,t)$ to an advection equation, given by

$$u_t + \epsilon u_x = 0, \tag{2.22}$$

where ϵ is a constant for simplicity. We assume the equation is defined for $x, t \geq 0$ and that the equation has boundary condition and initial conditions

$$u(0,t) = 1 \tag{2.23a}$$
$$u(x,0) = u_0(x) \tag{2.23b}$$

Let $x = x(s)$ and $t = t(s)$, yielding $u = u(x(s), t(s))$. We then have

$$\frac{du}{ds}(x(s),t(s)) = \frac{dt}{ds}\frac{\partial u}{\partial t} + \frac{dx}{ds}\frac{\partial u}{\partial x}. \tag{2.24}$$

The PDE (2.22) has essentially been reduced to the ODE $u'(s) = 0$ along the characteristics if we choose

$$\frac{dt}{ds} = 1, \tag{2.25a}$$
$$\frac{dx}{ds} = \epsilon, \tag{2.25b}$$

and from these we can find the characteristic equation $\frac{dt}{1} = \frac{dx}{\epsilon}$. Both sides of this equation are equal to the infinitesimal ds, and integrating relative this parametrization variable we obtain $t = t_0 + s$, and letting $t_0 = 0$, we find $x(t) = x_0 + \epsilon t$, where $x_0 \geq 0$ is some arbitrary initial point along the positive x axis we use as the starting point for the characteristic line. Using the initial condition we can now express the solution as

$$u(x,t) = u_0(x - \epsilon t). \tag{2.26}$$

Applying the boundary condition, it is then possible to predict that at the point $x_1 \geq 0$, $u(x_1, t) = 1$ for all time $t \geq \frac{x_1}{\epsilon}$.

2.2.2 Numerical Solution Methods

For most PDEs the solution can not be found exactly, and in these cases we must resort to solving the PDEs numerically. We will briefly describe two common numerical methods here, namely the *Finite Element* method and the *Finite Difference* method. Unlike analytical solution methods, which yield *exact* solutions to the PDEs, numerical methods only produce *approximate* solutions, and therefore could have stability issues if incorrect grid or step sizes are chosen.

2.2.2.1 Finite Element Method

The term finite element methods(FEM) refers in general to numerical methods for solving boundary value problems based on dividing the grid into smaller segments, termed as *finite elements*, finding the solution over each element, and then finally combining the solutions together simultaneously over the entire domain to make it satisfy the boundary conditions. For a more in depth treatment of FEM see f.ex. Chapra and Canale (1998). We will briefly illustrate the principle here on a 1D analogue of the Poisson equation, given by

$$u_{xx}(x) = f(x). \tag{2.27}$$

The FEM considered here is known as the *Galerkin method*(Hutton and Wu (2004)). Despite (2.27) only being an ODE, the principle is the same for PDEs albeit the calculations become more complicated to set up. Often for PDE problems where one of the independent variables is time, FEM can be combined with the *Method of Lines*, as described in Schiesser (2012), to make the solvers less computationally expensive.

Assume (2.27) is defined for $x \in [0, 1]$, and has boundary conditions $u_x(0) = u_l$ and $u_x(1) = u_r$. We split the domain into N segments, known as *elements*, each of size $\Delta_x = \frac{1}{N}$, by defining the sequence of equidistant points $0 < x_1 < \cdots < x_{N-1} < 1$(the finite element method can however also apply to variable element size).

Consider now the segment defined for $x_1 < x < x_2$. The next step is to define basis functions on which the approximate solution will be expressed. Using the linear basis functions $N_1(x) = 2 - \frac{x}{\Delta_x}$ and $N_2(x) = -1 + \frac{x}{\Delta_x}$(these are constructed so that $N_1(x_1) = N_2(x_2) = 1$ and $N_1(x_2) = N_2(x_1) = 0$), the solution is approximated over the element by

$$u(x) \approx u_1 N_1(x) + u_2 N_2(x), \tag{2.28}$$

where u_1 and u_2 are to be solved for. The order of the basis functions determines the method order and solution accuracy, with higher order basis functions yielding more accurate solutions but requiring more calculations. Integrating (2.27) multiplied by the basis functions $N_i(x)$ for $i = 1, 2$ over the elements and integrating by parts,

obtain

$$\int_{x_1}^{x_2} u_{xx} N_i(x) dx = -\int_{x_1}^{x_2} f(x) N_i(x) dx \tag{2.29a}$$

$$\Rightarrow \frac{1}{x_2 - x_1} \begin{bmatrix} 1 & -1 \\ -1 & 1 \end{bmatrix} \begin{bmatrix} u_1 \\ u_2 \end{bmatrix} = \begin{bmatrix} -u_x(x_1) \\ u_x(x_2) \end{bmatrix} + \begin{bmatrix} \int_{x_1}^{x_2} f(x) N_1(x) dx \\ \int_{x_1}^{x_2} f(x) N_2(x) dx \end{bmatrix}, \tag{2.29b}$$

which is a linear system that can be solved numerically. The corresponding equations are found for all elements, and together with the boundary conditions the approximate solution over all the elements can be solved simultaneously. Finally the solution over the entire domain can be pieced together from the individual solutions.

2.2.2.2 Finite Difference Method

The finite difference method(FDM) is one of the simplest numerical methods for PDEs, and it is based on a functions *Taylor expansion*. Consider perturbing the function $u(x,t)$ slightly a distance Δ_x along the x axis. The Taylor expansion then becomes

$$u(x + \Delta x, t) = u(x,t) + \sum_{n=1}^{\infty} \frac{(\Delta_x)^n}{n!} \frac{\partial^n u}{\partial x^n} \tag{2.30}$$

Using (2.30) and dropping all terms involving second order derivatives or higher, the following approximation can be found

$$u_x(x,t) \approx \frac{u(x + \Delta x) - u(x)}{\Delta x} \tag{2.31}$$

Consider the heat equation (2.4) defined for $x \in [0,1]$ and time $t \geq 0$. Let $c = 1$ and the boundary conditions be $u(0,t) = u_l(t)$ and $u(1,t) = u_r(t)$ whilst the initial conditions $u(x,0) = u_0(x)$. Consider dividing the domain into N segments as was done for the FEM example above, each segment being of length Δx. Let also time be discretized into steps of length Δt. We let the index $i \in \{1, \dots, N-1\}$ denote points along the x-axis defining the different segment boundaries, and the index $j \in \{1, 2, \dots\}$ be an index for the time steps. The notation $u(x,t) = u_i^j$ will be used where x is the spatial position corresponding with the index i and t is the time corresponding to the index j. By applying the forward difference scheme (2.31) once to the left hand side and twice to the right hand side of (2.4) the following expression can be obtained as

$$u_i^{j+1} \approx u_i^j + \frac{\Delta t}{(\Delta x)^2}(u_{i+1}^j - 2u_i^j + u_{i-1}^j), \tag{2.32}$$

which gives an explicit expression for the value of u at index i for the next time step. Combining with initial and boundary conditions, all the interior points in

the domain can be solved for with this expression simultaneously by setting up a linear system. Alternatively the solution can be found one time step at a time, in a so-called *time marching* solution.

The forward difference scheme presented here is only one of many FDM schemes which exist, see for example Wendt (2008) or Johnson (2016) for a more in depth treatment of the FDM. The text Strikwerda (2004) also provides an in depth treatment of stability analyis of FDM.

2.3 Infinite Dimensional Backstepping

Before explaining the basic theory behind deriving observers for boundary state estimation of PDEs, the underlying technique used will be briefly refreshed. This technique is known as *infinite dimensional backstepping*, sometimes also referred to as *continuum backstepping*, and is inspired from the original ODE backstepping method. We will first introduce ODE backstepping and subsequently show how it can be generalized to PDE backstepping. The book Krstic and Smyshlyaev (2008b) presents a similar discussion.

2.3.1 ODE Backstepping

Backstepping was a technique originally devised for designing control laws, and therefore the simple examples presented here to illustrate the technique will be based on designing control laws. For a more in depth treatment of the method, see for example Khalil (2002). In the next section it will be shown how the technique can be modified for observation problems. Consider the system with state $v(t) = [v_1(t), v_2(t), v_3(t)]^T$ and control input $U(t)$ given by

$$\dot{v}_1(t) = v_2(t) + 3v_1^3(t) \tag{2.33a}$$
$$\dot{v}_2(t) = -4v_3(t) + v_2(t) \tag{2.33b}$$
$$\dot{v}_3(t) = U(t) \tag{2.33c}$$

We wish to design the control input $U(t)$ to stabilize the states $v(t)$ of (2.33) to 0. Consider now the following target system

$$\dot{\beta}_1(t) = -5\beta_1(t) + \beta_2(t) \tag{2.34a}$$
$$\dot{\beta}_2(t) = -\beta_1(t) - 5\beta_2(t) + \beta_3(t) \tag{2.34b}$$
$$\dot{\beta}_3(t) = -\beta_2(t) - 5\beta_3(t) \tag{2.34c}$$

To see that this system is stable, put it in the form $\dot{\beta} = A\beta$, with

$$A = \begin{bmatrix} -5 & 1 & 0 \\ -1 & -5 & 1 \\ 0 & -1 & -5 \end{bmatrix} \tag{2.35}$$

and $\beta = [\beta_1, \beta_2, \beta_3]^T$. According to the *Lyapunov theorem*, as given in Theorem 5.5 of Chen (1998), the system $\dot{\beta} = A\beta$ is asymptotically stable if there exists a positive definite matrix M so that

$$A^T M + MA = -N \tag{2.36}$$

for all positive definite symmetric matrices N. By computing the sum $A^T + A$ we identify that $M = I_2$ and $N = 10I_2$, with I_2 denoting the 2×2 identity matrix, satisfy the equation. Hence (2.34) is asymptotically stable.

If a structure preserving invertible and differentiable mapping known as a *diffeomorphism* between (2.34) and (2.33) can be found, a control law can be discovered to make (2.33) behave as (2.34). In other words this would imply we have designed an asymptotically stabilizing control law.

The following transformation is recursively built up by considering the target system dynamics:

$$\beta_1 = v_1 \tag{2.37a}$$

$$\beta_2 = v_2 + 3v_1^3 + 5v_1 \tag{2.37b}$$

$$\beta_3 = v_3 - 5v_3 + v_2 + 9v_1^2(v_2 + 3v_1^3) + 5(v_2 + 3v_1^3) + v_1 + 5(v_2 + 3v_1^3 + 5v_1) \tag{2.37c}$$

The transformation (2.37) can trivially be seen to be invertible due to its cascade structure, and therefore a one-to-one correspondence between the target and original system can be found. Differentiating the equation for β_3 in (2.37) and setting it equal to the desired $\dot{\beta}_3$ in (2.34), the necessary control law $U(t) = U(v_1(t), v_2(t), v_3(t))$ can be found to be

$$\begin{aligned} U = \frac{1}{4}[&135v_1 + 78v_1^3 + 26v_2 + 5(v_2 - 4v_3 + (9v_1^2 + 5)(v_2 + 3v_1^3)) \\ &+(135v_1^4 + 90v_1^2 + 18v_2 + 26)(v_2 + 3v_1^3) + (9v_1^2 + 11)(v_2 - 4v_3)] \end{aligned} \tag{2.38}$$

2.3.2 The Infinite Dimensional Analogue

One can view the transformation (2.37) as being a transformation of the form $\beta = v - K(v)$, where K is some nonlinear "lower triangular" transformation with the structure $K = [K_1(v_1), K_2(v_1, v_2), K_3(v_1, v_2, v_3)]^T$. If we imagine that the number of states in v goes to infinity so that they fill all real numbers between 0 and 1, each individual scalar state in v can be specified through a number $x \in [0, 1]$. In other words v can be expressed as $v(x, t)$, and $U(t)$ can be seen as a boundary control input. A linear analogue to the transformation (2.37) could then be

$$\beta(x, t) = v(x, t) - \int_0^x k(x, \xi)v(\xi, t)d\xi, \tag{2.39}$$

where for a given $x_0 \in (0, 1)$, only states $v(x, t)$ for $0 \leq x \leq x_0$ will be featured in the transformation. $k(x, \xi)$ is referred to as the transformation *kernel*, and

acts as the analogue to the "lower triangular" transformation K used in the ODE backstepping case. The equation (2.39) is a linear *Volterra* integral equation of the second kind(Tricomi (1985)). Another type of integral equation that will be of interest in this thesis is the *Fredholm* integral equation of the second kind, defined in general as

$$w(x,t) = \gamma(x,t) + \lambda \int_a^b k(x,\xi)w(\xi,t)d\xi \tag{2.40}$$

where λ is some constant and the integration limits a and b are also both constant. The constant integration limits is the biggest difference between Fredholm and Volterra integral equations, where the latter has one variable integration limit.

Fredholm integral transformations can also be used as a tool within infinite dimensional backstepping controller and observer design. However, in contrast to Volterra integral transformations, Fredholm integral transformations are not trivially invertible and invertibility of a given transformation must hence be proven before it can be used.

The steps involved in the infinite dimensional version of backstepping are nearly analogous to the steps required for the ODE version. One must find a target system and prove its stability somehow, either by solving it explicitly or with a *Lyapunov* function. In the same way as the ODE backstepping transformation was differentiated, the integral transformation in the PDE case must be differentiated with respect to both space and time and combined with the target system dynamics. When comparing this to the original system dynamics, PDEs for the kernel $k(x,\xi)$ are found. The well-posedness of these kernel equations must be shown, a common method being to use the method of successive approximations after having transformed them into integral equations, and after this their solution must be found somehow. For cases when one is using backstepping to design boundary control laws, the control law typically features in one of the boundary conditions of the system. If we have some PDE with the distributed state $v(x,t)$ for $x \in [0,1]$ and $t \geq 0$, if the control input is at the right boundary a possible boundary condition could be $v(1,t) = U(t)$. Then, assuming that the target system has right boundary condition $\beta(1,t) = 0$, if the Volterra transformation (2.39) is used for designing the control law, after the kernel $k(x,\xi)$ has been solved for, the control law can be found by setting $x = 1$ into the transformation and then obtaining

$$U(t) = v(1,t) = \int_0^1 k(1,\xi)v(\xi,t)d\xi. \tag{2.41}$$

PDE controller design was the original goal when continuum backstepping was developed. Next we will discuss observers and how infinite dimensional backstepping can be applied to PDE observer design.

2.4 PDE Observer Structure and Design

2.4.1 Luenberger Observer Structure

The most common observer used for deterministic linear systems is the *Luenberger* observer, which bases itself on replicating the system dynamics but adding an extra term to account for errors in the estimate. For nondeterministic cases, for instance if the system is infected with an unknown noisy disturbance, it is common to instead use *Bayesian* filters such as *Kalman* or *particle* filters(see f.ex. Chen et al. (2003)), but these are outside the scope of this thesis so no more space will be devoted to them. Consider the following linear time-invariant ODE system

$$\dot{v}(t) = Av(t) + BU(t) \tag{2.42a}$$
$$y(t) = Cv(t) \tag{2.42b}$$

for a system with state $v = [v_1, \ldots, v_n]^T \in \mathbb{R}^n$, control inputs $U = [U_1, \ldots, U_m]^T \in \mathbb{R}^m$ and measurements $y = [y_1, \ldots, y_p]^T \in \mathbb{R}^p$, and A, B and C being constant matrices of appropriate dimensions. Often the control input U and measurement y are known quantities, but we need to know the states v which we can not measure directly. To solve this problem we try to come up with some algorithm for producing state estimates $\hat{v}(t)$. One naive approach is to simply replicate the model as $\dot{\hat{v}}(t) = A\hat{v}(t) + BU(t)$. However, a problem with this algorithm is that incorrect initial conditions or model errors will cause the estimates to be different from the real values with a high degree of probability, and being open-loop it has no way of correcting itself. Additionally, the measurement y has not been utilized at all. Consider therefore instead injecting the measurement into the dynamic model in the state estimation algorithm through comparing it with the value the measurement would have had if the system had the states predicted by the observer. The state estimation algorithm then looks like

$$\dot{\hat{v}}(t) = A\hat{v}(t) + BU(t) + P(y(t) - C\hat{v}(t)), \tag{2.43}$$

where P is referred to as the *observer gain* and is a matrix of appropriate dimension determining how much the measurement estimation error should be weighted in the estimation dynamics. Defining the error $\tilde{v} = v - \hat{v}$, the error in the ODE,

$$\dot{\tilde{v}}(t) = (A - PC)v(t) \tag{2.44}$$

is easily be found from (2.42) and (2.43). From (2.44) we see that if P is chosen so that $(A - PC)$ is Hurwitz(has eignevalues with negative real components), $\tilde{v}$ will converge to 0 and the output injection term $P(y(t) - C\hat{v}(t))$ in (2.43) has the effect of driving the state estimates towards the actual state values. The algorithm (2.43) is the Luenberger observer, and is described in any standard text on linear systems such as Chen (1998).

2.4.2 Generalizing to PDE Observers

Consider instead now a variant of the heat equation where λ is some constant

$$v_t(x,t) - v_{xx}(x,t) = \lambda v(x,t) \tag{2.45a}$$
$$y(t) = v(1,t) \tag{2.45b}$$

evolving for $t \geq 0$ on $x \in [0,1]$ and with the right boundary measurement $y(t)$. As with the analogy in the previous section, the state $v = v(x,t)$ can be seen as an infinite dimensional version of the state vector $v = [v_1, v_2, \dots]$ where each state corresponds to a real number x in the interval $[0,1]$. The measurement $y(t) = v(1,t)$ is analogous to the matrix C in (2.42) being of the form $C = [0, \dots, 0, 1]$.

We wish to design an observer with the Luenberger structure from (2.43) for creating estimates $\hat{v}(x,t)$ for the states of (2.45). The rows of $P = [P_1^T, \dots, P_n^T]^T$ in (2.43) correspond to the states in the state vector $v(t) = [v_1(t), \dots, v_n(t)]^T$, and to keep with this analogy, a corresponding observer gain for the distributed states $v(x,t)$ would be $P = P(x)$. In the case of (2.45) both the measurement and states are scalars so the observer gain is also a scalar function of x. We can now set up a Luenberger type observer for (2.45) as

$$\hat{v}_t(x,t) - \hat{v}_{xx}(x,t) = \lambda \hat{v}(x,t) + P(x)[y(t) - \hat{v}(1,t)]. \tag{2.46}$$

The next step is to find out what the function $P(x)$ needs to be for convergence of the estimates $\hat{v}$ to the actual states v to be guaranteed. We will now show how the infinite dimensional backstepping technique briefly covered in the previous section can be used to discover this function.

The state estimation error can be calculated as $\tilde{v}(x,t) = v(x,t) - \hat{v}(x,t)$. Considering that we want $\hat{v}(x,t) \to v(x,t)$, an equivalent objective to producing correct state estimates is to drive the error system with states $\tilde{v}$ towards 0, as we did with (2.44) for the ODE case. Subtracting (2.46) from the first line of (2.45), the error system dynamics can easily be seen to be

$$\tilde{v}_t(x,t) - \tilde{v}_{xx}(x,t) = \lambda \tilde{v}(x,t) - P(x)\tilde{v}(1,t). \tag{2.47}$$

This is now the system infinite dimensional backstepping will be applied to. As in the case for controller design, some target error system which vanishes must be set up, and an invertible integral transformation(typically Volterra integral equation of the second kind) is used to transform the original error system to the target error system. Partially differentiating this transformation with respect to relevant variables and combining with target and original error system dynamics, in a similar way to the controller design case, the expression for the observer gain function $P(x)$ can be discovered together with the kernel equation which must be solved before this expression can be applied.

2.4.3 Hyperbolic PDE Observer Convergence Time

For the PDE systems of interest in this thesis, namely systems of 2×2 and $n + m$(particularly for the case $n = m = 2$) first-order linear hyperbolic PDEs, observers and controllers that estimate system states correctly and drive the states to zero, respectively, in finite time can be devised. Hence the issue of convergence

time in designing these observers and controllers comes up. 2×2 systems have one equation, conventionally with state denoted as $v(x,t)$, representing information propagating from what is conventionally referred to as the right boundary to the left boundary with negative velocity $\mu(x)$, whereas the other equation represents a distributed state $u(x,t)$ convecting information from the left boundary to the right boundary with positive velocity $\lambda(x)$. For the $n+m$ case, which is a generalization of the 2×2 case(since the 2×2 case corresponds with $n = m = 1$), there are n equations with states $u_i(x,t)$, where $i \in \{1, \ldots, n\}$, representing information which convects in the rightward direction with respective velocities $\lambda_i(x)$, and m equations with states $v_j(x,t)$ $j \in \{1, \ldots, m\}$, representing information travelling in the leftward direction with relative velocities $\mu_j(x)$. Thus, the shortest amount of time it takes for information to travel from one boundary to the other for the respective states, referred to in Anfinsen (2018) as *transport delays*, can be calculated respectively as

$$t_{u,i} = \int_0^1 \frac{dx}{\lambda_i(x)} \tag{2.48a}$$

$$t_{v,j} = \int_0^1 \frac{dx}{\mu_j(x)} \tag{2.48b}$$

If a single boundary measurement is used, the smallest possible convergence time of an observer using this information will according to Woittennek et al. (2009) be

$$t_{1,min} = \max_{i \in \{1,\ldots,n\}} t_{u,i} + \max_{j \in \{1,\ldots,m\}} t_{v,j}. \tag{2.49}$$

This is the sum of propagation time of the slowest characteristic in each direction. However if both boundary measurements are used in the observer design, the convergence time can according to Li and Rao (2010) be brought down to

$$t_{2,min} = \max_{i \in \{1,\ldots,n\}, j \in \{1,\ldots,m\}} \{t_{u,i}, t_{v,j}\}. \tag{2.50}$$

In other words the convergence time in the case of measuring both boundaries is limited by *only* the propagation time of the slowest characteristic in the entire system. Clearly $t_{2,min} < t_{1,min}$ in general.

An observer which reaches its objective of producing correct state estimates within the time limit given by (2.49) or (2.50) for a single boundary or both boundary measurements, respectively, will be referred to as a *minimum time* observer. An observer which uses more time than the theoretical minimum for a given number of available measurements to achieve its objective will be referred to as a *non-minimum time* observer.

The next section of this thesis is devoted to deriving two minimum time observers for hyperbolic PDE systems. In the next chapter, Chapter 3, a minimum time observer for a $2+2$ system relying on a single boundary measurement which converges in time $t_{1,min}$ expressed by the relevant value of (2.49) for that specific

system is derived. Then in the subsequent chapter, Chapter 4, we derive a minimum time observer converging in time $t_{2,min}$, given by the relevant value of (2.50) for that system.

Part II

Observer Design

Chapter 3

Minimum Time $2+2$ Collocated Observer Design

3.1 Problem Statement

Consider the following first-order $2+2$ linear hyperbolic PDE system defined for $x \in [0,1]$ and $t \in [0,\infty)$ with states $\bar{u}(x,t) = [u_1(x,t), u_2(x,t)]^T$, $\bar{v}(x,t) = [v_1(x,t), v_2(x,t)]^T$ and dynamics governed by[1]

$$\bar{u}_t(x,t) + \Lambda^+(x)\bar{u}_x(x,t) = \Sigma^{+-}(x)\bar{v}(x,t), \tag{3.1a}$$
$$\bar{v}_t(x,t) - \Lambda^-(x)\bar{v}_x(x,t) = \Sigma^{-+}(x)\bar{u}(x,t) \tag{3.1b}$$

along with boundary conditions

$$\bar{u}(0,t) = Q_0\bar{v}(0,t), \tag{3.2a}$$
$$\bar{v}(1,t) = R_1\bar{u}(1,t) + U(t). \tag{3.2b}$$

The initial conditions, where we denote $\bar{u}_0(x) = [u_{1,0}(x), u_{2,0}(x)]^T$, $\bar{v}_0(x) = [v_{1,0}(x), v_{2,0}(x)]^T$, are given by

$$\bar{u}(x,0) = \bar{u}_0(x), \tag{3.3a}$$
$$\bar{v}(x,0) = \bar{v}_0(x). \tag{3.3b}$$

[1]Note that this $2+2$ system is not fully general, due to the commonly included terms $\Sigma^{++}(x)\bar{u}(x,t)$ and $\Sigma^{--}(x)\bar{v}(x,t)$ in the right hand side of respectively the $\bar{u}$ and $\bar{v}$ dynamics being absent. The relevance of this system will however become apparent in the next chapter of this section, Chapter 4, where a minimum time convergent *bilateral* observer, by which an observer utilizing measurements from both left and right boundary is implied, is derived or a 2×2 system based on the results from the current chapter.

We assume that $u_{1,0}(x), u_{2,0}(x), v_{1,0}(x), v_{2,0}(x) \in L^2([0,1])$. Our system is defined over the 1D continuous spatial domain $[0,1]$, and the position $x = 0$ is referred to as the *left boundary* whereas $x = 1$ is the *right boundary*. Assume that we have access to measurements at the right boundary and define therefore the measurement variable $y(t) = [\bar{y}_1(t), \bar{y}_2(t)]^T$ collocated with actuation, given as

$$y(t) = \begin{bmatrix} \bar{y}_1(t) \\ \bar{y}_2(t) \end{bmatrix} = \begin{bmatrix} u_1(1,t) \\ u_2(1,t) \end{bmatrix}. \tag{3.4}$$

The relevant matrices for this system are defined as

$$\Lambda^+(x) = \begin{bmatrix} \lambda_1(x) & 0 \\ 0 & \lambda_2(x) \end{bmatrix}, \qquad \Lambda^-(x) = \begin{bmatrix} \mu_1(x) & 0 \\ 0 & \mu_2(x) \end{bmatrix}, \tag{3.5a}$$

$$\Sigma^{+-}(x) = \begin{bmatrix} \sigma_{11}^{+-}(x) & \sigma_{12}^{+-}(x) \\ \sigma_{21}^{+-}(x) & \sigma_{22}^{+-}(x) \end{bmatrix}, \qquad \Sigma^{-+}(x) = \begin{bmatrix} \sigma_{11}^{-+}(x) & \sigma_{12}^{-+}(x) \\ \sigma_{21}^{-+}(x) & \sigma_{22}^{-+}(x) \end{bmatrix}, \tag{3.5b}$$

$$Q_0 = \begin{bmatrix} Q_{11} & Q_{12} \\ Q_{21} & Q_{22} \end{bmatrix}, \qquad R_1 = \begin{bmatrix} R_{11} & R_{12} \\ R_{21} & R_{22} \end{bmatrix}, \tag{3.5c}$$

$$U(t) = \begin{bmatrix} \bar{U}_1(t) \\ \bar{U}_2(t) \end{bmatrix}, \qquad y(t) = \begin{bmatrix} \bar{y}_1(t) \\ \bar{y}_2(t) \end{bmatrix}. \tag{3.5d}$$

The transport speeds $\lambda_1(x), \lambda_2(x), \mu_1(x), \mu_2(x) \in C^1([0,1])$, and are subject to the restriction[2]

$$-\mu_1(x) \leq -\mu_2(x) < 0 < \lambda_1(x) \leq \lambda_2(x), \tag{3.6}$$

whilst $\forall i, j, k, l \in \{1,2\}$ the coupling coefficients $\sigma_{ij}^{+-}(x), \sigma_{kl}^{-+}(x) \in C^0([0,1])$. In addition to this, $\forall i, j, k, l \in \{1,2\}$ the reflection coefficients q_{ij}, $\rho_{kl} \in \mathbb{R}$ are constants. The terms $\bar{U}_1(t), \bar{U}_2(t)$ are boundary control inputs, but their design is not the focus of this thesis but are placed in the model above for completeness.

The objective of this chapter is to design a minimum time convergent *collocated* observer, by which we mean an observer using measurements from the same side in which actuation signals $U(t)$ would potentially enter(in this case the right boundary), for the special case of $2+2$ systems given by (3.1) with boundary conditions (3.2) and initial conditions (3.3). Only utilizing measurements from one side of the domain, the criterion for our observer to be minimum time is that its estimates $\check{u}(t) = [\check{u}_1(t), \check{u}_2(t)]^T$ and $\check{v}(t) = [\check{v}_1(t), \check{v}_2(t)]^T$ converge to the correct values of the $2+2$ system states, $\bar{u}(t)$ and $\bar{v}(t)$ respectively, within in time $t_{1,min}$ given by (2.49). This convergence time can for our specific $2+2$ system be expressed using (2.49) as

[2]These restrictions on the transport speeds are present to ensure the observer kernel PDEs, which will be introduced at a later point in this chapter, have well-posed solutions. One can refer to Hu et al. (2016) for more details. For the special class of $2+2$ systems (3.1)–(3.2), the relative restriction between μ_1 and μ_2 is strictly not necessary, as long as $\mu_1, \mu_2 > 0$ is maintained, but the restriction is kept here for simplicity.

$$t_{1,min} = \int_0^1 \frac{dx}{\lambda_1(x)} + \int_0^1 \frac{dx}{\mu_2(x)}. \tag{3.7}$$

Chapter 3 is organized as follows. The problem statement has been defined here in Section 3.1. In Section 3.2 an already existing non-minimum time collocated observer for general first-order $n + m$ linear hyperbolic PDE systems, which was derived in Anfinsen and Aamo (2017b), is reviewed. This non-minimum time observer is then applied in Section 3.3 to the $2 + 2$ system we are interested in, and as a first step towards this chapter's main result an invertible Fredholm transformation is defined between the old error target system with boundary terms preventing minimum time convergence and a new minimum time convergent error target system. "Observer gains" to make the old non-minimum time convergent target error system vanish in minimum time are then succesfully derived. To complete the observer derivation, in Section 3.4 a Volterra transformation is defined between the $2 + 2$ observer error system and the old target error system with its new "observer gains", allowing the calculation of the necessary observer gains for a minimum time collocated observer for (3.1)–(3.5).

3.2 Non-Minimum Time Result for General $n+m$ System

In Anfinsen and Aamo (2017b) a non-minimum time collocated observer for a general $n + m$ linear hyperbolic system is given, a result which will be reproduced here. The $n + m$ systems with states $\bar{u}(x,t) = [u_1(x,t), \dots, u_n(x,t)]^T$, $\bar{v}(x,t) = [v_1(x,t), \dots, v_m(x,t)]^T$ as considered in f.ex. Hu et al. (2016), Auriol and Di Meglio (2016) and Anfinsen and Aamo (2017b), of which (3.1)–(3.5) is a special case, are reproduced with spatially varying coefficients as

$$\bar{u}_t(x,t) + \Lambda^+(x)\bar{u}_x(x,t) = \Sigma^{++}(x)\bar{u}(x,t) + \Sigma^{+-}(x)\bar{v}(x,t), \tag{3.8a}$$
$$\bar{v}_t(x,t) - \Lambda^-(x)\bar{v}_x(x,t) = \Sigma^{-+}(x)\bar{u}(x,t) + \Sigma^{--}(x)\bar{v}(x,t) \tag{3.8b}$$

together with boundary conditions

$$\bar{u}(0,t) = Q_0\bar{v}(0,t), \tag{3.9a}$$
$$\bar{v}(1,t) = R_1\bar{u}(1,t) + U(t). \tag{3.9b}$$

By denoting $\bar{u}_0(x) = [u_{1,0}(x), \dots, u_{n,0}(x)]^T$ and $\bar{v}_0(x) = [v_{1,0}(x), \dots, v_{m,0}(x)]^T$, we define the initial conditions as

$$\bar{u}(x,0) = \bar{u}_0(x), \tag{3.10a}$$
$$\bar{v}(x,0) = \bar{v}_0(x), \tag{3.10b}$$

where $\forall i \in \{1,\dots,n\}, j \in \{1,\dots,m\}$ it is assumed true that $u_{i,0}(x), v_{j,0}(x) \in L_2([0,1])$, implying square integrable initial conditions. Similarly to the $2+2$ system (3.1)–(3.5), the coefficients for the general $n+m$ system (3.8) with boundary conditions (3.9) are defined by the matrices

$$\Lambda^+(x) = diag\{\lambda_1(x),\dots,\lambda_n(x)\}, \quad \Lambda^-(x) = diag\{\mu_1(x),\dots,\mu_n(x)\}, \tag{3.11a}$$
$$\Sigma^{++}(x) = \{\sigma_{ij}^{++}(x)\}_{1\le i\le n, 1\le j\le n}, \quad \Sigma^{+-}(x) = \{\sigma_{ij}^{+-}(x)\}_{1\le i\le n, 1\le j\le m}, \tag{3.11b}$$
$$\Sigma^{-+}(x) = \{\sigma_{ij}^{-+}(x)\}_{1\le i\le m, 1\le j\le n}, \quad \Sigma^{--}(x) = \{\sigma_{ij}^{--}(x)\}_{1\le i\le m, 1\le j\le m}, \tag{3.11c}$$
$$Q_0 = \{Q_{ij}\}_{1\le i\le n, 1\le j\le m}, \quad R_1 = \{R_{ij}\}_{1\le i\le m, 1\le j\le n}, \tag{3.11d}$$
$$U(t) = [\bar{U}_1(t),\dots,\bar{U}_m(t)]^T, \quad y(t) = [\bar{y}_1(t),\dots,\bar{y}_n(t)]^T. \tag{3.11e}$$

Also we assume $\forall i \in \{1,\dots,n\}, j \in \{1,\dots,m\}$ that $\lambda_i(x), \mu_j(x) \in C^1[(0,1)]$. For this more general $n+m$ case where $\Sigma^{++}(x) \neq 0$ in general, the transport speeds must(see Anfinsen and Aamo (2017b)) be subject to the stronger restrictions[3]

$$-\mu_1(x) < \cdots < -\mu_m(x) < 0 < \lambda_1(x) < \cdots < \lambda_n(x). \tag{3.12}$$

The coupling coefficients are $\forall i,j,k,p \in \{1,\dots,n\}$ and $\forall l,o,q,r \in \{1,\dots,m\}$ subject to $\sigma_{ij}^{++}(x), \sigma_{kl}^{+-}(x), \sigma_{op}^{-+}(x), \sigma_{qr}^{--}(x) \in C^0([0,1])$. Note that according to Hu et al. (2015), without loss of generality it can always be assumed $\forall x \in [0,1]$ that $\sigma_{ii}^{++}(x) = \sigma_{jj}^{--}(x) = 0$, $i \in \{1,\dots,n\}$, $j \in \{1,\dots,m\}$. If this is not the case a coordinate transformation can always be found allowing this assumption(see f.ex. Coron et al. (2013) or Hu and Di Meglio (2015)). The change of variables suggested by Coron et al. (2013) takes with our notation the form

$$\bar{u}_i(x,t) = \underline{u}_i(x,t) e^{\int_0^x \frac{\sigma_{ii}^{++}(s)}{\lambda_i(s)} ds}, \tag{3.13a}$$
$$\bar{v}_j(x,t) = \underline{v}_j(x,t) e^{-\int_0^x \frac{\sigma_{jj}^{--}(s)}{\mu_j(s)} ds} \tag{3.13b}$$

where we then obtain $\forall i \in \{1,\dots,n\}, j \in \{1,\dots,m\}$ the new set of variables $\underline{u}_i(x,t)$ and $\underline{v}_j(x,t)$.

The reflection coefficients are here also assumed $\forall i,l \in \{1,\dots,n\}$ and $\forall j,k \in \{1,\dots,m\}$ to be real constants $q_{ij}, \rho_{kl} \in \mathbb{R}$. The functions $\bar{U}_i(t)$ are $\forall i \in \{1,\dots,m\}$ right boundary control inputs.

As inputs the non-minimum time collocated observer presented in Anfinsen and Aamo (2017b) relies on the right boundary measurements $y(t) = [\bar{y}_1(t),\dots,\bar{y}_n(t)]^T$,

[3] These stronger restrictions were imposed in Anfinsen and Aamo (2017b), which considered both controller and collocated observer design for the more general $n+m$ system (3.8)–(3.9), so that the controller and observer kernel PDEs there had well-posed solutions. In the observer kernel PDEs one gets the boundary condition $M_{ij}(x,1) = \frac{\sigma_{ij}^{++}}{\lambda_j - \lambda_i}, 1 \le j < i \le n$, whereas the for the controller kernel PDE one has boundary condition $L_{ij}(1,\xi) = \frac{\sigma_{ij}^{--}}{\mu_j - \mu_i}, 1 \le j < i \le n$. These boundary conditions end up not being well-defined if $\lambda_i = \lambda_j$ or $\mu_i = \mu_j$ for $i = j$.

with $y(t) = \bar{u}(1,t)$ being defined in the analogous way as in the $2+2$ case considered above. Let $\check{u}(x,t) = [\check{u}_1(x,t), \ldots, \check{u}_n(x,t)]^T$, $\check{v}(x,t) = [\check{v}_1(x,t), \ldots, \check{v}_m(x,t)]^T$ denote the estimates of the states $\bar{u}(x,t)$, $\bar{v}(x,t)$, respectively, of the $n+m$ system (3.8)–(3.11).

Now that the general $n+m$ system and its associated assumptions have been presented we can present the non-minimum time collocated observer we are interested in. The following result is presented as Theorem 9 in Anfinsen and Aamo (2017b) for the case of the transport speeds and coupling coefficients in (3.8) being constant. It has been slightly modified for the purpose of this thesis and also to take into account spatially varying transport speeds and coupling coefficients.

Theorem 3.1 (Modified from Theorem 9 in Anfinsen and Aamo (2017b))**.** *Consider the following observer for the system* (3.8)–(3.11)

$$\check{u}_t(x,t) + \Lambda^+(x)\check{u}_x(x,t) = \Sigma^{++}(x)\check{u}(x,t) + \Sigma^{+-}(x)\check{v}(x,t) + P^+(x)(y(t) - \check{u}(1,t)), \tag{3.14a}$$

$$\check{v}_t(x,t) - \Lambda^-(x)\check{v}_x(x,t) = \Sigma^{-+}(x)\check{u}(x,t) + \Sigma^{--}(x)\check{v}(x,t) + P^-(x)(y(t) - \check{u}(1,t)) \tag{3.14b}$$

with boundary conditions

$$\check{u}(0,t) = Q_0\check{v}(0,t), \tag{3.15a}$$

$$\check{v}(1,t) = R_1 y(t) + U(t) \tag{3.15b}$$

together with observer gains

$$P^+(x) = M(x,1)\Lambda^+(1), \tag{3.16a}$$

$$P^-(x) = N(x,1)\Lambda^+(1). \tag{3.16b}$$

Here $M(x,\xi) = \{M_{ij}(x,\xi)\}_{1\leq i,j\leq n}$ *and* $N(x,\xi) = \{N_{ij}(x,\xi)\}_{1\leq i\leq m, 1\leq j\leq n}$ *in* (3.16) *are solutions to the kernel PDE equations*

$$\begin{aligned}\Lambda^+(x)M_x(x,\xi) + M_\xi(x,\xi)\Lambda^+(\xi) + M(x,\xi)\Lambda^+_\xi(\xi) &= \Sigma^{++}(x)M(x,\xi) \\ &\quad + \Sigma^{+-}(x)N(x,\xi),\end{aligned} \tag{3.17a}$$

$$\begin{aligned}-\Lambda^-(x)N_x(x,\xi) + N_\xi(x,\xi)\Lambda^+(\xi) + N(x,\xi)\Lambda^+_\xi(\xi) &= \Sigma^{-+}(x)M(x,\xi) \\ &\quad + \Sigma^{--}(x)N(x,\xi)\end{aligned} \tag{3.17b}$$

with boundary conditions

$$\Lambda^+(x)M(x,x) = M(x,x)\Lambda^+(x) - \Sigma^{++}(x), \tag{3.18a}$$

$$\Lambda^-(x)N(x,x) = -N(x,x)\Lambda^+(x) + \Sigma^{-+}(x), \tag{3.18b}$$
$$Q_0 N(0,\xi) = M(0,\xi) + H(\xi), \tag{3.18c}$$
$$M_{ij}(x,1) = \frac{\sigma_{ij}^{++}(x)}{\lambda_j(x) - \lambda_i(x)}, 1 \leq j < i \leq n, \tag{3.18d}$$

and are defined over the upper triangular domain $\mathcal{T}_u = \{(x,\xi) \mid 0 \leq x \leq \xi \leq 1\}$. *Additionally* $H(x) = \{h_{ij}(x)\}_{1\leq i,j\leq n}$ *is defined as a strict lower triangular matrix with components*

$$h_{ij}(x) = \begin{cases} \sum_{k=1}^{m} Q_{ik}N_{kj}(0,x) - M_{ij}(0,x), & \text{for } 1 \leq j < i \leq n, \\ 0, & \text{otherwise.} \end{cases} \tag{3.19}$$

The estimates $\check{u}(x,t)$, $\check{v}(x,t)$ *generated by* (3.14)–(3.15) *converge to their true values* $\bar{u}(x,t)$, $\bar{v}(x,t)$, *representing the states of the system* (3.8)–(3.11), *within time* t_F, *where*

$$t_F = \int_0^1 \frac{dx}{\mu_m(x)} + \sum_{i=1}^{n} \int_0^1 \frac{dx}{\lambda_i(x)}. \tag{3.20}$$

Proof. The steps of the proof are identical to the steps followed in Anfinsen and Aamo (2017b) and are therefore omitted. □

As the $2+2$ system (3.1)–(3.5) fits into the $n+m$ framework defined by (3.8)–(3.11) as a special case, the observer presented in Theorem 3.1 can be applied to state estimation of this system, given that the observer kernel PDE (3.17)–(3.18) is well-posed. Since $\Sigma^{++}(x) = 0$ in (3.1)–(3.2), we find that $\sigma_{21}^{++}(x) = 0$. This implies that the boundary condition (3.18d) can be set to $M_{21}(x,1) = 0$ for our class of $2+2$ system, and therefore the more relaxed assumption (3.6) can be applied instead of (3.12).

Hence, applying the observer (3.14) for $n = m = 2$ will guarantee that the state estimates $\check{u}_1(x,t)$, $\check{u}_2(x,t)$, $\check{v}_1(x,t)$ and $\check{v}_2(x,t)$ all convergence to their true values within time given by (3.20), which for this case becomes $t_F = \int_0^1 \frac{dx}{\mu_2(x)} + \int_0^1 \frac{dx}{\lambda_1(x)} + \int_0^1 \frac{dx}{\lambda_2(x)} > t_{1,min}$, where $t_{1,min}$ is defined in (3.7).

To improve on this we will now derive an observer for the $2+2$ system (3.1)–(3.2) generating estimates which instead converge within time $t_{1,min} < t_F$. One of the boundary conditions in the target error system used to derive the observer given by Theorem 3.1 contained a term preventing the minimum time convergence. Next, in Section 3.3, an approach for removing this term by treating the target error system as the error system of an actual system together with its observer, and defining a new minimum time convergent target error, between which an invertible Fredholm transformation is defined, is presented. This will lay the foundation for finally deriving the minimum time observer with a Volterra transformation in Section 3.4.

3.3 Modifying Target Error System with Fredholm Transformation

For the remainder of this chapter, unless otherwise explicitly stated, we will refer to the system and corresponding coefficient assignments given in Section 3.1.

To start our observer derivation, let $\tilde{u}(x,t) = [\tilde{u}_1(x,t), \tilde{u}_2(x,t)]^T$ and $\tilde{v}(x,t) = [\tilde{v}_1(x,t), \tilde{v}_2(x,t)]^T$ denote the estimation errors for an observer using $\check{u}(x,t) = [\check{u}_1(x,t), \check{u}_2(x,t)]^T$ and $\check{v}(x,t) = [\check{v}_1(x,t), \check{v}_2(x,t)]^T$ as the estimates of the states $\bar{u}(x,t) = [u_1(x,t), u_2(x,t)]^T$, $\bar{v}(x,t) = [v_1(x,t), v_2(x,t)]^T$, respectively, for the system (3.1)–(3.5). The estimation errors are defined as

$$\tilde{u}(x,t) = \begin{bmatrix} u_1(x,t) - \check{u}_1(x,t) \\ u_2(x,t) - \check{u}_2(x,t) \end{bmatrix}, \tag{3.21a}$$

$$\tilde{v}(x,t) = \begin{bmatrix} v_1(x,t) - \check{v}_1(x,t) \\ v_2(x,t) - \check{v}_2(x,t) \end{bmatrix}. \tag{3.21b}$$

Applying the observer presented in Theorem 3.1 to the $2+2$ system (3.1)–(3.5), and applying the estimation error definitions (3.21), we get the error system

$$\tilde{u}_t(x,t) + \Lambda^+(x)\tilde{u}_x(x,t) = \Sigma^{+-}(x)\tilde{v}(x,t) - P^+(x)\tilde{u}(1,t), \tag{3.22a}$$

$$\tilde{v}_t(x,t) - \Lambda^-(x)\tilde{v}_x(x,t) = \Sigma^{-+}(x)\tilde{u}(x,t) - P^-(x)\tilde{u}(1,t) \tag{3.22b}$$

with boundary conditions

$$\tilde{u}(0,t) = Q_0\tilde{v}(0,t), \tag{3.23a}$$

$$\tilde{v}(1,t) = 0. \tag{3.23b}$$

As for the initial observer estimates, we set $\forall x \in [0,1]$ that $\hat{u}(x,0) = 0$ and $\hat{v}(x,0) = 0$, implying that the observer assumes nothing about the system states initially. The error system initial conditions then become

$$\tilde{u}(x,0) = \bar{u}(x,0) = \bar{u}_0(x), \tag{3.24a}$$

$$\tilde{v}(x,0) = \bar{v}(x,0) = \bar{v}_0(x), \tag{3.24b}$$

with $\bar{u}_0(x)$ and $\bar{v}_0(x)$ the same as in (3.3). For the error system (3.22)–(3.24) to vanish in minimum time $t_{1,min}$ rather than non-minimum time t_F, new observer gains $P^+(x)$ and $P^-(x)$ that allow this must be calculated.

Let $\tilde{\alpha}(t) = [\tilde{\alpha}_1(t), \tilde{\alpha}_2(t)]^T$ and $\tilde{\beta}(t) = [\tilde{\beta}_1(t), \tilde{\beta}_2(t)]^T$ denote states for a target error system. The approach taken in Anfinsen and Aamo (2017b) to calculate the observer gains $P^+(x)$, $P^-(x)$ guaranteeing convergence of the error system (3.22)

to zero within time t_F given by (3.20) was to first define the target error system

$$\tilde{\alpha}_t(x,t) + \Lambda^+(x)\tilde{\alpha}_x(x,t) = \Sigma^{+-}(x)\tilde{\beta}(x,t) - \int_x^1 D^+(x,\xi)\tilde{\beta}(\xi,t)d\xi, \tag{3.25a}$$

$$\tilde{\beta}_t(x,t) - \Lambda^-(x)\tilde{\beta}_x(x,t) = -\int_x^1 D^-(x,\xi)\tilde{\beta}(\xi,t)d\xi \tag{3.25b}$$

with boundary conditions

$$\tilde{\alpha}(0,t) = Q_0\tilde{\beta}(0,t) + \int_0^1 H(\xi)\tilde{\alpha}(\xi,t)d\xi, \tag{3.26a}$$

$$\tilde{\beta}(1,t) = 0 \tag{3.26b}$$

and then subsequently define a Volterra backstepping transformation of the form

$$\tilde{u}(x,t) = \tilde{\alpha}(x,t) + \int_x^1 M(x,\xi)\tilde{\alpha}(\xi,t)d\xi \tag{3.27a}$$

$$\tilde{v}(x,t) = \tilde{\beta}(x,t) + \int_x^1 N(x,\xi)\tilde{\alpha}(\xi,t)d\xi \tag{3.27b}$$

between the original error system (3.22)–(3.23) and the target error system (3.25)–(3.26). Here $D^+(x,\xi)$ and $D^-(x,\xi)$ are defined by the implicit relations

$$\begin{aligned} D^+(x,\xi) &= M(x,\xi)\Sigma^{+-}(\xi) - \int_\xi^x M(\xi,s)D^+(s,\xi)ds \\ D^-(x,\xi) &= N(x,\xi)\Sigma^{+-}(\xi) - \int_\xi^x N(\xi,s)D^+(s,\xi)ds \end{aligned} \tag{3.28}$$

and $M(x,\xi)$, $N(x,\xi)$ are 2×2 matrices which become

$$M(x,\xi) = \begin{bmatrix} M_{11}(x,\xi) & M_{12}(x,\xi) \\ M_{21}(x,\xi) & M_{22}(x,\xi) \end{bmatrix}, \tag{3.29a}$$

$$N(x,\xi) = \begin{bmatrix} N_{11}(x,\xi) & N_{12}(x,\xi) \\ N_{21}(x,\xi) & N_{22}(x,\xi) \end{bmatrix}, \tag{3.29b}$$

respectively, when written out.

The function $H(x)$ which appears in the term $\int_0^1 H(\xi)\tilde{\alpha}(\xi,t)d\xi$ of boundary condition (3.26a) is the same strictly lower triangular matrix presented in Theorem 3.1 with components defined in (3.19). For the $2+2$ case, this matrix therefore becomes

$$H(x) = \begin{bmatrix} 0 & 0 \\ h_{21}(x) & 0 \end{bmatrix}, \tag{3.30}$$

and $h_{21}(x)$ can from (3.19) be written out as

$$h_{21}(x) = Q_{21}N_{12}(0,x) + Q_{22}N_{22}(0,x) - M_{21}(0,x). \tag{3.31}$$

This term is the primary reason the observer from Theorem 3.1 does not converge in minimum time. To see this, as was shown in Anfinsen and Aamo (2017b), firstly $\tilde{\beta}(x,t)$ in (3.25)–(3.26) vanishes after $\int_0^1 \frac{dx}{\mu_2(x)}$ units of time. Therefore, $\forall t \geq \int_0^1 \frac{dx}{\mu_2(x)}$, the PDE (3.25a) with boundary condition (3.26a) can be written out as

$$\tilde{\alpha}_{1,t}(x,t) = -\lambda_1(x)\tilde{\alpha}_{1,x}(x,t) \tag{3.32a}$$
$$\tilde{\alpha}_{2,t}(x,t) = -\lambda_2(x)\tilde{\alpha}_{2,x}(x,t) \tag{3.32b}$$
$$\tilde{\alpha}_1(0,t) = 0 \tag{3.32c}$$
$$\tilde{\alpha}_2(0,t) = \int_0^1 h_{21}(\xi)\tilde{\alpha}_1(\xi,t)d\xi \tag{3.32d}$$

The state $\tilde{\alpha}_1(x,t)$ can be seen to vanish within time $\int_0^1 \frac{dx}{\lambda_1(x)}$ due to the zero boundary condition (3.32c). However, $\tilde{\alpha}_2(x,t)$ has the boundary condition (3.32d), which is nonzero during the time $\tilde{\alpha}_1(x,t) \neq 0$, which is for a duration of $\int_0^1 \frac{dx}{\mu_2(x)} + \int_0^1 \frac{dx}{\lambda_1(x)}$ units of time. We therefore get the non-minimum convergence time (3.20) when using (3.25)–(3.26) as a target system.

We will now attempt to remove the effect of the term in (3.26a) by modifying the target system with the help of a Fredholm transformation. The target error system (3.25)–(3.26), despite being a mathematically constructed error system, can be considered as representing the error system of an actual $2+2$ linear hyperbolic PDE system with states $\alpha(t) = [\alpha_1(t), \alpha_2(t)]^T$, $\beta(t) = [\beta_1(t), \beta_2(t)]^T$ and an observer generating state estimates $\hat{\alpha}(t) = [\hat{\alpha}_1(t), \hat{\alpha}_2(t)]^T$ and $\hat{\beta}(t) = [\hat{\beta}_1(t), \hat{\beta}_2(t)]^T$, respectively. From these we define $\tilde{\alpha}(t) = \alpha(t) - \hat{\alpha}(t)$ and $\tilde{\beta}(t) = \beta(t) - \hat{\beta}(t)$. Consider therefore

the cascade PDE system defined for $x \in [0,1]$ and $t \in [0,\infty)$ with dynamics

$$\alpha_t(x,t) + \Lambda^+(x)\alpha_x(x,t) = \Sigma^{+-}(x)\beta(x,t) - \int_x^1 D^+(x,\xi)\beta(\xi,t)d\xi, \tag{3.33a}$$

$$\beta_t(x,t) - \Lambda^-(x)\beta_x(x,t) = -\int_x^1 D^-(x,\xi)\beta(\xi,t)d\xi \tag{3.33b}$$

and boundary conditions

$$\alpha(0,t) = Q_0\beta(0,t) + \int_0^1 H(\xi)\alpha(\xi,t)d\xi, \tag{3.34a}$$

$$\beta(1,t) = R_1\alpha(1,t) + V(t). \tag{3.34b}$$

The initial conditions are given by

$$\alpha(x,0) = \alpha_0(x), \tag{3.35a}$$

$$\beta(x,0) = \beta_0(x), \tag{3.35b}$$

where it is defined that $\alpha_0(x) = [\alpha_{1,0}(x), \alpha_{2,0}(x)]^T$ and $\beta_0(x) = [\beta_{1,0}(x), \beta_{2,0}(x)]^T$ and the constraints $\alpha_{1,0}(x), \alpha_{2,0}(x), \beta_{1,0}(x), \beta_{2,0}(x) \in L_2([0,1])$ are imposed. We also have that $\Lambda^+(x)$, $\Lambda^-(x)$, $\Sigma^{+-}(x)$, Q_0 and R_0 are defined the same way as in (3.5), whilst $V(t) = [V_1(t), V_2(t)]^T$ is a vector of arbitrary boundary control inputs $V_1(t), V_2(t)$. The terms $D^+(x)$, $D^-(x)$ are defined in (3.28). Assume that the boundary collocated with control is available for measurement, and define therefore the measurement variable $\eta(t) = [\eta_1(t), \eta_2(t)]^T$ as $\eta(t) = \alpha(1,t)$.

The error system with states $\tilde{\alpha}(x,t)$ and $\tilde{\beta}(x,t)$ will for the remainder of this section be viewed as the original error system, and a new target error system, with states $\tilde{\gamma}(x,t) = [\tilde{\gamma}_1(x,t), \tilde{\gamma}_2(x,t)]^T$ and $\tilde{\nu}(x,t) = [\tilde{\nu}_1(x,t), \tilde{\nu}_2(x,t)]^T$, which vanishes in time $t_{1,min}$ given by (3.7) will be established. The "observer gain" term $T^+(x)$ is added to the $\tilde{\alpha}$ error system, and an invertible Fredholm backstepping transformation $\mathcal{F}$ mapping the $\tilde{\gamma}, \tilde{\nu}$ error system to the new $\tilde{\alpha}, \tilde{\beta}$ system with the extra "observer gain" term is defined. Using this transformation, the values of the "observer gain" $T^+(x)$ to guarantee that the $\tilde{\alpha}, \tilde{\beta}$ system vanishes within time $t_{1,min}$ is calculated.

When this intermediate derivation has been completed, the new $\tilde{\alpha}, \tilde{\beta}$ minimum time convergent error system with additional "observer gain" term $T^+(x)$ can be used as the target error system for calculating new observer gains $P^+(x)$ and $P^-(x)$ via a Volterra backstepping transformation $\mathcal{V}$. The final transformation mapping the minimum time convergent target error system $\tilde{\gamma}, \tilde{\nu}$ to the original error system $\tilde{u}, \tilde{v}$ will then be a function composition $\mathcal{V} \circ \mathcal{F}$ of the Volterra transformation composed

with the Fredholm transformation[4]. This approach can be visualized in Figure 3.1.

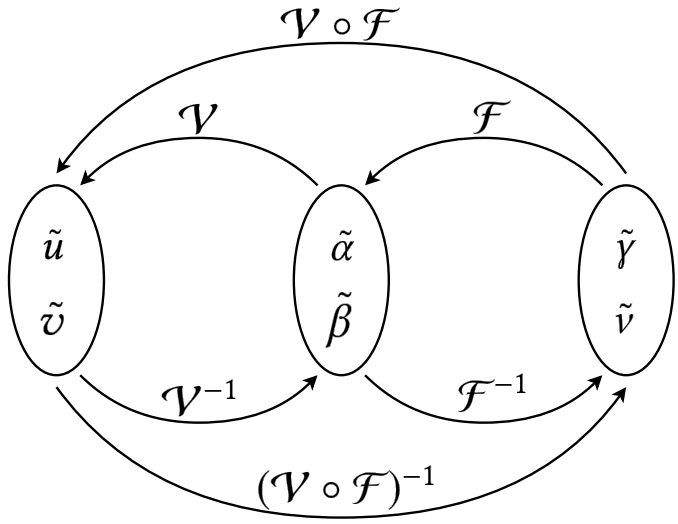

Figure 3.1: Composition diagram showing approach taken in deriving the minimum time convergent collocated observer for the $2 + 2$ system. The gains for the observer are calculated from the transformation $\mathcal{V} \circ \mathcal{F}$ between the final target error system with states $\tilde{\gamma}$, $\tilde{\nu}$ and the original error system with states $\tilde{u}$, $\tilde{v}$.

Thus, here in Section 3.3, we are primarily interested in the result pertaining to the transformation in the right half of Fig. 3.1. Then subsequently the result pertaining to the left half of Figure 3.1 is covered in Section 3.4.

Now the target error system with states $\tilde{\gamma}(x,t)$ and $\tilde{\nu}(x,t)$ in the far right of Fig. 3.1 will be introduced, and its convergence in minimum time $t_{1,min}$ given by (3.7) will be shown.

Lemma 3.2. *Consider the system with states* $\tilde{\gamma}(x,t) = [\tilde{\gamma}_1(x,t), \tilde{\gamma}_2(x,t)]^T$ *and* $\tilde{\nu}_1(x,t) = [\tilde{\nu}_1(x,t), \tilde{\nu}_2(x,t)]^T$*, governed by*

$$\tilde{\gamma}_t(x,t) + \Lambda^+(x)\tilde{\gamma}_x(x,t) = \Sigma^{+-}(x)\tilde{\nu}(x,t) - \int_x^1 D^+(x,\xi)\tilde{\nu}(\xi,t)d\xi - \int_0^1 \breve{K}_1(x,\xi)[\breve{\Sigma}^{+-}(\xi)\tilde{\nu}(\xi,t) - \int_\xi^1 \breve{D}^+(\xi,s)\tilde{\nu}(s,t)ds]d\xi, \tag{3.36a}$$

[4]For this approach to work it is critical that both transformations involved are invertible. Volterra integral equations are by their structure intrinsically invertible, but Fredholm integral equations do not have this guarantee. Therefore the Fredholm integral transformation must be proven to be invertible before it can be applied to a backstepping transformation. See Appendix B for more information on integral equations.

$$\tilde{\nu}_t(x,t) - \Lambda^-(x)\tilde{\nu}_x(x,t) = -\int_x^1 D^-(x,\xi)\tilde{\nu}(\xi,t)d\xi \tag{3.36b}$$

and with boundary conditions

$$\tilde{\gamma}(0,t) = Q_0\tilde{\nu}(0,t), \tag{3.37a}$$
$$\tilde{\nu}(1,t) = 0 \tag{3.37b}$$

Here $\Lambda^+(x)$, $\Lambda^-(x)$, $\Sigma^{+-}(x)$ *and* Q_0 *are as given by* (3.5), *whilst* $D^(x)$ *and* $D^-(x)$ *are given by* (3.28). *The remaining terms can be defined as*

$$\breve{K}_1(x,\xi) = \begin{bmatrix} 0 & 0 \\ 0 & k_{21}(x,\xi) \end{bmatrix}, \tag{3.38}$$

$$\breve{\Sigma}^{+-}(x) = \begin{bmatrix} 0 & 0 \\ \sigma_{11}^{+-}(x) & \sigma_{12}^{+-}(x) \end{bmatrix}, \tag{3.39}$$

$$\breve{D}^+(x,\xi) = \begin{bmatrix} 0 & 0 \\ d_{11}^+(x,\xi) & d_{12}^+(x,\xi) \end{bmatrix}. \tag{3.40}$$

Then $\forall x \in [0,1]$ *and* $\forall t \geq t_{1,min}$, *where* $t_{1,min}$ *is as defined in* (3.7), *the system states satisfy* $\tilde{\gamma}(x,t) = \tilde{\nu}(x,t) = 0$.

Proof. Observe that the target system (3.36)–(3.37) is a cascade system with the $\tilde{\gamma}$ subsystem depending on the $\tilde{\nu}$ subsystem, but the $\tilde{\nu}$ subsystem being independent. We start therefore by analyzing the convergence time of the $\tilde{\nu}$ subsystem

$$\tilde{\nu}_{1,t}(x,t) - \mu_1(x)\tilde{\nu}_{1,x}(x,t) = -\int_x^1 d_{11}^-(x,\xi)\tilde{\nu}_1(\xi,t)d\xi - \int_x^1 d_{12}^-(x,\xi)\tilde{\nu}_2(\xi,t)d\xi, \tag{3.41a}$$

$$\tilde{\nu}_{2,t}(x,t) - \mu_2(x)\tilde{\nu}_{2,x}(x,t) = -\int_x^1 d_{21}^-(x,\xi)\tilde{\nu}_1(\xi,t)d\xi - \int_x^1 d_{22}^-(x,\xi)\tilde{\nu}_2(\xi,t)d\xi, \tag{3.41b}$$

$$\tilde{\nu}_1(1,t) = 0, \tag{3.42a}$$
$$\tilde{\nu}_2(1,t) = 0. \tag{3.42b}$$

Observing the structure of the terms in the right hand sides of (3.41), we see that as $x \to 1$, these terms approach zero, implying that (3.41) approaches the

simplified equation $\tilde{\nu}_t - \Lambda^-(x)\tilde{\nu}_x = 0$. Therefore, by directly applying the method of characteristics to (3.41) at $x = 1$, we find $\forall i \in \{1, 2\}$ the equation for the characteristic originating at the point $x = 1$ is given by

$$\frac{dt}{1} = \frac{dx}{-\mu_i(x)}, \tag{3.43}$$

which by integrating we obtain

$$t_i(x) = \int_1^x \frac{ds}{-\mu_i(s)} = \int_x^1 \frac{ds}{\mu_i(s)}. \tag{3.44}$$

Hence, by applying the boundary condition (3.42) which is defined for $x = 1$, given the point $x_v \in [0, 1]$ we can deduce that $\forall x \in [x_v, 1]$ it is true that $\tilde{\nu}_i(x, t) = 0$, $\forall t \geq t_i(x_v)$. Therefore, after $t_1(0)$ units of time, we have $\forall x \in [0, 1]$ that $\tilde{\nu}_1(x, t) = 0$, and also after $t_2(0)$ units of time it is true $\forall x \in [0, 1]$ that $\tilde{\nu}_2(x, t) = 0$. Since $\mu_1(x) \geq \mu_2(x)$ due to (3.6), implying $t_1(0) \leq t_2(0)$, we find that (3.41) has vanished completely after time $t_H = t_2(0)$.

Observing the expression (3.36a), we see that $\forall t \geq t_H$ the $\tilde{\gamma}$ subsystem simplifies to

$$\tilde{\gamma}_{1,t}(x, t) + \lambda_1(x)\tilde{\gamma}_{1,x}(x, t) = 0 \tag{3.45a}$$
$$\tilde{\gamma}_{2,t}(x, t) + \lambda_2(x)\tilde{\gamma}_{2,x}(x, t) = 0 \tag{3.45b}$$

$$\tilde{\gamma}_1(0, t) = 0 \tag{3.46a}$$
$$\tilde{\gamma}_2(0, t) = 0 \tag{3.46b}$$

In a similar way to the $\tilde{\nu}$ subsystem, observe from (3.46) that the left boundary for the $\tilde{\gamma}$ subsytem is now equal to 0. Applying the same arguments as were applied above together with the fact that (3.45) contains positive transport speeds, we see the $\tilde{\gamma}$ subsystem vanishes in another $\int_0^1 \frac{dx}{\lambda_1(x)}$ units of time. Therefore both $\tilde{\nu}(x, t)$ and $\tilde{\gamma}(x, t)$ are identically zero across the spatial domain $[0, 1] \ni x$ after time t_{min} given in (3.7). □

Now that we have established a minimum-time convergent target system for the setup shown in Fig. 3.1, we would like to modify the old non-minimum time convergent target system (3.25)–(3.26) to make it converge in the same time as (3.36)–(3.37). Consider therefore incorporating the artificial observer gain $T^+(x)$ to (3.25a), resulting in the system

$$\tilde{\alpha}_t(x,t)+\Lambda^+(x)\tilde{\alpha}_x(x,t)=\Sigma^{+-}(x)\tilde{\beta}(x,t)-\int_x^1 D^+(x,\xi)\tilde{\beta}(\xi,t)d\xi-T^+(x)\tilde{\alpha}(1,t), \tag{3.47a}$$

$$\tilde{\beta}_t(x,t)-\Lambda^-(x)\tilde{\beta}_x(x,t)=-\int_x^1 D^-(x,\xi)\tilde{\beta}(\xi,t)d\xi, \tag{3.47b}$$

with boundary conditions

$$\tilde{\alpha}(0,t)=Q_0\tilde{\beta}(0,t)+\int_0^1 H(\xi)\tilde{\alpha}(\xi,t)d\xi, \tag{3.48a}$$

$$\tilde{\beta}(1,t)=0. \tag{3.48b}$$

We now present an invertible transformation mapping (3.36)–(3.37) into (3.47)–(3.48).

Lemma 3.3. *The Fredholm backstepping transformation $\mathcal{F}$ defined by*

$$\tilde{\alpha}(x,t)=\tilde{\gamma}(x,t)+\int_0^1 K_1(x,\xi)\tilde{\gamma}(\xi,t)d\xi, \tag{3.49a}$$

$$\tilde{\beta}(x,t)=\tilde{\nu}(x,t) \tag{3.49b}$$

is invertible. Here $K_1(x,\xi)$ has the structure

$$K_1(x,\xi)=\begin{bmatrix}0 & 0\\ k_{21}(x,\xi) & 0\end{bmatrix} \tag{3.50}$$

with $k_{21}(x,\xi)$ satisfying the kernel PDE

$$k_{21,x}(x,\xi)\lambda_2(x)+k_{21,\xi}(x,\xi)\lambda_1(\xi)=-k_{21}(x,\xi)\lambda_{1,\xi}(\xi) \tag{3.51}$$

with boundary conditions

$$k_{21}(0,\xi)=h_{21}(\xi), \tag{3.52a}$$

$$k_{21}(x,0) = 0 \tag{3.52b}$$

and defined over the square domain $\mathcal{S}_0 = \{(x,\xi) \mid 0 \leq x, \xi \leq 1\}$. *Here* $h_{21}(\xi)$ *is defined as in* (3.19). *The transformation* $\mathcal{F}$ *transforms the target system* (3.36)–(3.37) *into* (3.47)–(3.48), *where* $T^+(x)$ *is defined as*

$$T^+(x) = \begin{bmatrix} 0 & 0 \\ k_{21}(x,1)\lambda_1(1) & 0 \end{bmatrix}. \tag{3.53}$$

Proof. First the Fredholm transformation $\mathcal{F}$ is proven to be invertible. Let $\tilde{\delta} = [\tilde{\alpha}^T, \tilde{\beta}^T]^T$ and $\tilde{\omega} = [\tilde{\gamma}^T, \tilde{\nu}^T]^T$. The Fredholm transformation (3.49) can then be written as

$$\tilde{\delta}(x,t) = \tilde{\omega}(x,t) + \int_0^1 K(x,\xi)\tilde{\omega}(\xi,t)d\xi \tag{3.54}$$

with K having the structure

$$K(x,\xi) = \begin{bmatrix} K_1(x,\xi) & 0 \\ 0 & 0 \end{bmatrix}, \tag{3.55}$$

where K_1 is defined as the lower triangular matrix in (3.50). In Lemma 2 of Coron et al. (2017), which is reproduced with corresponding proof in Appendix B, it is proven that all Fredholm transformations of this form are invertible. Therefore the Fredholm transformation $\mathcal{F}$ must be invertible.

The $\tilde{\alpha}$ subsystem

Next, differentiating the expression for $\tilde{\alpha}(x,t)$ in the Fredholm transformation (3.49) with respect to time, substituting in the target system dynamics (3.36) and integrating by parts, obtain for $\tilde{\alpha}_1$ that

$$\begin{aligned} \tilde{\alpha}_{1,t}(x,t) = \tilde{\gamma}_{1,t}(x,t) = -\lambda_1(x)\tilde{\gamma}_{1,x}(x,t) + \sigma_{11}^{+-}(x)\tilde{\nu}_1(x,t) + \sigma_{12}^{+-}(x)\tilde{\nu}_2(x,t) \\ - \int_x^1 d_{11}^+(x,\xi)\tilde{\nu}_1(\xi,t)d\xi - \int_x^1 d_{12}^+(x,\xi)\tilde{\nu}_2(\xi,t)d\xi, \end{aligned} \tag{3.56}$$

whilst for $\tilde{\alpha}_2$ we get

$$\begin{aligned} \tilde{\alpha}_{2,t}(x,t) = \tilde{\gamma}_{2,t}(x,t) + \int_0^1 k_{21}(x,\xi)\tilde{\gamma}_{1,t}(\xi,t)d\xi \\ = -\lambda_2(x)\tilde{\gamma}_{2,x}(x,t) + \sigma_{21}^{+-}(x)\tilde{\nu}_1(x,t) + \sigma_{22}^{+-}(x)\tilde{\nu}_2(x,t) - \int_x^1 d_{21}^+(x,\xi)\tilde{\nu}_1(\xi,t)d\xi \end{aligned}$$

$$
\begin{aligned}
&-\int_x^1 d_{22}^+(x,\xi)\tilde{\nu}_2(\xi,t)d\xi-\int_0^1 k_{21}(x,\xi)[\sigma_{11}^{+-}(\xi)\tilde{\nu}_1(\xi,t)+\sigma_{12}^{+-}(\xi)\tilde{\nu}_2(\xi,t)\\
&-\int_\xi^1 d_{11}^+(\xi,s)\tilde{\nu}_1(s,t)ds-\int_\xi^1 d_{12}^+(\xi,s)\tilde{\nu}_2(s,t)ds]d\xi+\int_0^1 k_{21}(x,\xi)[-\lambda_1(\xi)\tilde{\gamma}_{1,\xi}(\xi,t)\\
&+\sigma_{11}^{+-}(\xi)\tilde{\nu}_1(\xi,t)+\sigma_{12}^{+-}(\xi)\tilde{\nu}_2(\xi,t)-\int_\xi^1 d_{11}^+(\xi,s)\tilde{\nu}_1(s,t)ds\\
&-\int_\xi^1 d_{12}^+(\xi,s)\tilde{\nu}_2(s,t)ds]d\xi\\
&=-\lambda_2(x)\tilde{\gamma}_{2,x}(x,t)-\int_0^1 k_{21}(x,\xi)\lambda_1(\xi)\tilde{\gamma}_{1,\xi}(\xi,t)d\xi+\sigma_{21}^{+-}(x)\tilde{\nu}_1(x,t)\\
&+\sigma_{22}^{+-}(x)\tilde{\nu}_2(x,t)\\
&-\int_x^1 d_{21}^+(x,\xi)\tilde{\nu}_1(\xi,t)d\xi-\int_x^1 d_{22}^+(x,\xi)\tilde{\nu}_2(\xi,t)d\xi-\int_0^1 k_{21}(x,\xi)[\sigma_{11}^{+-}(\xi)\tilde{\nu}_1(\xi,t)\\
&+\sigma_{12}^{+-}(\xi)\tilde{\nu}_2(\xi,t)-\int_\xi^1 d_{11}^+(\xi,s)\tilde{\nu}_1(s,t)ds-\int_\xi^1 d_{12}^+(\xi,s)\tilde{\nu}_2(s,t)ds]d\xi\\
&+\int_0^1 k_{21}(x,\xi)[\sigma_{11}^{+-}(\xi)\tilde{\nu}_1(\xi,t)+\sigma_{12}^{+-}(\xi)\tilde{\nu}_2(\xi,t)\\
&-\int_\xi^1 d_{11}^+(\xi,s)\tilde{\nu}_1(s,t)ds-\int_\xi^1 d_{12}^+(\xi,s)\tilde{\nu}_2(s,t)ds]d\xi\\
&=-\lambda_2(x)\tilde{\gamma}_{2,x}(x,t)-[k_{21}(x,1)\lambda_1(1)\tilde{\gamma}_1(1,t)-k_{21}(x,0)\lambda_1(0)\tilde{\gamma}_1(0,t)]\\
&+\int_0^1 k_{21,\xi}(x,\xi)\lambda_1(\xi)\tilde{\gamma}_1(\xi,t)d\xi+\int_0^1 k_{21}(x,\xi)\lambda_{1,\xi}(\xi)\tilde{\gamma}_1(\xi,t)d\xi\\
&+\sigma_{21}^{+-}(x)\tilde{\nu}_1(x,t)+\sigma_{22}^{+-}(x)\tilde{\nu}_2(x,t)-\int_x^1 d_{21}^+(x,\xi)\tilde{\nu}_1(\xi,t)d\xi-\int_x^1 d_{22}^+(x,\xi)\tilde{\nu}_2(\xi,t)d\xi,
\end{aligned}
$$

$$\Rightarrow \boxed{\begin{aligned}\tilde{\alpha}_{2,t}(x,t) &= -\lambda_2(x)\tilde{\gamma}_{2,x}(x,t) - k_{21}(x,1)\lambda_1(1)\tilde{\gamma}_1(1,t)\\ &\quad + k_{21}(x,0)\lambda_1(0)\tilde{\gamma}_1(0,t) + \int_0^1 [k_{21,\xi}(x,\xi)\lambda_1(\xi)\\ &\quad + k_{21}(x,\xi)\lambda_{1,\xi}(\xi)]\tilde{\gamma}_1(\xi,t)d\xi + \sigma_{21}^{+-}(x)\tilde{\nu}_1(x,t)\\ &\quad + \sigma_{22}^{+-}(x)\tilde{\nu}_2(x,t) - \int_x^1 d_{21}^{+}(x,\xi)\tilde{\nu}_1(\xi,t)d\xi - \int_x^1 d_{22}^{+}(x,\xi)\tilde{\nu}_2(\xi,t)d\xi\end{aligned}} \tag{3.57}$$

Likewise, differentiating expression for $\tilde{\alpha}(x,t)$ in the Fredholm transformation (3.49) with respect to space, obtain that

$$\tilde{\alpha}_{1,x}(x,t) = \tilde{\gamma}_{1,x}(x,t), \tag{3.58}$$

$$\tilde{\alpha}_{2,x}(x,t) = \tilde{\gamma}_{2,x}(x,t) + \int_0^1 k_{21,x}(x,\xi)\tilde{\gamma}_1(\xi,t)d\xi. \tag{3.59}$$

Next, combining (3.56), (3.57), (3.58) and (3.59) with the $\tilde{\alpha}$ subsystem dynamics from (3.47), obtain for $\tilde{\alpha}_1$ that

$$\begin{aligned}0 &= \tilde{\alpha}_{1,t}(x,t) + \lambda_1(x)\tilde{\alpha}_{1,x}(x,t) - \sigma_{11}^{+-}(x)\tilde{\beta}_1(x,t) - \sigma_{12}^{+-}(x)\tilde{\beta}_2(x,t)\\ &+ \int_x^1 d_{11}^{+}(x,\xi)\tilde{\beta}_1(\xi,t)d\xi + \int_x^1 d_{12}^{+}(x,\xi)\tilde{\beta}_2(\xi,t)d\xi + T_{11}^{+}(x)\tilde{\alpha}_1(1,t) + T_{12}^{+}(x)\tilde{\alpha}_2(1,t)\\ &= -\lambda_1(x)\tilde{\gamma}_{1,x}(x,t) + \sigma_{11}^{+-}(x)\tilde{\nu}_1(x,t) + \sigma_{12}^{+-}(x)\tilde{\nu}_2(x,t) - \int_x^1 d_{11}^{+}(x,\xi)\tilde{\nu}_1(\xi,t)d\xi\\ &- \int_x^1 d_{12}^{+}(x,\xi)\tilde{\nu}_2(\xi,t)d\xi + \lambda_1(x)\tilde{\gamma}_{1,x}(x,t) - \sigma_{11}^{+-}(x)\tilde{\beta}_1(x,t) - \sigma_{12}^{+-}(x)\tilde{\beta}_2(x,t)\\ &+ \int_x^1 d_{11}^{+}(x,\xi)\tilde{\beta}_1(\xi,t)d\xi + \int_x^1 d_{12}^{+}(x,\xi)\tilde{\beta}_2(\xi,t)d\xi + T_{11}^{+}(x)\tilde{\alpha}_1(1,t) + T_{12}^{+}(x)\tilde{\alpha}_2(1,t)\\ &= \underbrace{-\lambda_1(x)\tilde{\gamma}_{1,x}(x,t) + \lambda_1(x)\tilde{\gamma}_{1,x}(x,t)}_{=0} + \sigma_{11}^{+-}(x)[\underbrace{\tilde{\nu}_1(x,t) - \tilde{\beta}_1(x,t)}_{=0}]\\ &+ \sigma_{12}^{+-}(x)[\underbrace{\tilde{\nu}_2(x,t) - \tilde{\beta}_2(x,t)}_{=0}] + \int_x^1 d_{11}^{+}(x,\xi)[\underbrace{\tilde{\beta}_1(\xi,t) - \tilde{\nu}_1(\xi,t)}_{=0}]d\xi\end{aligned}$$

$$+\int_x^1 d_{12}^+(x,\xi)[\underbrace{\tilde{\beta}_2(\xi,t)-\tilde{\nu}_2(\xi,t)}_{=0}]d\xi+T_{11}^+(x)\tilde{\gamma}_1(1,t)$$

$$+T_{12}^+(x)[\tilde{\gamma}_2(1,t)+\int_0^1 k_{21}(1,\xi)\tilde{\gamma}_1(\xi,t)d\xi],$$

$$\Rightarrow \boxed{T_{11}^+(x)\tilde{\gamma}_1(1,t)+T_{12}^+(x)[\tilde{\gamma}_2(1,t)+\int_0^1 k_{21}(1,\xi)\tilde{\gamma}_1(\xi,t)d\xi]=0}, \qquad (3.60)$$

and the expression for $\tilde{\alpha}_2$ becomes

$$0=\tilde{\alpha}_{2,t}(x,t)+\lambda_2(x)\tilde{\alpha}_{2,x}(x,t)-\sigma_{21}^{+-}(x)\tilde{\beta}_1(x,t)-\sigma_{22}^{+-}(x)\tilde{\beta}_2(x,t)$$

$$+\int_x^1 d_{21}^+(x,\xi)\tilde{\beta}_1(\xi,t)d\xi+\int_x^1 d_{22}^+(x,\xi)\tilde{\beta}_2(\xi,t)d\xi+T_{21}^+(x)\tilde{\alpha}_1(1,t)+T_{22}^+(x)\tilde{\alpha}_2(1,t)$$

$$=-\lambda_2(x)\tilde{\gamma}_{2,x}(x,t)-k_{21}(x,1)\lambda_1(1)\tilde{\gamma}_1(1,t)+k_{21}(x,0)\lambda_1(0)\tilde{\gamma}_1(0,t)$$

$$+\int_0^1[k_{21,\xi}(x,\xi)\lambda_1(\xi)+k_{21}(x,\xi)\lambda_{1,\xi}(\xi)]\tilde{\gamma}_1(\xi,t)d\xi$$

$$+\sigma_{21}^{+-}(x)\tilde{\nu}_1(x,t)+\sigma_{22}^{+-}(x)\tilde{\nu}_2(x,t)-\int_x^1 d_{21}^+(x,\xi)\tilde{\nu}_1(\xi,t)d\xi-\int_x^1 d_{22}^+(x,\xi)\tilde{\nu}_2(\xi,t)d\xi$$

$$+\lambda_2(x)[\tilde{\gamma}_{2,x}(x,t)+\int_0^1 k_{21,x}(x,\xi)\tilde{\gamma}_1(\xi,t)d\xi]-\sigma_{21}^{+-}(x)\tilde{\beta}_1(x,t)-\sigma_{22}^{+-}(x)\tilde{\beta}_2(x,t)$$

$$+\int_x^1 d_{21}^+(x,\xi)\tilde{\beta}_1(\xi,t)d\xi+\int_x^1 d_{22}^+(x,\xi)\tilde{\beta}_2(\xi,t)d\xi$$

$$+T_{21}^+(x)\tilde{\gamma}_1(1,t)+T_{22}^+(x)[\tilde{\gamma}_2(1,t)+\int_0^1 k_{21}(1,\xi)\tilde{\gamma}_1(\xi,t)d\xi]$$

$$=\underbrace{-\lambda_2(x)\tilde{\gamma}_{2,x}(x,t)+\lambda_2(x)\tilde{\gamma}_{2,x}(x,t)}_{=0}+\sigma_{21}^{+-}(x)[\underbrace{\tilde{\nu}_1(x,t)-\tilde{\beta}_1(x,t)}_{=0}]$$

$$+\sigma_{22}^{+-}(x)[\underbrace{\tilde{\nu}_2(x,t)-\tilde{\beta}_2(x,t)}_{=0}]$$

$$+\int_x^1 d_{21}^+(x,\xi)[\underbrace{\tilde{\beta}_1(\xi,t)-\tilde{\nu}_1(\xi,t)}_{=0}]d\xi+\int_x^1[\underbrace{\tilde{\beta}_2(\xi,t)-\tilde{\nu}_2(\xi,t)}_{=0}]d\xi$$

$$+[T_{21}^{+}(x)-k_{21}(x,1)\lambda_1(1)]\tilde{\gamma}_1(1,t)+T_{22}^{+}(x)[\tilde{\gamma}_2(1,t)+\int_0^1 k_{21}(1,\xi)\tilde{\gamma}_1(\xi,t)d\xi]$$
$$+\int_0^1[k_{21,\xi}(x,\xi)\lambda_1(\xi)+k_{21}(x,\xi)\lambda_{1,\xi}(\xi)+\lambda_2(x)k_{21,x}(x,\xi)]\tilde{\gamma}_1(\xi,t)d\xi$$
$$+k_{21}(x,0)\lambda_1(0)\tilde{\gamma}_1(0,t),$$

$$\Rightarrow \boxed{\begin{aligned}&[T_{21}^{+}(x)-k_{21}(x,1)\lambda_1(1)]\tilde{\gamma}_1(1,t)+T_{22}^{+}(x)[\tilde{\gamma}_2(1,t)+\int_0^1 k_{21}(1,\xi)\tilde{\gamma}_1(\xi,t)d\xi]\\&+\int_0^1[k_{21,x}(x,\xi)\lambda_2(x)+k_{21,\xi}(x,\xi)\lambda_1(\xi)+k_{21}(x,\xi)\lambda_{1,\xi}(\xi)]\tilde{\gamma}_1(\xi,t)d\xi\\&+k_{21}(x,0)\lambda_1(0)\tilde{\gamma}_1(0,t)\\&=0\end{aligned}} \tag{3.61}$$

The $\tilde{\beta}$ subsystem

Performing the same differentiation of the $\tilde{\beta}(x,t)$ expression in the Fredholm transformation (3.49) with respect to both time and space we find

$$\tilde{\beta}_{1,t}(x,t)=\tilde{\nu}_{1,t}(x,t)=\mu_1(x)\tilde{\nu}_{1,x}(x,t)-\int_x^1 d_{11}^{-}(x,\xi)\tilde{\nu}_1(\xi,t)d\xi - \int_x^1 d_{12}^{-}(x,\xi)\tilde{\nu}_2(\xi,t)d\xi, \tag{3.62}$$

$$\tilde{\beta}_{2,t}(x,t)=\tilde{\nu}_{2,t}(x,t)=\mu_2(x)\tilde{\nu}_{2,x}(x,t)-\int_x^1 d_{21}^{-}(x,\xi)\tilde{\nu}_1(\xi,t)d\xi - \int_x^1 d_{22}^{-}(x,\xi)\tilde{\nu}_2(\xi,t)d\xi, \tag{3.63}$$

$$\tilde{\beta}_{1,x}(x,t)=\tilde{\nu}_{1,x}(x,t), \tag{3.64}$$

$$\tilde{\beta}_{2,x}(x,t)=\tilde{\nu}_{2,x}(x,t). \tag{3.65}$$

For the $\tilde{\beta}$ subsystem we have by combining (3.62), (3.63), (3.64) and (3.65)

together with (3.47) that

$$
\begin{aligned}
0 &= \tilde{\beta}_{1,t}(x,t) - \mu_1(x)\tilde{\beta}_{1,x}(x,t) + \int_x^1 d_{11}^-(x,\xi)\tilde{\beta}_1(\xi,t)d\xi + \int_x^1 d_{12}^-(x,\xi)\tilde{\beta}_2(\xi,t)d\xi \\
&= \mu_1(x)\tilde{\nu}_{1,x}(x,t) - \int_x^1 d_{11}^-(x,\xi)\tilde{\nu}_1(\xi,t)d\xi - \int_x^1 d_{12}^-(x,\xi)\tilde{\nu}_2(\xi,t)d\xi - \mu_1(x)\tilde{\beta}_{1,x}(x,t) \\
&\quad + \int_x^1 d_{11}^-(x,\xi)\tilde{\beta}_1(\xi,t)d\xi + \int_x^1 d_{12}^-(x,\xi)\tilde{\beta}_2(\xi,t)d\xi \\
&= \mu_1(x)[\underbrace{\tilde{\nu}_{1,x}(x,t) - \tilde{\beta}_{1,x}(x,t)}_{=0}] + \int_x^1 d_{11}^-(x,\xi)[\underbrace{\tilde{\beta}_1(\xi,t) - \tilde{\nu}_1(\xi,t)}_{=0}]d\xi \\
&\quad + \int_x^1 d_{12}^-(x,\xi)[\underbrace{\tilde{\beta}_2(\xi,t) - \tilde{\nu}_2(\xi,t)}_{=0}]d\xi = 0,
\end{aligned} \tag{3.66}
$$

and likewise for $\tilde{\beta}_2$

$$
\begin{aligned}
0 &= \tilde{\beta}_{2,t}(x,t) - \mu_2(x)\tilde{\beta}_{2,x}(x,t) + \int_x^1 d_{21}^-(x,\xi)\tilde{\beta}_1(\xi,t)d\xi + \int_x^1 d_{22}^-(x,\xi)\tilde{\beta}_2(\xi,t)d\xi \\
&= \mu_2(x)\tilde{\nu}_{2,x}(x,t) - \int_x^1 d_{21}^-(x,\xi)\tilde{\nu}_1(\xi,t)d\xi - \int_x^1 d_{22}^-(x,\xi)\tilde{\nu}_2(\xi,t)d\xi - \mu_2(x)\tilde{\beta}_{2,x}(x,t) \\
&\quad + \int_x^1 d_{21}^-(x,\xi)\tilde{\beta}_1(\xi,t)d\xi + \int_x^1 d_{22}^-(x,\xi)\tilde{\beta}_2(\xi,t)d\xi \\
&= \mu_2(x)[\underbrace{\tilde{\nu}_{2,x}(x,t) - \tilde{\beta}_{2,x}(x,t)}_{=0}] + \int_x^1 d_{21}^-(x,\xi)[\underbrace{\tilde{\beta}_1(\xi,t) - \tilde{\nu}_1(\xi,t)}_{=0}]d\xi \\
&\quad + \int_x^1 d_{22}^-(x,\xi)[\underbrace{\tilde{\beta}_2(\xi,t) - \tilde{\nu}_2(\xi,t)}_{=0}]d\xi = 0.
\end{aligned} \tag{3.67}
$$

This is as expected since (3.49) maps (3.36b) into (3.47b) via an identity transform.

Calculating "Observer Gains"

Considering that the errors $\tilde{\gamma}_1(x,t) \neq 0$ and $\tilde{\gamma}_2(x,t) \neq 0$ in (3.60) and (3.61), in general, obtain from (3.60) and (3.61) that $T_{11}^+(x) = T_{12}^+(x) = T_{22}^+(x) = 0$. Also

obtain the expression

$$T_{21}^{+}(x) = k_{21}(x,1)\lambda_1(1), \tag{3.68}$$

and the partial differential equation for $k_{21}(x,\xi)$ given by (3.51). One also finds the boundary condition

$$k_{21}(x,0) = 0. \tag{3.69}$$

For the other boundary condition for (3.51), set $x = 0$ into the Fredholm transformation (3.49) yielding

$$\tilde{\alpha}_2(0,t) = \tilde{\gamma}_2(0,t) + \int_0^1 k_{21}(0,\xi)\tilde{\gamma}_1(\xi,t)d\xi. \tag{3.70}$$

Comparing with the boundary conditions (3.48), obtain the kernel boundary condition

$$\tilde{\alpha}_2(0,t) = q_{21}\underbrace{\tilde{\nu}_1(0,t)}_{=\tilde{\beta}_1(0,t)} + q_{22}\underbrace{\tilde{\nu}_2(0,t)}_{=\tilde{\beta}_2(0,t)} + \int_0^1 k_{21}(0,\xi)\underbrace{\tilde{\gamma}_1(\xi,t)}_{=\tilde{\alpha}_1(\xi,t)}d\xi.$$

$$\Rightarrow \boxed{k_{21}(0,\xi) = h_{21}(\xi)} \tag{3.71}$$

□

An important detail for our design is that the kernel PDE (3.51)–(3.52) is well-posed, so that it admits a unique and well-defined solution $k_{21}(x,\xi)$ on which the observer gains can be based. In Coron et al. (2017), the solution was found explicitly for equations having the same form, thus ensuring well-posedness. With Lemma 3.3 we laid the groundwork for setting up a minimum time "observer" for the α, β system. The final step which remains before we can move on to designing the minimum time collocated observer for our $2 + 2$ system (3.1)–(3.5) is to explicitly set up the "observer" for the α, β system (3.33)–(3.34) using the gain $T^{+}(x)$ from Lemma 3.3 and prove that this "observer" generates estimates $\hat{\alpha}, \hat{\beta}$ which converge to their true values within time $t_{1,min}$, and this is done as shown in the following result.

Lemma 3.4. *Consider the collocated observer*

$$\hat{\alpha}_t(x,t) + \Lambda^{+}(x)\hat{\alpha}_x(x,t) = \Sigma^{+-}(x)\hat{\beta}(x,t) - \int_x^1 D^{+}(x,\xi)\hat{\beta}(\xi,t)d\xi + T^{+}(x)(\eta(t) - \hat{\alpha}(1,t)) \tag{3.72a}$$

$$\hat{\beta}_t(x,t) - \Lambda^-(x)\hat{\beta}_x(x,t) = -\int_x^1 D^-(x,\xi)\hat{\beta}(\xi,t)d\xi \tag{3.72b}$$

$$\hat{\alpha}(0,t) = Q_0\hat{\beta}(0,t) + \int_0^1 H(\xi)\hat{\alpha}(\xi,t)d\xi \tag{3.72c}$$

$$\hat{\beta}(1,t) = R_1\eta(t) + V(t) \tag{3.72d}$$

relying on the right boundary measurement $\eta(t) = \alpha(1,t)$ *where the observer gain* $T^+(x)$ *is defined as* (3.53)*, and all other coefficients are defined in the same way as in* (3.33)–(3.34)*. Then,* $\forall t \geq t_{min} = \int_0^1 \frac{dx}{\mu_2(x)} + \int_0^1 \frac{dx}{\lambda_1(x)}$*, the estimates* $\hat{\alpha}(x,t)$*,* $\hat{\beta}(x,t)$ *generated by* (3.72) *have converged to their true values* $\alpha(x,t)$ *and* $\beta(x,t)$

Proof. Using the estimation errors $\tilde{\alpha}(x,t) = \alpha(x,t) - \hat{\alpha}(x,t)$ and $\tilde{\beta}(x,t) = \beta(x,t) - \hat{\beta}(x,t)$, subtract the estimation system dynamics and boundary conditions (3.72) of the collocated observer from the system dynamics (3.33) with boundary conditions (3.34) to obtain the error system (3.47) with boundary conditions (3.48) as presented in Lemma 3.3.

Thanks to Lemma 3.3 we know the Fredholm transformation $\mathcal{F}$ given by (3.49) is invertible, and therefore the error system (3.33) with boundary conditions (3.34) is equivalent to the target system (3.36) with boundary conditions (3.37).

This further implies that the target error system (3.36)–(3.37) will vanish within the same amount of time as the error system (3.33)–(3.34), and therefore analyzing either of them will yield the same convergence time.

It is thus guaranteed that the entire target system (3.36)–(3.37) is zero $\forall t \geq t_{1,min} = \int_0^1 \frac{dx}{\mu_2(x)} + \int_0^1 \frac{dx}{\lambda_1(x)}$ and hence also the estimates $\hat{\alpha}(x,t)$ and $\hat{\beta}(x,t)$ generated by (3.72) will also have converged to their correct values within this time.

□

3.4 Minimum Time Result for $2 + 2$ System

Now that an invertible Fredholm transformation $\mathcal{F}$ that transforms the minimum time convergent target system (3.36)–(3.37) into the error system (3.33)–(3.34) has been found, in turn allowing us to calculate the necessary observer gains $T^+(x)$ to guarantee minimum time convergence of the observer estimates, the focus will be shifted to the left half of Figure 3.1. The error system (3.47)–(3.48) will now be used as the target error system, and a Volterra transformation $\mathcal{V}$ will be defined which allows the transformation from this target system into a system of the form (3.22)–(3.23), but with new observer gains $P^+(x)$ and $P^-(x)$ which will guarantee convergence of the estimates $\hat{u}$, $\hat{v}$ to their true values in minimum time $t_{1,min}$. The Lemma and subsequent Theorem that will now be presented pertain to this result.

Lemma 3.5. *The Volterra backstepping transformation $\mathcal{V}$ defined in* (3.27) *transforms the target error system* (3.47) *with boundary conditions* (3.48) *into the error system* (3.22) *with boundary conditions* (3.23)*, but with $P^+(x)$, $P^-(x)$ defined as*

$$P^+(x) = M(x,1)\Lambda^+(1) + T^+(x) + \int_x^1 M(x,\xi)T^+(\xi)d\xi, \tag{3.73a}$$

$$P^-(x) = N(x,1)\Lambda^+(1) + \int_x^1 N(x,\xi)T^+(\xi)d\xi, \tag{3.73b}$$

respectively. $T^+(x)$ and $\Lambda^+(x)$ are as defined in (3.53) *and* (3.5) *respectively, whilst $M(x,\xi)$, $N(x,\xi)$ which can be denoted as in* (3.29) *satisfy the kernel PDE*

$$\Lambda^+(x)M_x(x,\xi) + M_\xi(x,\xi)\Lambda^+(\xi) + M(x,\xi)\Lambda^+_\xi(\xi) = \Sigma^{+-}(x)N(x,\xi), \tag{3.74a}$$

$$-\Lambda^-(x)N_x(x,\xi) + N_\xi(x,\xi)\Lambda^+(\xi) + N(x,\xi)\Lambda^+_\xi(\xi) = \Sigma^{-+}(x)M(x,\xi) \tag{3.74b}$$

with boundary conditions

$$\Lambda^+(x)M(x,x) - M(x,x)\Lambda^+(x) = 0, \tag{3.75a}$$

$$\Lambda^-(x)N(x,x) + N(x,x)\Lambda^+(x) = \Sigma^{-+}(x), \tag{3.75b}$$

$$Q_0N(0,\xi) = M(0,\xi) + H(\xi), \tag{3.75c}$$

$$M_{21}(x,1) = 0 \tag{3.75d}$$

defined over the upper triangular domain $\mathcal{T}_u = \{(x,\xi) \mid 0 \le x \le \xi \le 1\}$. Additionally the terms $\Lambda^-(x)$, $\Sigma^{+-}(x)$, $\Sigma^{-+}(x)$, Q_0 and $H(x)$ are all defined in Lemma 3.3.

Proof. **The $\tilde{u}$ subsystem**

Differentiating expression for $\tilde{u}(x,t)$ in the Volterra transformation (3.27) with respect to time, substituting the relevant target system dynamics from (3.47)–(3.48) and integrating by parts to obtain

$$\tilde{u}_t(x,t) = \tilde{\alpha}_t(x,t) + \int_x^1 M(x,\xi)\tilde{\alpha}_t(\xi,t)d\xi = -\Lambda^+(x)\tilde{\alpha}_x(x,t) + \Sigma^{+-}(x)\tilde{\beta}(x,t)$$
$$-\int_x^1 D^+(x,\xi)\tilde{\beta}(\xi,t)d\xi - T^+(x)\tilde{\alpha}(1,t) + \int_x^1 M(x,\xi)[-\Lambda^+(\xi)\tilde{\alpha}_\xi(\xi,t)$$

$$+\Sigma^{+-}(\xi)\tilde{\beta}(\xi,t)-\int_{\xi}^{1}D^{+}(\xi,s)\tilde{\beta}(s,t)ds-T^{+}(\xi)\tilde{\alpha}(1,t)]d\xi$$

$$\Rightarrow\quad\boxed{\begin{aligned}\tilde{u}_t(x,t)=&-\Lambda^{+}(x)\tilde{\alpha}_x(x,t)+\Sigma^{+-}(x)\tilde{\beta}(x,t)+\int_{x}^{1}[M(x,\xi)\Sigma^{+-}(\xi)\\&-D^{+}(x,\xi)-\int_{\xi}^{x}M(\xi,z)D^{+}(z,\xi)dz]\tilde{\beta}(\xi,t)d\xi\\&-M(x,1)\Lambda^{+}(1)\tilde{\alpha}(1,t)+M(x,x)\Lambda^{+}(x)\tilde{\alpha}(x,t)\\&+\int_{x}^{1}[M_{\xi}(x,\xi)\Lambda^{+}(\xi)+M(x,\xi)\Lambda_{\xi}^{+}(\xi)]\tilde{\alpha}(\xi,t)d\xi\\&-T^{+}(x)\tilde{\alpha}(1,t)-\int_{x}^{1}M(x,\xi)T^{+}(\xi)\tilde{\alpha}(1,t)d\xi.\end{aligned}}\tag{3.76}$$

Likewise, differentiating $\tilde{u}(x,t)$ in the Volterra transformation (3.27) with respect to space and applying the Leibniz integral rule, obtain

$$\begin{aligned}\tilde{u}_x(x,t)&=\tilde{\alpha}_x(x,t)+\frac{d}{dx}\int_{x}^{1}M(x,\xi)\tilde{\alpha}(\xi,t)d\xi\\&=\tilde{\alpha}_x(x,t)-M(x,x)\tilde{\alpha}(x,t)+\int_{x}^{1}M_x(x,\xi)\tilde{\alpha}(\xi,t)d\xi.\end{aligned}\tag{3.77}$$

Combining (3.76) and (3.77) with the original error system dynamics (3.25)–(3.26), the following is found for the $\tilde{u}$ subsystem

$$\begin{aligned}0&=\tilde{u}_t(x,t)+\Lambda^{+}(x)\tilde{u}_x(x,t)-\Sigma^{+-}(x)\tilde{v}(x,t)+P^{+}(x)\tilde{u}(1,t)\\&=\int_{x}^{1}[M(x,\xi)\Sigma^{+-}(\xi)-D^{+}(x,\xi)-\int_{\xi}^{x}M(\xi,s)D^{+}(s,\xi)ds]\tilde{\beta}(\xi,t)d\xi\\&-M(x,1)\Lambda^{+}(1)\tilde{\alpha}(1,t)+M(x,x)\Lambda^{+}(x)\tilde{\alpha}(x,t)+\int_{x}^{1}[M_{\xi}(x,\xi)\Lambda^{+}(\xi)\\&+M(x,\xi)\Lambda_{\xi}^{+}(\xi)]\tilde{\alpha}(\xi,t)d\xi-T^{+}(x)\tilde{\alpha}(1,t)-\int_{x}^{1}M(x,\xi)T^{+}(\xi)\tilde{\alpha}(1,t)d\xi\end{aligned}$$

$$\underbrace{-\Lambda^+(x)\tilde{\alpha}_x(x,t)+\Lambda^+(x)[\tilde{\alpha}_x(x,t)}_{=0}-M(x,x)\tilde{\alpha}(x,t)+\int_x^1 M_x(x,\xi)\tilde{\alpha}(\xi,t)d\xi]$$

$$\underbrace{\Sigma^{+-}(x)\tilde{\beta}(x,t)-\Sigma^{+-}(x)[\tilde{\beta}(x,t)}_{=0}+\int_x^1 N(x,\xi)\tilde{\alpha}(\xi,t)d\xi]+P^+(x)\tilde{\alpha}(1,t)$$

$$\Rightarrow \boxed{\begin{aligned}&[M(x,x)\Lambda^+(x)-\Lambda^+(x)M(x,x)]\tilde{\alpha}(x,t)\\&+\int_x^1[M_\xi(x,\xi)\Lambda^+(\xi)+M(x,\xi)\Lambda_\xi^+(\xi)+\Lambda^+(x)M_x(x,\xi)\\&-\Sigma^{+-}(x)N(x,\xi)]\tilde{\alpha}(\xi,t)d\xi\\&+\int_x^1[M(x,\xi)\Sigma^{+-}(\xi)-D^+(x,\xi)-\int_\xi^x M(\xi,s)D^+(s,\xi)ds]\tilde{\beta}(\xi,t)d\xi\\&+[P^+(x)-M(x,1)\Lambda^+(1)-T^+(x)-\int_x^1 M(x,\xi)T^+(\xi)d\xi]\tilde{\alpha}(1,t)\\&=0.\end{aligned}} \tag{3.78}$$

The $\tilde{v}$ subsystem

Performing the corresponding calculations for the $\tilde{v}(x,t)$ subsystem in (3.27) we find the equation corresponding to the time derivative is

$$\tilde{v}_t(x,t)=\tilde{\beta}_t(x,t)+\int_x^1 N(x,\xi)\tilde{\alpha}_t(\xi,t)d\xi=\Lambda^-(x)\tilde{\beta}_x(x,t)-\int_x^1 D^-(x,\xi)\tilde{\beta}(\xi,t)d\xi$$
$$+\int_x^1 N(x,\xi)[-\Lambda^+(\xi)\tilde{\alpha}_\xi(\xi,t)+\Sigma^{+-}(\xi)\tilde{\beta}(\xi,t)-\int_\xi^1 D^+(\xi,s)\tilde{\beta}(s,t)ds$$
$$-T^+(\xi)\tilde{\alpha}(1,t)]d\xi$$

$$\Rightarrow \boxed{\begin{aligned}\tilde{v}_t(x,t) &= \Lambda^-(x)\tilde{\beta}_x(x,t) + \int_x^1 [N(x,\xi)\Sigma^{+-}(\xi) - D^-(x,\xi) \\ &\quad - \int_\xi^x N(\xi,s)D^+(s,\xi)ds]\tilde{\beta}(\xi,t)d\xi - N(x,1)\Lambda^+(1)\tilde{\alpha}(1,t) \\ &\quad + N(x,x)\Lambda^+(x)\tilde{\alpha}(x,t) + \int_x^1 [N_\xi(x,\xi)\Lambda^+(\xi) \\ &\quad + N(x,\xi)\Lambda_\xi^+(\xi)]\tilde{\alpha}(\xi,t)d\xi - \int_x^1 N(x,\xi)T^+(\xi)\tilde{\alpha}(1,t)d\xi\end{aligned}} \tag{3.79}$$

and the one corresponding to the space derivative becomes

$$\begin{aligned}\tilde{v}_x(x,t) &= \tilde{\beta}_x(x,t) + \frac{d}{dx}\int_x^1 N(x,\xi)\tilde{\alpha}(\xi,t)d\xi \\ &= \tilde{\beta}_x(x,t) - N(x,x)\tilde{\alpha}(x,t) + \int_x^1 N_x(x,\xi)\tilde{\alpha}(\xi,t)d\xi.\end{aligned} \tag{3.80}$$

As with the $\tilde{u}$ subsystem, combining (3.79) and (3.80) with (3.25)–(3.26) for the $\tilde{v}$ subsystem we likewise obtain

$$\begin{aligned}0 &= \tilde{v}_t(x,t) - \Lambda^-(x)\tilde{v}_x(x,t) - \Sigma^{-+}(x)\tilde{u}(x,t) + P^-(x)\tilde{u}(1,t) \\ &= \int_x^1 [N(x,\xi)\Sigma^{+-}(\xi) - D^-(x,\xi) - \int_\xi^x N(\xi,s)D^+(s,\xi)ds]\tilde{\beta}(\xi,t)d\xi \\ &\quad -N(x,1)\Lambda^+(1)\tilde{\alpha}(1,t) + N(x,x)\Lambda^+(x)\tilde{\alpha}(x,t) \\ &\quad + \int_x^1 [N_\xi(x,\xi)\Lambda^+(\xi) + N(x,\xi)\Lambda_\xi^+(\xi)]\tilde{\alpha}(\xi,t)d\xi \\ &\quad - \int_x^1 N(x,\xi)T^+(\xi)\tilde{\alpha}(1,t)d\xi + \underbrace{\Lambda^-(x)\tilde{\beta}_x(x,t) - \Lambda^-(x)[\tilde{\beta}_x(x,t)}_{=0} - N(x,x)\tilde{\alpha}(x,t) \\ &\quad + \int_x^1 N_x(x,\xi)\tilde{\alpha}(\xi,t)d\xi] - \Sigma^{-+}(x)[\tilde{\alpha}(x,t) + \int_x^1 M(x,\xi)\tilde{\alpha}(\xi,t)d\xi] + P^-(x)\tilde{\alpha}(1,t)\end{aligned}$$

$$
\Rightarrow \boxed{\begin{aligned}
&[N(x,x)\Lambda^+(x) + \Lambda^-(x)N(x,x) - \Sigma^{-+}(x)]\tilde{\alpha}(x,t) \\
&+ \int_x^1 [N_\xi(x,\xi)\Lambda^+(\xi) + N(x,\xi)\Lambda_\xi^+(\xi) \\
&- \Lambda^-(x)N_x(x,\xi) - \Sigma^{-+}(x)M(x,\xi)]\tilde{\alpha}(\xi,t)d\xi \\
&+ \int_x^1 [N(x,\xi)\Sigma^{+-}(\xi) - D^-(x,\xi) - \int_\xi^x N(\xi,s)D^+(s,\xi)ds]\tilde{\beta}(\xi,t)d\xi \\
&+ [P^-(x) - N(x,1)\Lambda^+(1) - \int_x^1 N(x,\xi)T^+(\xi)d\xi]\tilde{\alpha}(1,t) \\
&= 0
\end{aligned}} \tag{3.81}
$$

Calculating Observer Gains

Arguing in (3.78) and (3.81) that the errors $\tilde{\alpha}(x,t) \neq 0$, $\tilde{\beta}(x,t) \neq 0$, in general, one obtains the kernel PDEs (3.74) and first two boundary conditions from (3.75). Next, set $x = 0$ in (3.27) and substitute this into (3.23a), and applying (3.34a) yields

$$
\int_0^1 H(\xi)\tilde{\alpha}(\xi,t)d\xi = \int_0^1 [Q_0 N(0,\xi) - M(0,\xi)]\tilde{\alpha}(\xi,t)d\xi, \tag{3.82}
$$

from which we find (3.75c). For the general $n + m$ case, in Hu et al. (2016) and Anfinsen and Aamo (2017b) the boundary condition (3.18d) is added. However, in this case $\sigma_{21}^{++}(x) = 0$ which yields the fourth boundary condition from (3.75). The definitions for $D^+(x,\xi)$ and $D^-(x,\xi)$ as presented in (3.28) are also obtained, and the new definitions of $P^+(x)$ and $P^-(x)$ as given in (3.73) can be calculated. □

The well-posedness of the observer kernel PDEs are guaranteed by Theorem 3.2 from Hu et al. (2016)[5], which proves well-posedness of equations which have the same form as (3.74)–(3.75). As discussed previously in this chapter, the kernel boundary conditions forcing the restriction (3.12) can be modified for the 2+2 system (3.1)–(3.2), since isotachic[6] states do not cause ill-defined boundary conditions.

Finally, the main result for this chapter, which gives a minimum time convergent collocated observer for the original $2 + 2$ system (3.1) with boundary conditions (3.2) can be now presented and proved. This is done in the following theorem.

[5]Note that in Hu et al. (2016) the well-posedness proof was performed for the case of constant system coefficients, but Remark 1 from that paper stated that the same methods can be carried out for spatially varying coefficients, albeit more technical calculations being involved.

[6]Different states that have the same transport velocity.

Theorem 3.6 (Minimum time collocated observer for 2 + 2 system)**.** *Consider the collocated observer*

$$\check{u}_t(x,t) + \Lambda^+(x)\check{u}_x(x,t) = \Sigma^{+-}(x)\check{v}(x,t) + P^+(x)(y(t) - \check{u}(1,t)), \tag{3.83a}$$
$$\check{v}_t(x,t) - \Lambda^-(x)\check{v}_x(x,t) = \Sigma^{-+}(x)\check{u}(x,t) + P^-(x)(y(t) - \check{u}(1,t)), \tag{3.83b}$$
$$\check{u}(0,t) = Q_0\check{v}(0,t), \tag{3.83c}$$
$$\check{v}(1,t) = R_1 y(t) + U(t) \tag{3.83d}$$

relying on the right boundary measurement $y(t) = \bar{u}(1,t)$*. The observer gains* $P^+(x)$ *and* $P^-(x)$ *are defined by* (3.73)*, and the other coefficients are defined the same way as in* (3.5)*. The estimates* $\check{u}(x,t)$*,* $\check{v}(x,t)$ *generated by* (3.83) *converge to their true values* $\bar{u}(x,t)$*,* $\bar{v}(x,t)$ *representing the states of the original* $2+2$ *system* (3.1)–(3.2) *within minimum time* $t_{1,min} = \int_0^1 \frac{dx}{\mu_2(x)} + \int_0^1 \frac{dx}{\lambda_1(x)}$.

Proof. Using the estimation errors $\tilde{u}(x,t) = \bar{u}(x,t) - \check{u}(x,t)$, $\tilde{v}(x,t) = \bar{v}(x,t) - \check{v}(x,t)$, subtract the collocated observer (3.83) from the original system dynamics (3.1) with boundary conditions (3.2), and obtain the error system (3.25)–(3.26) having $P^+(x)$ and $P^-(x)$ as defined in (3.73). We know from Lemma 3.5 that the Volterra transformation (3.27) transforms the target system given by (3.47)–(3.48) to this error system. As Volterra backstepping transformations are always invertible due to their "triangular structure", the convergence properties of these two systems must be identical.

Also, according to Lemma 3.4, the observer given by (3.72) produces estimates $\hat{\alpha}(x,t)$, $\hat{\beta}(x,t)$ of the states $\alpha(x,t)$, $\beta(x,t)$, respectively, of the system (3.33)–(3.34) that converge to their true values exponentially within time $t_{1,min} = \int_0^1 \frac{dx}{\mu_2(x)} + \int_0^1 \frac{dx}{\lambda_1(x)}$. Applying the definition of the error variables $\tilde{\alpha}(x,t) = \alpha(x,t) - \hat{\alpha}(x,t)$, $\tilde{\beta}(x,t) = \beta(x,t) - \hat{\beta}(x,t)$, this in turn implies that the target error system (3.47)–(3.48) vanishes within time t_{min}.

Hence also the error system (3.25)–(3.26) vanishes within time t_{min}. From the definition of the error system the only logical conclusion is that the estimates $\check{u}(x,t)$, $\check{v}(x,t)$ generated by (3.83) converge to their true values $\bar{u}(x,t)$, $\bar{v}(x,t)$ respectively within time $t_{1,min}$ given by (3.7). □

This concludes the derivation of the minimum time convergent collocated observer for the $2+2$ system (3.1)–(3.2). In the next section the theory developed here will be applied to derive an observer for a 2×2 system which relies on measurements from both left and right boundaries and which can be shown to converge quicker, in general, than an observer only relying on a single boundary measurement.

Chapter 4

Minimum Time 2×2 Bilateral Observer Design

4.1 Problem Statement

Consider the following first-order coupled 2×2 linear hyperbolic PDE system defined for $x \in [0, 1]$ and $t \in [0, \infty)$ with scalar states $u(x, t)$ and $v(x, t)$ and dynamics governed by

$$u_t(x,t) + \lambda(x)u_x(x,t) = \sigma^+(x)v(x,t), \tag{4.1a}$$
$$v_t(x,t) - \mu(x)v_x(x,t) = \sigma^-(x)u(x,t), \tag{4.1b}$$

along with boundary conditions

$$u(0,t) = Qv(0,t) + U_1(t) \tag{4.2a}$$
$$v(1,t) = Ru(1,t) + U_2(t) \tag{4.2b}$$

and the initial conditions defined by

$$u(x,0) = u_0(x), \tag{4.3a}$$
$$v(x,0) = v_0(x), \tag{4.3b}$$

where it is assumed that $u_0(x), v_0(x) \in L_2([0, 1])$. The transport speeds $\lambda(x), \mu(x) \in C^1([0, 1])$ and are both defined as positive functions, so that

$$\lambda(x) > 0, \tag{4.4a}$$
$$\mu(x) > 0. \tag{4.4b}$$

To facilitate our design, we introduce without loss of generality[1] the assumption[2]

$$\lambda(x) \leq \overline{\lambda} \leq \underline{\mu} \leq \mu(x), \tag{4.5}$$

where clearly $\overline{\lambda} = \max_{x\in(0,1)} \lambda(x)$ and $\underline{\mu} = \min_{x\in(0,1)} \mu(x)$.

For the coupling coefficients, it is assumed that the functions are satisfying $\sigma^+(x), \sigma^-(x) \in C^0([0,1])$. The terms $U_1(t)$ and $U_2(t)$ are considered boundary control inputs. From (4.2), with our definition that $x = 0$ is the left boundary and $x = 1$ is the right boundary, we see that $U_1(t)$ is the left boundary control input, whereas $U_2(t)$ is the right boundary control input. Their design is not the focus of this dissertation, but they are placed in the model above for completeness and for the possibility of implementing a controller actuating both sides of the spatial domain. Finally, the reflection coefficients $Q, R \in \mathbb{R}$ are real constants.

We assume that both the right boundary measurement $y_1(t)$ and left boundary measurement $y_2(t)$, defined as

$$y_1(t) = u(1,t), \tag{4.6a}$$
$$y_2(t) = v(0,t), \tag{4.6b}$$

are available. The goal of this chapter is to derive a bilateral observer for (4.1)–(4.2) utilizing both measurements $y_1(t)$ and $y_2(t)$ in (4.6) which can be guaranteed to produce state estimates converging to their correct values quicker, ideally within time $t_{2,min}$, than the theoretical minimal convergence time $t_{1,min}$ for an observer using only a single boundary measurement. The relationship between the two convergence times $t_{1,min}$ and $t_{2,min}$, which are based on the definitions given in (2.49)–(2.50), can for 2×2 systems of the form (4.1)–(4.2) be expressed as

$$\max\left\{\int_0^1 \frac{dx}{\mu(x)}, \int_0^1 \frac{dx}{\lambda(x)}\right\} = t_{2,min} < t_{1,min} = \int_0^1 \frac{dx}{\mu(x)} + \int_0^1 \frac{dx}{\lambda(x)}. \tag{4.7}$$

One should note that an immediate consequence of (4.5) is that $t_{2,min}$ in (4.7) is

$$t_{2,min} = \int_0^1 \frac{dx}{\lambda(x)} \tag{4.8}$$

Theoretical results derived in Chapter 3 will be applied to achieve this. Chapter 4 is thus organized as follows. Firstly the problem to be solved has been defined in Section 4.1. Next, in Section 4.2, it will be shown how the 2×2 system (4.1)–(4.2) can be transformed to take the form of the $2 + 2$ system (3.1)–(3.2), laying the groundwork for applying the observer results for the $2 + 2$ system to the 2×2 system. Finally, Section 4.3 presents the minimum time bilateral observer for the

[1] In view of the symmetry of (4.1)–(4.2), λ and μ can be relabelled if necessary.

[2] Note that for constant transport speeds this assumption is implicit. Due to the way the bilateral observer here is derived, the assumption is needed in order to help in satisfying (3.6), which is a prerequisite for well-posedness of the observer kernels, as was discussed in Chapter 3.

2×2 system, and proves its minimum time convergence. This completes the 2×2 minimum time observer derivation.

4.2 Transforming 2×2 System to $2 + 2$ System

First it will be shown that the 2×2 system (4.1)–(4.2) can be transformed into a $2 + 2$ system of the form (3.1)–(3.2) by splitting the spatial domain at an interior point $x_s \in (0, 1)$ and subsequently defining a spatial coordinate transformation which is a function of this splitting point. The approach taken here can be visualized as in Figure 4.1, which shows the original 2×2 system being split at the interior point, and subsequently Figure 4.2 showing the new $2 + 2$ system after reassigning the states within the $2 + 2$ framework. Within the scope of this chapter we use $\bar{x} \in [0, 1]$ to denote the spatial variable of the $2 + 2$ system (3.1)–(3.2), to illustrate that it is different from the spatial variable x over which the 2×2 system (4.1)–(4.2) is defined.

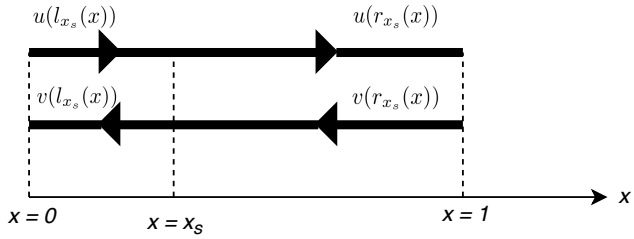

Figure 4.1: The original 2×2 system on the x domain is split at some $x_s \in (0, 1)$.

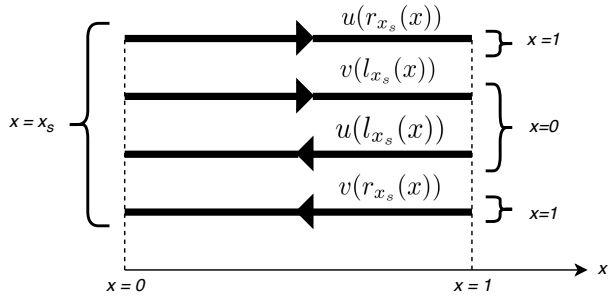

Figure 4.2: The 2×2 system x domain is folded over the splitting point x_s and stretched to fit into the $2 + 2$ system x domain.

In order to perform this transformation, we start by introducing the coordinate transforms r_{x_s} and l_{x_s}, with $r_{x_s} : [x_s, 1] \to [0, 1]$ defined as

$$r_{x_s}(x) = \frac{x - x_s}{1 - x_s} \tag{4.9}$$

and $l_{x_s} : [0, x_s] \to [0, 1]$ defined by

$$l_{x_s}(x) = \frac{x_s - x}{x_s}. \tag{4.10}$$

These can easily be seen to be invertible with respective inverses, $r_{x_s}^{-1} : [0,1] \to [x_s, 1]$, defined as

$$r_{x_s}^{-1}(x) = x_s + x(1 - x_s), \tag{4.11}$$

and $l_{x_s}^{-1} : [0,1] \to [0, x_s]$ given by

$$l_{x_s}^{-1}(x) = x_s(1 - x). \tag{4.12}$$

We can now use these spatial coordinate transformations to express the states of u and v in the left and right sub-domains, as functions of a spatial variable $x \in [0,1]$ in the following manner. u and v in the left sub-domain can be given as

$$u(l_{x_s}^{-1}(x)) = u(x_s(1 - x)) \tag{4.13a}$$
$$v(l_{x_s}^{-1}(x)) = v(x_s(1 - x)) \tag{4.13b}$$

whilst u and v in the right sub-domain become

$$u(r_{x_s}^{-1}(x)) = u(x_s + x(1 - x_s)) \tag{4.14a}$$
$$v(r_{x_s}^{-1}(x)) = v(x_s + x(1 - x_s)) \tag{4.14b}$$

Comparing (4.13)–(4.14) to Fig. 4.1 and Fig. 4.2, we see that (4.13a) and (4.14b) could be assigned to v_1 and v_2 in the $2 + 2$ system (3.1)–(3.2), whilst (4.13b) and (4.14a) can be assigned to the states u_1 and u_2. Due to the four possible ways these assignments can be done, we can define four state transformations $\mathscr{T}_{i,x_s} : (L_2([0,1]))^2 \to (L_2([0,1]))^4$, $i \in \{1, \ldots, 4\}$ as follows.

$$\mathscr{T}_{1,x_s}[u,v](x) = \left(\begin{bmatrix} u(x_s + x(1 - x_s)) \\ v(x_s(1 - x), t) \end{bmatrix}, \begin{bmatrix} u(x_s(1 - x)) \\ v(x_s + x(1 - x_s)) \end{bmatrix} \right) \tag{4.15a}$$
$$\mathscr{T}_{2,x_s}[u,v](x) = \left(\begin{bmatrix} v(x_s(1 - x), t) \\ u(x_s + x(1 - x_s)) \end{bmatrix}, \begin{bmatrix} u(x_s(1 - x)) \\ v(x_s + x(1 - x_s)) \end{bmatrix} \right) \tag{4.15b}$$
$$\mathscr{T}_{3,x_s}[u,v](x) = \left(\begin{bmatrix} u(x_s + x(1 - x_s)) \\ v(x_s(1 - x), t) \end{bmatrix}, \begin{bmatrix} v(x_s + x(1 - x_s)) \\ u(x_s(1 - x)) \end{bmatrix} \right) \tag{4.15c}$$
$$\mathscr{T}_{4,x_s}[u,v](x) = \left(\begin{bmatrix} v(x_s(1 - x), t) \\ u(x_s + x(1 - x_s)) \end{bmatrix}, \begin{bmatrix} v(x_s + x(1 - x_s)) \\ u(x_s(1 - x)) \end{bmatrix} \right) \tag{4.15d}$$

The four transformations (4.15) can also be shown to be invertible, with inverses

$\mathscr{T}_{i,x_s}^{-1}:(L_2([0,1]))^4\to(L_2([0,1]))^2$ defined as

$$\mathscr{T}_{1,x_s}^{-1}[\bar{u},\bar{v}](x)=\begin{cases}(v_1(\frac{x_s-x}{x_s}),u_2(\frac{x_s-x}{x_s})), & x\in[0,x_s]\\(u_1(\frac{x-x_s}{1-x_s}),v_2(\frac{x-x_s}{1-x_s})), & x\in[x_s,1]\end{cases}\tag{4.16a}$$

$$\mathscr{T}_{2,x_s}^{-1}[\bar{u},\bar{v}](x)=\begin{cases}(v_1(\frac{x_s-x}{x_s}),u_1(\frac{x_s-x}{x_s})), & x\in[0,x_s]\\(u_2(\frac{x-x_s}{1-x_s}),v_2(\frac{x-x_s}{1-x_s})), & x\in[x_s,1]\end{cases}\tag{4.16b}$$

$$\mathscr{T}_{3,x_s}^{-1}[\bar{u},\bar{v}](x)=\begin{cases}(v_2(\frac{x_s-x}{x_s}),u_2(\frac{x_s-x}{x_s})), & x\in[0,x_s]\\(u_1(\frac{x-x_s}{1-x_s}),v_1(\frac{x-x_s}{1-x_s})), & x\in[x_s,1]\end{cases}\tag{4.16c}$$

$$\mathscr{T}_{4,x_s}^{-1}[\bar{u},\bar{v}](x)=\begin{cases}(v_2(\frac{x_s-x}{x_s}),u_1(\frac{x_s-x}{x_s})), & x\in[0,x_s]\\(u_2(\frac{x-x_s}{1-x_s}),v_1(\frac{x-x_s}{1-x_s})), & x\in[x_s,1]\end{cases}\tag{4.16d}$$

After transforming the 2×2 system to a $2+2$ system, the goal is to apply the collocated $2+2$ observer (3.83) to find a bilateral 2×2 observer. An important detail, therefore, when transforming is to maintain well-posedness of the observer kernel equations (3.74)–(3.75) and (3.51)–(3.52), which follows if (3.6) is satisfied. Depending on $\lambda(x)$ and $\mu(x)$ in (4.1)–(4.2) and the splitting point $x_s\in(0,1)$, due to the definitions of (4.9) and (4.10), it will be seen that this can be guaranteed if one of the following four pairs of inequalities hold $\forall x\in[0,1]$:

$$\frac{\lambda(x_s+x(1-x_s))}{1-x_s}\le\frac{\mu(x_s(1-x))}{x_s},\frac{\lambda(x_s(1-x))}{x_s}\ge\frac{\mu(x_s+x(1-x_s))}{1-x_s},\tag{4.17a}$$

$$\frac{\lambda(x_s+x(1-x_s))}{1-x_s}\ge\frac{\mu(x_s(1-x))}{x_s},\frac{\lambda(x_s(1-x))}{x_s}\ge\frac{\mu(x_s+x(1-x_s))}{1-x_s},\tag{4.17b}$$

$$\frac{\lambda(x_s+x(1-x_s))}{1-x_s}\le\frac{\mu(x_s(1-x))}{x_s},\frac{\lambda(x_s(1-x))}{x_s}\le\frac{\mu(x_s+x(1-x_s))}{1-x_s},\tag{4.17c}$$

$$\frac{\lambda(x_s+x(1-x_s))}{1-x_s}\ge\frac{\mu(x_s(1-x))}{x_s},\frac{\lambda(x_s(1-x))}{x_s}\le\frac{\mu(x_s+x(1-x_s))}{1-x_s},\tag{4.17d}$$

Depending on which of (4.17) $\forall x\in[0,1]$, if any, the correct transformation from (4.15) should be chosen accordingly[3]. We now present a result defining how the $2+2$ system coefficients will be defined in terms of 2×2 system coefficients when applying the transformations (4.15).

Lemma 4.1. *Consider the 2×2 linear hyperbolic PDE system (4.1)–(4.2) and choose a point $x_s\in(0,1)$. Assume that of the four cases (4.17), case i, where $i\in\{1,\dots,4\}$, holds true. Assigning*

$$(\bar{u}(x,t),\bar{v}(x,t))=\mathscr{T}_{i,x_s}[u,v](x,t)\tag{4.18}$$

will map the 2×2 system (4.1)-(4.2) into the $2+2$ linear hyperbolic system (3.1)–(3.2), where the coefficients are as defined in Appendix A.

[3]The inequality pairs in (4.17) have been listed so they correspond directly to the transformations in (4.15); for example, if (4.17a) holds, then the transformation (4.15a) should be used.

Proof. The proof will be conducted assuming $\mathscr{T}_{3,x_s}$ in (4.15c) has been applied. The steps of the proof for the three other cases (4.15a)–(4.15b) and (4.15d) are identical to the steps presented here, so they will be omitted.

Applying $(u(x,t), v(x,t)) = \mathscr{T}_{3,x_s}^{-1}[u_1, u_2, v_1, v_2](x,t)$ directly, we obtain

$$\bar{u}(x,t) = \begin{bmatrix} u_1(x,t) \\ u_2(x,t) \end{bmatrix} = \begin{bmatrix} u(x_s + x(1-x_s), t) \\ v(x_s(1-x), t) \end{bmatrix} \tag{4.19}$$

and $\bar{v}(\bar{x},t) = [v_1(\bar{x},t), v_2(\bar{x},t)]^T$ as

$$\bar{v}(x,t) = \begin{bmatrix} v_1(x,t) \\ v_2(x,t) \end{bmatrix} = \begin{bmatrix} v(x_s + x(1-x_s), t) \\ u(x_s(1-x), t) \end{bmatrix}. \tag{4.20}$$

Next, differentiating (4.19) and (4.20) with respect to time the following will be obtained:

$$\bar{u}_t(x,t) = \begin{bmatrix} u_t(x_s + x(1-x_s), t) \\ v_t(x_s(1-x), t) \end{bmatrix}, \tag{4.21a}$$

$$\bar{v}_t(x,t) = \begin{bmatrix} v_t(x_s + x(1-x_s), t) \\ u_t(x_s(1-x), t) \end{bmatrix}. \tag{4.21b}$$

Likewise, differentiating (4.19) and (4.20) with respect to x we obtain that

$$\bar{u}_x(x,t) = \begin{bmatrix} (1-x_s)u_x(x_s + x(1-x_s), t) \\ -x_s v_x(x_s(1-x), t) \end{bmatrix}, \tag{4.22a}$$

$$\bar{v}_{\bar{x}}(\bar{x},t) = \begin{bmatrix} (1-x_s)v_x(x_s + x(1-x_s), t) \\ -x_s u_x(x_s(1-x), t) \end{bmatrix}. \tag{4.22b}$$

Next, inserting (4.21)–(4.22) into the $2 + 2$ system framework (3.1), and comparing to (4.1), one obtains the coefficients assignments

$$\Lambda^+(x) = \begin{bmatrix} \lambda_1(x) & 0 \\ 0 & \lambda_2(x) \end{bmatrix} = \begin{bmatrix} \frac{\lambda(x_s + x(1-x_s))}{1-x_s} & 0 \\ 0 & \frac{\mu(x_s(1-x))}{x_s} \end{bmatrix}, \tag{4.23a}$$

$$\Lambda^-(x) = \begin{bmatrix} \mu_1(x) & 0 \\ 0 & \mu_2(x) \end{bmatrix} = \begin{bmatrix} \frac{\mu(x_s + x(1-x_s))}{1-x_s} & 0 \\ 0 & \frac{\lambda(x_s(1-x))}{x_s} \end{bmatrix}, \tag{4.23b}$$

from which we can readily confirm that (4.17c) and (3.6) represent the same relation.

The coupling coefficients are found as

$$\Sigma^{+-}(x) = \begin{bmatrix} \sigma_{11}^{+-}(x) & \sigma_{12}^{+-}(x) \\ \sigma_{21}^{+-}(x) & \sigma_{22}^{+-}(x) \end{bmatrix} = \begin{bmatrix} \sigma^{+}(x_s + x(1-x_s)) & 0 \\ 0 & \sigma^{-}(x_s(1-x)) \end{bmatrix}, \tag{4.24a}$$

$$\Sigma^{-+}(x) = \begin{bmatrix} \sigma_{11}^{-+}(x) & \sigma_{12}^{-+}(x) \\ \sigma_{21}^{-+}(x) & \sigma_{22}^{-+}(x) \end{bmatrix} = \begin{bmatrix} \sigma^{-}(x_s + x(1-x_s)) & 0 \\ 0 & \sigma^{+}(x_s(1-x)) \end{bmatrix}. \tag{4.24b}$$

In order to obtain boundary conditions from the 2×2 system that fit into the $2+2$ framework boundary conditions (3.2), start by setting $x = 0$ and $x = 1$ into (4.19) and (4.20) which gives

$$\bar{u}(0,t) = \begin{bmatrix} u_1(0,t) \\ u_2(0,t) \end{bmatrix} = \begin{bmatrix} u(x_s,t) \\ v(x_s,t) \end{bmatrix}, \tag{4.25a}$$

$$\bar{v}(0,t) = \begin{bmatrix} v_1(0,t) \\ v_2(0,t) \end{bmatrix} = \begin{bmatrix} v(x_s,t) \\ u(x_s,t) \end{bmatrix}, \tag{4.25b}$$

and

$$\bar{u}(1,t) = \begin{bmatrix} u_1(1,t) \\ u_2(1,t) \end{bmatrix} = \begin{bmatrix} u(1,t) \\ v(0,t) \end{bmatrix}, \tag{4.26a}$$

$$\bar{v}(1,t) = \begin{bmatrix} v_1(1,t) \\ v_2(1,t) \end{bmatrix} = \begin{bmatrix} v(1,t) \\ u(0,t) \end{bmatrix}, \tag{4.26b}$$

respectively. From (4.25) observe that $u_1(0,t) = v_2(0,t)$ and $u_2(0,t) = v_1(0,t)$. Comparing this with the left boundary conditions for the $2+2$ system given in (3.1), the left reflection coefficients

$$Q_0 = \begin{bmatrix} Q_{11} & Q_{12} \\ Q_{21} & Q_{22} \end{bmatrix} = \begin{bmatrix} 0 & 1 \\ 1 & 0 \end{bmatrix} \tag{4.27}$$

are easily obtained. For the right reflection coefficient matrix R_1, substitute the individual equations in (4.26) into the 2×2 boundary conditions (4.2), and comparing with the $2+2$ right boundary conditions in (3.2) one finds

$$R_1 = \begin{bmatrix} R_{11} & R_{12} \\ R_{21} & R_{22} \end{bmatrix} = \begin{bmatrix} Q & 0 \\ 0 & R \end{bmatrix} \tag{4.28}$$

and additionally the right boundary control can be assigned as

$$U(t) = \begin{bmatrix} \bar{U}_1(t) \\ \bar{U}_2(t) \end{bmatrix} = \begin{bmatrix} U_2(t) \\ U_1(t) \end{bmatrix}. \tag{4.29}$$

□

4.3 Minimum Time Observer Result for 2×2 System

Now that it has been shown that the 2×2 system (4.1)–(4.2) can be transformed into a $2+2$ system of the form (3.1)–(3.2), the minimum time collocated observer for $2+2$ systems of this form derived in the previous chapter can be applied to obtain a bilateral observer for the 2×2 system (4.1)–(4.2). Consider the bilateral observer

$$\begin{aligned}
\hat{u}_t(x,t) + \lambda(x)\hat{u}_x(x,t) &= \sigma^+(x)\hat{v}(x,t) + P^{++}(x)(y_1(t) - \hat{u}(1,t)) \\
&\quad + P^{+-}(x)(y_2(t) - \hat{v}(0,t)), && \text{(4.30a)} \\
\hat{v}_t(x,t) - \mu(x)\hat{v}_x(x,t) &= \sigma^-(x)\hat{u}(x,t) + P^{-+}(x)(y_1(t) - \hat{u}(1,t)) \\
&\quad + P^{--}(x)(y_2(t) - \hat{v}(0,t)), && \text{(4.30b)} \\
\hat{u}(0,t) &= Qy_2(t) + U_1(t), && \text{(4.30c)} \\
\hat{v}(1,t) &= Ry_1(t) + U_2(t), && \text{(4.30d)}
\end{aligned}$$

relying on measurements $y_1(t)$ and $y_2(t)$ defined in (4.6), where P^{++}, P^{+-}, P^{-+} and P^{--} are output injection gains to be designed. The next result presents assignments of these in terms of the output injection gains P^+ and P^- of a $2+2$ collocated observer for a $2+2$ hyperbolic system defined in terms of one of the four mappings (4.15).

Lemma 4.2. *Consider the collocated observer* (3.83) *for the* $2+2$ *linear hyperbolic system defined by applying transformation* $\mathscr{T}_{i,x_s}$ *in* (4.18)*. Applying the inverse transform* $\mathscr{T}_{i,x_s}^{-1}$ *to the state estimates* $\check{u}, \check{v}$ *produced by* (3.83)*, we can define*

$$(\hat{u}(x,t), \hat{v}(x,t)) = \mathscr{T}_{i,x_s}^{-1}[\check{u}_1, \check{u}_2, \check{v}_1, \check{v}_2](x,t). \tag{4.31}$$

Then $\hat{u}$*,* $\hat{v}$ *are state estimates generated by the bilateral observer* (4.30) *with observer gains defined in Appendix A.*

Proof. Since one of the four (4.17) was assumed when defining the $2+2$ system according to (4.18), the kernel equations (3.74)–(3.75) and (3.51)–(3.52) will be well-posed, implying the observer gains (3.73) are well-defined.

For the remainder of the proof we assume (4.16c) is applied. The steps of the first section for the three other cases (4.16a)–(4.16c) and (4.16d) are identical to the steps presented here, so they will be omitted. Due to (4.15c) having been applied to define the $2+2$ hyperbolic system, we know from Lemma 4.1 that $\check{u}$ is defined as

$$\breve{u}(x,t) = \begin{bmatrix} \hat{u}(x_s + x(1-x_s), t) \\ \hat{v}(x_s(1-x), t) \end{bmatrix} \tag{4.32}$$

and $\breve{v}$ is

$$\breve{v}(x,t) = \begin{bmatrix} \hat{v}(x_s + x(1-x_s), t) \\ \hat{u}(x_s(1-x), t) \end{bmatrix}. \tag{4.33}$$

Substituting (4.32)–(4.33), along with their respective spatial and temporal derivatives, which take the same form as in Lemma 4.1, and the coefficient assignments (4.23)–(4.24), into the minimum time $2+2$ collocated observer presented in Theorem 3.6 we find

$$\begin{aligned}
\hat{u}_t(x_s + x(1-x_s), t) &= -\frac{\lambda(x_s + x(1-x_s))}{1-x_s}(1-x_s)\hat{u}_x(x_s + x(1-x_s), t) \\
&\quad + \sigma^+(x_s + x(1-x_s))\hat{v}(x_s + x(1-x_s), t) \\
&\quad + P_{11}^+(x)[\bar{y}_1(t) - \hat{u}(1,t)] + P_{12}^+(x)[\bar{y}_2(t) - \hat{v}(0,t)], \qquad (4.34a) \\
\hat{v}_t(x_s(1-x), t) &= -\frac{\mu(x_s(1-x))}{x_s}(-x_s)\hat{v}_x(x_s(1-x), t) \\
&\quad + \sigma^-(x_s(1-x))\hat{u}(x_s(1-x)) \\
&\quad + P_{21}^+(x)[\bar{y}_1(t) - \hat{u}(1,t)] + P_{22}^+(x)[\bar{y}_2(t) - \hat{v}(0,t)], \qquad (4.34b) \\
\hat{v}_t(x_s + x(1-x_s), t) &= \frac{\mu(x_s + x(1-x_s))}{1-x_s}(1-x_s)\hat{v}_x(x_s + x(1-x_s), t) \\
&\quad = \sigma^-(x_s + x(1-x_s))\hat{u}(x_s + x(1-x_s)) \\
&\quad + P_{11}^-(x)[\bar{y}_1(t) - \hat{u}(1,t)] + P_{12}^-(x)[\bar{y}_2(t) - \hat{v}(0,t)], \qquad (4.34c) \\
\hat{u}_t(x_s(1-x), t) &= \frac{\lambda(x_s(1-x))}{x_s}(-x_s)\hat{u}_x(x_s(1-x), t) \\
&\quad + \sigma^+(x_s(1-x))\hat{v}(x_s(1-x), t) \\
&\quad + P_{21}^-(x)[\bar{y}_1(t) - \hat{u}(1,t)] + P_{22}^-(x)[\bar{y}_2(t) - \hat{v}(0,t)]. \qquad (4.34d)
\end{aligned}$$

The measurement assignment

$$y(t) = \begin{bmatrix} \bar{y}_1(t) \\ \bar{y}_2(t) \end{bmatrix} = \begin{bmatrix} y_1(t) \\ y_2(t) \end{bmatrix} \tag{4.35}$$

is easily obtained by observing the error terms that are multiplied by the observer gains in (4.34). Next, comparing the four equations (4.34) with the two first equations of the bilateral observer (4.30), one can see that these two sets of equations represent the same observer, with two of the equations in (4.34) being for all points in the left sub-domain $[0, x_s]$, and the other two equations representing the observer for all points in the right sub-domain $[x_s, 1]$. Applying the spatial coordinate transformations $l_{x_s} : [0, x_s] \to [0, 1]$ defined in (4.9) to (4.34d) and (4.34b) we find

the following observer PDEs $\forall x \in [0, x_s)$,

$$\hat{u}_t(x,t) + \lambda(x)\hat{u}_x(x,t) - \sigma^+(x)\hat{v}(x,t) = P_{21}^-(\frac{x_s - x}{x})[y_1(t) - \hat{u}(1,t)] \tag{4.36a}$$

$$+ P_{22}^-(\frac{x_s - x}{x})[y_2(t) - \hat{v}(0,t)], \tag{4.36b}$$

$$\hat{v}_t(x,t) - \mu(x)\hat{v}_x(x,t) - \sigma^-(x)\hat{u}(x,t) = P_{21}^+(\frac{x_s - x}{x})[y_1(t) - \hat{u}(1,t)] \tag{4.36c}$$

$$+ P_{22}^+(\frac{x_s - x}{x})[y_2(t) - \hat{v}(0,t)] \tag{4.36d}$$

whereas $\forall x \in [x_s, 1]$ we obtain by applying $r_{x_s} : [x_s, 1] \to [0, 1]$ to (4.34a) and (4.34c) that

$$\hat{u}_t(x,t) + \lambda(x)\hat{u}_x(x,t) - \sigma^+(x)\hat{v}(x,t) = P_{11}^+(\frac{x - x_s}{1 - x_s})[y_1(t) - \hat{u}(1,t)] \tag{4.37a}$$

$$+ P_{12}^+(\frac{x - x_s}{1 - x_s})[y_2(t) - \hat{v}(0,t)], \tag{4.37b}$$

$$\hat{v}_t(x,t) - \mu(x)\hat{v}_x(x,t) = \sigma^-(x)\hat{u}(x,t) = P_{11}^-(\frac{x - x_s}{1 - x_s})[y_1(t) - \hat{u}(1,t)] \tag{4.37c}$$

$$+ P_{12}^-(\frac{x - x_s}{1 - x_s})[y_2(t) - \hat{v}(0,t)] \tag{4.37d}$$

Comparing with (4.30), the observer gains are easily seen to be

$$P^{++}(x) = \begin{cases} P_{21}^-(\frac{x_s - x}{x_s}), & 0 \le x < x_s \\ P_{11}^+(\frac{x - x_s}{1 - x_s}), & x_s \le x \le 1 \end{cases}, \tag{4.38a}$$

$$P^{+-}(x) = \begin{cases} P_{22}^-(\frac{x_s - x}{x_s}), & 0 \le x < x_s \\ P_{12}^+(\frac{x - x_s}{1 - x_s}), & x_s \le x \le 1 \end{cases}, \tag{4.38b}$$

$$P^{-+}(x) = \begin{cases} P_{21}^+(\frac{x_s - x}{x_s}), & 0 \le x < x_s \\ P_{11}^-(\frac{x - x_s}{1 - x_s}), & x_s \le x \le 1 \end{cases}, \tag{4.38c}$$

$$P^{--}(x) = \begin{cases} P_{22}^+(\frac{x_s - x}{x_s}), & 0 \le x < x_s \\ P_{12}^-(\frac{x - x_s}{1 - x_s}), & x_s \le x \le 1 \end{cases}. \tag{4.38d}$$

□

We have now defined a bilateral observer (4.30) for 2 × 2 hyperbolic systems (4.1)–(4.2). Next we establish a closed interval $I \subset (0, 1)$ in which x_s can be chosen so that, given one of the four (4.17) is true, the observer (4.30) with observer gains defined for the corresponding case in Appendix A will produce estimates that converge in minimum time for bilateral sensing.

Theorem 4.3. *Consider the bilateral observer* (4.30). *Define* $f : [0,1] \to F \subset \mathbb{R}$ *as*

$$f(x) = \int_x^1 \frac{ds}{\lambda(s)} - \int_0^x \frac{ds}{\mu(s)} \tag{4.39}$$

and $g : [0,1] \to G \subset \mathbb{R}$ *as*

$$g(x) = \int_0^x \frac{ds}{\lambda(s)} - \int_x^1 \frac{ds}{\mu(s)}, \tag{4.40}$$

and have inverses denoted as $f^{-1} : F \to [0,1]$ *and* $g^{-1} : G \to [0,1]$, *respectively. Define the interval* $I = [g^{-1}(0), f^{-1}(0)]$, *and let the splitting point* x_s *be chosen so that* $x_s \in I$. *Assuming one of* (4.17) *is true, using the corresponding observer gains from Appendix A in the bilateral observer* (4.30) *will produce estimates* $\hat{u}(x,t)$, $\hat{v}(x,t)$ *that converge to their true values* $u(x,t)$, $v(x,t)$, *respectively, within time* (4.8).

Proof. First we must show that the interval I can be constructed. From (4.39)–(4.40) we find

$$f'(x) = -\frac{1}{\lambda(x)} - \frac{1}{\mu(x)} \tag{4.41a}$$

$$g'(x) = \frac{1}{\lambda(x)} + \frac{1}{\mu(x)}. \tag{4.41b}$$

Hence $\forall x \in [0,1]$ we have $f'(x) < 0$ and $g'(x) > 0$. From their respective definitions we therefore see f and g are bijective, and their inverses f^{-1} and g^{-1} exist. Additionally,

$$f(0) = \int_0^1 \frac{ds}{\lambda(s)}, \qquad f(1) = -\int_0^1 \frac{ds}{\mu(s)} \tag{4.42a}$$

$$g(0) = -\int_0^1 \frac{ds}{\mu(s)}, \qquad g(1) = \int_0^1 \frac{ds}{\lambda(s)} \tag{4.42b}$$

which implies $f^{-1}(0), g^{-1}(0) \in (0,1)$. Also, from the definitions of f and g in (4.39)–(4.40) together with the assumption (4.5), it is clear that

$$g^{-1}(0) \leq f^{-1}(0). \tag{4.43}$$

Therefore the closed interval $I = [g^{-1}(0), f^{-1}(0)]$ is well-defined. From Theorem 3.6 we know the collocated observer (3.83) converges within time $t_{1,min} = \int_0^1 \frac{d\bar{x}}{\mu_2(\bar{x})} +$

$\int_0^1 \frac{d\bar{x}}{\lambda_1(\bar{x})}$. Due to (3.6), this convergence time $t_{1,min}$ can be written in terms of the transport speeds $\mu(x)$, $\lambda(x)$ for the 2×2 system (4.1)–(4.2) as

$$\begin{aligned} t_{1,min} = &\max\left\{\int_0^1 \frac{1-x_s}{\mu(x_s+\bar{x}(1-x_s))}d\bar{x}, \int_0^1 \frac{x_s}{\lambda(x_s(1-\bar{x}))}d\bar{x}\right\} \\ &+ \max\left\{\int_0^1 \frac{x_s}{\mu(x_s(1-\bar{x}))}d\bar{x}, \int_0^1 \frac{1-x_s}{\lambda(x_s+\bar{x}(1-x_s))}d\bar{x}\right\}. \end{aligned} \tag{4.44}$$

Applying a spatial change of variables using the left and right sub-domain spatial transformations $\bar{x} = l_{x_s}$ to the second and third integrals, and $\bar{x} = r_{x_s}$ to the first and fourth integrals, respectively, we can express (4.44) as the convergence time t_2 of the 2×2 observer as

$$\begin{aligned} t_2 &= \max\left\{\int_{x_s}^1 \frac{1-x_s}{\mu(x)}\frac{dx}{1-x_s}, \int_{x_s}^0 \frac{x_s}{\lambda(x)}\frac{-dx}{x_s}\right\} \\ &+ \max\left\{\int_{x_s}^0 \frac{x_s}{\mu(x)}\frac{-dx}{x_s}, \int_{x_s}^1 \frac{1-x_s}{\lambda(x)}\frac{dx}{1-x_s}\right\} \\ &= \max\left\{\int_{x_s}^1 \frac{dx}{\mu(x)}, \int_0^{x_s} \frac{dx}{\lambda(x)}\right\} + \max\left\{\int_0^{x_s} \frac{dx}{\mu(x)}, \int_{x_s}^1 \frac{dx}{\lambda(x)}\right\}. \end{aligned} \tag{4.45}$$

The minimal convergence time $t_{2,min}$ of the bilateral observer can then be found by performing a minimization over (4.45) with respect to $x_s \in (0,1)$. This minimization problem can be posed as

$$t_{2,min} = \min_{x_s \in (0,1)} \left\{\max\left\{\int_{x_s}^1 \frac{dx}{\mu(x)}, \int_0^{x_s} \frac{dx}{\lambda(x)}\right\} + \max\left\{\int_0^{x_s} \frac{dx}{\mu(x)}, \int_{x_s}^1 \frac{dx}{\lambda(x)}\right\}\right\}. \tag{4.46}$$

The open interval $(0,1)$ is now partitioned into three disjoint subintervals, namely $(0, g^{-1}(0))$, I and $(f^{-1}(0), 1)$ and the convergence time of the observer (4.30) when x_s is chosen in these three intervals is analyzed.

Firstly, when $x_s \in (0, g^{-1}(0))$, due to the strictly decreasing and increasing properties of $f(x)$ and $g(x)$ respectively, we have that $f(x_s) > 0$ and $g(x_s) < 0$, something which in turn implies

$$\int_{x_s}^1 \frac{dx}{\lambda(x)} > \int_0^{x_s} \frac{dx}{\mu(x)} \tag{4.47a}$$

$$\int_{x_s}^{1} \frac{dx}{\mu(x)} > \int_{0}^{x_s} \frac{dx}{\lambda(x)}. \tag{4.47b}$$

Therefore, for x_s in this interval, the convergence time can be found from (4.45) to be

$$t_{2,left}(x_s) = \int_{x_s}^{1} \frac{dx}{\lambda(x)} + \int_{x_s}^{1} \frac{dx}{\mu(x)}. \tag{4.48}$$

In the same sense, when $x_s \in (f^{-1}(0), 1)$, from $f(x_s) < 0$ and $g(x_s) > 0$ being true in this region, the inequalities

$$\int_{x_s}^{1} \frac{dx}{\lambda(x)} < \int_{0}^{x_s} \frac{dx}{\mu(x)} \tag{4.49a}$$

$$\int_{x_s}^{1} \frac{dx}{\mu(x)} < \int_{0}^{x_s} \frac{dx}{\lambda(x)}. \tag{4.49b}$$

are satisfied and therefore the convergence time becomes

$$t_{2,right}(x_s) = \int_{0}^{x_s} \frac{dx}{\mu(x)} + \int_{0}^{x_s} \frac{dx}{\lambda(x)}. \tag{4.50}$$

Finally, for the closed interval I, $f(x_s) \geq 0$ and $g(x_s) \geq 0$ which implies

$$\int_{0}^{x_s} \frac{dx}{\mu(x)} \leq \int_{x_s}^{1} \frac{dx}{\lambda(x)}, \tag{4.51a}$$

$$\int_{x_s}^{1} \frac{dx}{\mu(x)} \leq \int_{0}^{x_s} \frac{dx}{\lambda(x)}. \tag{4.51b}$$

Applying the inequalities (4.51) to (4.45), obtain that the observer converges in time $t_{2,middle}$ when x_s is chosen to satisfy $f^{-1}(0) \leq \bar{x}_s \leq g^{-1}(0)$, where

$$t_{2,middle} = \int_{0}^{x_s} \frac{dx}{\lambda(x)} + \int_{x_s}^{1} \frac{dx}{\lambda(x)} = \int_{0}^{1} \frac{dx}{\lambda(x)}. \tag{4.52}$$

To see that (4.52) is a solution to the minimization problem (4.46), observe from (4.48) that $t'_{2,left}(x_s) < 0$, whilst from (4.50) we have $t'_{2,right}(x_s) > 0$. Also, at

$f^{-1}(0)$, $\int_{x_s}^{1} \frac{dx}{\lambda(x)} = \int_{0}^{x_s} \frac{dx}{\mu(x)}$ which implies that $t_{2,right}(f^{-1}(0)) = t_{2,middle}$ and at $g^{-1}(0)$ it is true that $\int_{0}^{x_s} \frac{dx}{\lambda(x)} = \int_{x_s}^{1} \frac{dx}{\mu(x)}$, implying that $t_{2,left}(g^{-1}(0)) = t_{2,middle}$. Hence $t_{2,middle} = t_{2,min}$ is a solution to the minimization problem (4.46). □

An issue with the observer presented in Theorem 4.3 is that depending on the value of $x_s \in (0,1)$ chosen and the definitions of $\lambda(x)$ and $\mu(x)$, one of the four pairs of inequalities in (4.17) may or may not be true $\forall x \in [0,1]$, implying the observer gains will not necessarily be well-defined. It would therefore be beneficial to pin down a value of x_s which will guarantee that the observer gains to always be well-defined and produce correct estimates within the theoretical minimum time (4.8), given (4.5).

Consider choosing $x_s = \frac{1}{2}$. A transform $\mathscr{T}$ with this value of x_s "hardwired" can then be defined in terms of $\mathscr{T}_{3,x_s}$ as

$$\mathscr{T} = \mathscr{T}_{3,\frac{1}{2}}. \tag{4.53}$$

The transform $\mathscr{T}$ can then be stated as

$$\mathscr{T}[u,v](x) = \left(\begin{bmatrix} u(\frac{1}{2}(1+x)) \\ v(\frac{1}{2}(1-x)) \end{bmatrix}, \begin{bmatrix} v(\frac{1}{2}(1+x)) \\ u(\frac{1}{2}(1-x)) \end{bmatrix} \right) \tag{4.54}$$

with inverse given by(from setting $x_s = \frac{1}{2}$ into (4.16c))

$$\mathscr{T}^{-1}[\bar{u},\bar{v}] = \begin{cases} (v_2(1-2x), u_2(1-2x)), & x \in [0, \frac{1}{2}] \\ (u_1(2x-1), v_1(2x-1)), & x \in [\frac{1}{2}, 1] \end{cases} \tag{4.55}$$

Using (4.54) allows us to state a bilateral observer for (4.1)–(4.2) that will always converge in minimum time (4.8) and always have well-defined observer gains, given (4.5). This result can be seen as a direct consequence of Theorem 4.3, and is therefore presented as a Corollary.

Corollary 4.4. *The invertible change of coordinates* $(\hat{u}(x,t), \hat{v}(x,t)) = \mathscr{T}^{-1}[\check{u}_1, \check{u}_2, \check{v}_1, \check{v}_2](x,t)$ *maps the collocated* $2+2$ *observer* (3.83) *with coefficients for* (3.83a)–(3.83b) *defined as*

$$\Lambda^{+}(x) = \begin{bmatrix} 2\lambda(\frac{1}{2}(1+x)) & 0 \\ 0 & 2\mu(\frac{1}{2}(1-x)) \end{bmatrix}, \tag{4.56a}$$

$$\Lambda^{-}(x) = \begin{bmatrix} 2\mu(\frac{1}{2}(1+x)) & 0 \\ 0 & 2\lambda(\frac{1}{2}(1-x)) \end{bmatrix}, \tag{4.56b}$$

$$\Sigma^{+-}(x) = \begin{bmatrix} \sigma^{+}(\frac{1}{2}(1+x)) & 0 \\ 0 & \sigma^{-}(\frac{1}{2}(1-x)) \end{bmatrix}, \tag{4.56c}$$

$$\Sigma^{-+}(x) = \begin{bmatrix} \sigma^{-}(\frac{1}{2}(1+x)) & 0 \\ 0 & \sigma^{+}(\frac{1}{2}(1-x)) \end{bmatrix}, \tag{4.56d}$$

corresponding observer gains $P^+(x)$, $P^-(x)$ *given by* (3.73), *measurement assignments* (4.35) *and boundary coefficient assignments* (4.27)–(4.29), *into the bilateral* 2×2 *observer* (4.30) *with observer gains given in terms of* (3.73) *as*

$$P^{++}(x) = \begin{cases} P_{21}^-(1-2x), & 0 \leq x < \frac{1}{2} \\ P_{11}^+(2x-1), & \frac{1}{2} \leq x \leq 1 \end{cases}, \tag{4.57a}$$

$$P^{+-}(x) = \begin{cases} P_{22}^-(1-2x), & 0 \leq x < \frac{1}{2} \\ P_{12}^+(2x-1), & \frac{1}{2} \leq x \leq 1 \end{cases}, \tag{4.57b}$$

$$P^{-+}(x) = \begin{cases} P_{21}^+(1-2x), & 0 \leq x < \frac{1}{2} \\ P_{11}^-(2x-1), & \frac{1}{2} \leq x \leq 1 \end{cases}, \tag{4.57c}$$

$$P^{--}(x) = \begin{cases} P_{22}^+(1-2x), & 0 \leq x < \frac{1}{2} \\ P_{12}^-(2x-1), & \frac{1}{2} \leq x \leq 1 \end{cases}. \tag{4.57d}$$

Moreover, the observer gains (4.57) *are always well-defined and the states* $\hat{u}(x,t)$, $\hat{v}(x,t)$ *converge to their true values* $u(x,t)$, $v(x,t)$ *in finite time given by* (4.8).

Proof. The system coefficients (4.56) are trivially found by setting $x_s = \frac{1}{2}$ into (4.23)–(4.24), and setting $x_s = \frac{1}{2}$ into (4.3) gives us (4.57). Setting $x_s = \frac{1}{2}$ into (4.17c), we find the inequalities

$$\lambda(\frac{1}{2}(1+x)) \leq \mu(\frac{1}{2}(1-x)), \lambda(\frac{1}{2}(1-x)) \leq \mu(\frac{1}{2}(1+x)), \tag{4.58}$$

which must be satisfied $\forall x \in [0,1]$ in order for (4.57) to be well-defined. Both inequalities (4.58) as satisfied due to (4.5).

The convergence time of the $2+2$ collocated observer (3.83) with transport speeds (4.56a)–(4.56b) is according to Theorem 3.6 given by

$$t_{min} = \int_0^1 \frac{d\bar{x}}{2\lambda(\frac{1}{2}(1+\bar{x}))} + \int_0^1 \frac{d\bar{x}}{2\lambda(\frac{1}{2}(1-\bar{x}))} \tag{4.59}$$

Applying the change of variables $\bar{x} = 2x - 1$ to the first integral and $\bar{x} = 1 - 2x$ to the second integral, we find

$$\begin{aligned} t_{min} &= \int_{\frac{1}{2}}^1 \frac{2dx}{2\lambda(x)} + \int_{\frac{1}{2}}^0 \frac{-2dx}{2\lambda(x)} = \int_{\frac{1}{2}}^1 \frac{dx}{\lambda(x)} + \int_0^{\frac{1}{2}} \frac{dx}{\lambda(x)} \\ &= \int_0^1 \frac{dx}{\lambda(x)} \end{aligned} \tag{4.60}$$

which is (4.8). Since (4.54) is invertible, (4.8) is also convergence time of the bilateral observer (4.30) with output injection gains (4.57). □

If the transport speeds in the 2×2 system (4.1)–(4.2) are defined as being constant, an analytic expression for the range the splitting point x_s should be chosen within to guarantee minimum time convergence can be found[4]. Consider therefore setting $\lambda(x) = \lambda$ and $\mu(x) = \mu$, with $\lambda, \mu \in \mathbb{R}^+$ positive real constants, in (4.1) to obtain the 2×2 linear hyperbolic PDE system

$$u_t(x,t) + \lambda u_x(x,t) = \sigma^+(x)v(x,t) \tag{4.61a}$$
$$v_t(x,t) - \mu v_x(x,t) = \sigma^-(x)u(x,t) \tag{4.61b}$$

which also has boundary conditions (4.2). The result which follows, also being a Corollary of Theorem 4.3, presents an observer for this special case of the 2×2 system with constant transport speeds along with analytic expressions for the boundaries of the interval within x_s must be chosen to guarantee minimum time convergence.

Corollary 4.5. *Consider the bilateral observer*

$$\hat{u}_t(x,t) + \lambda \hat{u}_x(x,t) = \sigma^+(x)\hat{v}(x,t) + P^{++}(x)(y_1(t) - \hat{u}(1,t)) \tag{4.62a}$$
$$+ P^{+-}(x)(y_2(t) - \hat{v}(0,t)), \tag{4.62b}$$
$$\hat{v}_t(x,t) - \mu \hat{v}_x(x,t) = \sigma^-(x)\hat{u}(x,t) + P^{-+}(x)(y_1(t) - \hat{u}(1,t)) \tag{4.62c}$$
$$+ P^{--}(x)(y_2(t) - \hat{v}(0,t)), \tag{4.62d}$$
$$\hat{u}(0,t) = Qy_2(t) + U_1(t), \tag{4.62e}$$
$$\hat{v}(1,t) = Ry_1(t) + U_2(t), \tag{4.62f}$$

relying on measurements $y_1(t) = u(1,t)$, $y_2(t) = v(0,t)$. The observer gains $P^{++}(x)$, $P^{+-}(x)$, $P^{-+}(x)$ and $P^{--}(x)$ are defined in Appendix A. If the splitting point x_s is chosen to lie in the closed interval $I \subset (0,1)$ defined as being all real numbers between and including both $x_\mu \in (0,1)$, which can be calculated as

$$x_\mu = \frac{\mu}{\mu + \lambda}, \tag{4.63}$$

and $x_\lambda \in (0,1)$, defined as

$$x_\lambda = \frac{\lambda}{\mu + \lambda}, \tag{4.64}$$

then the observer (4.62) *generates estimates $\hat{u}(x,t)$, $\hat{v}(x,t)$ which converge to their true values $u(x,t)$, $v(x,t)$ representing the states of the PDE system* (4.61) *with boundary conditions* (4.2) *within time $t_{2,min}$, where*

$$t_{2,min} = \max\{\frac{1}{\mu}, \frac{1}{\lambda}\}. \tag{4.65}$$

[4]Additionally the restriction (4.5) will hold trivially for constant transport speeds, in light of it being imposed without loss of generality.

Proof. Since $\lambda(x)$ and $\mu(x)$ are constant, (4.5) will always hold true since it is imposed without loss of generality, and therefore one of the four cases in (4.17) will always be true implying the observer gains defined accordingly in Appendix A will be well-defined. For the observer (4.62), $f(x)$ and $g(x)$ from Theorem 4.3 can be written as

$$f(x) = \frac{1}{\lambda}\int_x^1 ds - \frac{1}{\mu}\int_0^x ds = \frac{1-x}{\lambda} - \frac{x}{\mu}, \tag{4.66a}$$

$$g(x) = \frac{1}{\lambda}\int_0^x ds - \frac{1}{\mu}\int_x^1 ds = \frac{x}{\lambda} - \frac{1-x}{\mu}. \tag{4.66b}$$

The points $f^{-1}(0)$ and $g^{-1}(0)$ can then be solved for by setting

$$0 = f(x) = \frac{1-x}{\lambda} - \frac{x}{\mu} \Rightarrow f^{-1}(0) = \frac{\mu}{\mu+\lambda} = x_\mu, \tag{4.67a}$$

$$0 = g(x) = \frac{x}{\lambda} - \frac{1-x}{\mu} \Rightarrow g^{-1}(0) = \frac{\lambda}{\mu+\lambda} = x_\lambda, \tag{4.67b}$$

For the convergence time of the observer (4.62), using the general version of the convergence time (4.8) from Theorem 4.3, which is

$$t_{2,min} = \max\{\int_0^1 \frac{dx}{\lambda(x)}, \int_0^1 \frac{dx}{\mu(x)}\}, \tag{4.68}$$

we obtain

$$t_{2,min} = \max\{\frac{1}{\mu}\int_0^1 dx, \frac{1}{\lambda}\int_0^1 dx\} = \max\{\frac{1}{\mu}, \frac{1}{\lambda}\}. \tag{4.69}$$

□

This concludes the derivation of the minimum time bilateral observer for systems of coupled 2×2 linear hyperbolic PDEs considered in this thesis. The next section will focus on simulating the observers, giving an empirical confirmation of the theory, and additionally applying the theory developed to an oil well drilling example.

Part III

Simulations and Application

Chapter 5

Numerical Solution Method

5.1 Introduction

A minimum time bilateral observer for the 2×2 system (4.1)–(4.2) has been derived, and we wish to demonstrate this observer in practice on various examples. For simplicity we assume the equations in our simulations have constant transport speeds λ and μ respectively, and the observer given in Corollary 4.5 can then be applied.

To demonstrate the observer for various cases given in Appendix A, we will firstly in Chapter 6 demonstrate the observer on two *toy* examples, by which we mean cases where the coefficients in the 2×2 cases are picked without any underlying physical motivation. In one of the simulations we have $\lambda > \mu$, whilst in the other case $\mu > \lambda$. Picking that $x_s = 0.5$, which lies according to Corollary 4.5 in the possible interval for minimum time convergence for both of these cases, we see that for the first simulation we must assign our $2 + 2$ system according to *Case II* in Appendix A, whilst the second simulations uses the coefficient assignments corresponding to *Case III*.

Next, to show the applicability of the theory developed in this thesis to a practical example, we demonstrate in Chapter 7 that a linearized model of a drill string can be transformed to fit into our 2×2 system framework (4.1)–(4.2). The transport velocities can in this case be calculated from physical quantities and we will see that they will both be equal and constant.

This chapter is organized as follows. First, for comparison reasons, we introduce an alternative observer for 2×2 linear hyperbolic systems that only uses single boundary sensing, in Section 5.2. In order to implement our 2×2 system minimum time bilateral observer on a computer, we need to solve the kernel equations for the $2 + 2$ system minimum time collocated observer that results from transforming the 2×2 system to a $2 + 2$ system. Section 5.3 will explain how these kernel equations are numerically solved(and additionally how the kernel equations for the alternative single boundary 2×2 system observer are solved). After having solved the kernel PDEs we can calculate observer gains that can then be used in a simulation for the 2×2 system together with observers, and Section 5.4 takes care of explaining how the 2×2 system and the corresponding observer algorithms are numerically marched forward in time, giving an overview over the entire simulator structure.

5.2 Alternative Observer: 2×2 Single Boundary Observer

In order to highlight the improvement in convergence our 2×2 bilateral observer offers, we compare it to a previously derived observer relying on a single boundary measurement, only. Consider the *unilateral* observer, implying an observer for (4.1)–(4.2) relying on measurement from a single boundary, only, with constant transport speeds $\lambda(x) = \lambda$, $\mu(x) = \mu$, based on the observer from Vazquez et al. (2011), given by[1]

$$\hat{u}_t(x,t) + \lambda \hat{u}_x(x,t) = \sigma^+(x)\hat{v}(x,t) + \bar{P}^+(x)[y_1(t) - \hat{u}(1,t)], \tag{5.1a}$$
$$\hat{v}_t(x,t) - \mu \hat{v}_x(x,t) = \sigma^-(x)\hat{u}(x,t) + \bar{P}^-(x)[y_1(t) - \hat{u}(1,t)], \tag{5.1b}$$
$$\hat{u}(0,t) = Q\hat{v}(0,t) + U_1(t), \tag{5.1c}$$
$$\hat{v}(1,t) = Ry_1(t) + U_2(t). \tag{5.1d}$$

The output injection gains $\bar{P}^+$, $\bar{P}^-$ are given by

$$\bar{P}^+(x) = \lambda \bar{M}(x,1), \tag{5.2a}$$
$$\bar{P}^-(x) = \lambda \bar{N}(x,1) \tag{5.2b}$$

with $\bar{M}$, $\bar{N}$ being solutions to the kernel PDE

$$\lambda \bar{M}_x(x,\xi) + \lambda \bar{M}_\xi(x,\xi) = \sigma^+(x)\bar{N}(x,\xi) \tag{5.3a}$$
$$-\mu \bar{N}_x(x,\xi) + \lambda \bar{N}_\xi(x,\xi) = \sigma^-(x)\bar{M}(x,\xi) \tag{5.3b}$$

with boundary conditions

$$\bar{M}(0,\xi) = Q\bar{N}(0,\xi), \tag{5.4a}$$
$$\bar{N}(x,x) = \frac{\sigma^-(x)}{\lambda + \mu}. \tag{5.4b}$$

The kernel PDE (5.3)–(5.4) is defined over the upper triangular domain $\mathcal{T}_u$. According to Theorem 2 of Vazquez et al. (2011), the observer (5.1) produces

[1]This observer is presented here with constant transport speeds, since that is what will be implemented in the simulation. However, the observer was originally presented with spatially varying transport speeds in Vazquez et al. (2011). Another slight difference is that in Vazquez et al. (2011), only a boundary control input actuating the boundary $x = 1$ was applied, so the observer there was referred to as *collocated*, as sensing for this observer is also at the same boundary $x = 1$. In this case we have two "dummy" control inputs actuating both $x = 0$ and $x = 1$, so the term collocated does not apply for this observer within the scope of this thesis.

estimates $\hat{u}(x,t)$, $\hat{v}(x,t)$ that converge to the states $u(x,t)$, $v(x,t)$ of (4.1)–(4.2) within time

$$t_{1,min} = \frac{1}{\lambda} + \frac{1}{\mu}. \tag{5.5}$$

5.3 Kernel Solvers

5.3.1 Method introduction

In this section we are interested in finding a solution to the two sets of 2×2 matrix valued PDE equations (3.74)–(3.75), the single kernel PDE (3.51)–(3.52)[2], and kernel PDE system (5.3)–(5.4). Solving these(for constant transport speeds) will allow us to compute output injection gains $P^{++}(x)$, $P^{+-}(x)$, $P^{-+}(x)$,$P^{--}(x)$ for the 2×2 bilateral observer (4.62), and output injection gains $\bar{P}^{+}(x)$, $\bar{P}^{-}(x)$ for the 2×2 unilateral observer (5.1).

Let $w(x,\xi) \in C^1(\mathcal{T}_u)$ or $C^1(\mathcal{S}_0)$ and $f(x,\xi) \in C^0(\mathcal{T}_u)$ or $C^0(\mathcal{S}_0)$ be two functions defined over $\mathcal{T}_u$ or $\mathcal{S}_0$. When written out component-wise, all the PDEs in (3.74)–(3.75), (3.51)–(3.52) and (5.3)–(5.4) can be written in the form

$$\epsilon_1 w_x(x,\xi) + \epsilon_2 w_\xi(x,\xi) = f(x,\xi). \tag{5.6}$$

where ϵ_1 and ϵ_2 are used to denote the transport velocities. Analyzing (5.6) with the method of characteristics by setting $x = x(s)$ and $\xi = \xi(s)$, with s some underlying artificial variable, we find that along the characteristic lines that can be calculated from

$$\frac{dx}{ds} = \epsilon_1, \tag{5.7a}$$

$$\frac{d\xi}{ds} = \epsilon_2, \tag{5.7b}$$

where the PDE (5.6) corresponds with the ODE $w'(s) = f(s)$. Since we have assumed constant transport velocities, each equation has characteristics propagating in the direction given by the unit vector

$$\delta_s = \frac{1}{\sqrt{\epsilon_1^2 + \epsilon_2^2}} \begin{bmatrix} \epsilon_1 \\ \epsilon_2 \end{bmatrix} \tag{5.8}$$

For the kernel PDE (3.51)–(3.52) defined over the square domain $\mathcal{S}_0$, a standard finite difference scheme is used. However, for the kernel PDEs defined over the upper triangular domain $\mathcal{T}_u$, a slightly modified finite difference scheme is applied. In order to find the solution to the PDEs evolving over $\mathcal{T}_u$ numerically, we use the finite difference method originally proposed in Anfinsen and Aamo (2017a). An alternative method is used in Anfinsen and Aamo (2017b) where first the method of characteristics is used to find the characteristic lines, the resultant ODEs are

[2]Note that (3.51)–(3.52) can be solved analytically, as was shown for equations of the same form in Coron et al. (2017). However, we solve the PDE numerically instead in our implementation.

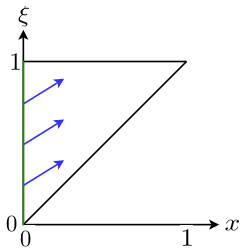

(a) $\epsilon_1, \epsilon_2 > 0$ in (5.6), the boundary condition is known along $(0, \xi)$ and the PDE evolves over $\mathcal{T}_u$.

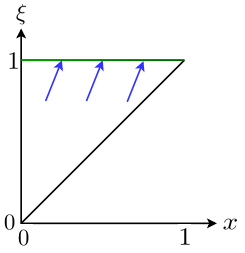

(b) $\epsilon_1, \epsilon_2 > 0$ in (5.6), the boundary condition is known along $(x, 1)$ and the PDE evolves over $\mathcal{T}_u$.

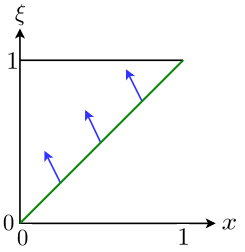

(c) $\epsilon_1 < 0$ whilst $\epsilon_2 > 0$ in (5.6), the boundary condition is known along (x, x) and the PDE evolves over $\mathcal{T}_u$.

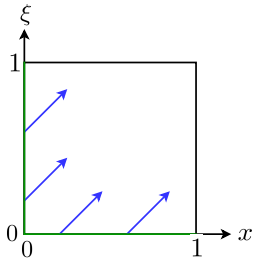

(d) $\epsilon_1, \epsilon_2 > 0$ in (5.6), the boundary condition is known along both $(x, 0)$ and $(0, \xi)$ and the PDE evolves over $\mathcal{S}_0$.

Figure 5.1: Illustration of characteristics and boundary conditions in the respective domains of kernel PDEs we are interested in solving. The blue arrows are characteristics and the boundary conditions are defined along the green lines.

integrated along these lines and the method of successive approximations is used approximate the solution iteratively.

We briefly introduce the method from Anfinsen and Aamo (2017a) here. Instead of calculating the finite difference approximation along the x and ξ axis, the method used in Anfinsen and Aamo (2017a) approximates the derivative along the direction of the characteristic given by the unit vector δ_s defined in (5.8). After discretizing a square domain into an $\hat{N} \times \hat{N}$ grid, we wish to find the solution for grid points $1 \leq i \leq j \leq \hat{N}$, where i is the grid index along the x axis and j is the grid index along the ξ axis.

Depending on the relevant situation from Fig. 5.1, the finite difference approximation is defined so that the function approximation over a given grid point (i, j) is found from neighbouring grid points which lie in the direction defined by δ_s towards the boundary with a boundary condition defined on it. Unless $\epsilon_1 = \epsilon_2$ the characteristic will not go through two grid points which lie diagonal to each other, and then interpolation must be used to obtain the correct value. By defining a step length ς and using the notation $x_i = \Delta i$, $\xi_j = \Delta j$, where $\Delta = \frac{1}{\hat{N}-1}$, the finite difference approximation in order to approximately solve the case in Fig. 5.1c can

be given by (Anfinsen and Aamo (2017a))

$$\epsilon_1 L_x(x_i,\xi_j)+\epsilon_2 L_\xi(x,\xi)\approx\frac{\sqrt{\epsilon_1^2+\epsilon_2^2}}{\varsigma}(L(x_i,\xi_j)-L(x_i-\delta_{s,1}\varsigma,\xi_j-\delta_{s,2}\varsigma)) \quad (5.9)$$

where $\delta_{s,1}$ and $\delta_{s,2}$ denote the first and second component of the vector δ_s, respectively.

To solve the PDEs defined over triangular domains, MATLAB code(written by Henrik Anfinsen) to solve

$$\varepsilon_1(z)K_z(z,\zeta)-\eta_1(\zeta)K_\zeta(z,\zeta)=a_1(z,\zeta)K(z,\zeta)+a_2(z,\zeta)L(z,\zeta)+a_3(z,\zeta)P(z,\zeta) \quad (5.10a)$$

$$\varepsilon_2(z)L_z(z,\zeta)-\eta_2(\zeta)L_\zeta(z,\zeta)=b_1(z,\zeta)K(z,\zeta)+b_2(z,\zeta)L(z,\zeta)+b_3(z,\zeta)P(z,\zeta) \quad (5.10b)$$

$$\nu(z)P_z(z,\zeta)+\nu(\zeta)P_\zeta(z,\zeta)=c_1(z,\zeta)K(z,\zeta)+c_2(z,\zeta)L(z,\zeta)+c_3(z,\zeta)P(z,\zeta) \quad (5.10c)$$

with boundary conditions

$$K(z,z)=f_1(z) \quad (5.11a)$$

$$L(z,z)=f_2(z) \quad (5.11b)$$

$$P(z,0)=\varrho_1 K(z,0)+\varrho_2 L(z,0) \quad (5.11c)$$

over the lower triangular domain $\mathcal{T}_l=\{(z,\zeta)\mid 1\le\zeta\le z\le 1\}$ using the finite difference scheme just described was used as a starting point. The kernel PDEs (5.3)–(5.4) for the unilateral 2×2 observer can, as will be shown, be put into the form (5.10)–(5.11), so the solver written to solve these kernel PDEs was sufficient for that observer. However, (5.10)–(5.11) was not sufficient to solve the bilateral 2×2 observer kernel PDEs (3.74)–(3.75), so the code had to be extended for this case.

The rest of this section is structured as follows. In Subsection 5.3.2 we explain how the finite difference scheme just described is applied to solve the unilateral kernel PDE system (5.3)–(5.4). Then in Subsection 5.3.3 we explain how the kernel PDE system (3.74)–(3.75) is solved, and then how (3.51)–(3.52) is solved.

5.3.2 Unilateral observer kernel numerics

For the kernel equations (5.3) for the unilateral 2×2 observer, setting $x\to\zeta$ and $\xi\to z$, we obtain

$$\lambda\bar{M}_\zeta(\zeta,z)+\lambda\bar{N}_z(\zeta,z)=\sigma^+(\zeta)\bar{N}(\zeta,z), \quad (5.12a)$$

$$-\mu\bar{N}_\zeta(\zeta,z)+\lambda\bar{N}_z(\zeta,z)=\sigma^-(\zeta)\bar{M}(\zeta,z), \quad (5.12b)$$

These can be transformed to fit into the framework (5.10) with

$$K(z,\zeta) = \bar{N}(\zeta,z) \tag{5.13a}$$
$$P(z,\zeta) = \bar{M}(\zeta,z) \tag{5.13b}$$

and coefficient assignments

$$\epsilon_1(z) = \lambda, \quad \epsilon_2(z) = 0, \quad \eta_1(z) = \mu, \quad \eta_2(z) = 0, \tag{5.14a}$$
$$a_1(z,\zeta) = 0, \quad a_1(z,\zeta) = 0, \quad a_3(z,\zeta) = \sigma^-(\zeta), \quad \nu(z) = \lambda, \tag{5.14b}$$
$$b_1(z,\zeta) = 0, \quad b_2(z,\zeta) = 0, \quad b_3(z,\zeta) = 0, \tag{5.14c}$$
$$c_1(z,\zeta) = \sigma^{+-}(\zeta), \quad c_2(z,\zeta) = 0, \quad c_3(z,\zeta) = 0. \tag{5.14d}$$

The boundary conditions (5.4) become

$$N(\zeta,\zeta) = \frac{\sigma^-(\zeta)}{\lambda+\mu} \tag{5.15a}$$
$$M(z,0) = QN(z,0) \tag{5.15b}$$

and hence fit into (5.11) with

$$f_1(z) = \frac{\sigma^{-+}(z)}{\lambda+\mu}, \tag{5.16a}$$
$$f_2(z) = 0, \tag{5.16b}$$
$$\varrho_1 = Q, \varrho_2 = 0. \tag{5.16c}$$

The solver already written using the finite difference scheme from Anfinsen and Aamo (2017a) to solve systems for the form (5.10)–(5.11) was therefore applied directly to solve (5.3)–(5.4).

5.3.3 Bilateral observer kernel numerics

5.3.3.1 Triangular domain kernels

Given that we have constant transport velocities, the kernel equations from the first matrix PDE in (3.74) can equation-wise be written out as using the notation from (3.29) as

$$\lambda_1 M_{11,x}(x,\xi) + \lambda_1 M_{11,\xi}(x,\xi) = \sigma_{11}^{+-}(x)N_{11}(x,\xi) + \sigma_{12}^{+-}(x)N_{21}(x,\xi), \tag{5.17a}$$
$$\lambda_1 M_{12,x}(x,\xi) + \lambda_2 M_{12,\xi}(x,\xi) = \sigma_{11}^{+-}(x)N_{12}(x,\xi) + \sigma_{12}^{+-}(x)N_{22}(x,\xi), \tag{5.17b}$$
$$\lambda_2 M_{21,x}(x,\xi) + \lambda_1 M_{21,\xi}(x,\xi) = \sigma_{21}^{+-}(x)N_{11}(x,\xi) + \sigma_{22}^{+-}(x)N_{21}(x,\xi), \tag{5.17c}$$
$$\lambda_2 M_{22,x}(x,\xi) + \lambda_2 M_{22,\xi}(x,\xi) = \sigma_{21}^{+-}(x)N_{12}(x,\xi) + \sigma_{22}^{+-}(x)N_{22}(x,\xi), \tag{5.17d}$$

whilst the second matrix PDE becomes

$$-\mu_1 N_{11,x}(x,\xi) + \lambda_1 N_{11,\xi}(x,\xi) = \sigma_{11}^{-+}(x) M_{11}(x,\xi) + \sigma_{12}^{-+}(x) M_{21}(x,\xi), \quad (5.18a)$$
$$-\mu_1 N_{12,x}(x,\xi) + \lambda_2 N_{12,\xi}(x,\xi) = \sigma_{11}^{-+}(x) M_{12}(x,\xi) + \sigma_{12}^{-+}(x) M_{22}(x,\xi), \quad (5.18b)$$
$$-\mu_2 N_{21,x}(x,\xi) + \lambda_1 N_{21,\xi}(x,\xi) = \sigma_{21}^{-+}(x) M_{11}(x,\xi) + \sigma_{22}^{-+}(x) M_{21}(x,\xi), \quad (5.18c)$$
$$-\mu_2 N_{22,x}(x,\xi) + \lambda_2 N_{22,\xi}(x,\xi) = \sigma_{21}^{-+}(x) M_{12}(x,\xi) + \sigma_{22}^{-+}(x) M_{22}(x,\xi). \quad (5.18d)$$

The boundary conditions for these two coupled sets of PDEs can be found from (3.75) to be

$$M_{11}(0,\xi) = Q_{11} N_{11}(0,\xi) + Q_{12} N_{21}(0,\xi), \quad (5.19a)$$
$$M_{12}(0,\xi) = Q_{11} N_{12}(0,\xi) + Q_{12} N_{22}(0,\xi), \quad (5.19b)$$
$$M_{21}(x,1) = 0 \quad (5.19c)$$
$$M_{22}(0,\xi) = Q_{21} N_{12}(0,\xi) + Q_{22} N_{22}(0,\xi), \quad (5.19d)$$

and

$$N_{11}(x,x) = \frac{\sigma_{11}^{-+}(x)}{\mu_1 + \lambda_1}, \quad (5.20a)$$
$$N_{12}(x,x) = \frac{\sigma_{12}^{-+}(x)}{\mu_1 + \lambda_2}, \quad (5.20b)$$
$$N_{21}(x,x) = \frac{\sigma_{21}^{-+}(x)}{\mu_2 + \lambda_1}, \quad (5.20c)$$
$$N_{22}(x,x) = \frac{\sigma_{22}^{-+}(x)}{\mu_2 + \lambda_2}, \quad (5.20d)$$

respectively. These all evolve and need to be solved over the upper triangular domain $\mathcal{T}_u = \{(x,\xi) \mid 0 \leq x \leq \xi \leq 1\}$.

By comparing the general form (5.6) with the PDEs in (5.17), we see that $\epsilon_1, \epsilon_2 > 0$ for all of them, something which implies that the characteristics propagate for this set of equations in the upwards-right direction. The boundary conditions for this set of equations are found in (5.19), and for M_{11}, M_{12} and M_{22} we have a boundary condition defined on the line $(0,\xi)$. Fig. 5.1a shows a visual representation of the characteristics as blue arrows and the boundary they propagate from as a green line. Hence, in order to solve for M_{11}, M_{12} and M_{22} we start at the left boundary $(0,\xi)$ in their respective domains and propagate the boundary information into the domain. For M_{21} however, we have information about the values lying along the line $(x,1)$, and this information must then instead be propagated backwards into the domain when solving the corresponding PDE as Fig. 5.1b illustrates.

Likewise, comparing (5.6) to the PDEs (5.18), we see all the PDEs here have

characteristics propagating in the upper-left direction. The boundary conditions (5.20) are all defined along the right diagonal (x, x), so Fig. 5.1c illustrates the flow of information when calculating the solution to N_{11}, N_{12}, N_{21} and N_{22}.

Observing the PDEs (5.17) and (5.18) along with their respective boundary conditions (5.19) and (5.20), it can be noted that the $M_{11}(x,\xi)$, $M_{21}(x,\xi)$, $N_{11}(x,\xi)$ and $N_{21}(x,\xi)$ must be solved simultaneously, but can be treated separately from the group $M_{12}(x,\xi)$, $M_{22}(x,\xi)$, $N_{12}(x,\xi)$ and $N_{22}(x,\xi)$.

Due to the kernel PDEs here splitting into two systems of four PDEs each, the `MATLAB` code for solving (5.10)–(5.11) only needed to be extended to solve systems of the form

$$\begin{aligned}
\varepsilon_1(z)K_z(z,\zeta) - \eta_1(\zeta)K_\zeta(z,\zeta) &= a_1(z,\zeta)K(z,\zeta) + a_2(z,\zeta)L(z,\zeta) \\
&\quad + a_3(z,\zeta)P(z,\zeta) + a_4(z,\zeta)R(z,\zeta) && \text{(5.21a)} \\
\varepsilon_2(z)L_z(z,\zeta) - \eta_2(\zeta)L_\zeta(z,\zeta) &= b_1(z,\zeta)K(z,\zeta) + b_2(z,\zeta)L(z,\zeta) \\
&\quad + b_3(z,\zeta)P(z,\zeta) + b_4(z,\zeta)R(z,\zeta) && \text{(5.21b)} \\
\varepsilon_3(z)P_z(z,\zeta) + \eta_3(\zeta)P_\zeta(z,\zeta) &= c_1(z,\zeta)K(z,\zeta) + c_2(z,\zeta)L(z,\zeta) \\
&\quad + c_3(z,\zeta)P(z,\zeta) + c_4(z,\zeta)R(z,\zeta) && \text{(5.21c)} \\
\varepsilon_4(z)R_z(z,\zeta) + \eta_4(\zeta)R_\zeta(z,\zeta) &= d_1(z,\eta)K(z,\zeta) + d_2(z,\zeta)L(z,\zeta) \\
&\quad + d_3(z,\zeta)P(z,\zeta) + d_4(z,\zeta)R(z,\zeta) && \text{(5.21d)}
\end{aligned}$$

To apply this code to solve the set of PDEs we are interested in, the equations must be transformed from the upper triangular domain $\mathcal{T}_u$ to the lower triangular domain $\mathcal{T}_l$ through a coordinate transformation $(x,\xi) \to (z,\zeta)$. For the set of PDEs defining relationships between $M_{12}(x,\xi)$, $M_{22}(x,\xi)$, $N_{12}(x,\xi)$ and $N_{22}(x,\xi)$, mapping $\xi \to z$ and $x \to \zeta$ and defining

$$\begin{aligned}
K(z,\zeta) &= N_{12}(\zeta,z) && \text{(5.22a)} \\
L(z,\zeta) &= N_{22}(\zeta,z) && \text{(5.22b)} \\
P(z,\zeta) &= M_{12}(\zeta,z) && \text{(5.22c)} \\
R(z,\zeta) &= M_{22}(\zeta,z) && \text{(5.22d)}
\end{aligned}$$

will put this PDE set into the form (5.21) with the necessary coefficient assignments defined as

$$\varepsilon_1(z) = \lambda_2, \qquad \varepsilon_2(z) = \lambda_2, \qquad \varepsilon_3(z) = \lambda_2, \qquad \varepsilon_4(z) = \lambda_2 \tag{5.23a}$$

$$\eta_1(\zeta) = \mu_1, \qquad \eta_2(\zeta) = \mu_2, \qquad \eta_3(\zeta) = \lambda_1, \qquad \eta_3(\zeta) = \lambda_2 \tag{5.23b}$$

$$a_1(z,\zeta) = 0, \qquad a_2(z,\zeta) = 0, \qquad a_3(z,\zeta) = \sigma_{11}^{-+}(\zeta), \quad a_4(z,\zeta) = \sigma_{12}^{-+}(\zeta) \tag{5.23c}$$

$$b_1(z,\zeta) = 0, \quad b_2(z,\zeta) = 0, \quad b_3(z,\zeta) = \sigma_{21}^{-+}(\zeta), \quad b_4(z,\zeta) = \sigma_{22}^{-+}(\zeta) \tag{5.23d}$$

$$c_1(z,\zeta) = \sigma_{11}^{+-}(\zeta), \quad c_2(z,\zeta) = \sigma_{12}^{+-}(\zeta), \quad c_3(z,\zeta) = 0, \quad c_4(z,\zeta) = 0 \tag{5.23e}$$

$$d_1(z,\zeta) = \sigma_{21}^{+-}(\zeta), \quad d_2(z,\zeta) = \sigma_{22}^{+-}(\zeta), \quad d_3(z,\zeta) = 0, \quad d_4(z,\zeta) = 0 \tag{5.23f}$$

As for the boundary conditions of (5.21), they will in this case be of the form

$$K(z,z) = f_1(z) \tag{5.24a}$$
$$L(z,z) = f_2(z) \tag{5.24b}$$
$$P(z,0) = \varrho_1 K(z,0) + \varrho_2 L(z,0) \tag{5.24c}$$
$$R(z,0) = \varrho_3 K(z,0) + \varrho_4 L(z,0) \tag{5.24d}$$

with

$$f_1(z) = \frac{\sigma_{12}^{-+}(z)}{\mu_1 + \lambda_2}, \qquad f_2(z) = \frac{\sigma_{22}^{-+}(z)}{\mu_2 + \lambda_2} \tag{5.25a}$$
$$\varrho_1 = Q_{11}, \qquad \varrho_2 = Q_{12}, \tag{5.25b}$$
$$\varrho_3 = Q_{21}, \qquad \varrho_4 = Q_{22} \tag{5.25c}$$

For $M_{11}(x,\xi)$, $M_{21}(x,\xi)$, $N_{11}(x,\xi)$ and $N_{21}(x,\xi)$, by applying the same transformation $x \to \zeta$ and $\xi \to z$, we obtain that the PDEs can be put in the form (5.21) with

$$K(z,\zeta) = N_{11}(\zeta,z) \tag{5.26a}$$
$$L(z,\zeta) = N_{21}(\zeta,z) \tag{5.26b}$$
$$P(z,\zeta) = M_{11}(\zeta,z) \tag{5.26c}$$
$$R(z,\zeta) = M_{21}(\zeta,z) \tag{5.26d}$$

and coefficient assignments

$$\varepsilon_1(z) = \lambda_1, \quad \varepsilon_2(z) = \lambda_1, \quad \varepsilon_3(z) = \lambda_1, \quad \varepsilon_4(z) = \lambda_1 \tag{5.27a}$$

$$\eta_1(\zeta) = \mu_1, \quad \eta_2(\zeta) = \mu_2, \quad \eta_3(\zeta) = \lambda_1, \quad \eta_4(\zeta) = \lambda_2 \tag{5.27b}$$

$$a_1(z,\zeta) = 0, \quad a_2(z,\zeta) = 0, \quad a_3(z,\zeta) = \sigma_{11}^{-+}(\zeta), \quad a_4(z,\zeta) = \sigma_{12}^{-+}(\zeta) \tag{5.27c}$$

$$b_1(z,\zeta) = 0, \quad b_2(z,\zeta) = 0, \quad b_3(z,\zeta) = \sigma_{21}^{-+}(\zeta), \quad b_4(z,\zeta) = \sigma_{22}^{-+}(\zeta) \tag{5.27d}$$

$$c_1(z,\zeta) = \sigma_{11}^{+-}(\zeta), \quad c_2(z,\zeta) = \sigma_{12}^{+-}(\zeta), \quad c_3(z,\zeta) = 0, \quad c_4(z,\zeta) = 0 \tag{5.27e}$$

$$d_1(z,\zeta) = \sigma_{21}^{+-}(\zeta), \quad d_2(z,\zeta) = \sigma_{22}^{+-}(\zeta), \quad d_3(z,\zeta) = 0, \quad d_4(z,\zeta) = 0 \tag{5.27f}$$

Due to one of the boundary conditions for $M_{21}(x,\xi)$ being defined along the line $(x,1)$ rather than $(0,\xi)$, the boundary conditions in this case become of the form

$$K(z,z) = f_1(z) \tag{5.28a}$$
$$L(z,z) = f_2(z) \tag{5.28b}$$
$$P(z,0) = \varrho_1 K(z,0) + \varrho_2 L(z,0) \tag{5.28c}$$
$$R(1,\zeta) = 0 \tag{5.28d}$$

where we can define

$$f_1(z) = \frac{\sigma_{11}^{-+}(z)}{\mu_1 + \lambda_1}, \qquad f_2(z) = \frac{\sigma_{21}^{+-}(z)}{\mu_2 + \lambda_1} \tag{5.29a}$$
$$\varrho_1 = Q_{11}, \qquad \varrho_2 = Q_{12} \tag{5.29b}$$

Observe, however, that the boundary condition (5.24) is a simple extension of the boundary condition (5.11), whereas (5.28) breaks this pattern. By looking at the coefficient assignments in Appendix A, we can see that either $\sigma_{11}^{+-}(x) = \sigma_{11}^{-+}(x) = \sigma_{22}^{+-}(x) = \sigma_{22}^{-+}(x) = 0$ or $\sigma_{12}^{+-}(x) = \sigma_{12}^{-+}(x) = \sigma_{21}^{+-}(x) = \sigma_{21}^{-+}(x) = 0$. This can be exploited to simplify fitting the boundary condition, $M_{21}(x,1) = 0$, into the framework already established. Depending on the situation, only either $N_{11}(x,\xi)$ or $N_{21}(x,\xi)$ will be coupled with $M_{21}(x,\xi)$ point-wise in the domain, the other one will only be coupled via the boundary condition.

From Appendix A we see that for *Cases I & IV* the equations are coupled as

$$-\mu_1 N_{11,x}(x,\xi) + \lambda_1 N_{11,\xi}(x,\xi) = \sigma_{12}^{-+}(x) M_{21}(x,\xi) \tag{5.30a}$$
$$\lambda_2 M_{21,x}(x,\xi) + \lambda_1 M_{21,\xi}(x,\xi) = \sigma_{21}^{+-}(x) N_{21}(x,\xi) \tag{5.30b}$$

and

$$-\mu_2 N_{21,x}(x,\xi) + \lambda_1 N_{21,\xi}(x,\xi) = \sigma_{21}^{-+}(x) M_{11}(x,\xi) \tag{5.31a}$$
$$\lambda_1 M_{11,x}(x,\xi) + \lambda_1 M_{11,\xi}(x,\xi) = \sigma_{12}^{+-}(x) N_{21}(x,\xi) \tag{5.31b}$$

with respect to being connected point-wise in the domain interior. However, for

Cases II & III they are instead coupled as

$$-\mu_1 N_{11,x}(x,\xi) + \lambda_1 N_{11,\xi}(x,\xi) = \sigma_{11}^{-+}(x) M_{11}(x,\xi) \tag{5.32a}$$
$$\lambda_1 M_{11,x}(x,\xi) + \lambda_1 M_{11,\xi}(x,\xi) = \sigma_{11}^{+-}(x) N_{11}(x,\xi) \tag{5.32b}$$

and

$$-\mu_2 N_{21,x}(x,\xi) + \lambda_1 N_{21,\xi}(x,\xi) = \sigma_{22}^{-+}(x) M_{21}(x,\xi) \tag{5.33a}$$
$$\lambda_2 M_{21,x}(x,\xi) + \lambda_1 M_{21,\xi}(x,\xi) = \sigma_{22}^{+-}(x) N_{21}(x,\xi) \tag{5.33b}$$

respectively. Consider instead the coordinate transformations $x \to (1-z)$ and $\xi \to (1-\zeta)$ for (5.30) and (5.33). Apply also the coordinate transformations $x \to \zeta$ and $\xi \to z$ for (5.31) and (5.32). For (5.30) and (5.31) we obtain the same definitions as in (5.26) for $L(z,\zeta)$ and $P(z,\zeta)$, but for $K(z,\zeta)$ and $R(z,\zeta)$ we instead have

$$K(z,\zeta) = N_{11}(1-z, 1-\zeta), \tag{5.34a}$$
$$R(z,\zeta) = M_{21}(1-z, 1-\zeta). \tag{5.34b}$$

For (5.32) and (5.33) the assignments for $K(z,\zeta)$ and $P(z,\zeta)$ are the same as (5.26), but the definitions $L(z,\zeta)$ and $R(z,\zeta)$ become

$$L(z,\zeta) = N_{21}(1-z, 1-\zeta), \tag{5.35a}$$
$$R(z,\zeta) = M_{21}(1-z, 1-\zeta). \tag{5.35b}$$

Applying the coordinate transformation $x \to (1-z)$ and $\xi \to (1-\zeta)$ along with the chain rule to (5.30), we obtain

$$\mu_1 N_{11,z}(1-z,1-\zeta) - \lambda_1 N_{11,\zeta}(1-z,1-\zeta) = \sigma_{12}^{-+}(1-z) M_{21}(1-z,1-\zeta) \tag{5.36a}$$
$$-\lambda_2 M_{21,z}(1-z,1-\zeta) - \lambda_1 M_{21,\zeta}(1-z,1-\zeta) = \sigma_{21}^{+-}(1-z) N_{11}(1-z,1-\zeta) \tag{5.36b}$$

For (5.31) we apply $x \to \zeta$ and $\xi \to z$, therefore obtaining

$$-\mu_2 N_{21,\zeta}(\zeta,z) + \lambda_1 N_{21,z}(\zeta,z) = \sigma_{21}^{-+}(\zeta) M_{11}(\zeta,z) \tag{5.37a}$$
$$\lambda_1 M_{11,\zeta}(\zeta,z) + \lambda_1 M_{11,z}(\zeta,z) = \sigma_{12}^{+-}(\zeta) N_{21}(\zeta,z) \tag{5.37b}$$

Thus, by applying the definitions of $L(z,\zeta)$ and $P(z,\zeta)$ given by (5.26) and

$K(z,\zeta)$ and $R(z,\zeta)$ found in (5.34), we find by comparing to (5.21) the following coefficient assignments can be used for *Case I & IV*

$$\varepsilon_1(z)=\mu_1, \quad \varepsilon_2(z)=\lambda_1, \quad \varepsilon_3(z)=\lambda_1, \quad \varepsilon_4(z)=\lambda_2 \tag{5.38a}$$

$$\eta_1(\zeta)=\lambda_1, \quad \eta_2(\zeta)=\mu_2, \quad \eta_3(\zeta)=\lambda_1, \quad \eta_4(\zeta)=\lambda_1 \tag{5.38b}$$

$$a_1(z,\zeta)=0, \quad a_2(z,\zeta)=0, \quad a_3(z,\zeta)=0, \quad a_4(z,\zeta)=\sigma_{12}^{-+}(1-z) \tag{5.38c}$$

$$b_1(z,\zeta)=0, \quad b_2(z,\zeta)=0, \quad b_3(z,\zeta)=\sigma_{21}^{-+}(\zeta), \quad b_4(z,\zeta)=0 \tag{5.38d}$$

$$c_1(z,\zeta)=0, \quad c_2(z,\zeta)=\sigma_{12}^{+-}(\zeta), \quad c_3(z,\zeta)=0, \quad c_4(z,\zeta)=0 \tag{5.38e}$$

$$d_1(z,\zeta)=-\sigma_{21}^{+-}(1-z), \quad d_2(z,\zeta)=0, \quad d_3(z,\zeta)=0, \quad d_4(z,\zeta)=0 \tag{5.38f}$$

For *Cases II & III* we apply $x\to\zeta$ and $\xi\to z$ to (5.32), giving us

$$-\mu_1 N_{11,\zeta}(\zeta,z)+\lambda_1 N_{11,z}(\zeta,z)=\sigma_{11}^{-+}(\zeta)M_{11}(\zeta,z) \tag{5.39a}$$

$$\lambda_1 M_{11,\zeta}(\zeta,z)+\lambda_1 M_{11,z}(\zeta,z)=\sigma_{11}^{+-}(\zeta)N_{11}(\zeta,z) \tag{5.39b}$$

and we also apply $x\to(1-z)$ and $\xi\to(1-\zeta)$ so that

$$\mu_2 N_{21,z}(1-z,1-\zeta)-\lambda_1 N_{21,\zeta}(1-z,1-\zeta)=\sigma_{22}^{-+}(1-z)M_{21}(1-z,1-\zeta), \tag{5.40a}$$

$$-\lambda_2 M_{21,z}(1-z,1-\zeta)-\lambda_1 M_{21,\zeta}(1-z,1-\zeta)=\sigma_{22}^{+-}(1-z)N_{21}(1-z,1-\zeta). \tag{5.40b}$$

This gives us the coefficient assignments

$$\varepsilon_1(z)=\lambda_1, \quad \varepsilon_2(z)=\mu_2, \quad \varepsilon_3(z)=\lambda_1, \quad \varepsilon_4(z)=\lambda_2 \tag{5.41a}$$

$$\eta_1(\zeta)=\mu_1, \quad \eta_2(\zeta)=\lambda_1, \quad \eta_3(\zeta)=\lambda_1, \quad \eta_4(\zeta)=\lambda_1 \tag{5.41b}$$

$$a_1(z,\zeta)=0, \quad a_2(z,\zeta)=0, \quad a_3(z,\zeta)=\sigma_{11}^{-+}(\zeta), \quad a_4(z,\zeta)=0 \tag{5.41c}$$

$$b_1(z,\zeta)=0, \quad b_2(z,\zeta)=0, \quad b_3(z,\zeta)=0, \quad b_4(z,\zeta)=\sigma_{22}^{-+}(1-z) \tag{5.41d}$$

$$c_1(z,\zeta)=\sigma_{11}^{+-}(\zeta), \quad c_2(z,\zeta)=0, \quad c_3(z,\zeta)=0, \quad c_4(z,\zeta)=0 \tag{5.41e}$$

$$d_1(z,\zeta) = 0, \qquad d_2(z,\zeta) = -\sigma_{22}^{+-}(1-z), \quad d_3(z,\zeta) = 0, \qquad d_4(z,\zeta) = 0 \tag{5.41f}$$

For *Cases I & IV*, we see from Appendix A that $Q_{21} = Q_{12} = 0$, and for *Cases II & III* $Q_{11} = Q_{22} = 0$. Applying this fact together with the boundary conditions (5.19) and (5.20), we can obtain by applying the appropriate transformations for *Case I & IV*

$$N_{11}(1-z,1-z) = 0 \tag{5.42a}$$
$$N_{21}(\zeta,\zeta) = \frac{\sigma_{21}^{-+}(\zeta)}{\mu_2 + \lambda_1} \tag{5.42b}$$
$$M_{11}(z,0) = Q_{11}N_{11}(1,1-z) \tag{5.42c}$$
$$M_{21}(z,0) = 0 \tag{5.42d}$$

and for *Cases II & III*

$$N_{11}(\zeta,\zeta) = \frac{\sigma_{11}^{-+}(\zeta)}{\mu_1 + \lambda_1} \tag{5.43a}$$
$$N_{21}(1-z,1-z) = 0 \tag{5.43b}$$
$$M_{11}(z,0) = Q_{12}N_{21}(1,1-z) \tag{5.43c}$$
$$M_{21}(z,0) = 0 \tag{5.43d}$$

Recognizing that the boundary (ζ,ζ) is equivalent to (z,z) the boundary conditions can be seen to be of the form

$$K(z,z) = f_1(z) \tag{5.44a}$$
$$L(z,z) = f_2(z) \tag{5.44b}$$
$$P(z,0) = \varrho_1 K(1,1-z) + \varrho_2 L(1,1-z) \tag{5.44c}$$
$$R(z,0) = \varrho_3 K(1,1-z) + \varrho_4 (L(1,1-z) \tag{5.44d}$$

and for *Cases I & IV* we get

$$f_1(z) = 0, \qquad f_2(z) = \frac{\sigma_{21}^{-+}(z)}{\mu_2 + \lambda_1} \tag{5.45a}$$
$$\varrho_1 = 1, \qquad \varrho_2 = 0, \tag{5.45b}$$
$$\varrho_3 = 0, \qquad \varrho_4 = 0 \tag{5.45c}$$

whilst for *Cases II & III*

$$f_1(z) = \frac{\sigma_{11}^{-+}(z)}{\mu_1 + \lambda_1}, \qquad f_2(z) = 0 \tag{5.46a}$$

$$\varrho_1 = 0, \qquad \varrho_2 = 1, \tag{5.46b}$$

$$\varrho_3 = 0, \qquad \varrho_4 = 0. \tag{5.46c}$$

5.3.3.2 Square domain kernels

Finally, k_{21} in (3.51)–(3.52) must be solved over the square domain $\mathcal{S}_0 = \{(x,\xi) \mid 0 \leq x,\xi \leq 1\}$., and comparing to (5.6) we find upwards-right convecting characteristics and boundary conditions (5.48) for both $(x,0)$ and $(0,\xi)$, as can be seen from Fig. 5.1d. It is reproduced here as

$$\lambda_2 k_{21,x}(x,\xi) + \lambda_1 k_{21,\xi}(x,\xi) = 0, \tag{5.47}$$

and with boundary conditions reproduced from (3.71) as

$$k_{21}(x,0) = 0, \tag{5.48a}$$

$$k_{21}(0,\xi) = h_{21}(\xi), \tag{5.48b}$$

where $h_{21}(\xi) = Q_{21}N_{11}(0,\xi) + Q_{22}N_{21}(0,\xi) - M_{21}(0,\xi)$ appearing in the second boundary condition of (5.48) depends on the solution to the PDE set (5.17)–(5.20).

Through relabelling $t \to \xi$, (5.47)–(5.48) can be written as the advection equation (2.22) with $\epsilon = \frac{\lambda_2}{\lambda_1}$. Let $\mathcal{S}_0$ be divided into an $\hat{N} \times \hat{M}$ grid, where $\Delta_x = \frac{1}{\hat{N}-1}$ and $\Delta_\xi = \frac{1}{\hat{M}-1}$ are the grid dimensions along the x and ξ axis, respectively. Additionally the indices $1 \leq i \leq \hat{N}$ and $1 \leq j \leq \hat{M}$ are used to specify grid coordinates. We see that (5.47) can be put into the form (5.6) with $\epsilon_1 = \epsilon$, $\epsilon_2 = 1$ and $f(x,\xi) = 0$. Denoting $w_i^j = w(i\Delta_x, j\Delta_\xi)$, we discretize (5.47) using first order backward difference along both the x and ξ axis, which gives us in the notation just introduced that

$$\epsilon \frac{w_i^j - w_{i-1}^j}{\Delta_x} + \frac{w_i^j - w_i^{j-1}}{\Delta_\xi} = 0. \tag{5.49}$$

Solving for w_i^j then gives us

$$w_i^j = \frac{\frac{\epsilon}{\Delta_x} w_{i-1}^j + \frac{1}{\Delta_\xi} w_i^{j-1}}{\frac{\epsilon}{\Delta_x} + \frac{1}{\Delta_\xi}}. \tag{5.50}$$

Using (5.50) for all interior grid points $(i,j) \in \{2,\ldots,\hat{N}\} \times \{2,\ldots,\hat{M}\}$, a linear system can be set up allowing the solution of all interior points to be found simultaneously from the boundary conditions defined for the grid points

$\{(1, j) \mid j \in \{1, \ldots, \hat{M}\}\}$ and $\{(i, 1) \mid i \in \{1, \ldots, \hat{N}\}\}$.

5.4 Simulator Structure

The simulation code is structured in the following manner. Firstly the parameters along with boundary and initial conditions of the 2×2 system are initialized together with other relevant variables. In order to calculate the minimum time bilateral observer gains, a $2+2$ system is initialized based on the 2×2 system according to the assignments from Appendix A. The kernel equations for the resultant $2+2$ system are set up and solved, the details of which have been explained in Section 5.3. Next the minimum time observer gains can be calculated by applying (3.53) and (3.73). In order to evaluate the integrals appearing in, for example, (3.73), trapezoidal integration was used for numerically approximating the integrals in the implementation written for this thesis. See Appendix B for more information on trapezoidal integration. After the $2+2$ minimum time collocated observer gains had been calculated, the minimum time bilateral observer gains could be found from these by also applying the relevant equations from Appendix A.

To calculate the observer gains for the single boundary 2×2 observer which will be used to benchmark the bilateral 2×2 observer performance, the observer kernels (5.3)–(5.4) need to be solved, which has also been explained in Section 5.3. The observer gains are then calculated with (5.2).

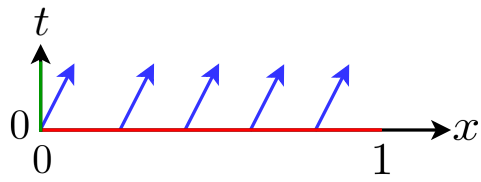

(a) Characteristics for $u(x,t)$ are given by the blue arrows. The red line describes where the initial conditions $u(x,0)$ are defined whereas the boundary condition $u(0,t)$ is defined along the green line.

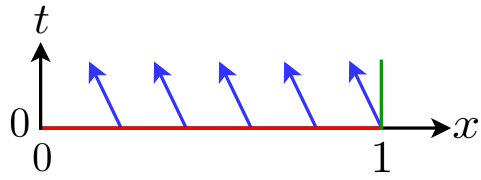

(b) Characteristics for $v(x,t)$ are given by the blue arrows. The red line describes where the initial conditions $v(x,0)$ are defined whereas the boundary condition $v(1,t)$ is defined along the green line.

Figure 5.2: Illustration of characteristics and boundary conditions in the respective domains of kernel PDEs we are interested in solving. The blue arrows are characteristics, the boundary conditions are defined along the green line whilst the initial conditions are found along the red line.

When both unilateral and bilateral minimum time observer gains have been

calculated, the actual simulation can be started. A finite difference time marching scheme is used for both the actual 2×2 system and the two 2×2 observer algorithms. Measurements $y_1(t)$ and $y_2(t)$ from both sides of the domain are provided to the bilateral observer, whereas only the right boundary measurement $y_1(t)$ is provided to the unilateral observer. Assuming that we are at time t, the 2×2 system states $u(x,t)$ and $v(x,t)$ are calculated based on information about the previous states $u(x,t-h)$ and $v(x,t-h)$ respectively and relevant boundary conditions, where h is the size of the time step used. Applying the method of characteristics to the 2×2 system (4.1) with constant λ and μ, we see that the characteristics for $u(x,t)$ move along the line $x(t)=x_0+\lambda t$, whilst the characteristics for $v(x,t)$ move along $x(t)=x_0-\mu t$. This can be visualized by Fig. 5.2 where the red line represents the region where initial conditions are defined, the green line is the boundary condition and the blue arrows represent characteristic lines.

The direction of the characteristics shown in Fig. 5.2 must be taken into account when setting up the finite scheme for $u(x,t)$ and $v(x,t)$. Let the x domain be discretized into $\hat{N}$ grid points, with spacing $\Delta=\frac{1}{\hat{N}-1}$. The time step is given by h. Fig. 5.2a shows that $u(x,t)$ propagates information towards the left and uses the left boundary, so a first order finite difference *upwind* scheme for $u(x,t)$ with the notation $u_i^n=u(i\Delta,nh)$ is

$$\frac{u_i^{n+1}-u_i^n}{h}+\lambda\frac{u_i^n-u_{i-1}^n}{\Delta}=\sigma^+(i\Delta)v_i^n. \tag{5.51}$$

Likewise we see from Fig. 5.2b that information must be taken from the right of the point being calculated, and therefore the first order finite difference *downwind* scheme appropriate for $v(x,t)$, using the notation $v_i^n=v(i\Delta,nh)$, is

$$\frac{v_i^{n+1}-v_i^n}{h}-\mu\frac{v_{i+1}^n-v_i^n}{\Delta}=\sigma^-(i\Delta)u_i^n. \tag{5.52}$$

Both (5.51) and (5.52) allow the value of $u(x,t)$ and $v(x,t)$ to be calculated from the boundary conditions $u(0,t)$ and $v(1,t)$ along with states $u(x,t-h)$ and $v(x,t-h)$, respectively, of the previous time step.

The observer algorithms are both implemented with similar finite difference schemes to (5.51) for $\hat{u}(x,t)$ and (5.52) for $\hat{v}(x,t)$, the biggest difference being that the observer gains multiplied by measurement errors are added to the right hand side. After the simulation has been run for the desired amount of time, the results are output and plots are generated. Fig. 5.3 summarizes the simulator description just given.

Next, in Chapter 6, plots generated from simulations using the simulator just described for two toy examples are given. After this, in Chapters 7 and 8, the simulator is applied again but for an oil drilling application.

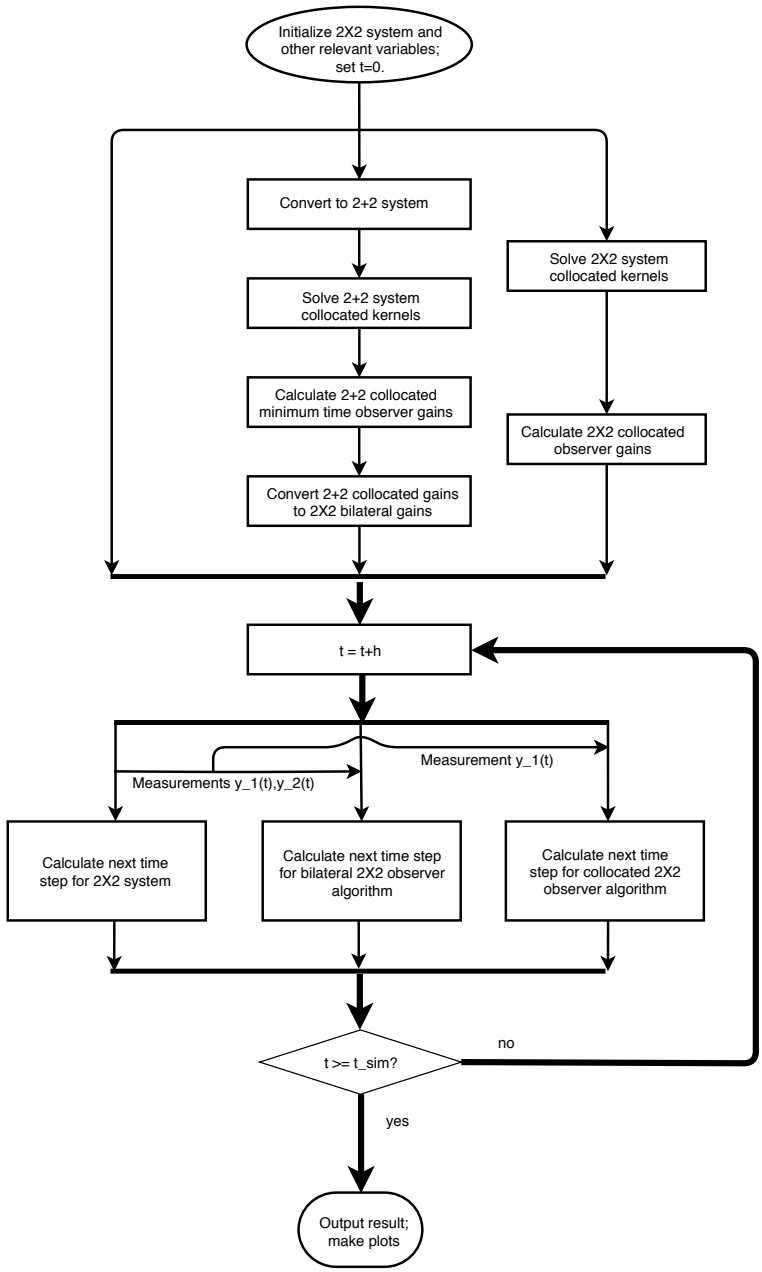

Figure 5.3: Flowchart summarizing simulator used for comparing the performance of the bilateral 2×2 observer derived in the dissertation with a previously derived 2×2 unilateral observer.

Chapter 6

2×2 Observer Simulations

6.1 Introduction

The 2×2 system (4.1)–(4.2) with constant transport velocities $\lambda(x) = \lambda$ and $\mu(x) = \mu$ and its minimum time bilateral observer (4.62) were implemented in MATLAB in the way described in Chapter 5. To showcase the performance of the bilateral observer, it is compared with a previously derived unilateral observer (5.1) for the 2×2 system, also implemented in MATLAB.

The simulations shown here are for two *toy* examples, so neither the system coefficients nor the initial and boundary conditions are physically motivated. For the first example, $\lambda > \mu$, whereas in the second example $\mu > \lambda$. The reason these two examples are shown is that they represent different cases in Appendix A, namely *Case II* and *Case III* respectively.

The following plots are given for both simulations:

1. Firstly plots of the 2×2 system states $u(x,t)$ and $v(x,t)$, which are to be estimated by the observers, are given.

2. Next, to compare with each other and the actual states, the estimates $\hat{u}(x,t)$ and $\hat{v}(x,t)$ from both the bilateral and the unilateral observers are shown.

3. However, since it is difficult to see from the state estimates how quickly the observers produce correct estimates, the observer estimation errors $\tilde{u}(x,t)$ and $\tilde{v}(x,t)$ for both observers are shown.

4. After this the Euclidean norm $||\tilde{u}(t)|| = \sqrt{\int_0^1 \tilde{u}^2(x,t)dx}$ and $||\tilde{v}(t)|| = \sqrt{\int_0^1 \tilde{v}^2(x,t)dx}$ of the estimation errors are shown, to get an indication of when estimation errors across the spatial domain have entirely vanished for both observers.

5. For completeness the bilateral observer gains $P^{++}(x)$, $P^{+-}(x)$, $P^{-+}(x)$ and $P^{--}(x)$ used in the simulation are shown, followed by the unilateral observer gains $\bar{P}^{+}(x)$ and $\bar{P}^{-}(x)$.

6. Additionally the solution to the $2+2$ collocated kernels $M_{11}(x,\xi)$, $M_{12}(x,\xi)$, $M_{21}(x,\xi)$, $M_{22}(x,\xi)$, $N_{11}(x,\xi)$, $N_{12}(x,\xi)$, $N_{21}(x,\xi)$, $N_{22}(x,\xi)$ over $\mathcal{T}_u$ and $K_{21}(x,\xi)$ over $\mathcal{S}_0$ from which the 2×2 bilateral observer gains were calculated are shown. Also the 2×2 unilateral observer kernel equation solutions $\bar{M}(x,\xi)$ and $\bar{N}(x,\xi)$ over $\mathcal{T}_u$ are shown.

When running the simulations, the initial conditions $u(x,0) = u_0(x)$ and $v(x,0) = v_0(x)$ are assumed unknown to the observers. Instead the observers are initialized with the estimates $\hat{u}(x,0) = 0$ and $\hat{v}(x,0) = 0$, representing that the observers know nothing about the states initially. Additionally no control inputs are used, so $U_1(t) = U_2(t) = 0$.

6.2 Simulation 1: $\lambda > \mu$

The 2×2 system implemented in the simulations shown in this section and for which observers were computed and implemented can be specified by the values in Table 6.1. Apart from the criterion that $\lambda > \mu$, the parameters were chosen so that the 2×2 system stayed marginally stable during the duration of the simulation, as will be seen from the plots of the system states.

λ	$\frac{2}{3}$
μ	$\frac{1}{2}$
$\sigma^+(x)$	x^2
$\sigma^-(x)$	$-\sin(3x)$
Q	1
R	$\frac{1}{2}$
$u_0(x)$	$\cos(8x)$
$v_0(x)$	e^{-x}

Table 6.1: Coefficients, boundary and initial conditions for simulations in Section 6.2

For Section 6.2 the spatial coordinate $x \in [0,1]$ whilst time $t \in [0,5]$. The x axis is discretized into $\hat{N} = 240$ grid points, and a time step $h = 0.001$ was used. For ease of implementation however, the $2+2$ collocated observer gains are solved over a grid of dimension $\frac{\hat{N}}{2}\times\frac{\hat{N}}{2}$, and hence the $2+2$ collocated observer gains were found over an x axis discretized into $\frac{\hat{N}}{2}$ grid points. The 2×2 unilateral observer kernels are solved directly over a grid of dimension $\hat{N}\times\hat{N}$.

6.2.1 Simulation Plots

System States

The evolution of $u(x,t)$ and $v(x,t)$ described by (4.1)–(4.2) for $(x,t) \in [0,1]\times[0,5]$ with parameters specified in Table 6.1 is shown in Fig. 6.1, with Fig. 6.1a showing $u(x,t)$ and Fig. 6.1b showing $v(x,t)$.

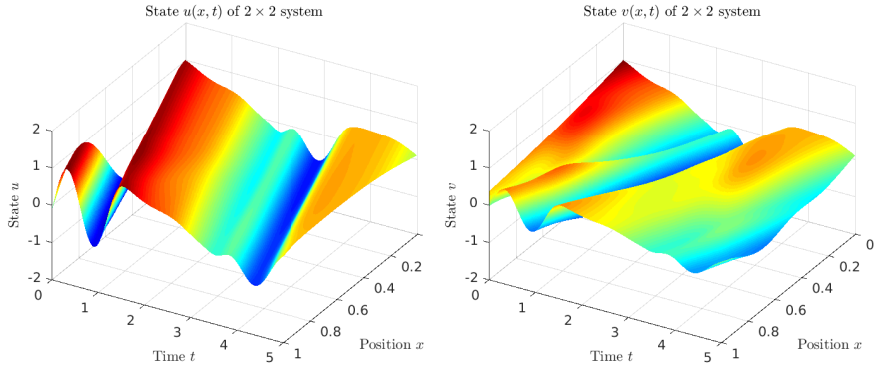

(a) State $u(x,t)$. **(b)** State $v(x,t)$.

Figure 6.1: States $u(x,t)$ and $v(x,t)$ of 2×2 system (4.1)–(4.2) evolving over the spatial interval $x \in [0,1]$ and time interval $t \in [0,5]$ when using the system parameters and initial conditions as given in Table 6.1

Observer Estimates

The plots shown in Fig. 6.2 show the estimates $\hat{u}(x,t)$ and $\hat{v}(x,t)$ produced by the 2×2 bilateral observer (4.62) when using the model with parameters given by Table 6.1. The former estimate can be seen from Fig. 6.2a whereas the latter are in Fig. 6.2b. The bilateral observer gains which were used are shown further down in this section.

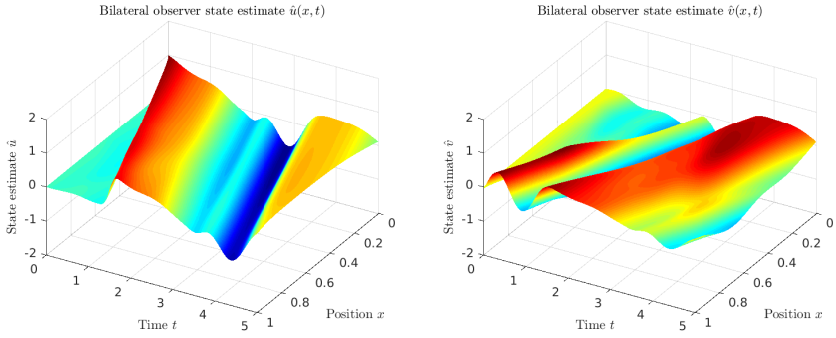

(a) Bilateral observer estimate $\hat{u}(x,t)$ **(b)** Bilateral observer estimate $\hat{v}(x,t)$

Figure 6.2: Bilateral observer estimates $\hat{u}(x,t)$ and $\hat{v}(x,t)$ produced by (4.62) for estimating the states $u(x,t)$ and $v(x,t)$, respectively, of the 2×2 system (4.1)–(4.2) using measurements $y_1(t) = u(1,t)$ and $y_2(t) = v(0,t)$. The model parameters used are in Table 6.1.

In Fig. 6.3 we see the state estimates $\hat{u}(x,t)$ and $\hat{v}(x,t)$ produced by the 2×2 unilateral observer (5.1) with model parameters from Table 6.1. Fig. 6.3a shows $\hat{u}(x,t)$ and Fig. 6.3b shows $\hat{v}(x,t)$. For the unilateral 2×2 observer gains used, see

the relevant graph further down this section.

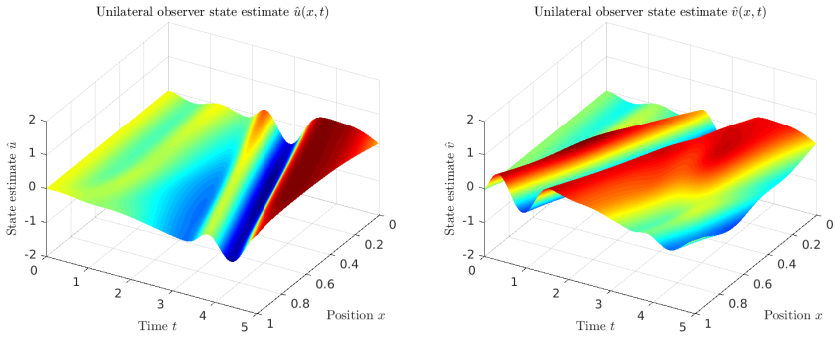

(a) Unilateral observer estimate $\hat{u}(x,t)$ **(b)** Unilateral observer estimate $\hat{v}(x,t)$

Figure 6.3: Unilateral observer estimates $\hat{u}(x,t)$ and $\hat{v}(x,t)$ produced by (5.1) for estimating the states $u(x,t)$ and $v(x,t)$, respectively, of the 2×2 system (4.1)–(4.2) using right boundary measurement $y(t) = u(1,t)$. The model parameters used are in Table 6.1.

By comparing Fig. 6.2 and Fig. 6.3 it is difficult to precisely see the difference in performance between the bilateral and unilateral 2×2 observers, especially with respect to convergence time. However, in Fig. 6.2a, we see the bilateral observer is able to quickly estimate a sharp transient moving from the left to right boundary early on, something which is present in the actual state $u(x,t)$ in Fig. 6.1a. As can be seen from Fig. 6.3a, the unilateral observer does however not pick this up. The estimates $\hat{v}(x,t)$ in from the bilateral and unilateral observers, in Fig. 6.2b and Fig. 6.3b respectively, appear similar, but also here we can see some slightly more efficient transient estimation from the bilateral observers side by comparing these plots to Fig. 6.1b.

Observer Estimation Errors

In Fig. 6.4 we see the estimation errors $\tilde{u}(x,t) = u(x,t) - \hat{u}(x,t)$ and $\tilde{v}(x,t) = v(x,t) - \hat{v}(x,t)$ when the estimates $\hat{u}(x,t)$ and $\hat{v}(x,t)$ are produced by the bilateral observer (4.62), with the 2×2 model defined by Table 6.1. Essentially Fig. 6.4a represents the values in Fig. 6.2a subtracted from the states $u(x,t)$ shown in Fig. 6.1a, whilst Fig. 6.4b represents values from Fig. 6.2b subtracted from values in Fig. 6.1b.

The corresponding errors in estimation $\tilde{u}(x,t)$ and $\tilde{v}(x,t)$ the unilateral observer (5.1) commits can be seen in Fig. 6.5, with Fig. 6.5a representing $\tilde{u}(x,t)$ and Fig. 6.5b displaying $\tilde{v}(x,t)$.

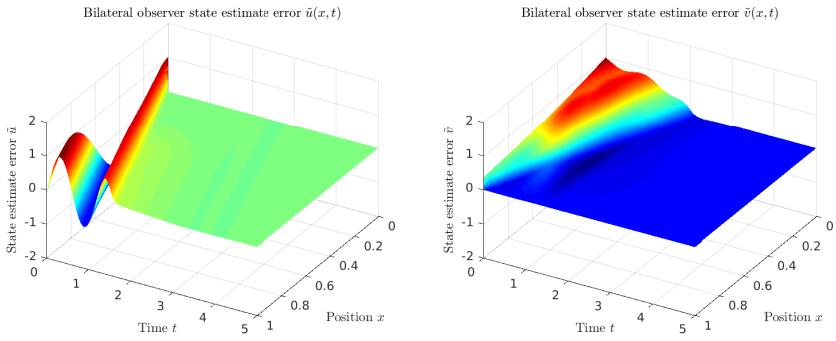

(a) Bilateral error $\tilde{u}(x,t)$ **(b)** Bilateral error $\tilde{v}(x,t)$

Figure 6.4: Bilateral observer estimation errors $\tilde{u}(x,t)$ and $\tilde{v}(x,t)$ when trying to estimate the states $u(x,t)$ and $v(x,t)$ of (4.1)–(4.2) using estimates $\hat{u}(x,t)$ and $\hat{v}(x,t)$ from the bilateral observer (4.62). The model parameters used are in Table 6.1.

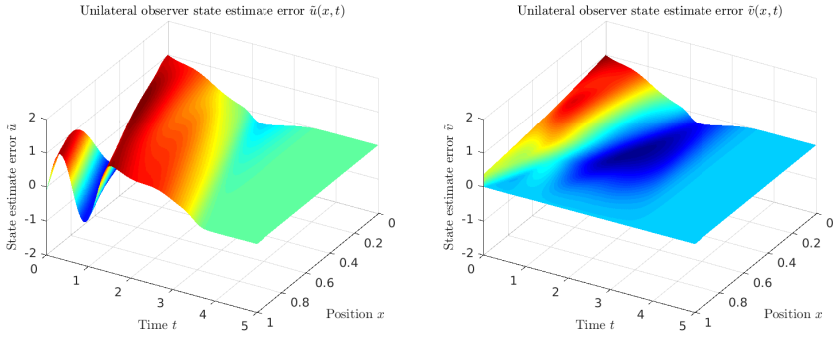

(a) Unilateral observer error $\tilde{u}(x,t)$. **(b)** Unilateral observer error $\tilde{v}(x,t)$.

Figure 6.5: Unilateral observer estimation errors $\tilde{u}(x,t)$ and $\tilde{v}(x,t)$ when trying to estimate the states $u(x,t)$ and $v(x,t)$ of (4.1)–(4.2) using estimates $\hat{u}(x,t)$ and $\hat{v}(x,t)$ from (5.1). The model parameters used are in Table 6.1.

The plots in Fig. 6.4 and Fig. 6.5 give a better indication of the efficiency of the two observers in producing correct state estimates than just observing the plots of the estimates $\hat{u}(x,t)$ and $\hat{v}(x,t)$. This is due to the fact that the closer the errors $\tilde{u}(x,t)$ and $\tilde{v}(x,t)$ are to 0, the better the estimate is. Comparing Fig. 6.4a to Fig. 6.5a, the error $\tilde{u}(x,t)$ seems to vanish much more quickly in the former than the latter. Fig. 6.4b compared to Fig. 6.5b also shows some improvement in efficiency of prediction when using measurements from both sides of the domain rather than only the right boundary, but the difference is not as dramatic as it was for $\tilde{u}(x,t)$ since $\tilde{v}(x,t)$ is not far from vanishing in Fig. 6.5b when it seems to have converged to 0 in Fig. 6.4b.

A useful indicator of the absolute magnitude of the estimation error for cases such as these when it is continuously distributed across a spatial domain is the

Euclidean norm of the error, defined in general by (1.1). Structural information with respect to where along the spatial domain the errors are located is lost, but instead it gives us a digest of the total estimation summarized by a single number, making it easier to observe when the total estimation error has vanished than it was in Fig. 6.4 and Fig. 6.5.

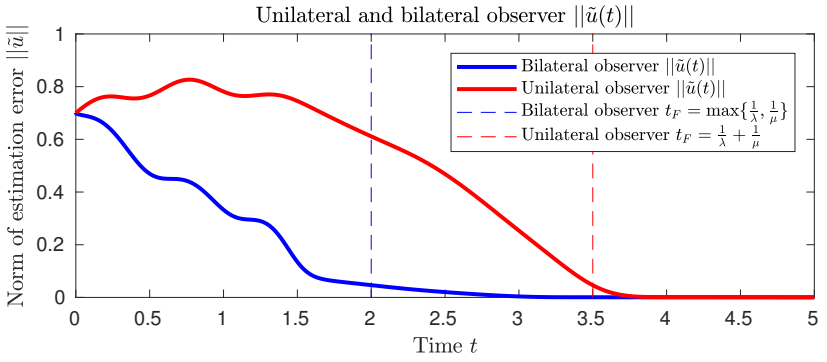

(a) Euclidean norms $||\tilde{u}(t)||$ of estimation errors $\tilde{u}(x,t)$.

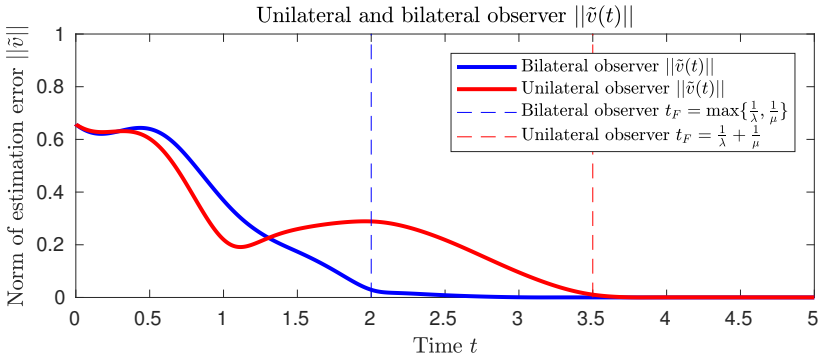

(b) Euclidean norms $||\tilde{v}(t)||$ of estimation errors $\tilde{v}(x,t)$.

Figure 6.6: Euclidean norms $||\tilde{u}(t)||$ and $||\tilde{v}(t)||$ of estimation errors $\tilde{u}(x,t)$ and $\tilde{v}(x,t)$ respectively for both bilateral and unilateral observers. The blue line shows the error norm for the bilateral observer estimates, whereas the red line shows the error norm for the unilateral observer estimate. The blue dashed line shows the expected theoretical convergence time $t_{2,min}$ of the bilateral observer, whereas the red dashed line shows the expected theoretical convergence time $t_{1,min}$ of the unilateral observer. The 2×2 model used parameters specified in Table 6.1.

In Fig. 6.6 we see the Euclidean norms $||\tilde{u}(t)|| = \sqrt{\int_0^1 \tilde{u}^2(x,t)dx}$ and $||\tilde{v}(t)|| = \sqrt{\int_0^1 \tilde{v}^2(x,t)dx}$ of the estimation errors $\tilde{u}(x,t)$ and $\tilde{v}(x,t)$ which can be found in Fig. 6.4 and Fig. 6.5 respectively. Fig. 6.6a shows the former norm whereas Fig. 6.6b shows the latter. For ease of direct comparison the error norms of both estimation

errors due to the estimates made by the bilateral observer are shown in the same plot as the estimates made by the unilateral observer. The blue line shows the error norm due to the bilateral observer, whilst the red line shows the one corresponding to the unilateral observer. Additionally, the expected theoretical convergence time is shown by a dashed line in both figures, with the dashed blue line showing the time $t_{2,min} = \max\{\frac{1}{\lambda}, \frac{1}{\mu}\}$ within which the bilateral observer estimate should match the 2×2 system states, and the red dashed line showing the time $t_{1,min} = \frac{1}{\lambda} + \frac{1}{\mu}$ when we should expect the unilateral observer estimation errors to have converged to 0.

Comparing Fig. 6.6a to Fig. 6.6b, it is clear that there is a much higher improvement in efficiency for estimating $u(x,t)$ than $v(x,t)$ when using the bilateral rather than unilateral 2×2 observer. Despite this, for both states the bilateral observer performs better than the unilateral observer. One possible explanation for the greater discrepancy in estimation error between the bilateral and unilateral observer when estimating $u(x,t)$ compared to $v(x,t)$ is that both observers have access to the right boundary measurement $y_1(t) = u(1,t)$ and can therefore incorporate this value directly into their right boundary condition $\hat{v}(1,t) = Ru(1,t)$, something which directly affects the estimate $\hat{v}(x,t)$. However, only the bilateral observer has access to the left boundary measurement $y_2(t) = v(0,t)$. Therefore the left boundary condition of the bilateral observer becomes $\hat{u}(0,t) = Qv(0,t)$, whereas the unilateral observer must instead input an estimate into the boundary condition, yielding $\hat{u}(0,t) = Q\hat{v}(0,t)$. This could cause producing estimates $\hat{u}(x,t)$ more difficult for the unilateral than bilateral observer. But of course the states are coupled with each other point-wise in the domain, so a larger estimation error in one of the states will affect the estimation error in the other state, and partially this is why the bilateral observer still produces correct estimates $\hat{v}(x,t)$ more quickly than the unilateral observer, despite the correct boundary condition value being fully available to both.

By the point in time the blue dashed line in Fig. 6.6 appears, the bilateral observer error norms $||\tilde{u}(t)||$ and $||\tilde{v}(t)||$ should have vanished in both plots. However, they are slightly nonzero for both cases. The same is true for the unilateral observer error norms. This is most likely due to numerical computation errors as all steps in their computation have been numerically approximated by first-order methods rather than calculated exactly.

6.2.2 Observer Gains and Kernel PDE Solutions

Bilateral 2×2 Observer Gains

The four plots in Fig. 6.7 show the 2×2 bilateral observer gains $P^{++}(x)$, $P^{+-}(x)$, $P^{-+}(x)$ and $P^{--}(x)$ across the spatial domain $[0,1] \ni x$ which have been used in producing the state estimates $\hat{u}(x,t)$ and $\hat{v}(x,t)$. These estimates are displayed in Fig. 6.2 and have been generated using the observer (4.62) when using model parameters from Table 6.1.

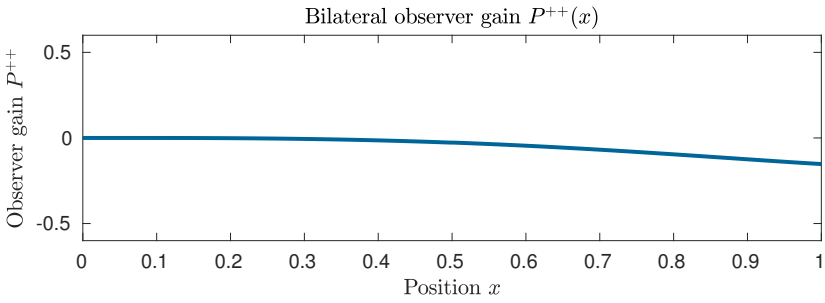

(a) Bilateral observer gain $P^{++}(x)$.

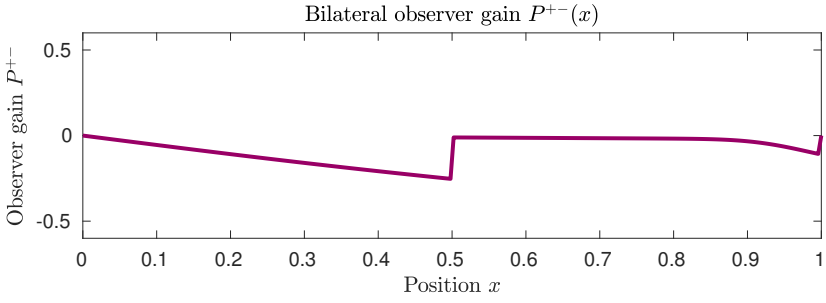

(b) Bilateral observer gain $P^{+-}(x)$.

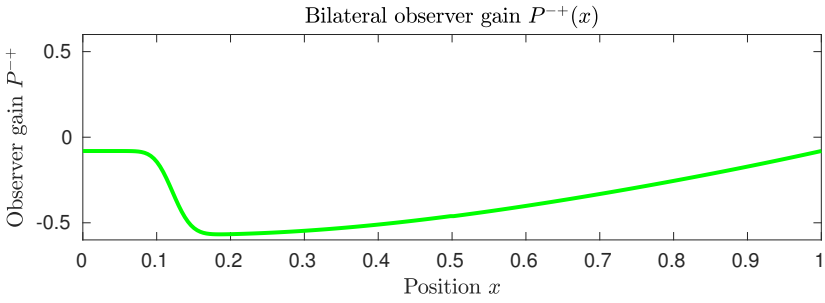

(c) Bilateral observer gain $P^{-+}(x)$.

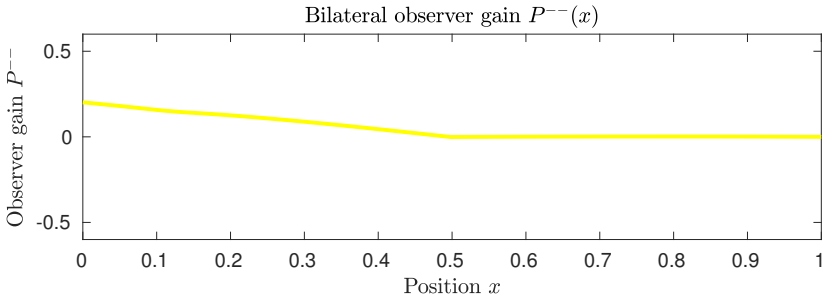

(d) Bilateral observer gain $P^{--}(x)$.

Figure 6.7: Bilateral observer gains used to calculate the state estimates $\hat{u}(x,t)$ and $\hat{v}(x,t)$ using the bilateral observer (4.62) for estimating the states $u(x,t)$ and $v(x,t)$ of the 2×2 system (4.1)–(4.2). The model parameters used are summarized in Table 6.1.

Fig. 6.7a shows the gain $P^{++}(x)$ which gets multiplied by the error term $y_1(t) - \hat{u}(1,t)$ in the PDE for $\hat{u}(x,t)$, Fig. 6.7b shows the gain $P^{+-}(x)$ which gets multiplied by the error term $y_2(t) - \hat{v}(0,t)$ in the PDE for $\hat{u}(x,t)$, Fig. 6.7c shows the gain $P^{-+}(x)$ which gets multiplied by the error term $y_1(t) - \hat{u}(1,t)$ in the PDE for $\hat{v}(x,t)$, and Fig. 6.7d shows the gain $P^{--}(x)$ which is multiplied by the error $y_2(t) - \hat{v}(0,t)$ featuring in the PDE for $\hat{v}(x,t)$. These gains were calculated from minimum time $2+2$ collocated kernels according to (A.14) in Appendix A. The $2+2$ gains used in (A.14) to calculate the 2×2 gains were calculated from (3.73). The numerical kernel PDE solutions used for these calculations can be seen further down in Section 6.2.

Unilateral 2×2 Observer Gains

In Fig. 6.8 we find the observer gains defined over the real number interval $[0,1] \ni x$ used to produce the 2×2 unilateral observer estimates $\hat{u}(x,t)$ and $\hat{v}(x,t)$ from (5.1). The estimates this observer produces given that the system parameters used are summarized in Table 6.1 are shown in Fig. 6.3.

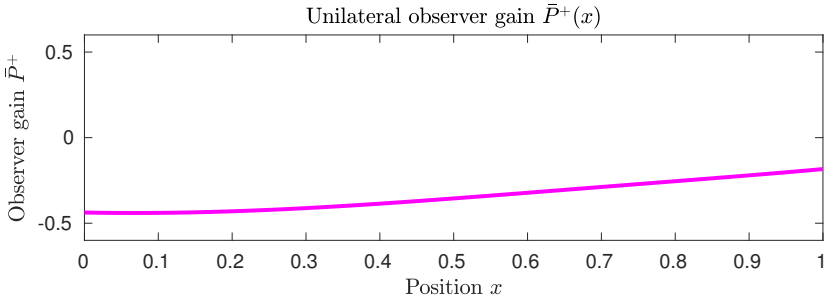

(a) Unilateral observer gain $\bar{P}^{+}(x)$.

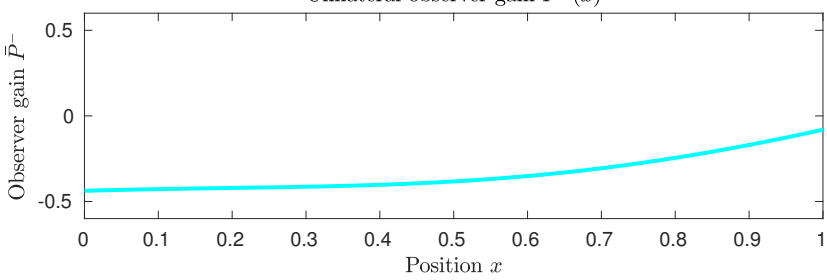

(b) Unilateral observer gain $\bar{P}^{-}(x)$.

Figure 6.8: Unilateral observer gains used to calculate the state estimates $\hat{u}(x,t)$ and $\hat{v}(x,t)$ using the unilateral observer (5.1) for estimating the states $u(x,t)$ and $v(x,t)$ of the 2×2 system (4.1)–(4.2). The model parameters used are summarized in Table 6.1.

We find in Fig. 6.8a the 2×2 unilateral observer gain $\bar{P}^{+}(x)$ which gets multiplied by the only error term $y(t) - \hat{u}(1,t)$ in the PDE for $\hat{u}(x,t)$, whilst Fig. 6.8b shows the other observer gain $\bar{P}^{-}(x)$ which gets multiplied by the same error term $y(t) - \hat{u}(1,t)$,

but appearing in the PDE for $\hat{v}(x,t)$. These observer gains are computed from (5.2). The numerical approximate solution to the kernel PDEs used here are given further down in Section 6.2.

Collocated $2+2$ Minimum Time Observer Kernel Solutions

To produce the observer gains shown in Fig. 6.7 to be used in conjunction with observer (4.62) for estimating states $u(x,t)$ and $v(x,t)$ of the 2×2 system (4.1)–(4.2) with parameters from Table 6.1, they were as mentioned earlier calculated from $2+2$ collocated observer gains according to (A.14), which in turn were calculated from (3.73). The four components of the $M(x,\xi)$ matrix kernel solution used in this calculation are shown in Fig. 6.9, with $(x,\xi) \in \mathcal{T}_u$.

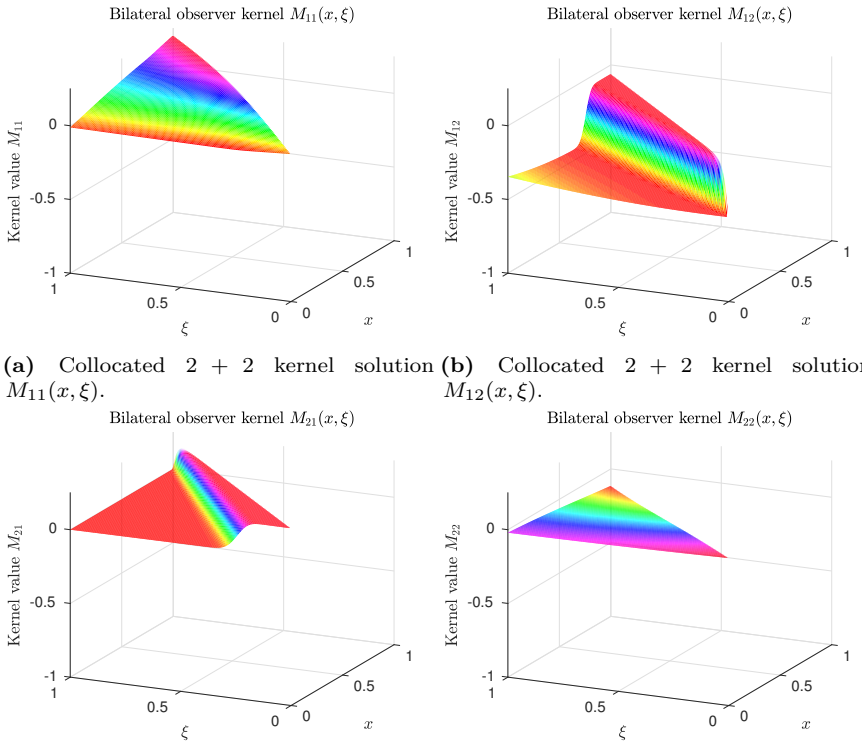

(a) Collocated $2+2$ kernel solution $M_{11}(x,\xi)$.

(b) Collocated $2+2$ kernel solution $M_{12}(x,\xi)$.

(c) Collocated $2+2$ kernel solution $M_{21}(x,\xi)$.

(d) Collocated $2+2$ kernel solution $M_{22}(x,\xi)$.

Figure 6.9: Collocated $2+2$ kernel solutions $M(x,\xi)$ over the upper triangular domain $\mathcal{T}_u$ to the first matrix PDE in (3.74) with boundary conditions (3.75), where the $2+2$ system parameters are defined according to *Case II* in Appendix A, which again are based on the 2×2 parameters defined in Table 6.1.

Fig. 6.9a shows $M_{11}(x,\xi)$ which corresponds with the top left matrix entry of $M(x,\xi)$, Fig. 6.9b shows $M_{12}(x,\xi)$ corresponding to the top right entry, Fig. 6.9c displays $M_{21}(x,\xi)$ which represents the values from the bottom left entry, and

Fig. 6.9d display $M_{22}(x,\xi)$ which are the values found in the bottom right entry of the 2×2 matrix $M(x,\xi)$.

$M(x,\xi)$ and $N(x,\xi)$ are solutions to the matrix PDE (3.74)–(3.75) with the $2+2$ system parameters found from *Case II* in Appendix A, which in turn are calculated from the 2×2 coefficients in Table 6.1. See Section 5.3 for an explanation of how these matrix kernel solutions were found. The four components of the $N(x,\xi)$ matrix kernel solution are shown in Fig. 6.10. Fig. 6.10a shows $N_{11}(x,\xi)$ which is the top left component of the 2×2 matrix $N(x,\xi)$, Fig. 6.10b shows $N_{12}(x,\xi)$ which is the top right component, the bottom left component $N_{21}(x,\xi)$ is in Fig. 6.10c and Fig. 6.10d shows the bottom right component $N_{22}(x,\xi)$.

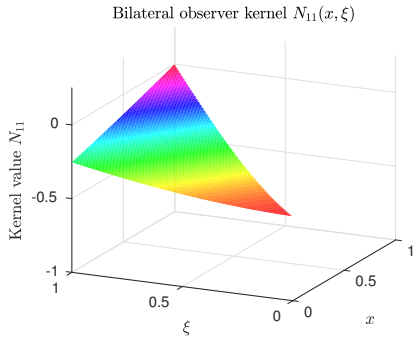

(a) Collocated 2+2 kernel solution $N_{11}(x,\xi)$.

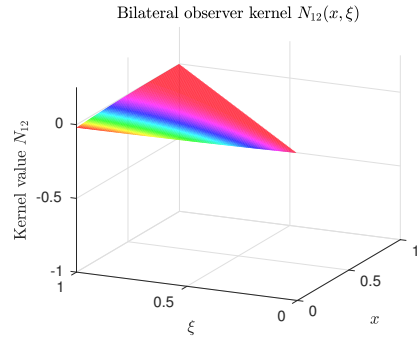

(b) Collocated $2+2$ kernel solution $N_{12}(x,\xi)$.

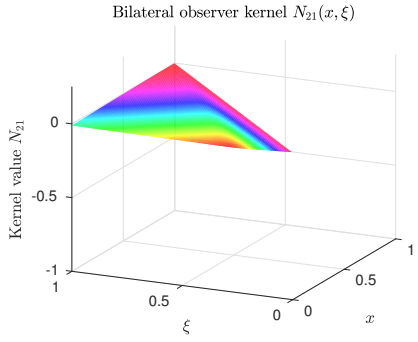

(c) Collocated 2+2 kernel solution $N_{21}(x,\xi)$.

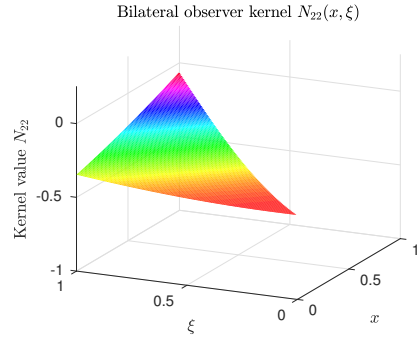

(d) Collocated $2+2$ kernel solution $N_{22}(x,\xi)$.

Figure 6.10: Collocated $2+2$ kernel solutions $N(x,\xi)$ over the upper triangular domain $\mathcal{T}_u$ to the second matrix PDE in (3.74) with boundary conditions (3.75), where the $2+2$ system parameters are defined according to *Case II* in Appendix A, which again are based on the 2×2 parameters defined in Table 6.1.

In addition to $2+2$ system transport velocities and the kernel matrix solutions $M(x,\xi)$ and $N(x,\xi)$, the $2+2$ collocated observer gains in (3.73) contain the lower triangular matrix $T^{+}(x)$ which is defined in (3.53). This term is dependent on the kernel solution $k_{21}(x,\xi)$ over $\mathcal{S}_0$ of (3.51)–(3.71), which is here in Fig. 6.11. The boundary condition for this PDE depends on the solution to the $M(x,\xi)$ and

$N(x,\xi)$ matrix PDEs shown in Fig. 6.9 and Fig. 6.10 respectively, so these were solved first, and $k_{21}(x,\xi)$ was solved for subsequently.

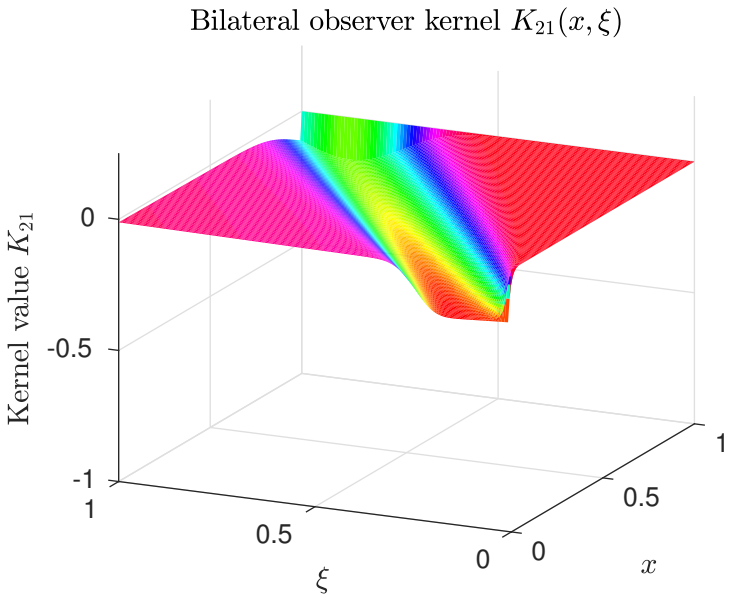

Figure 6.11: Collocated $2+2$ minimum time kernel solution $k_{21}(x,\xi)$ to (3.51)–(3.71) for the case when the $2+2$ system parameters are defined according to *Case II* in Appendix A which in turn are defined by 2×2 parameters from Table 6.1.

Unilateral 2×2 Observer Kernel Solutions

In order to calculate the 2×2 observer kernel gains shown in Fig. 6.8, of which there were only two, the PDE system (5.3)–(5.4) with scalar solutions $\bar{M}(x,\xi)$ and $\bar{N}(x,\xi)$ needed to be solved over the upper triangular domain $\mathcal{T}_u$. The solution to this system when the 2×2 system parameters are specified as in Table 6.1 is shown in Fig. 6.12. Here Fig. 6.12a shows the solution $\bar{M}(x,\xi)$ whereas Fig. 6.12b shows $\bar{N}(x,\xi)$.

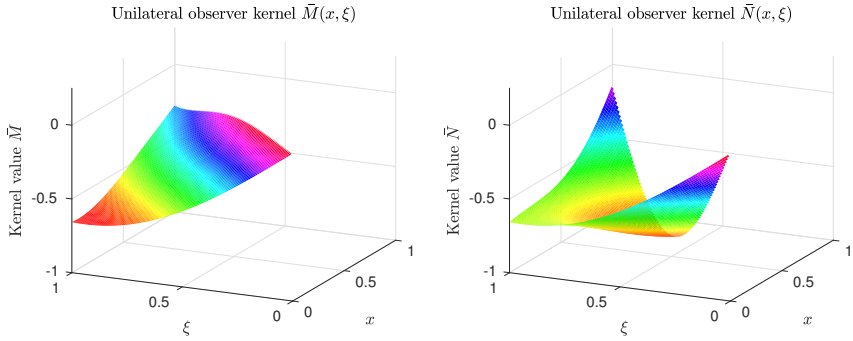

(a) Unilateral 2×2 kernel solution $\bar{M}(x,\xi)$. **(b)** Unilateral 2×2 kernel solution $\bar{N}(x,\xi)$.

Figure 6.12: Unilateral 2×2 kernel solutions to the PDE system (5.3)–(5.4) using system parameters defined in Table 6.1.

6.3 Simulation 2: $\lambda < \mu$

In order to test the 2×2 bilateral observer in a case where the 2×2 system (4.1)–(4.2) must be converted to a $2 + 2$ system in a different manner than the one the simulations shown in Section 6.2, which based itself on *Case II* from Appendix A, a case where instead the rightwards propagating transport velocity λ is smaller than the leftwards propagating transport velocity μ is considered here in Section 6.3. This corresponds to *Case III* from Appendix A. As in Section 6.2, apart from the criterion that $\mu > \lambda$, the parameters of the 2×2 system (4.1)–(4.2) were chosen to make the 2×2 system (4.1)–(4.2) marginally stable. They are summarized in Table 6.2.

λ	$\frac{1}{2}$
μ	1
$\sigma_+(x)$	$-2e^{-\sin(x^3)}$
$\sigma_-(x)$	$-1 + x - x^2$
Q	$\frac{3}{2}$
R	2
$u_0(x)$	$\frac{1}{5}e^{(0.5-x^2)}$
$v_0(x)$	$-\sin(6x)$

Table 6.2: Coefficients, boundary and initial conditions for simulations in Section 6.3

Here also the spatial coordinate $x \in [0, 1]$, but instead the time $t \in [0, 4]$. The reason the plots in Section 6.3 last for 1 second less than the plots in Section 6.2 is for visibility, as the transients can be seen more clearly this way. The x axis is here also discretized into $\hat{N} = 240$ grid points, and the time step used was here also $h = 0.001$. Also the observers are initialized with $\hat{u}(x, 0) = 0$ and $\hat{v}(x, 0) = 0$.

6.3.1 Simulation Plots

System States

The evolution of $u(x,t)$ and $v(x,t)$ described by (4.1)–(4.2) for $(x,t) \in [0,1] \times [0,4]$ with parameters specified in Table 6.2 is shown in Fig. 6.13, with Fig. 6.13a showing $u(x,t)$ and Fig. 6.13b showing $v(x,t)$.

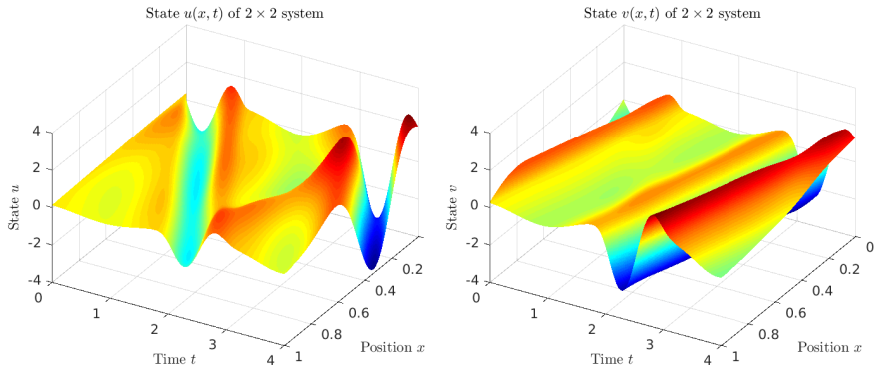

(a) State $u(x,t)$. **(b)** State $v(x,t)$.

Figure 6.13: States $u(x,t)$ and $v(x,t)$ of 2×2 system (4.1)–(4.2) evolving over the spatial interval $x \in [0,1]$ time interval $t \in [0,4]$ when using the system parameters and initial conditions as given in Table 6.2.

Observer Estimates

The plots shown in Fig. 6.14 show the estimates $\hat{u}(x,t)$ and $\hat{v}(x,t)$ produced by the 2×2 bilateral observer (4.62) when using the model with parameters given by Table 6.2. The former estimate can be seen from 6.14a whereas the latter are in 6.14b. The bilateral observer gains which were used are shown further down in this section.

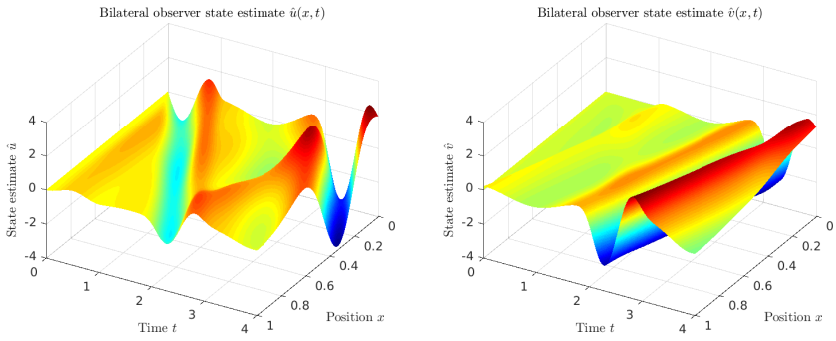

(a) Bilateral observer estimate $\hat{u}(x,t)$. **(b)** Bilateral observer estimate $\hat{v}(x,t)$.

Figure 6.14: Bilateral observer estimates $\hat{u}(x,t)$ and $\hat{v}(x,t)$ produced by (4.62) for estimating the states $u(x,t)$ and $v(x,t)$, respectively, of the 2×2 system (4.1)–(4.2) using measurements $y_1(t) = u(1,t)$ and $y_2(t) = v(0,t)$. The model parameters used are in Table 6.2.

In Fig. 6.15 we see the state estimates $\hat{u}(x,t)$ and $\hat{v}(x,t)$ produced by the 2×2 unilateral observer (5.1) with model parameters from Table 6.2. Fig. 6.15a shows $\hat{u}(x,t)$ and Fig. 6.15b shows $\hat{v}(x,t)$. For the unilateral 2×2 observer gains used, see the relevant graph further down this section.

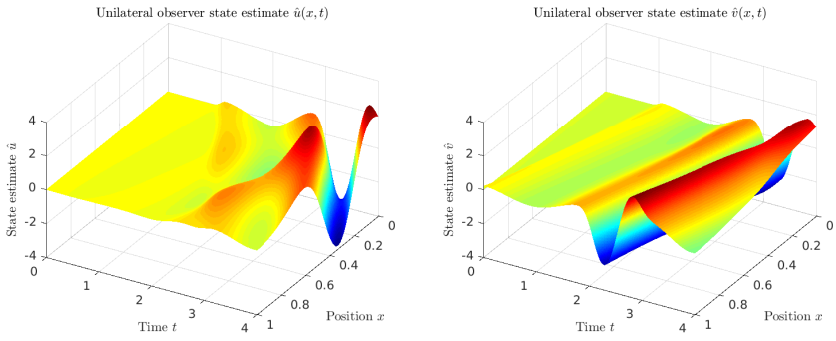

(a) Unilateral observer estimate $\hat{u}(x,t)$. **(b)** Unilateral observer estimate $\hat{v}(x,t)$.

Figure 6.15: Unilateral observer estimates $\hat{u}(x,t)$ and $\hat{v}(x,t)$ produced by (5.1) for estimating the states $u(x,t)$ and $v(x,t)$, respectively, of the 2×2 system (4.1)–(4.2) using right boundary measurement $y(t) = u(1,t)$. The model parameters used are in Table 6.2.

Comparing Fig. 6.14a and Fig. 6.15a with Fig. 6.13a, we see that in this case the bilateral observer produces estimates $\hat{u}(x,t)$ which are much closer to the actual state $u(x,t)$ very early on than the corresponding estimates produced by the single boundary observer. It is difficult however to see much difference between the bilateral observer estimate $\hat{v}(x,t)$ in Fig. 6.14b and corresponding unilateral observer estimate in Fig. 6.15b. Neither are able to estimate the initial sharp

transient present in $u(x,t)$ as seen in Fig. 6.13b very well. However after this they both seem to produce fairly accurate estimates.

Observer Estimation Errors

In Fig. 6.16 we see the estimation errors $\tilde{u}(x,t) = u(x,t) - \hat{u}(x,t)$ and $\tilde{v}(x,t) = v(x,t) - \hat{v}(x,t)$ when the estimates $\hat{u}(x,t)$ and $\hat{v}(x,t)$ are produced by the bilateral observer (4.62) and the 2×2 model is defined by Table 6.2. Essentially Fig. 6.16a represents the values in Fig. 6.14a subtracted from the states $u(x,t)$ shown in Fig. 6.13a, whilst Fig. 6.16b represents values from Fig. 6.14b subtracted from values in Fig. 6.13b.

The corresponding errors in the estimation of $\tilde{u}(x,t)$ and $\tilde{v}(x,t)$, the collocated observer (5.1) commits can be seen in Fig. 6.17, with Fig. 6.17a representing $\tilde{u}(x,t)$ and Fig. 6.17b displaying $\tilde{v}(x,t)$.

The observation from Fig. 6.14a that the bilateral observer has small errors in its estimation $\hat{u}(x,t)$ of the state $u(x,t)$ overall is confirmed in Fig. 6.16a, which primarily shows that the error $\tilde{u}(x,t)$ of the bilateral observers estimation has transients with small values that disappear quickly. Comparing this to Fig. 6.17a we can see that the unilateral observer indeed struggles much more in finding estimates which are correct. Additionally, the fact that Fig. 6.14b looks similar to Fig. 6.15b is reflected in the similarities between Fig. 6.16b and Fig. 6.17b. Both of these plots contain a sharp transient early on which reflects the sharp transient in $v(x,t)$ both observers fail to capture. The main difference between these plots is that the latter contains some slight transients in $\tilde{v}(x,t)$ later on which are not present in the former. Hence the bilateral observer estimates $\hat{v}(x,t)$ still converge more quickly than the corresponding estimates from the unilateral observer, despite $\tilde{v}(x,t)$ in Fig. 6.17b having nearly but not entirely vanished after $\tilde{v}(x,t)$ in Fig. 6.16b vanishes.

In Fig. 6.18 we see the Euclidean norms $||\tilde{u}(t)|| = \sqrt{\int_0^1 \tilde{u}^2(x,t)dx}$ and $||\tilde{v}(t)|| = \sqrt{\int_0^1 \tilde{v}^2(x,t)dx}$. These are shown separately in Fig. 6.18a and Fig. 6.18b respectively, where the former shows the norm of the estimation errors $\tilde{u}(x,t)$ whilst the latter shows the norm of $\tilde{v}(x,t)$, which respectively can be found in Fig. 6.16 and Fig. 6.17 respectively.

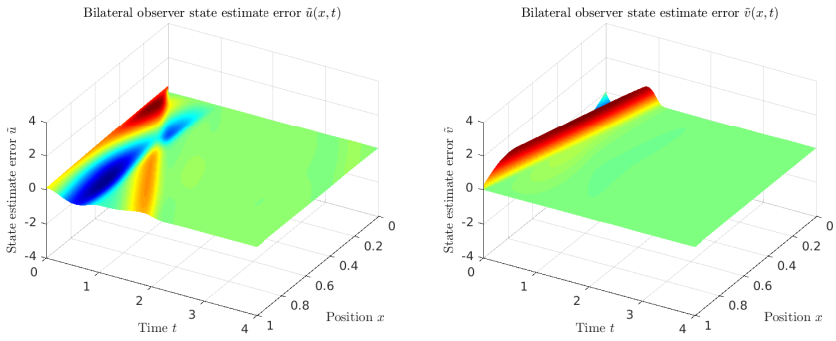

(a) Bilateral observer error $\tilde{u}(x,t)$ **(b)** Bilateral observer error $\tilde{v}(x,t)$

Figure 6.16: Bilateral observer estimation errors $\tilde{u}(x,t)$ and $\tilde{v}(x,t)$ when trying to estimate the states $u(x,t)$ and $v(x,t)$ of (4.1)–(4.2) using estimates $\hat{u}(x,t)$ and $\hat{v}(x,t)$ from the bilateral observer (4.62). The model parameters used are in Table 6.2.

In Fig. 6.18a we find a large difference between the efficiency at which the bilateral observer produces correct estimates of $u(x,t)$ and the ones produced by the unilateral observer. The error norm $||\tilde{u}(t)||$ of the estimation error corresponding to the unilateral observer is much larger than the error norm for the bilateral observer for most of the convergence time interval. However, Fig. 6.18b tells an entirely different story, with the error norms for both observers being nearly identical all the way through. The error norm $||\tilde{v}(t)||$ corresponding to the bilateral observer does truly vanish before the one for the unilateral observer, but the latter estimation norm only slightly hovers above zero before finally vanishing after three seconds.

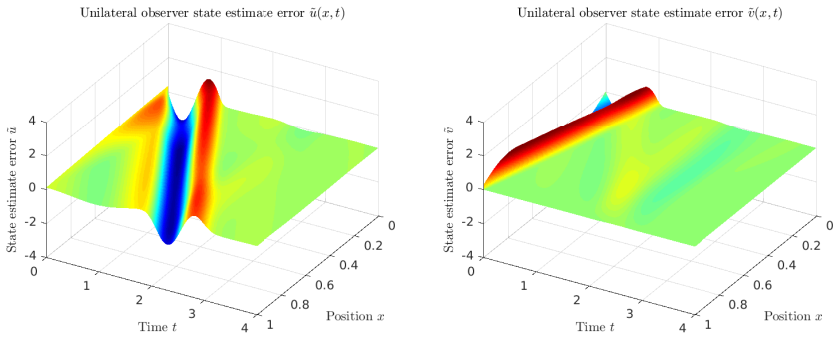

(a) Unilateral error $\tilde{u}(x,t)$. **(b)** Unilateral error $\tilde{v}(x,t)$.

Figure 6.17: Unilateral observer estimation errors $\tilde{u}(x,t)$ and $\tilde{v}(x,t)$ when trying to estimate the states $u(x,t)$ and $v(x,t)$ of (4.1)–(4.2) using estimates $\hat{u}(x,t)$ and $\hat{v}(x,t)$ from (5.1). The model parameters used are in Table 6.2.

Also as in Fig. 6.6 from Section 6.2, the error norms are for the most part not entirely equal to 0 by the time the theoretical convergence time comes around, most likely due to numerical errors. Although in this case $||\tilde{u}(t)||$ for the unilateral

observer is the most severe perpetrator of this, with the three other error norms being largely close to 0 at the correct time.

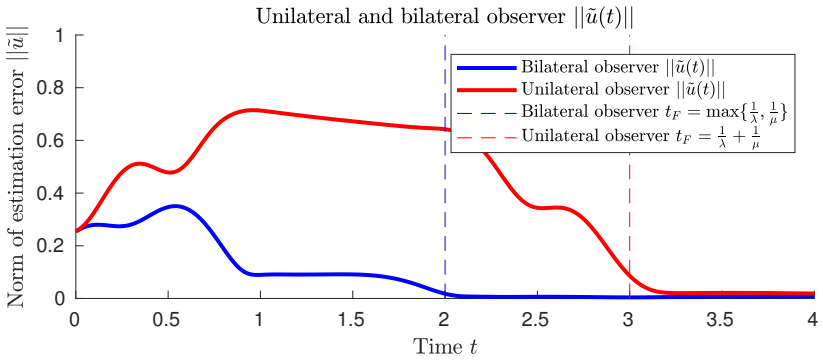

(a) Euclidean norms $||\tilde{u}(t)||$ of estimation errors $\tilde{u}(x,t)$.

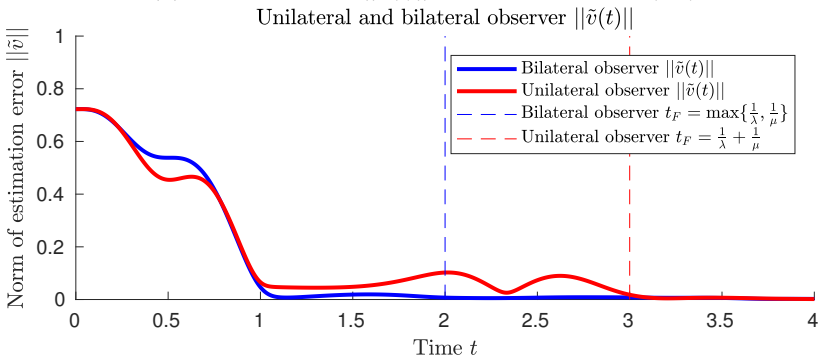

(b) Euclidean norms $||\tilde{v}(t)||$ of estimation errors $\tilde{v}(x,t)$.

Figure 6.18: Euclidean norms $||\tilde{u}(t)||$ and $||\tilde{v}(t)||$ of estimation errors $\tilde{u}(x,t)$ and $\tilde{v}(x,t)$ respectively for both bilateral and unilateral observers. The blue line shows the error norm for the bilateral observer estimates, whereas the red line shows the error norm for the unilateral observer estimate. The blue dashed line shows the expected theoretical convergence time $t_{2,min}$ of the bilateral observer, whereas the red dashed line shows the expected theoretical convergence time $t_{1,min}$ of the unilateral observer. The 2×2 model used parameters specified in Table 6.2.

6.3.2 Observer Gains and Kernel PDE Solutions

Bilateral 2×2 Observer Gains

The four plots in Fig. 6.19 show the bilateral observer gains $P^{++}(x)$, $P^{+-}(x)$, $P^{-+}(x)$ and $P^{--}(x)$ across $[0,1] \ni x$ used to produce the state estimates $\hat{u}(x,t)$ and $\hat{v}(x,t)$. These estimates are displayed in Fig. 6.14 and have been generated using the observer (4.62) when using model parameters from Table 6.2.

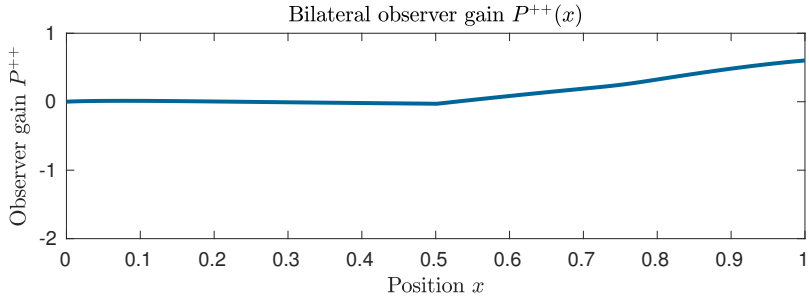

(a) Bilateral observer gain $P^{++}(x)$.

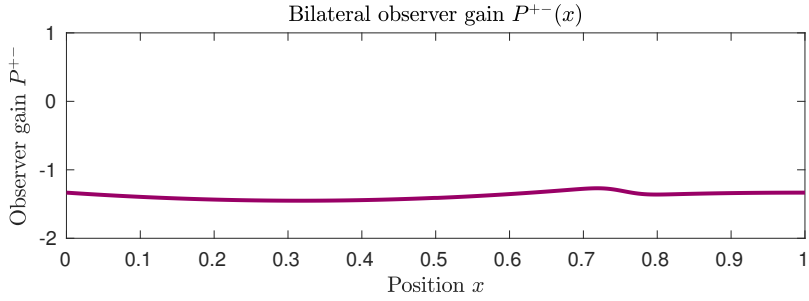

(b) Bilateral observer gain $P^{+-}(x)$.

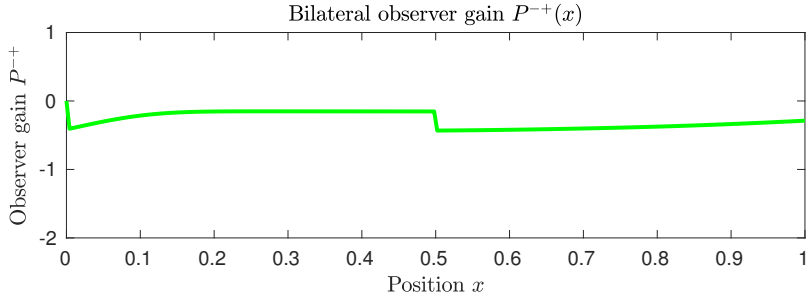

(c) Bilateral observer gain $P^{-+}(x)$.

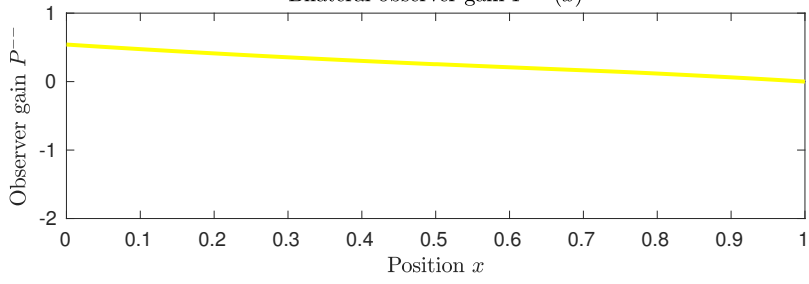

(d) Bilateral observer gain $P^{--}(x)$.

Figure 6.19: Bilateral observer gains used to calculate the state estimates $\hat{u}(x,t)$ and $\hat{v}(x,t)$ using the bilateral observer (4.62) for estimating the states $u(x,t)$ and $v(x,t)$ of the 2×2 system (4.1)–(4.2). The model parameters used are summarized in Table 6.2.

Fig. 6.19a shows the gain $P^{++}(x)$ which gets multiplied by the error term $y_1(t) - \hat{u}(1,t)$ in the PDE for $\hat{u}(x,t)$, Fig. 6.19b shows the gain $P^{+-}(x)$ which gets multiplied by the error term $y_2(t) - \hat{v}(0,t)$ in the PDE for $\hat{u}(x,t)$, Fig. 6.19c shows the gain $P^{-+}(x)$ which gets multiplied by the error term $y_1(t) - \hat{u}(1,t)$ in the PDE for $\hat{v}(x,t)$, and Fig. 6.19d shows the gain $P^{--}(x)$ which is multiplied by the error $y_2(t) - \hat{v}(0,t)$ featuring in the PDE for $\hat{v}(x,t)$. These gains were calculated from minimum time $2+2$ collocated kernels according to (A.21) in Appendix A. The $2+2$ gains used in (A.21) to calculate the 2×2 gains were calculated from (3.73). The numerical kernel PDE solutions used for these calculations can be seen further down in Section 6.2.

Unilateral 2×2 Observer Gains

In Fig. 6.20 we find the unilateral observer gains $\bar{P}^+(x)$ and $\bar{P}^-(x)$ defined over the real number interval $[0,1] \ni x$ used to produce the single boundary observer estimates $\hat{u}(x,t)$ and $\hat{v}(x,t)$ from (5.1). The estimates this observer produces, given that the system parameters used are summarized in Table 6.2, are shown in Fig. 6.3.

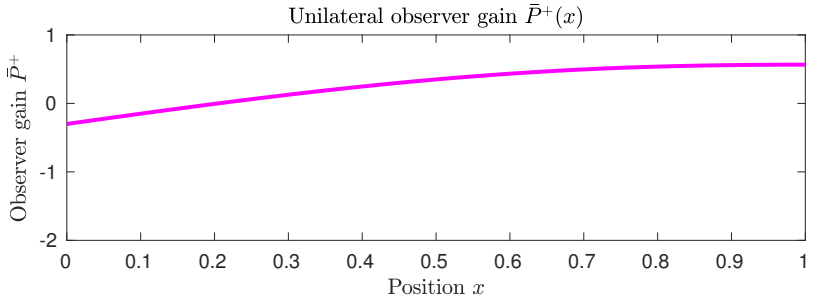

(a) Unilateral observer gain $\bar{P}^+(x)$.

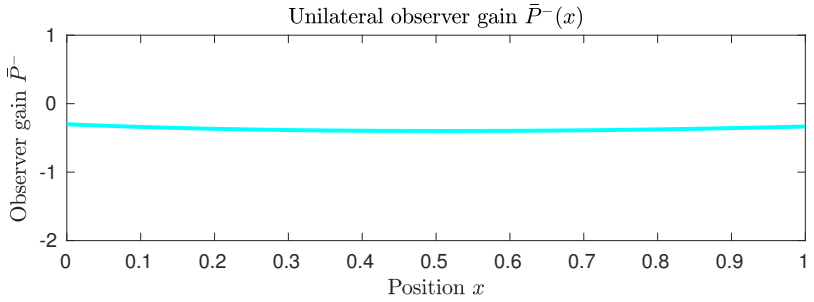

(b) Unilateral observer gain $\bar{P}^-(x)$.

Figure 6.20: Unilateral observer gains used to calculate the state estimates $\hat{u}(x,t)$ and $\hat{v}(x,t)$ using the collocated observer (5.1) for estimating the states $u(x,t)$ and $v(x,t)$ of the 2×2 system (4.1)–(4.2). The model parameters used are summarized in Table 6.2.

We find in Fig. 6.20a the 2×2 unilateral observer gain $\bar{P}^+(x)$ which gets multiplied by the only error term $y(t) - \hat{u}(1,t)$ in the PDE for $\hat{u}(x,t)$, whilst Fig. 6.20b shows the other observer gain $\bar{P}^-(x)$ which gets multiplied by the same

error term $y(t) - \hat{u}(1,t)$, but appearing in the PDE for $\hat{v}(x,t)$. These observer gains are computed from (5.2). The numerical approximate solution to the kernel PDEs used here are given further down in Section 6.2.

Collocated $2+2$ Minimum Time Observer Kernel Solutions

The four components of the $M(x,\xi)$ matrix kernel solution used for calculating the observer gains shown in Fig. 6.19 from (A.21) which again were calculated from (3.73) are shown in Fig. 6.21, with $(x,\xi) \in \mathcal{T}_u$.

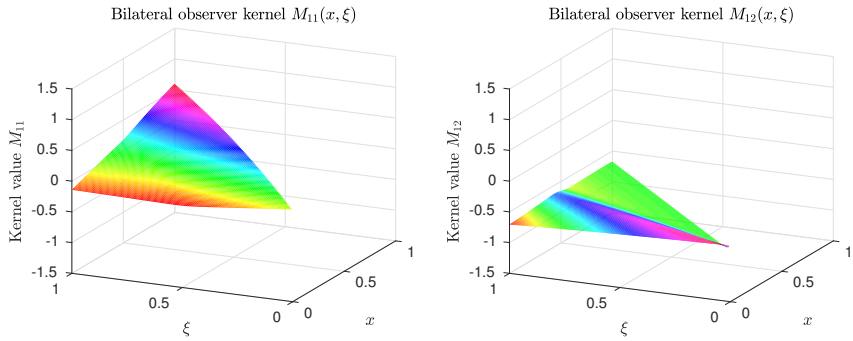

(a) Collocated $2+2$ kernel solution $M_{11}(x,\xi)$. **(b)** Collocated $2+2$ kernel solution $M_{12}(x,\xi)$.

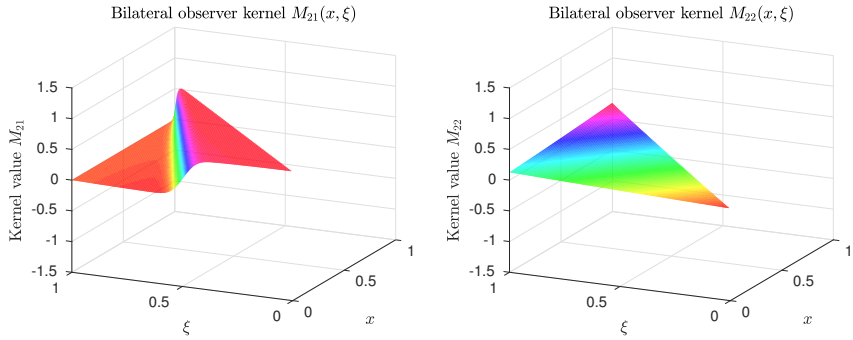

(c) Collocated $2+2$ kernel solution $M_{21}(x,\xi)$. **(d)** Collocated $2+2$ kernel solution $M_{22}(x,\xi)$.

Figure 6.21: Collocated $2+2$ kernel solutions $M(x,\xi)$ over the upper triangular domain $\mathcal{T}_u$ to the first matrix PDE in (3.74) with boundary conditions (3.75), where the $2+2$ system parameters are defined according to *Case III* in Appendix A, which again are based on the 2×2 parameters defined in Table 6.2.

Fig. 6.21a shows $M_{11}(x,\xi)$ which corresponds with the top left matrix entry of $M(x,\xi)$, Fig. 6.21b shows $M_{12}(x,\xi)$ corresponding to the top right entry, Fig. 6.21c displays $M_{21}(x,\xi)$ which represents the values from the bottom left entry, and Fig. 6.21d display $M_{22}(x,\xi)$ which are the values found in the bottom right entry of the matrix 2×2 matrix $M(x,\xi)$.

$M(x,\xi)$ and $N(x,\xi)$ are solutions to the matrix PDE (3.74)–(3.75) with the

$2+2$ system parameters found from *Case III* in Appendix A, which in turn are calculated from the 2×2 coefficients in Table 6.2. See Section 5.3 for an explanation of how these matrix kernel solutions were found. The four components of the $N(x,\xi)$ matrix kernel solution are shown in Fig. 6.22. Fig. 6.22a shows $N_{11}(x,\xi)$ which is the the top left component of the 2×2 matrix $N(x,\xi)$, Fig. 6.22b shows $N_{12}(x,\xi)$ which is the top right component, the bottom left component $N_{21}(x,\xi)$ is in Fig. 6.22c and Fig. 6.22d shows the bottom right component $N_{22}(x,\xi)$.

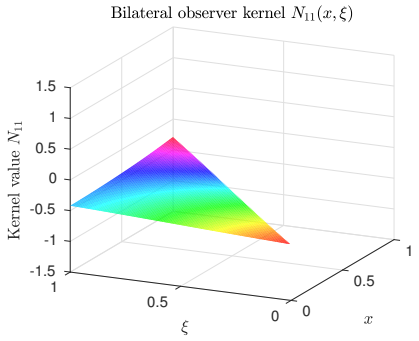

(a) Collocated 2+2 kernel solution $N_{11}(x,\xi)$.

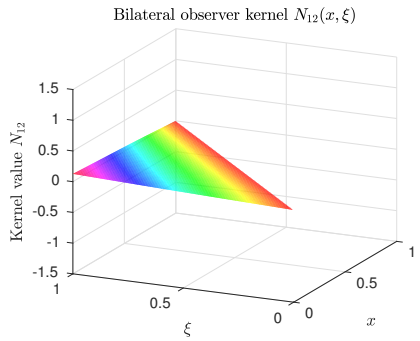

(b) Collocated $2+2$ kernel solution $N_{12}(x,\xi)$.

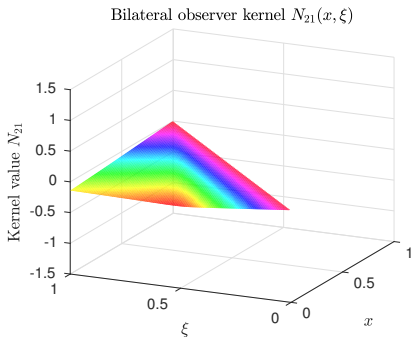

(c) Collocated 2+2 kernel solution $N_{21}(x,\xi)$.

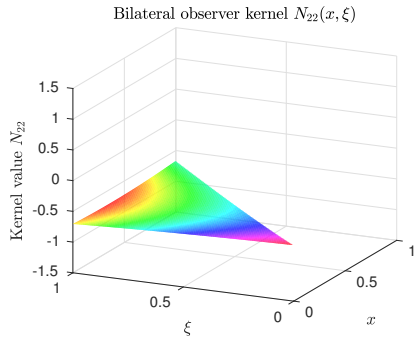

(d) Collocated $2+2$ kernel solution $N_{22}(x,\xi)$.

Figure 6.22: Collocated $2+2$ kernel solutions $N(x,\xi)$ over the lower triangular domain $\mathcal{T}_u$ to the second matrix PDE in (3.74) with boundary conditions (3.75), where the $2+2$ system parameters are defined according to *Case III* in Appendix A, which again are based on the 2×2 parameters defined in Table 6.2.

The kernel solution $k_{21}(x,\xi)$ over $\mathcal{S}_0$ of (3.51)–(3.71) is here in Fig. 6.23. Note that the boundary condition for this PDE depends on the solution to the $M(x,\xi)$ and $N(x,\xi)$ matrix PDEs shown in Fig. 6.21 and Fig. 6.22 respectively, so these were solved first, and $k_{21}(x,\xi)$ was solved for subsequently.

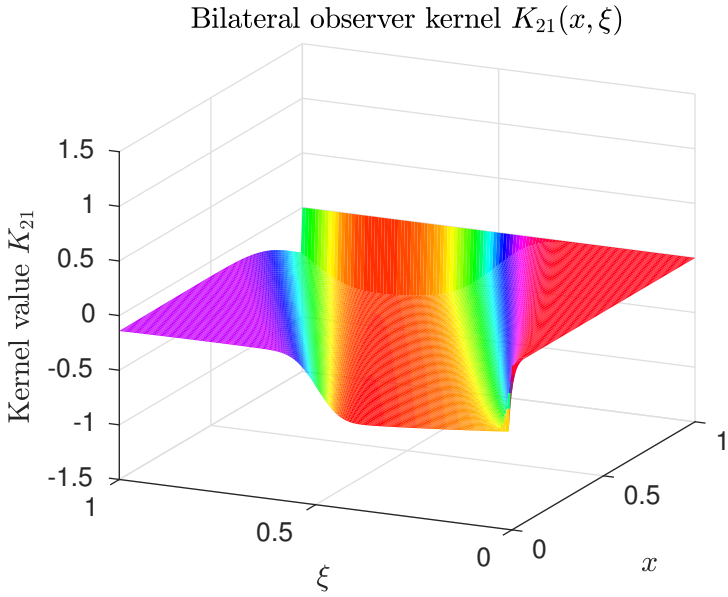

Figure 6.23: Collocated $2+2$ minimum time kernel solution $k_{21}(x,\xi)$ to (3.51)–(3.71) for the case when the $2+2$ system parameters are defined according to *Case III* in Appendix A which in turn are defined by 2×2 parameters from Table 6.2.

Unilateral 2×2 Observer Kernel Solutions

In order to calculate the 2×2 observer kernel gains shown in Fig. 6.20, of which there were only two, the PDE system (5.3)–(5.4) with scalar solutions $\bar{M}(x,\xi)$ and $\bar{N}(x,\xi)$ needed to be solved over the upper triangular domain $\mathcal{T}_u$. The solution to this system when the 2×2 system parameters are specified as in Table 6.2 is shown in Fig. 6.24. Here Fig. 6.24a shows the solution $\bar{M}(x,\xi)$ whereas Fig. 6.24b shows $\bar{N}(x,\xi)$.

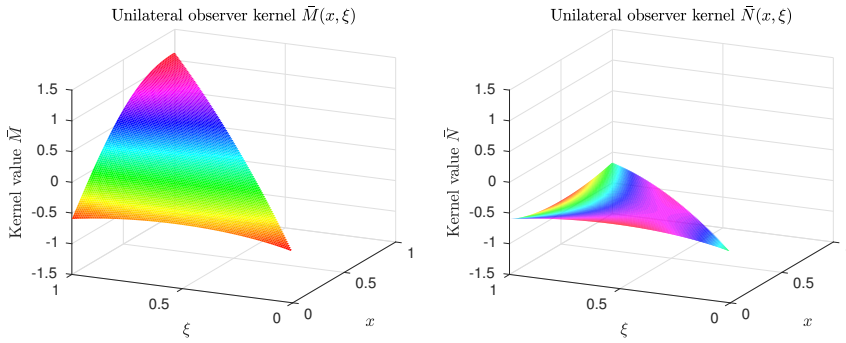

(a) Unilateral 2×2 kernel solution $\bar{M}(x,\xi)$. **(b)** Unilateral 2×2 kernel solution $\bar{N}(x,\xi)$.

Figure 6.24: Unilateral 2×2 kernel solutions to the PDE system (5.3)–(5.4) using system parameters defined in Table 6.2.

This concludes the 2×2 observer toy simulations. In the next chapter we introduce a technical application case for the observers, showing how they can be used to estimate the flow and pressure dynamics of the drilling mud in a drill string.

Chapter 7

Application to Estimation of Flow and Pressure in Oil Well Drilling

7.1 Introduction

During oil and gas drilling operations, typically a water-based drilling fluid referred to as *mud* is circulated throughout the *drill string*. The mud gets pumped into the top of the drill string, flows downwards to the *drill-bit* at the bottom, flowing through the bit and into the well. In addition to cooling down and lubricating the drill-bit whilst concurrently acting as a pressure barrier against the formation, the mud picks up cuttings left over from drilling and brings them back up into annulus between the surrounding casing and the drill string itself(Landet et al. (2013)). A schematic of this setup is shown in Fig. 7.1, similar to the schematic from Aarsnes et al. (2016).

By its very nature drilling for oil is a highly uncertain activity, with changes in the operating conditions at the far end of the drill string having the potential to happen suddenly. Here incorrect or missing responses could have far reaching consequences for the environment, machinery and personnel involved. One common phenomenon which could occur suddenly whilst drilling is a *kick*, which is an influx of hydrocarbons into the drill string occurring when the *formation pore pressure* gets larger than pressure in the *wellbore*(Ahmed et al. (2016)). The opposite of a kick situation is referred to by petroleum engineers as a *loss*, occurring when mud instead escapes into the formation due to the mud pressure being greater than the reservoir pressure(Alsaba et al. (2014)). Severe loss situations could result in collapse of the well. Kicks have the possibility of developing into *blowouts*, being the situation when hydrocarbons from the well start flowing uncontrollably into the wellbore and surrounding environment (Tamim et al. (2017)). Kicks can according to Grace (2017) happen for multiple reasons, including that the mud weight is less than the formation pressure, *swabbing* occurs whilst *tripping* or there is a loss of circulation in the mud.

Within drilling, one can as in NORSOK (2004) classify two main levels of *well*

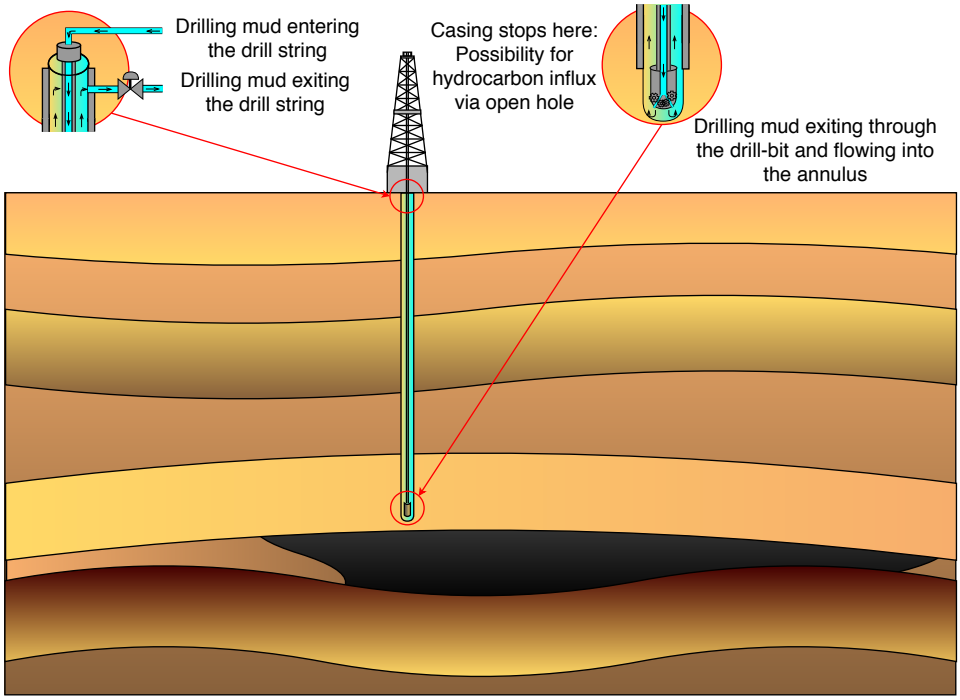

Figure 7.1: Schematic of a drilling system. The black region in the lower section of the figure represents hydrocarbons the drill string is approaching. The figure is not to scale, with hydrocarbons commonly being trapped in pockets several kilometers under the ground.

barriers between the rig and the reservoir, whose purpose is to prevent unintended fluids from flowing out of the formation to the surface, namely *primary* and *secondary* well barriers. Primary barriers are the first line of defense, with the mud column typically serving this purpose. If primary barriers should fail to contain the influx, secondary barriers might be necessary to prevent the situation from developing into a disaster, with typically *blowout preventers(BOP)*(see Aadnoy et al. (2011)) being used for this purpose. We will here only focus on the primary well barrier, specifically by actively estimating(and controlling) the flow and pressure of the drill string mud for this purpose.

Traditionally, in *conventional* drilling, the mud exits at the top of the wellbore through a *bell nipple* into an open vessel(Malloy et al. (2009)). Usually an inherently *overbalanced* drilling situation, implying that a purposefully overly heavy mud is used, is created during conventional drilling. This will most likely imply loss of mud into the formation. The estimated mud weight is calculated from a *pore pressure analysis*, see for example Zhang (2011) for details on this, and a safety margin added to create the overbalanced state. With the formation pressure increasing as the drill string reaches further into the ground, the mud weight is increased at finite depth intervals. Overbalanced drilling is in contrast to the *underbalanced* case where the mud is purposefully made too light in order to not compromise the productivity

potential of the well during drilling (see Rehm et al. (2013)).

The conventional drilling method just described has two main disadvantages. Firstly the safety margin in mud weight implies that often much drilling fluid will be lost into the formation, which is expensive. Also if the safety margin is too high the formation could crack, causing the well to collapse. Secondly, the pressure of the drilling mud imposes on the formation it is drilling into can not be updated quickly, so it can not react to sudden unexpected changes in the operating conditions. To improve on this, a drilling technique known as *managed pressure drilling(MPD)* has been developed to be able to actively balance the pressure from the drilling fluid column against the formation pore pressure and continuously update the pressure whilst having the possibility of quickly adapting itself to changing downhole conditions. Instead of having mud exit into an open pit as is the case of conventional drilling, in MPD the top of the borehole is sealed and the mud instead exits through a choke. This choke can be actively controlled to precisely regulate the pressure of the mud without changing its density (Aamo (2013)).

As explained in Nayeem et al. (2016), a kick can occur without it immediately developing into a critical situation such as a blowout, and with correct and swift reaction the drilling system can be stabilized and brought under control. Often when drilling into new regions, the formation pressure could change unexpectedly. For example in Fig. 7.1, when the drill string reaches the pocket of hydrocarbons a sudden jump in pressure could occur. The information one has of the region that is being drilled is typically from geological surveys, which are inherently uncertain(Suslick et al. (2009)).

Assume that a sudden jump in the reservoir pressure to an unknown value occurs. The following will then occur. Since the mud weight and pressure will not be sufficient to balance against the reservoir, influx will happen causing an underbalanced drilling situation. Since the reservoir pressure is unknown, the state estimates of mud flow and pressure will become incorrect, and hence an attenuating controller relying on correct state estimates to function correctly will not be able to perform its job. The following three steps would be necessary to effectively handle the kick in such a situation:

1. The new reservoir pressure must be estimated.
2. New state estimates of the flow and pressure must be made.
3. An attenuating controller must regulate the mud in the drill string to cancel out the disturbance and bring the flow and pressure of the mud to the new set-point for a stable well.

The time it takes for each of these three steps to complete affects the total time before the well can be brought under control, and a decrease in time for any of them will reduce the probability of a severe and expensive occurrence such as a blowout happening. We will here focus on the second step, and apply the 2×2 bilateral observer developed previously and investigate whether this algorithm can assist in reducing the time for kick handling. For the first step, an adaptive estimation scheme for estimating the downhole pressure online such as the one presented in Stamnes et al. (2011) could be used, which estimates the downhole pressure from topside measurements. After step two, which involves estimating the pressure and flow in the drill pipe, has been completed, an example of an

attenuating controller which could be used for step three(assuming downhole in addition to topside actuation is possible) is the 2×2 hyperbolic PDE bilateral controller presented in Vazquez and Krstic (2016), given that the 2×2 system it operates on gets transformed to the MPD model which will be presented in the next section.

Using *wired drill pipe(WDP)* technology, which allows bi-directional real time data transfer between sensors and actuators placed downhole and the rig(Gravdal et al. (2010)), efficient drilling systems which can handle kicks more quickly and safely than topside limited MPD systems can be realized. WDP technology can as explained in Fosse (2015) be contrasted with the conventional techniques of *mud pulse telemetry(MPT)* and *electromagnetic telemetry(EMT)*. MPT is based on equipment installed on the *bottomhole assembly(BHA)* creating pulses in the drilling mud, which travel upwards the drill string and can be received at the top. A disadvantage of MPT is that the speed the pulses travel at is limited by the speed pressure waves can travel through the mud. On the other hand, EMT bases itself on sending low-frequency electromagnetic waves from the BHA. A disadvantage of this communication technology is that the signal strength is quickly attenuated, implying it is most useful when drilling shallow wells in practice. In contrast to these two communication methods, WDP technology relies on wired communication. As explained in Fosse (2015), the physical setup of a WDP can be explained as follows. From the topside computer system, the data travels via the *surface cabling* into the *data swivel*, which is physically installed as part of the *top drive*. From here the data is communicated through the wired drill pipe segments, and between each segment coils are present to allow data to be transferred from segment to segment. The main advantage of WDP compared to MPT and EMT lies in its speed and capacity of data transmission. By applying this technology, observers capitalizing on both topside and downhole measurements for quicker state estimation and additionally controllers attenuating disturbances faster by actuating both sides of the drill string can be implemented.

The main purpose of Chapter 7 is to present the background for and introduce a WDP MPD system model that will be applied in simulations in Chapter 8 to compare the performance between two observers performing step two in the kick handling scenario above. One of the observers will use both topside and downhole measurements, whilst the other will only have the ability of incorporating topside[1] measurements. This section, Section 7.1, has been devoted to present the problem background. The next section, Section 7.2, will present the precise mathematical model used to describe the drilling system and the simulation case specified. After this in Section 7.3 it will be shown how this model can be transformed to fit into the 2×2 system (4.1)–(4.2) framework, hence allowing the bilateral observer developed in Chapter 4 to be applied.

[1]If downhole measurements are available, this observer could just as well use downhole instead of topside measurements, depending on which side of the drill string is actuated(if any). However, the important point here is that this second observer is only able to use measurements from one of the two sides of the drill string, and its performance will be compared to the first observer which is uses measurements from both sides in its state estimation algorithm.

7.2 Problem Statement

In Landet et al. (2013), a one-dimensional, linearized model of the pressure and volumetric flow of the mud in a drill string for the *heave problem* in offshore MPD was derived. As the model is one dimensional whereas fluid flow is a three dimensional phenomenon in reality, the model assumes that the mud flow and pressure is constant across the annular cross-section of the drill string. This model was in Holta et al. (2017) presented in modified form to the application of kick attenuation during drilling using topside actuation via the choke the mud exits through as it leaves the wellbore. Assuming that the choke dynamics are significantly faster than the rest of the system, it was argued there that topside pressure could be used directly as the control input, yielding the topside control signal $p_l(t)$.

Despite control design not being the focus of this thesis, we assume that within our MPD system with a WDP we have the possibility of controlling the flow through the bit with the signal $q_{bit}(t)$. The MPD model then becomes

$$p_t(z,t) = -\frac{\beta}{A_1} q_z(z,t) \tag{7.1a}$$

$$q_t(z,t) = -\frac{A_1}{\rho} p_z(z,t) - \frac{F_1}{\rho} q(z,t) - A_1 g \tag{7.1b}$$

with boundary conditions

$$q(0,t) = J(p_r(t) - p(0,t)) + q_{bit}(t) \tag{7.2a}$$

$$p(l,t) = p_l(t) \tag{7.2b}$$

where l is the well depth, $z \in [0, l]$ represents locations along the drill string, $q(z,t)$ denotes the volumetric flow of the mud in the drill pipe, $p(z,t)$ denotes the pressure of the mud along the drill pipe, β denotes the bulk modulus of the mud, A_1 is the cross-sectional area of the annulus, ρ denotes the density of the mud, F_1 is a friction factor, g denotes the acceleration of gravity, and finally J is the reservoir *productivity index*.

Since we are using a WDP, it will be assumed that we have access to both topside pressure and flow measurements, $\iota_1(t) = p(l,t)$ and $\iota_2(t) = q(l,t)$ respectively, from sensors on the rig and the corresponding downhole measurements $\iota_3(t) = p(0,t)$ and $\iota_4(t) = q(0,t)$, which are measured using sensors on the BHA and transmitted to the rig via the WDP. It will be assumed that the downhole data can be transmitted upwards via the WDP in a negligible amount of time, so they are available to the observer in practice simultaneously as the topside measurements.

To investigate what advantages, if any, using the downhole measurements $\iota_3(t)$ and $\iota_4(t)$ will have on the efficiency of flow and pressure state estimation in a kick handling scenario, the case that will be considered in the drilling simulations presented in Chapter 8 can be explained as follows. An MPD system is drilling at a given depth l, and knows the current reservoir pressure $p_{r,0}$ along with correct estimates of the pressure $p(z,t)$ and flow $q(z,t)$. At a point in time t_K, the drill string hits a region with much higher but unknown pressure $p_{r,1} > p_{r,0}$, causing a

kick. This is modelled as a step increase in the reservoir pressure, so the reservoir pressure $p_r(t)$ in the simulation becomes

$$p_r(t) = \begin{cases} p_{r,0} \text{ for } t \leq t_K \\ p_{r,1} \text{ for } t > t_K \end{cases} \tag{7.3}$$

In order to attenuate this kick, the three steps presented in Section 7.1 must be applied. Thus, the reservoir pressure estimate $\hat{p}_r$ must first converge to the new reservoir pressure $p_{r,1}$. The specific way this is achieved is not the focus of this thesis(a possible algorithm was suggested in Section 7.1), so the reservoir estimation algorithm providing the observer with the reservoir pressure is modeled as a simple time delay as $\hat{p}_r(t) = p_r(t - t_D)$, with t_D being the time the algorithm uses to calculate the correct "estimate".

This "parameter estimation" time delay t_D will essentially cause the observer pressure and flow estimates, $\hat{p}(z,t)$ and $\hat{q}(z,t)$ respectively, which were correct before the t_K, to get pushed away from the correct values. When the observer receives at time $t_K + t_D$ the correct reservoir pressure estimate $\hat{p}_r(t) = p_{r,1}$, it can start attempting to find the correct state estimates $\hat{p}(z,t)$ and $\hat{q}(z,t)$ again.

The performance of a state observer having access to both topside and downhole measurements in the kick scenario just described will be contrasted to an observer on a rig drilling with a normal drill pipe rather than WDP, and hence only having access to the topside measurements $\iota_1(t)$ and $\iota_2(t)$.

Now that the drilling scenario we are interested in investigating in our simulations has been precisely defined, we will in the next section, Section 7.3 show how the drilling model (7.1)–(7.2) can be transformed to fit into the form (4.1)–(4.2). Hence the bilateral observer (4.62) from Corollary 4.5 can be applied to estimate states for the MPD system with WDP having access to topside and downhole measurements, whereas the unilateral observer (5.1) can be applied to estimate states for the MPD system without WDP only having access to topside measurements. This will allow possible advantages of combining topside with downhole measurements to be discerned.

7.3 Feasibility of Design

We will now show that the MPD system (7.1)–(7.2) can be put into the form (4.1)–(4.2). Consider the general 2×2 system (4.1)–(4.2) rewritten as

$$u_t(x,t) + \lambda u_x(x,t) = \sigma^+(x)v(x,t) \tag{7.4a}$$
$$v_t(x,t) - \mu v_x(x,t) = \sigma^-(x)u(x,t) \tag{7.4b}$$
$$u(0,t) = Qv(0,t) + [V(t) + \Theta(t)] \tag{7.4c}$$
$$v(1,t) = Ru(1,t) + U_2(t) \tag{7.4d}$$

We have here split $U_1(t) = V(t) + \Theta(t)$. In this form, $V(t)$ denotes a control input and $\Theta(t)$ is an external parameter. We also assume that the measurements $y_1(t) = v(0,t)$ and $y_2(t) = u(1,t)$ are available.

The necessary coordinate transformation between (7.4) and (7.1) is now presented.

Lemma 7.1 (Modified from Lemma 10 in Aamo (2013))**.** *Consider the coordinate transformation*

$$u(x,t) = \frac{1}{2}(q(xl,t) + \frac{A_1}{\sqrt{\beta\rho}}(p(xl,t) - p_{sp} + \rho g l x)) \times e^{\frac{lF_1}{2\sqrt{\beta\rho}}x} \tag{7.5a}$$

$$v(x,t) = \frac{1}{2}(q(xl,t) - \frac{A_1}{\sqrt{\beta\rho}}(p(xl,t) - p_{sp} + \rho g l x)) \times e^{-\frac{lF_1}{2\sqrt{\beta\rho}}x} \tag{7.5b}$$

Using this transform, the system (7.1)–(7.2) *is mapped into* (7.4) *with*

$$\lambda = \mu = \frac{1}{l}\sqrt{\frac{\beta}{\rho}} \tag{7.6a}$$

$$\sigma^+(x) = -\frac{1}{2}\frac{F_1}{g} \times e^{\frac{lF_1}{\sqrt{\beta\rho}}x} \tag{7.6b}$$

$$\sigma^-(x) = -\frac{1}{2}\frac{F_1}{g} \times e^{-\frac{lF_1}{\sqrt{\beta\rho}}x} \tag{7.6c}$$

$$Q = -\frac{1 - J\frac{\sqrt{\beta\rho}}{A_1}}{1 + J\frac{\sqrt{\beta\rho}}{A_1}} \tag{7.6d}$$

$$R = e^{-\frac{lF_1}{\sqrt{\beta\rho}}} \tag{7.6e}$$

$$V(t) = \frac{1}{1 + J\frac{\sqrt{\beta\rho}}{A_1}}(q_{bit}(t) + Jp_{sp}) \tag{7.6f}$$

$$\Theta(t) = \frac{J}{1 + J\frac{\sqrt{\beta\rho}}{A_1}}p_r(t) \tag{7.6g}$$

$$U_2(t) = \frac{A_1}{\sqrt{\beta\rho}}(p_l(t) - p_{sp} + \rho g l) \times e^{-\frac{lF_1}{\sqrt{\beta\rho}}} \tag{7.6h}$$

$$y_1(t) = \frac{1}{2}(\iota_4(t) - \frac{A_1}{\sqrt{\beta\rho}}(\iota_3(t) - p_{sp})) \tag{7.6i}$$

$$y_2(t) = \frac{1}{2}(\iota_2(t) + \frac{A_1}{\sqrt{\beta\rho}}(\iota_1(t) - p_{sp} + \rho g l)) \times e^{\frac{lF_1}{2\sqrt{\beta\rho}}} \tag{7.6j}$$

Proof. Define the following change of variables

$$\bar{p}(z,t) = p(z,t) - p_{sp} + \rho g z. \tag{7.7}$$

Differentiating with respect to time and space obtain

$$\bar{p}_t(z,t) = p_t(z,t), \tag{7.8a}$$

$$\bar{p}_z(z,t) = p_z(z,t) + \rho g, \tag{7.8b}$$

and substituting this into the model (7.1) obtain that

$$\bar{p}_t(z,t) = -\frac{\beta}{A_1} q_z(z,t) \tag{7.9a}$$

$$q_t(z,t) = -\frac{A_1}{\rho}[\bar{p}_z(z,t) - \rho g] - \frac{F_1}{\rho} q(z,t) - A_1 g \tag{7.9b}$$

$$\Rightarrow q_t(z,t) = -\frac{A_1}{\rho}\bar{p}_z(z,t) - \frac{F_1}{\rho} q(z,t). \tag{7.9c}$$

Obtain also the boundary conditions

$$q(0,t) = J(p_r(t) - [\bar{p}(0,t) + p_{sp}]) + q_{bit}(t) \tag{7.10a}$$

$$\bar{p}(l,t) = p_l(t) - p_{sp} + \rho g l. \tag{7.10b}$$

Define

$$\bar{u}(z,t) = \frac{1}{2}(q(z,t) + \frac{A_1}{\sqrt{\beta\rho}}\bar{p}(z,t)) \tag{7.11a}$$

$$\bar{v}(z,t) = \frac{1}{2}(q(z,t) - \frac{A_1}{\sqrt{\beta\rho}}\bar{p}(z,t)) \tag{7.11b}$$

Adding and subtracting the equations in (7.11) we find

$$q(z,t) = \bar{u}(z,t) + \bar{v}(z,t) \tag{7.12a}$$

$$\bar{p}(z,t) = \frac{\sqrt{\beta\rho}}{A_1}(\bar{u}(z,t) - \bar{v}(z,t)) \tag{7.12b}$$

Differentiating (7.12) with respect to time and space obtain

$$q_t(z,t) = \bar{u}_t(z,t) + \bar{v}_t(z,t) \tag{7.13a}$$

$$q_z(z,t) = \bar{u}_z(z,t) + \bar{v}_z(z,t) \tag{7.13b}$$

$$\bar{p}_t(z,t) = \frac{\sqrt{\beta\rho}}{A_1}(\bar{u}_t(z,t) - \bar{v}_t(z,t)) \tag{7.13c}$$

$$\bar{p}_z(z,t) = \frac{\sqrt{\beta\rho}}{A_1}(\bar{u}_t(z,t) - \bar{v}_t(z,t)). \tag{7.13d}$$

Substituting then (7.13) into (7.9) we find

$$\bar{u}_t(z,t) - \bar{v}_t(z,t) = -\sqrt{\frac{\beta}{\rho}}(\bar{u}_z(z,t) + \bar{v}_z(z,t)) \tag{7.14a}$$

$$\bar{u}_t(z,t) + \bar{v}_t(z,t) = -\sqrt{\frac{\beta}{\rho}}(\bar{u}_t(z,t) - \bar{v}_t(z,t)) - \frac{F_1}{\rho}(\bar{u}(z,t) + \bar{v}(z,t)) \tag{7.14b}$$

and substituting into the boundary conditions (7.10) we get

$$\bar{u}(0,t) + \bar{v}(0,t) = J(p_r(0,t) - [\frac{\sqrt{\beta\rho}}{A_1}(\bar{u}(0,t) - \bar{v}(0,t)) + p_{sp}]) + q_{bit}(t) \tag{7.15a}$$

$$\bar{u}(l,t) - \bar{v}(l,t) = \frac{A_1}{\sqrt{\beta\rho}}(p_l(t) - p_{sp} + \rho g l). \tag{7.15b}$$

Adding and subtracting the PDEs (7.14) obtain

$$\bar{u}_t(z,t) = -\sqrt{\frac{\beta}{\rho}}\bar{u}_z(z,t) - \frac{1}{2}\frac{F_1}{\rho}(\bar{u}(z,t) + \bar{v}(z,t)) \tag{7.16a}$$

$$\bar{v}_t(z,t) = \sqrt{\frac{\beta}{\rho}}\bar{v}_z(z,t) - \frac{1}{2}\frac{F_1}{\rho}(\bar{u}(z,t) + \bar{v}(z,t)) \tag{7.16b}$$

and rearranging of the boundary conditions (7.15) we find

$$\bar{u}(0,t) = -\frac{1 - J\frac{\sqrt{\beta\rho}}{A_1}}{1 + J\frac{\sqrt{\beta\rho}}{A_1}}\bar{v}(0,t) + \frac{J}{1 + J\frac{\sqrt{\beta\rho}}{A_1}}(p_r(t)) + \frac{1}{1 + J\frac{\sqrt{\beta\rho}}{A_1}}(q_{bit}(t) + Jp_{sp}) \tag{7.17a}$$

$$\bar{v}(l,t) = \bar{u}(l,t) - \frac{A_1}{\sqrt{\beta\rho}}(p_l(t) - p_{sp} + \rho g l) \tag{7.17b}$$

Define

$$u(x,t) = \bar{u}(xl,t)e^{\frac{lF_1}{2\sqrt{\beta\rho}}x} \tag{7.18a}$$

$$v(x,t) = \bar{v}(xl,t)e^{-\frac{lF_1}{2\sqrt{\beta\rho}}x} \tag{7.18b}$$

Then

$$\bar{u}_t(xl,t) = u_t(x,t)e^{-\frac{lF_1}{2\sqrt{\beta\rho}}x} \tag{7.19a}$$

$$\bar{v}_t(xl,t) = v_t(x,t)e^{\frac{lF_1}{2\sqrt{\beta\rho}}x} \tag{7.19b}$$

$$\bar{u}_x(xl,t) = u_x(x,t)e^{-\frac{lF_1}{2\sqrt{\beta\rho}}x} - \frac{lF_1}{2\sqrt{\beta\rho}}\bar{u}(xl,t) \tag{7.19c}$$

$$\bar{v}_x(xl,t) = v_x(x,t)e^{\frac{lF_1}{2\sqrt{\beta\rho}}x} + \frac{lF_1}{2\sqrt{\beta\rho}}\bar{v}(xl,t) \tag{7.19d}$$

Considering that $z = xl$ something which implies $l\bar{u}_z = \bar{u}_x$ and $l\bar{v}_z = \bar{v}_x$ we obtain

$$u_t(x,t)e^{-\frac{lF_1}{2\sqrt{\beta\rho}}x} = -\sqrt{\frac{\beta}{\rho}}[\frac{1}{l}u_x(x,t)e^{\frac{-lF_1}{2\sqrt{\beta\rho}}x} - \frac{F_1}{2\sqrt{\beta\rho}}\bar{u}(xl,t)] - \frac{1}{2}\frac{F_1}{\rho}(\bar{u}(xl,t)+\bar{v}(xl,t)) \tag{7.20a}$$

$$\Rightarrow u_t(x,t) = -\frac{1}{l}\sqrt{\frac{\beta}{\rho}}u_x(x,t) - \frac{1}{2}\frac{F_1}{\rho}v(x,t)e^{\frac{lF_1}{\sqrt{\beta\rho}}x}, \tag{7.20b}$$

$$v_t(x,t)e^{\frac{lF_1}{2\sqrt{\beta\rho}}x} = \sqrt{\frac{\beta}{\rho}}[\frac{1}{l}v_x(x,t)e^{\frac{lF_1}{2\sqrt{\beta\rho}}x} + \frac{F_1}{2\sqrt{\beta\rho}}\bar{v}(xl,t)] - \frac{1}{2}\frac{F_1}{\rho}(\bar{u}(xl,t)+\bar{v}(xl,t)) \tag{7.21a}$$

$$\Rightarrow v_t(x,t) = \frac{1}{l}\sqrt{\frac{\beta}{\rho}}v_x(x,t) - \frac{1}{2}\frac{F_1}{\rho}u(x,t)e^{-\frac{lF_1}{\sqrt{\beta\rho}}x}, \tag{7.21b}$$

from which we obtain (7.6a)–(7.6c) by comparing (7.20)–(7.21) to (7.4a)–(7.4b). For the boundary conditions, $u(0,t) = \bar{u}(0,t)$, $v(0,t) = \bar{v}(0,t)$, $u(1,t) = \bar{u}(l,t)e^{\frac{lF_1}{2\sqrt{\beta\rho}}}$, $v(1,t) = \bar{v}(l,t)e^{-\frac{lF_1}{2\sqrt{\beta\rho}}}$, yielding

$$u(0,t) = -\frac{1 - J\frac{\sqrt{\beta\rho}}{A_1}}{1 + J\frac{\sqrt{\beta\rho}}{A_1}}v(0,t) + \frac{J}{1 + J\frac{\sqrt{\beta\rho}}{A_1}}(p_r(t)) + \frac{1}{1 + J\frac{\sqrt{\beta\rho}}{A_1}}(q_{bit}(t) + Jp_{sp}) \tag{7.22a}$$

$$v(1,t) = u(1,t)e^{-\frac{lF_1}{\sqrt{\beta\rho}}} - \frac{A_1}{\sqrt{\beta\rho}}(p_l(t) - p_{sp} + \rho gl)e^{-\frac{lF_1}{\sqrt{\beta\rho}}}. \tag{7.22b}$$

Comparing then (7.22) to (7.4c)–(7.4d), we find (7.6d)–(7.6h). Using that $y_1(t) = v(0,t)$ and $y_2(t) = u(1,t)$, applying (7.5), we obtain

$$y_1(t) = \frac{1}{2}(q(0,t) - \frac{A_1}{\sqrt{\beta\rho}}(p(0,t) - p_{sp})) \tag{7.23a}$$

$$y_2(t) = \frac{1}{2}(q(l,t) - \frac{A_1}{\sqrt{\beta\rho}}(p(l,t) - p_{sp} + \rho g l))e^{\frac{-lF_1}{\sqrt{2\beta\rho}}} \tag{7.23b}$$

which by using $\iota_1(t) = p(l,t)$, $\iota_2(t) = q(l,t)$, $\iota_3(t) = p(0,t)$ and $\iota_4(t) = q(0,t)$ we get (7.6i)–(7.6j).

□

Now that we see that (7.1)–(7.2) admits the form (4.1)–(4.2), we can present simulations with the bilateral observer from Chapter 4 applied to estimate the states of the MPD system (7.1)–(7.2), and compare its performance to the previously derived unilateral observer. This is the focus of Chapter 8.

Chapter 8

Oil Well Drilling Simulations

8.1 Introduction

The drilling system (7.1)–(7.2) along with observers for estimating pressure and flow was implemented in MATLAB. The implementation was done in the way described in Chapter 5 with help from Lemma 7.1[1]. One observer, having access to topside measurements of the flow and pressure of the mud in addition to downhole measurements of the corresponding quantities via a WDP, is implemented alongside and contrasted to another observer only having access to topside measurements. We will refer to the former observer as the WDP observer and the latter as the topside observer. The benefit of combining topside and downhole measurements through using the bilateral observer derived in this dissertation in order to estimate drill string flow and pressure during a kick handling situation can then be quantified.

Recall from Chapter 7 that if a kick occurs following a sudden but unknown increase in the reservoir pressure during drilling, we can identify three steps, namely estimation of the new reservoir pressure, estimation of flow and pressure in the drill string and regulation of the drill string flow and pressure, to handle the kick and bring the well under control again, hopefully mitigating a potential blowout.

The simulation will occur in the following manner to reflect this. A well with production index $J = 1.1 \times 10^{-8}$ $\mathrm{m^3\,s^{-1}\,Pa^{-1}}$ is being drilled at a depth of $l = 3000$ m. Initially the reservoir pressure is at $p_{r,0} = 4 \times 10^7$ Pa, and the downhole pressure setpoint p_{sp} is set to this constant value throughout the simulation. The mud used has bulk modulus of $\beta = 7.317 \times 10^7$ Pa and density of $\rho = 1250$ $\mathrm{kg\,m^{-3}}$. The drill string annulus has a cross sectional area of $A_1 = 0.024$ $\mathrm{m^2}$, and the friction factor between the mud and the drill string wall is $F_1 = 600$ $\mathrm{kg\,m^{-3}\,s^{-1}}$. After $t_K = 5$ s have passed, the reservoir pressure suddenly increases by 5×10^7 Pa, causing a kick. To reflect that the new reservoir pressure must be estimated before the observers can use this information, a time delay of $t_D = 10$ s is implemented before the new reservoir pressure is passed into the observer algorithms, implying that the observers receive the new correct reservoir pressure $p_{r,1} = 9 \times 10^7$ Pa at time

[1] In practice the 2×2 system (7.4) and its corresponding single and double boundary observers were implemented, using coefficients assigned according to Lemma 7.1. Then when plotting, the states and estimates were converted from (u, v) coordinates to (p, q) coordinates, also using Lemma 7.1

$t_K + t_D = 15$ s. Additionally the value of $g = 9.81\ \mathrm{m\,s^{-2}}$ is used for the acceleration due to gravity. The simulation parameters used are summarized in Table 8.1.

Environment and Well Parameters	
$p_{r,0}$	4×10^7 Pa
$p_{r,1}$	9×10^7 Pa
J	$1.1 \times 10^{-8}\ \mathrm{m^3\,s^{-1}\,Pa^{-1}}$
g	$9.81\ \mathrm{m\,s^{-2}}$
t_K	5 s
Drilling System Related Parameters	
β	7.317×10^7 Pa
ρ	$1250\ \mathrm{kg\,m^{-3}}$
A_1	$0.024\ \mathrm{m^2}$
F_1	$600\ \mathrm{kg\,m^{-3}\,s^{-1}}$
l	3000 m
p_{sp}	4×10^7 Pa
$p_l(t)$	3.2125×10^6 Pa
$q_{bit}(t)$	$\frac{1}{60}\ \mathrm{m^3\,s^{-1}}$
$p_0(z)$	$4 \times 10^7 - 12262.5z$ Pa
$q_0(z)$	$0.9\ \mathrm{m^3\,s^{-1}}$
t_D	10 s

Table 8.1: Physical values used for the drilling simulations. The first sub-table shows parameters related to the well and physical environment. The second sub-table contains values related to the drilling system.

It is assumed that the reservoir pressure estimation algorithm relies only on topside measurements, and the same one is implemented for both the WDP and topside observer. This is so that exclusively the flow and pressure estimation capabilities of the two observers can be compared in the simulation. In practice attenuating controllers would be implemented for kick handling after the state estimates from the observers have converged, but this step is omitted from the simulations. For the rig with a WDP, a controller utilizing both topside pressure control $p_l(t)$ and downhole flow control $q_{bit}(t)$ could be implemented, whereas for the rig using a conventional drill string and only having access to topside actuation a controller using only the topside pressure control $p_l(t)$ could be implemented, with $q_{bit}(t) = q_p$ being constant. Here q_p denotes the constant flow rate from the main pump on the rig pumping mud into the drill string

The following plots from the simulation are presented in Section 8.2.

1. The pressure $p(z,t)$ and volumetric flow $q(z,t)$ in the drill string for the duration of the simulation is first shown.

2. Next the estimates $\hat{p}(z,t)$ and $\hat{q}(z,t)$ of the pressure and volumetric flow, respectively, the WDP and topside observers produce throughout the simulation are shown.

3. Again it is difficult to see from the estimate plots which estimates are closer to the physical states in the drill string, so the estimation error $\tilde{p}(z,t)$ and $\tilde{q}(z,t)$ from both observers are next displayed.

4. The Euclidean norms $||\tilde{p}(t)|| = \sqrt{\frac{1}{l}\int_0^l \tilde{p}^2(z,t)dz}$ and $||\tilde{q}(t)|| = \sqrt{\frac{1}{l}\int_0^l \tilde{q}^2(z,t)dz}$ of the pressure and flow estimate errors from both observers of the entire drill string are shown, to get a more condensed indicator of their relative performance.

5. The observer gains which were used for the WDP and topside observer are both presented in their 2×2 form over the domain $[0,1] \ni x$. These are $P^{++}(x)$, $P^{+-}(x)$, $P^{-+}(x)$ and $P^{--}(x)$ for the WDP observer, and $\bar{P}^{+}(x)$ and $\bar{P}^{-}(x)$ for the topside observer.

6. Also the PDE kernel solutions used to calculate the observer gains are presented. These are for the WDP observer $M_{11}(x,\xi)$, $M_{12}(x,\xi)$, $M_{21}(x,\xi)$, $M_{22}(x,\xi)$, $N_{11}(x,\xi)$, $N_{12}(x,\xi)$, $N_{21}(x,\xi)$ and $N_{22}(x,\xi)$ over the triangular domain $\mathcal{T}_u$ and $K_{21}(x,\xi)$ over the square domain $\mathcal{S}_0$. The kernels $\bar{M}(x,\xi)$ and $\bar{N}(x,\xi)$ over $\mathcal{T}_u$ for the topside observer are also presented.

With respect to the actual implementation of the WDP observer for the MPD system (7.1)–(7.2), from Lemma 7.1 we see that $\lambda = \mu$ are constant, so either *Case I* or *Case IV* in Appendix A can be utilized. In the simulations here presented, *Case I* was used. It was assumed that the observers already had converged to the correct state estimates at time $t = 0$, so $\hat{p}(z,0) = p_0(z)$ and $\hat{q}(z,0) = q_0(z)$ for both observers.

The drill string was discretized into $\hat{N} = 200$ grid points, whilst the simulation was run for time in the interval $t \in [0, 30]$. A time step of $h = 0.001$ s was used. In the same way as for the simulations presented in Chapter 6, the $2 + 2$ collocated gains which were used to calculate observer gains for the WDP observer were solved over a grid of dimension $\frac{\hat{N}}{2} \times \frac{\hat{N}}{2}$, whereas the observer gains for the topside observer were solved over a grid of dimension $\hat{N} \times \hat{N}$.

8.2 Simulation

8.2.1 Simulation Plots

Drill String Mud Pressure and Flow

How the pressure $p(z,t)$[Pa] and volumetric flow $q(z,t)$, for $z \in [0,l]$, varies along the length of the drill string as time progresses through the interval $t \in [0, 30]$ is shown in Fig. 8.1. Here Fig. 8.1a shows the pressure and Fig. 8.1b shows the flow.

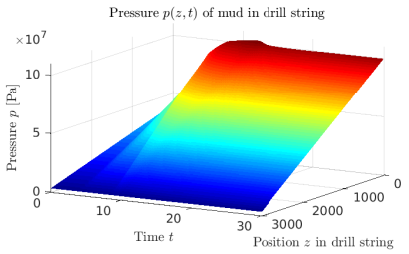

(a) Pressure $p(z,t)$ of the mud in drill string.

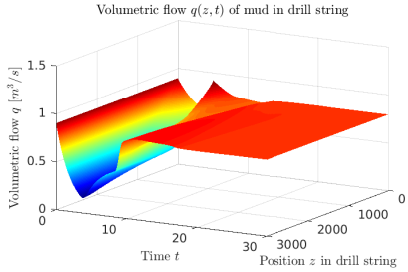

(b) Volumetric flow $q(z,t)$ of the mud in the drill string.

Figure 8.1: Pressure $p(z,t)$[Pa] and volumetric flow $q(z,t)[\mathrm{m}^3\,\mathrm{s}^{-1}]$ of mud in drill string, calculated with the model (7.1)–(7.2) using the values given in Table 8.1. A kick occurs at time $t_K = 5$ s, and the entire simulation lasts for 30 s.

At $t_K = 5$ s a kick occurs, and this is reflected in the behaviour of both plots in Fig. 8.1. There is a change in the pressure gradient in Fig. 8.1a before the kick occurs and afterwards, whereas the plot in Fig. 8.1b experiences a sudden change in its behaviour around this time.

Observer Mud Pressure and Flow Estimates

The plots in Fig. 8.2 show the estimates $\hat{p}(z,t)$ and $\hat{q}(z,t)$ produced by the observer (4.62), having access to both topside and downhole measurements $\iota_1(t) = p(l,t)$, $\iota_2(t) = q(l,t)$, $\iota_3(t) = p(0,t)$ and $\iota_4(t) = q(0,t)$. Lemma 7.1 is used for necessary coordinate transformations. Of the plots, Fig. 8.2a shows the pressure estimate, whereas Fig. 8.2b shows the estimate of the flow. The gains which were used to produce these estimates are shown further down in this section.

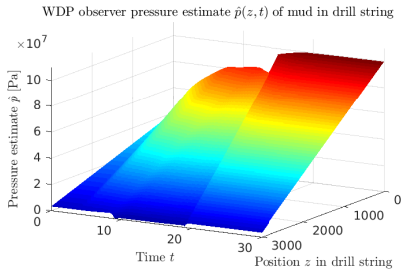

(a) WDP observer pressure estimate $\hat{p}(z,t)$.

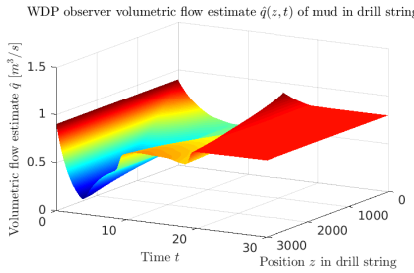

(b) WDP observer flow estimate $\hat{q}(z,t)$.

Figure 8.2: Estimates $\hat{p}(z,t)$ and $\hat{q}(z,t)$ of the pressure $p(z,t)$[Pa] and volumetric flow $q(z,t)[\mathrm{m}^3\,\mathrm{s}^{-1}]$ of the flow in a drill string described by (7.1)–(7.2), utilizing topside measurements $\iota_1(t) = p(l,t)$ and $\iota_2(t) = q(l,t)$ in addition to downhole measurements $\iota_3(t) = p(0,t)$ and $\iota_4(t) = q(0,t)$. The estimates are produced by (4.62) with help from Lemma 7.1 for coordinate transforms. The physical parameters used are defined in Table 8.1.

In Fig. 8.3 we see the drill string state estimates $\hat{p}(z,t)$ and $\hat{q}(z,t)$ produced

by the observer (5.1) combined with the coordinate transformation from Lemma 7.1, having access to only topside measurements $\iota_1(t) = p(l,t)$ and $\iota_2(t) = q(l,t)$. Fig. 8.3a shows the estimate of pressure from the topside observer and Fig. 8.3b shows the flow estimate from the topside observer.

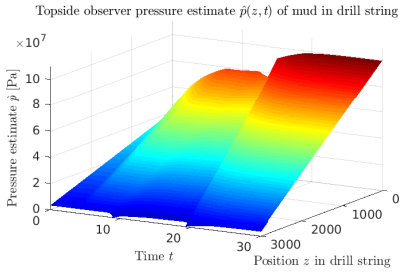

(a) Topside observer pressure estimate $\hat{p}(z,t)$.

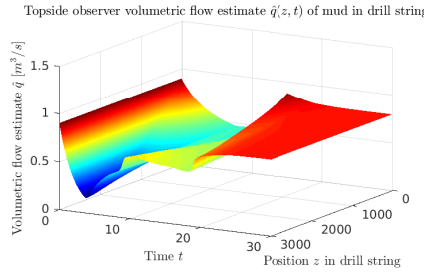

(b) Topside observer flow estimate $\hat{q}(z,t)$.

Figure 8.3: Estimates $\hat{p}(z,t)$ and $\hat{q}(z,t)$ of the pressure $p(z,t)$[Pa] and volumetric flow $q(z,t)[\mathrm{m}^3\,\mathrm{s}^{-1}]$ of the flow in a drill string described by (7.1)–(7.2), utilizing only topside measurements $\iota_1(t) = p(l,t)$ and $\iota_2(t) = q(l,t)$. The estimates are produced by (5.1) with help from Lemma 7.1 for coordinate transforms. The physical parameters used are defined in Table 8.1.

Observing Fig. 8.2 and Fig. 8.3, we see the kick at time $t_K = 5$ s affects the estimates despite them not having access to the correct reservoir pressure $p_{r,1}$ until after the estimation delay $t_D = 10$ s. Comparing these to Fig. 8.1, where we can identify that the behaviour in both plots changes most drastically when the kick occurs, we see instead in both Fig. 8.2 and Fig. 8.3 that there are two points in time where the behaviour changes most drastically. In addition to changing at the kick, the behaviour of both $\hat{p}(z,t)$ and $\hat{q}(z,t)$ for both observers changes some time after the correct reservoir pressure has been fed to them, most likely as a result of the state estimates converging to the correct values. Looking closely, we can observe nuanced differences between the plots of $\hat{p}(z,t)$ in Fig. 8.2a and Fig. 8.3a, and additionally the plots of $\hat{q}(z,t)$ in Fig. 8.2b and Fig. 8.3b. However, it is from these plots difficult to see which observer produces correct state estimates more efficiently.

Observer Mud Pressure and Flow Estimate Errors

Shown in Fig. 8.4 are the estimation errors $\tilde{p}(z,t) = p(z,t) - \hat{p}(z,t)$ and $\tilde{q}(z,t) = q(z,t) - \hat{q}(z,t)$ which are a result of the WDP observer estimating pressure $p(z,t)$[Pa] and flow $q(z,t)[\mathrm{m}^3\,\mathrm{s}^{-1}]$ using the estimates $\hat{p}(z,t)$ and $\hat{q}(z,t)$ produced from the observer (4.62) combined with Lemma 7.1. Table 8.1 defines the physical parameters used. Essentially Fig. 8.4a represents the values in Fig. 8.2a subtracted from the pressure plot in Fig. 8.1a. Likewise Fig. 8.4b represents the plot in Fig. 8.4b subtracted from Fig. 8.1b.

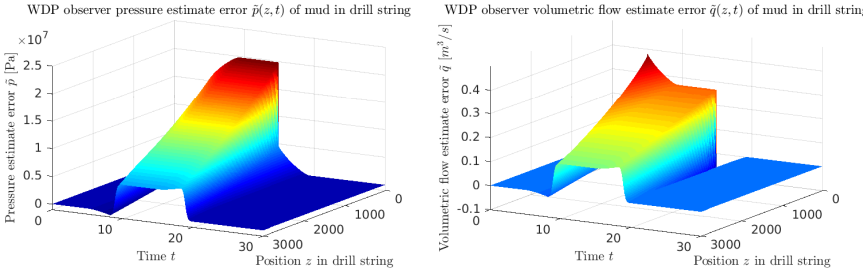

(a) WDP observer pressure estimation error $\tilde{p}(z,t)$.

(b) WDP observer flow estimation error $\tilde{q}(z,t)$.

Figure 8.4: Estimation errors $\tilde{p}(z,t)$ and $\tilde{q}(z,t)$ of the estimates $\hat{p}(z,t)$ and $\hat{q}(z,t)$ from the WDP observer, when it is trying to estimate the drill string pressure $p(z,t)$[Pa] and flow $q(z,t)[\mathrm{m}^3\,\mathrm{s}^{-1}]$, respectively. The physical parameters used are defined in Table 8.1.

The corresponding errors $\tilde{p}(z,t)$ and $\tilde{q}(z,t)$ which result from the estimation error in estimating $p(z,t)$[Pa] and $q(z,t)[\mathrm{m}^3\,\mathrm{s}^{-1}]$ with $\hat{p}(z,t)$ and $\hat{q}(z,t)$ generated by the topside observer using (5.1) together with Lemma 7.1 is shown in Fig. 8.5. Fig. 8.5a represents Fig. 8.3a subtracted from Fig. 8.1a, and in a similar way we obtain the values plotted in Fig. 8.5b from subtracting Fig. 8.3b from Fig. 8.1b.

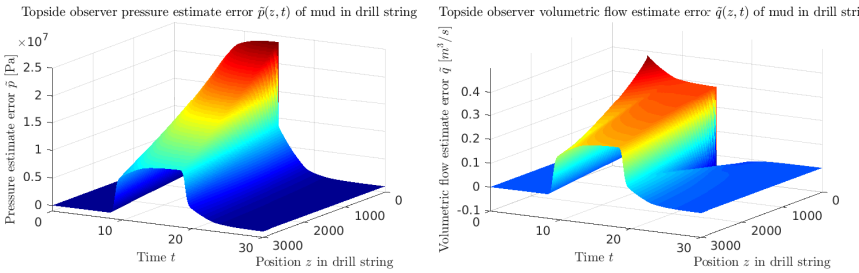

(a) Topside observer pressure estimation error $\tilde{p}(z,t)$.

(b) Topside observer flow estimation error $\tilde{q}(z,t)$.

Figure 8.5: Estimation errors $\tilde{p}(z,t)$ and $\tilde{q}(z,t)$ of the estimates $\hat{p}(z,t)$ and $\hat{q}(z,t)$ from the topside observer, when it is trying to estimate the drill string pressure $p(z,t)$[Pa] and flow $q(z,t)[\mathrm{m\,s}^{-3}]$, respectively. The physical parameters used are defined in Table 8.1.

Comparing Fig. 8.4 with Fig. 8.5 we can identify two main differences. Firstly, both $\tilde{p}(z,t)$ in Fig. 8.4a and $\tilde{q}(z,t)$ in Fig. 8.4b attain lower error values than the corresponding estimates in respectively Fig. 8.5a and Fig. 8.5b during the time interval when the estimates are pushed away from their correct values. The second difference that can be identified is that the re-convergence to zero after the correct pressure reservoir is given to the observers is sharper in the estimation errors from the WDP observer compared to the topside observer. To investigate the difference further we next present the Euclidean norm of the errors during the simulation.

In Fig. 8.6 the Euclidean norms $||\tilde{p}(t)|| = \sqrt{\frac{1}{l}\int_0^l \tilde{p}^2(z,t)dz}$ and $||\tilde{q}(t)|| = \sqrt{\frac{1}{l}\int_0^l \tilde{q}^2(z,t)dz}$, of the pressure and flow error respectively for both observers are presented. The norms related to both the WDP observer and topside observer are presented in the same plots so they can be compared easily, with Fig. 8.6a being devoted to the Euclidean norms of the pressure estimation error, and Fig. 8.6b displaying the Euclidean norms of the flow estimation error.

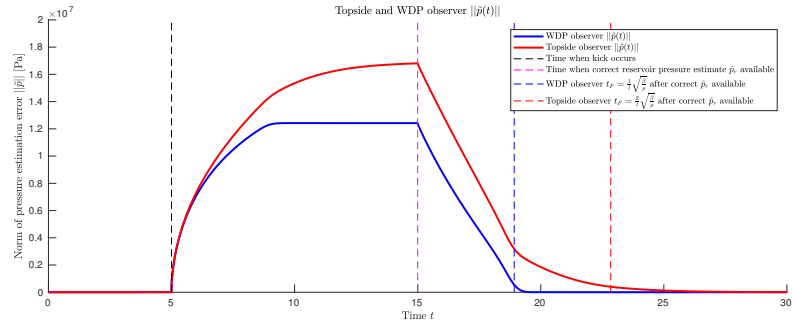

(a) Euclidean norms $||\tilde{p}(t)||$ of the pressure estimation errors $\tilde{p}(z,t)$.

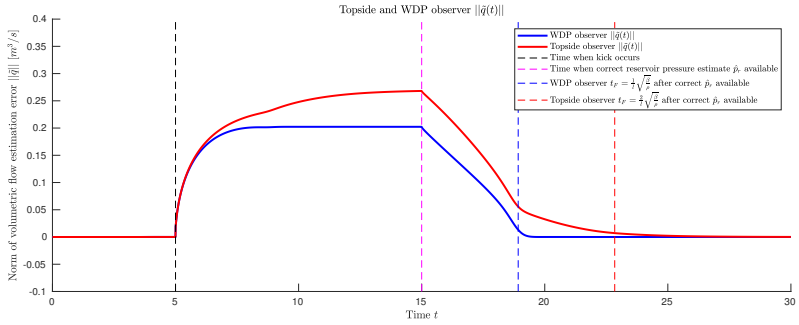

(b) Euclidean norms $||\tilde{q}(t)||$ of the flow estimation errors $\tilde{q}(z,t)$.

Figure 8.6: Euclidean norms $||\tilde{p}(t)||$ and $||\tilde{q}(t)||$ of estimation errors $\tilde{p}(z,t)$ and $\tilde{q}(z,t)$ respectively for both WDP and topside observer. The blue line shows the error norm for the WDP observer, whereas the red line is the error norm for the topside observer. The dashed black line represents t_K, when the kick occurs. Next, the pink dashed line is drawn at time $t_K + t_D$ to represent the time at which the observers are fed the correct new reservoir pressure $p_{r,1}$. The dashed blue line shows when the WDP observer estimates should theoretically have converged, whereas the dashed red line shows the theoretical convergence time for the topside observer. The physical parameters used are specified in Table 8.1.

In both sub-figures, the blue line represents the norm associated with the WDP observer, whereas the red line is for the topside observer. Critical times during the simulation are displayed by dashed lines, with the time of kick being represented by

a dashed black line and the time that the observers receive new correct reservoir pressure $p_{r,1}$ is represented by the dashed pink line. $\frac{1}{l}\sqrt{\frac{\beta}{\rho}}$ seconds after the WDP observer receives the new correct reservoir pressure $p_{r,1}$, the estimates $\hat{p}(z,t)$ and $\hat{q}(z,t)$ produced by this observer should have converged to the correct values $p(z,t)$[Pa] and $q(z,t)$[$\mathrm{m}^3\,\mathrm{s}^{-1}$]. This is represented by the dashed blue line in Fig. 8.6, and the corresponding time of $\frac{2}{l}\sqrt{\frac{\beta}{\rho}}$ seconds that the topside observer should use to come up with correct pressure and flow estimates is given by the dashed red line.

Both of the plots Fig. 8.6a and Fig. 8.6b shows that the WDP observer is more efficient at producing correct state estimates than the WDP observer. For the interval of time between t_K and t_D when the observers do not know the value of $p_{r,1}$ but are using the incorrect value of $p_{r,0}$ as the reservoir pressure estimate instead, the WDP observer is able to keep the offset of $\hat{p}(z,t)$ and $\hat{q}(z,t)$ away from the correct values smaller than the topside observer in general. Also, the WDP observer has its estimation errors $\tilde{p}(z,t)$ and $\tilde{q}(z,t)$ vanish across the entire drill string earlier than those related to the topside observer. Despite this, the topside observer has surprisingly good performance and the improvement introduced by using the extra downhole measurements are marginal. However the improvement is present and in a kick handling situation an attenuating controller using the WDP observer in the loop can start doing its work earlier than a controller waiting for the state estimates from the topside observer.

8.2.2 Observer Gains and Kernel PDE Solutions

WDP Observer Gains

The four plots in Fig. 8.7 show the bilateral observer gains $P^{++}(x)$, $P^{+-}(x)$, $P^{-+}(x)$ and $P^{--}(x)$ across the spatial domain $[0,1] \ni x$ which have been used in producing the WDP observer state estimates $\hat{p}(z,t)$ and $\hat{q}(z,t)$. These estimates are displayed in Fig. 8.2 and have been generated using the observer (4.62) together with Lemma 7.1 when using model parameters from Table 8.1.

Fig. 8.7a shows the gain $P^{++}(x)$, Fig. 8.7b shows the gain $P^{+-}(x)$, Fig. 8.7c shows the gain $P^{-+}(x)$, and Fig. 8.7d shows the gain $P^{--}(x)$, all of which get used by the WDP observer in generating the state estimates $\hat{p}(z,t)$ and $\hat{q}(z,t)$ with the measurements $\iota_1(t) = p(l,t)$, $\iota_2(t) = q(l,t)$, $\iota_3(t) = p(0,t)$ and $\iota_4(t) = q(0,t)$ as input. These gains were calculated from minimum time $2+2$ collocated kernels according to (A.7) in Appendix A. The $2+2$ gains used in (A.7) to calculate the 2×2 gains were calculated from (3.73). The numerical kernel PDE solutions used for these calculations can be seen further down in Section 8.2.

Topside Observer Gains

In Fig. 8.8 we find the unilateral observer gains $\bar{P}^{+}(x)$ and $\bar{P}^{-}(x)$ defined over the real number interval $[0,1] \ni x$ used to produce the topside observer estimates $\hat{p}(z,t)$ and $\hat{q}(z,t)$ using (5.1) and Lemma 7.1. The estimates this observer produces, given that the system parameters are summarized in Table 8.1, are shown in Fig. 8.3.

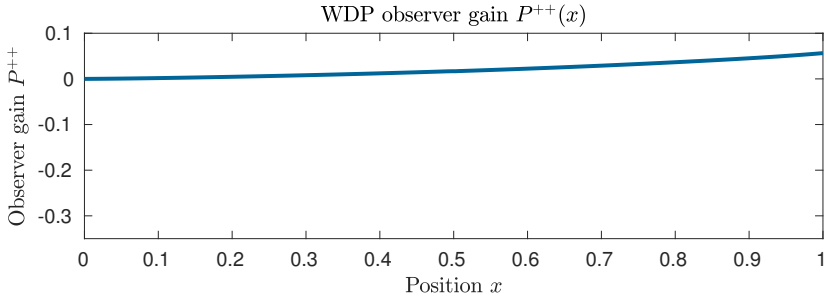

(a) WDP observer gain $P^{++}(x)$.

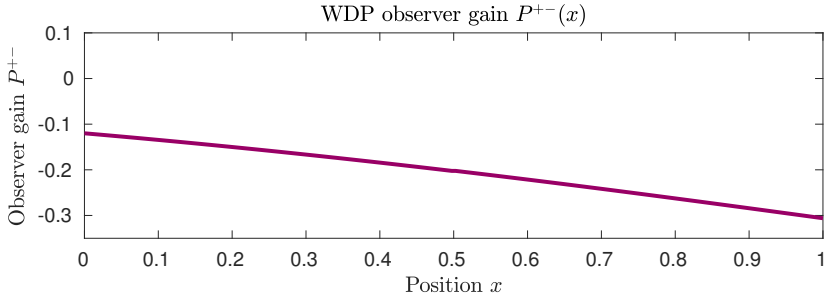

(b) WDP observer gain $P^{+-}(x)$.

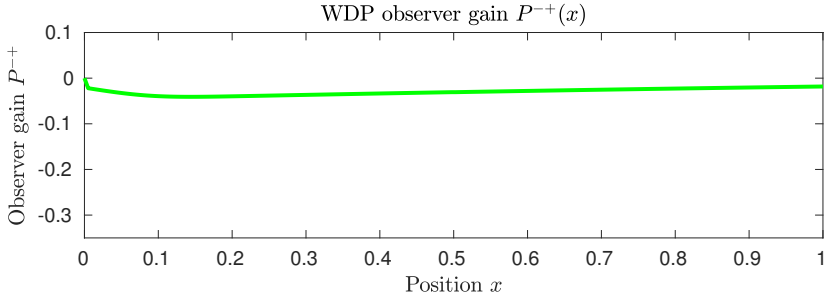

(c) WDP observer gain $P^{-+}(x)$.

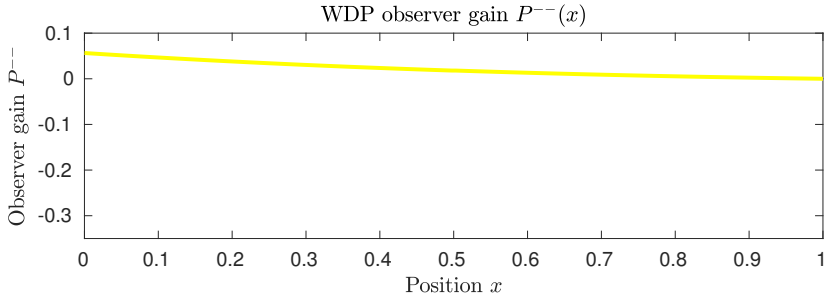

(d) WDP observer gain $P^{--}(x)$.

Figure 8.7: WDP observer gains used to calculate the pressure $\hat{p}(z,t)$ and $\hat{q}(z,t)$ estimates using the bilateral observer (4.62) together with Lemma 7.1 for estimating pressure $p(z,t)$[Pa] and flow $q(z,t)[\mathrm{m}^3\,\mathrm{s}^{-1}]$ of the drilling system model (7.1)–(7.2). The model parameters used are summarized in Table 8.1.

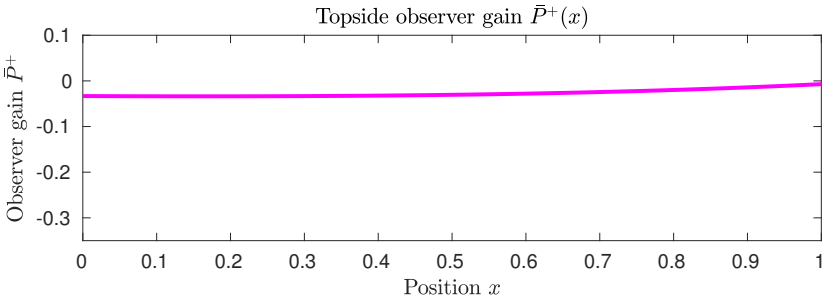

(a) Topside observer gain $\bar{P}^+(x)$.

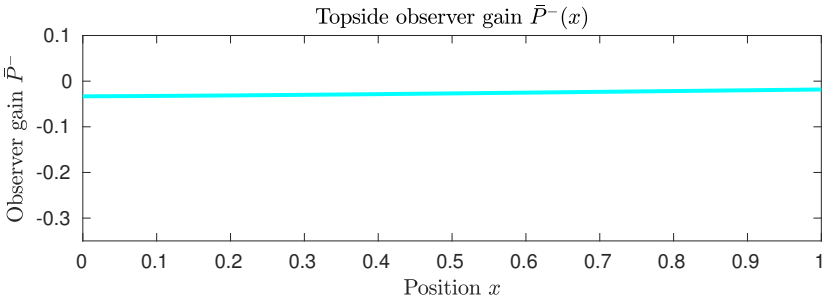

(b) Topside observer gain $\bar{P}^-(x)$.

Figure 8.8: Topside observer gains used to calculate the pressure estimate $\hat{p}(z,t)$ and $\hat{q}(z,t)$ using the collocated observer (5.1) for estimating the states $p(z,t)$[Pa] and $v(x,t)[\mathrm{m}^3\,\mathrm{s}^{-1}]$ of the drilling system (7.1)–(7.2). The model parameters used are summarized in Table 8.1.

We find in Fig. 8.8a the topside observer gain $\bar{P}^+(x)$, whilst Fig. 8.8b shows the other observer gain $\bar{P}^-(x)$, both of which get used by the topside observer to generate estimates $\hat{p}(z,t)$ and $\hat{q}(z,t)$ using topside measurements $\iota_1(t) = p(l,t)$ and $\iota_2(t) = q(l,t)$. These observer gains are computed from (5.2). The numerical approximate solution to the kernel PDEs used here are given further down in Section 8.2.

WDP Observer Kernel Solutions

The four components of the $M(x,\xi)$ matrix kernel solution used for calculating the observer gains shown in Fig. 8.7 from (A.7) which again were calculated from (3.73) are shown in Fig. 8.9, with $(x,\xi) \in \mathcal{T}_u$.

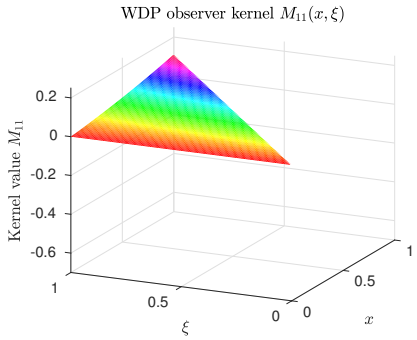

(a) Collocated 2+2 kernel solution $M_{11}(x,\xi)$ for WDP observer.

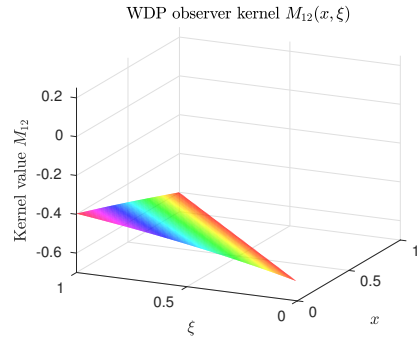

(b) Collocated 2+2 kernel solution $M_{12}(x,\xi)$ for WDP observer.

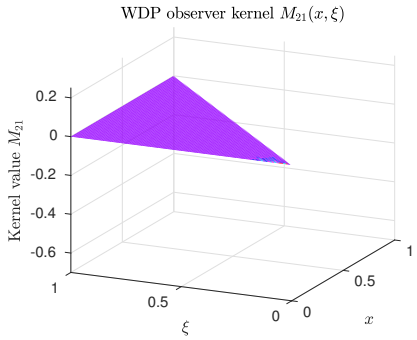

(c) Collocated 2+2 kernel solution $M_{21}(x,\xi)$ for WDP observer.

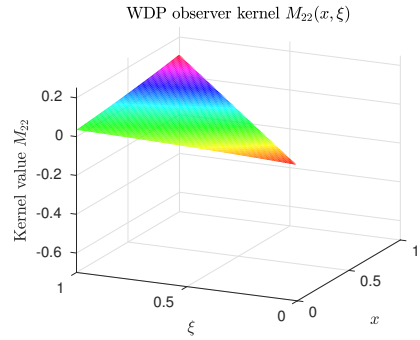

(d) Collocated 2+2 kernel solution $M_{22}(x,\xi)$ for WDP observer.

Figure 8.9: Collocated $2+2$ kernel solutions $M(x,\xi)$ over the upper triangular domain $\mathcal{T}_u$ to the first matrix PDE in (3.74) with boundary conditions (3.75), where the $2+2$ system parameters are defined according to *Case I* in Appendix A, which again are based on the 2×2 system from applying Lemma 7.1 with parameters from Table 8.1.

Fig. 8.9a shows $M_{11}(x,\xi)$ which corresponds with the top left matrix entry of $M(x,\xi)$, Fig. 8.9b shows $M_{12}(x,\xi)$ corresponding to the top right entry, Fig. 8.9c displays $M_{21}(x,\xi)$ which represents the values from the bottom left entry, and Fig. 8.9d display $M_{22}(x,\xi)$ which are the values found in the bottom right entry of the 2×2 matrix $M(x,\xi)$.

$M(x,\xi)$ and $N(x,\xi)$ are solutions to the matrix PDE (3.74)–(3.75) with the $2+2$ system parameters found from *Case I* in Appendix A, which in turn are calculated from Lemma 7.1 using Table 8.1. See Section 5.3 for an explanation of how these matrix kernel solutions were found. The four components of the $N(x,\xi)$ matrix kernel solution are shown in Fig. 8.10. Fig. 8.10a shows $N_{11}(x,\xi)$ which is the the

top left component of the 2×2 matrix $N(x, \xi)$, Fig. 8.10b shows $N_{12}(x, \xi)$ which is the top right component, the bottom left component $N_{21}(x, \xi)$ is in Fig. 8.10c and Fig. 8.10d shows the bottom right component $N_{22}(x, \xi)$.

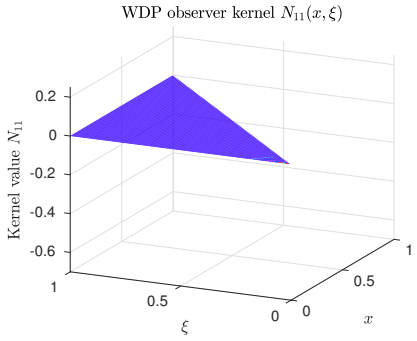

(a) Collocated $2+2$ kernel solution $N_{11}(x, \xi)$ for WDP observer.

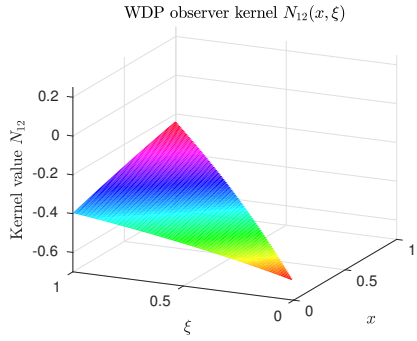

(b) Collocated $2+2$ kernel solution $N_{12}(x, \xi)$ for WDP observer.

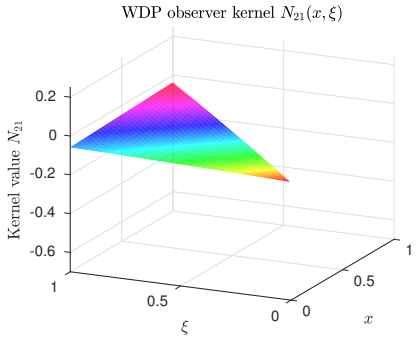

(c) Collocated $2+2$ kernel solution $N_{21}(x, \xi)$ for WDP observer.

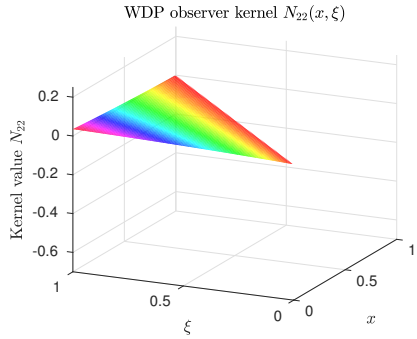

(d) Collocated $2+2$ kernel solution $N_{22}(x, \xi)$ for WDP observer.

Figure 8.10: Collocated $2 + 2$ kernel solutions $N(x, \xi)$ over the upper triangular domain $\mathcal{T}_u$ to the second matrix PDE in (3.74) with boundary conditions (3.75), where the $2 + 2$ system parameters are defined according to *Case I* in Appendix A, which again are based on the 2×2 system from applying Lemma 7.1 with parameters from Table 8.1.

The kernel solution $k_{21}(x, \xi)$ over $\mathcal{S}_0$ of (3.51)–(3.71) is here in Fig. 8.11. Note that the boundary condition for this PDE depends on the solution to the $M(x, \xi)$ and $N(x, \xi)$ matrix PDEs shown in Fig. 8.9 and Fig. 8.10 respectively, so these were solved first, and $k_{21}(x, \xi)$ was solved for subsequently.

Topside Observer Kernel Solutions

In order to calculate the topside observer kernel gains shown in Fig. 8.8, of which there were only two, the PDE system (5.3)–(5.4) with scalar solutions $\bar{M}(x, \xi)$ and $\bar{N}(x, \xi)$ needed to be solved over the upper triangular domain $\mathcal{T}_u$. The solution to this system when the system parameters are specified by Lemma 7.1 and Table 8.1

is shown in Fig. 8.12. Here Fig. 8.12a shows the solution $\bar{M}(x,\xi)$ whereas Fig. 8.12b shows $\bar{N}(x,\xi)$.

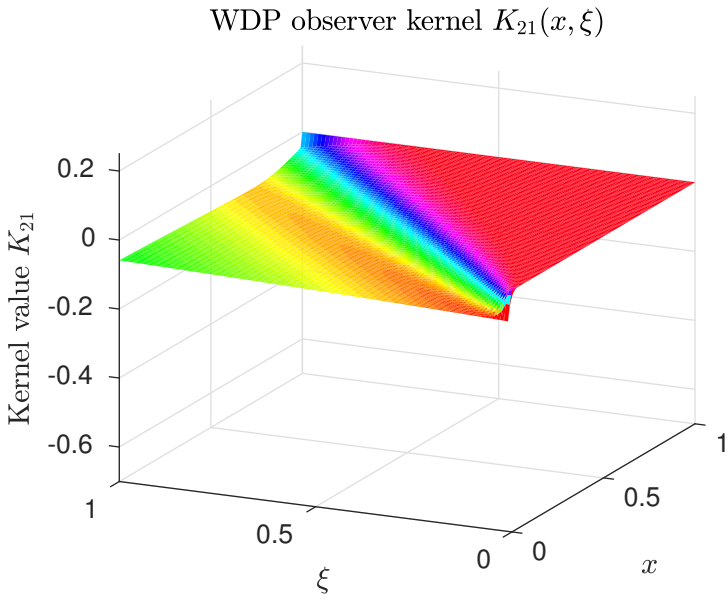

Figure 8.11: Collocated $2+2$ minimum time kernel solution $k_{21}(x,\xi)$ to (3.51) - (3.71) for the case when the $2+2$ system parameters are defined according to *Case I* in Appendix A, which again are based on the 2×2 system from applying Lemma 7.1 with parameters from Table 8.1.

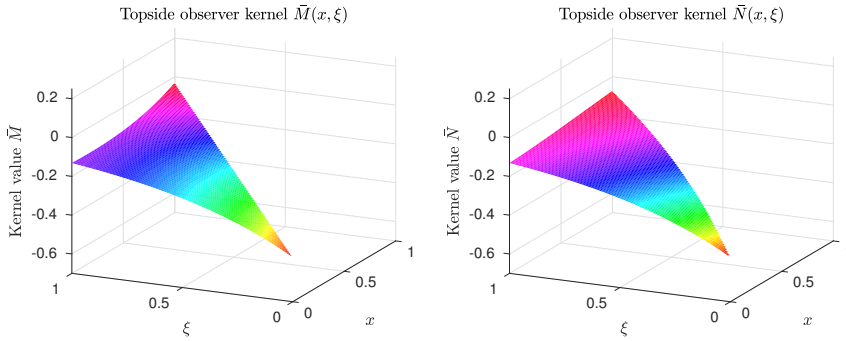

(a) Unilateral 2×2 kernel solution $\bar{M}(x,\xi)$ for topside observer.

(b) Unilateral 2×2 kernel solution $\bar{N}(x,\xi)$ for topside observer.

Figure 8.12: Unilateral 2×2 kernel solutions to the PDE system (5.3)–(5.4) and using system parameters defined in from Lemma 7.1 and Table 8.1.

Part IV

Conclusions

Chapter 9

Conclusions and future work

In this thesis, a minimum time bilateral observer for first order 2×2 linear hyperbolic PDEs relying on boundary from both the left and right boundary has been derived. It was shown that this observer can converge more quickly than an observer only using a single boundary measurement.

The derivation was based on going via a $2+2$ first order linear hyperbolic PDE system, and in doing so a special case of the non-minimum time $n+m$ collocated observer from Anfinsen and Aamo (2017b), for $n=m=2$, was extended to converge in minimum time. With the minimum time $2+2$ collocated observer having been developed, the minimum time 2×2 bilateral observer could be found by splitting its domain at a point $x_s\in(0,1)$ and subsequently folding its domain over to coincide with the $2+2$ system. The necessary splitting points x_s to achieve minimum time convergence within this framework was also found.

After having derived the theory, two toy simulations for the 2×2 bilateral observer were first implemented. In one of the simulations the leftward convecting transport velocity was higher than the rightward one, and vice versa for the second toy simulation. The performance of the bilateral observer was contrasted to an observer only having access to right boundary measurements. These simulations showed that the bilateral observer produced estimates which truly converged to their correct values more quickly than an observer using only a single boundary measurement.

To demonstrate a practical application of the theory developed, an oil drilling case was presented. It was suggested that an efficient observer could be useful during a kick handling situation, as full state information is usually needed to implement attenuating feedback controllers. The bilateral observer was therefore implemented as an observer relying on both topside and downhole measurements via a wired drill pipe, and demonstrated in a simulation where a drilling system is drilling into a reservoir that suddenly experiences a jump in the reservoir pressure. After some time delay, the correct reservoir pressure is revealed to the observer. Upon receiving this information, the observer had to generate pressure and flow estimates which re-converged to their correct values. As a benchmark, an observer using only topside measurements was implemented in parallel. It was found that the observer using both topside and downhole measurements generated estimates that converged to their correct values twice as quickly as the observer only relying on

topside measurements. However, the observer only relying on topside measurements still estimated the drill string pressure and flow surprisingly well, with its estimates nearly having converged to their correct value when the bilateral observer had converged. One possible reason the bilateral observer only showed a marginal improvement in estimation efficiency relative the unilateral observer when applied to a kick handling situation could be that the kick was modeled as a step input, being a very low bandwidth signal. As was seen in Chapter 6, a bigger difference in performance could be noted when the estimation error was a more "interesting" signal. Perhaps a larger difference in performance could be seen if a more realistic model of a kick is implemented instead.

With respect to future work, from a theoretical perspective some natural extensions could be to generalize the observer results to more general systems of first order linear hyperbolic PDEs. From the perspective of the practical application considered, only observation has been considered in this thesis, and possible further work could include implementing an attenuating controller in addition to the observer to see how quickly a kick situation could be handled. Possible future work could therefore include:

1. Extending the $2 + 2$ minimum time collocated observer result to a general $n + m$ setting.

2. Extending the 2×2 minimum time bilateral observer result to a general $n + m$ setting.

3. Extend the minimum time bilateral 2×2 observer to handle adaptive situations when parameters in its model are unknwon.

4. Implement a bilateral controller in the loop with the bilateral observer and investigate the performance of the entire feedback loop.

5. Test the observer in a more realistic drilling simulator.

Appendix A

Coefficient and Observer Gain Assignments between $2+2$ and 2×2 Systems

A.1 Case I

The invertible changes of coordinates

$$\begin{aligned}(\bar{u}(x,t),\bar{v}(x,t)) &= \mathscr{T}_{1,x_s}[u,v](x,t),\\ (\check{u}(x,t),\check{v}(x,t)) &= \mathscr{T}_{1,x_s}[\hat{u},\hat{v}](x,t),\end{aligned} \tag{A.1}$$

with $\mathscr{T}_{1,x_s}$ defined in (4.15a), are applied to map (4.1)–(4.2) into (3.1)–(3.2) and (4.30) into (3.83), respectively. We can then make coefficient assignments as follows:

$$\Lambda^+(x) = \begin{bmatrix}\lambda_1(x) & 0\\ 0 & \lambda_2(x)\end{bmatrix} = \begin{bmatrix}\frac{\lambda(x_s+x(1-x_s))}{1-x_s} & 0\\ 0 & \frac{\mu(x_s(1-x))}{x_s}\end{bmatrix} \tag{A.2a}$$

$$\Lambda^-(x) = \begin{bmatrix}\mu_1(x) & 0\\ 0 & \mu_2(x)\end{bmatrix} = \begin{bmatrix}\frac{\lambda(x_s(1-x))}{x_s} & 0\\ 0 & \frac{\mu(x_s+x(1-x_s))}{1-x_s}\end{bmatrix} \tag{A.2b}$$

$$\Sigma^{+-}(x) = \begin{bmatrix}\sigma_{11}^{+-}(x) & \sigma_{12}^{+-}(x)\\ \sigma_{21}^{+-}(x) & \sigma_{22}^{+-}(x)\end{bmatrix} = \begin{bmatrix}0 & \sigma^+(x_s+x(1-x_s))\\ \sigma^-(x_s(1-x)) & 0\end{bmatrix} \tag{A.3a}$$

$$\Sigma^{-+}(x) = \begin{bmatrix}\sigma_{11}^{-+}(x) & \sigma_{12}^{-+}(x)\\ \sigma_{21}^{-+}(x) & \sigma_{22}^{-+}(x)\end{bmatrix} = \begin{bmatrix}0 & \sigma^+(x_s(1-x))\\ \sigma^-(x_s+x(1-x_s)) & 0\end{bmatrix} \tag{A.3b}$$

$$Q_0 = \begin{bmatrix}Q_{11} & Q_{12}\\ Q_{21} & Q_{22}\end{bmatrix} = \begin{bmatrix}1 & 0\\ 0 & 1\end{bmatrix} \tag{A.4a}$$

$$R_1 = \begin{bmatrix} R_{11} & R_{12} \\ R_{21} & R_{22} \end{bmatrix} = \begin{bmatrix} 0 & Q \\ R & 0 \end{bmatrix} \tag{A.4b}$$

$$U(t) = \begin{bmatrix} \bar{U}_1(t) \\ \bar{U}_2(t) \end{bmatrix} = \begin{bmatrix} U_1(t) \\ U_2(t) \end{bmatrix} \tag{A.5}$$

$$y(t) = \begin{bmatrix} \bar{y}_1(t) \\ \bar{y}_2(t) \end{bmatrix} = \begin{bmatrix} y_1(t) \\ y_2(t) \end{bmatrix} \tag{A.6}$$

$$P^+(x) = \begin{bmatrix} P_{11}^+(x) & P_{12}^+(x) \\ P_{21}^+(x) & P_{22}^+(x) \end{bmatrix} = \begin{bmatrix} P^{++}(x_s + x(1-x_s)) & P^{+-}(x_s + x(1-x_s)) \\ P^{-+}(x_s(1-x)) & P^{--}(x_s(1-x)) \end{bmatrix} \tag{A.7a}$$

$$P^-(x) = \begin{bmatrix} P_{11}^-(x) & P_{12}^-(x) \\ P_{21}^-(x) & P_{22}^-(x) \end{bmatrix} = \begin{bmatrix} P^{++}(x_s(1-x)) & P^{+-}(x_s(1-x)) \\ P^{-+}(x_s + x(1-x_s)) & P^{--}(x_s + x(1-x_s)) \end{bmatrix} \tag{A.7b}$$

A.2 Case II

The invertible changes of coordinates

$$\begin{aligned} (\bar{u}(x,t), \bar{v}(x,t)) &= \mathscr{T}_{2,x_s}[u,v](x,t), \\ (\check{u}(x,t), \check{v}(x,t)) &= \mathscr{T}_{2,x_s}[\hat{u},\hat{v}](x,t), \end{aligned} \tag{A.8}$$

with $\mathscr{T}_{2,x_s}$ defined in (4.15b), are applied to map (4.1)–(4.2) into (3.1)–(3.2) and (4.30) into (3.83), respectively. We can then make coefficient assignments as follows:

$$\Lambda^+(x) = \begin{bmatrix} \lambda_1(x) & 0 \\ 0 & \lambda_2(x) \end{bmatrix} = \begin{bmatrix} \frac{\mu(x_s(1-x))}{x_s} & 0 \\ 0 & \frac{\lambda(x_s + x(1-x_s))}{1-x_s} \end{bmatrix} \tag{A.9a}$$

$$\Lambda^-(x) = \begin{bmatrix} \mu_1(x) & 0 \\ 0 & \mu_2(x) \end{bmatrix} = \begin{bmatrix} \frac{\lambda(x_s(1-x))}{x_s} & 0 \\ 0 & \frac{\mu(x_s + x(1-x_s))}{1-x_s} \end{bmatrix} \tag{A.9b}$$

$$\Sigma^{+-}(x) = \begin{bmatrix} \sigma_{11}^{+-}(x) & \sigma_{12}^{+-}(x) \\ \sigma_{21}^{+-}(x) & \sigma_{22}^{+-}(x) \end{bmatrix} = \begin{bmatrix} \sigma^-(x_s(1-x)) & 0 \\ 0 & \sigma^+(x_s + x(1-x_s)) \end{bmatrix} \tag{A.10a}$$

$$\Sigma^{-+}(x) = \begin{bmatrix} \sigma_{11}^{-+}(x) & \sigma_{12}^{-+}(x) \\ \sigma_{21}^{-+}(x) & \sigma_{22}^{-+}(x) \end{bmatrix} = \begin{bmatrix} \sigma^+(x_s(1-x)) & 0 \\ 0 & \sigma^-(x_s + x(1-x_s)) \end{bmatrix} \tag{A.10b}$$

$$Q_0 = \begin{bmatrix} Q_{11} & Q_{12} \\ Q_{21} & Q_{22} \end{bmatrix} = \begin{bmatrix} 0 & 1 \\ 1 & 0 \end{bmatrix} \tag{A.11a}$$

$$R_1 = \begin{bmatrix} R_{11} & R_{12} \\ R_{21} & R_{22} \end{bmatrix} = \begin{bmatrix} Q & 0 \\ 0 & R \end{bmatrix} \tag{A.11b}$$

$$U(t) = \begin{bmatrix} \bar{U}_1(t) \\ \bar{U}_2(t) \end{bmatrix} = \begin{bmatrix} U_1(t) \\ U_2(t) \end{bmatrix} \tag{A.12}$$

$$y(t) = \begin{bmatrix} \bar{y}_1(t) \\ \bar{y}_2(t) \end{bmatrix} = \begin{bmatrix} y_2(t) \\ y_1(t) \end{bmatrix} \tag{A.13}$$

$$P^+(x) = \begin{bmatrix} P_{11}^+(x) & P_{12}^+(x) \\ P_{21}^+(x) & P_{22}^+(x) \end{bmatrix} = \begin{bmatrix} P^{--}(x_s(1-x)) & P^{-+}(x_s(1-x)) \\ P^{+-}(x_s + x(1-x_s)) & P^{++}(x_s + x(1-x_s)) \end{bmatrix} \tag{A.14a}$$

$$P^-(x) = \begin{bmatrix} P_{11}^-(x) & P_{12}^-(x) \\ P_{21}^-(x) & P_{22}^-(x) \end{bmatrix} = \begin{bmatrix} P^{+-}(x_s(1-x)) & P^{++}(x_s(1-x)) \\ P^{--}(x_s + x(1-x_s)) & P^{-+}(x_s + x(1-x_s)) \end{bmatrix} \tag{A.14b}$$

A.3 Case III

The invertible changes of coordinates

$$\begin{aligned} (\bar{u}(x,t), \bar{v}(x,t)) &= \mathscr{T}_{3,x_s}[u,v](x,t), \\ (\check{u}(x,t), \check{v}(x,t)) &= \mathscr{T}_{3,x_s}[\hat{u},\hat{v}](x,t), \end{aligned} \tag{A.15}$$

with $\mathscr{T}_{2,x_s}$ defined in (4.15c), are applied to map (4.1)–(4.2) into (3.1)–(3.2) and (4.30) into (3.83), respectively. We can then make coefficient assignments as follows:

$$\Lambda^+(x) = \begin{bmatrix} \lambda_1(x) & 0 \\ 0 & \lambda_2(x) \end{bmatrix} = \begin{bmatrix} \frac{\lambda(x_s + x(1-x_s))}{1-x_s} & 0 \\ 0 & \frac{\mu(x_s(1-x))}{x_s} \end{bmatrix} \tag{A.16a}$$

$$\Lambda^-(x) = \begin{bmatrix} \mu_1(x) & 0 \\ 0 & \mu_2(x) \end{bmatrix} = \begin{bmatrix} \frac{\mu(x_s + x(1-x_s))}{1-x_s} & 0 \\ 0 & \frac{\lambda(x_s(1-x))}{x_s} \end{bmatrix} \tag{A.16b}$$

$$\Sigma^{+-}(x) = \begin{bmatrix} \sigma_{11}^{+-}(x) & \sigma_{12}^{+-}(x) \\ \sigma_{21}^{+-}(x) & \sigma_{22}^{+-}(x) \end{bmatrix} = \begin{bmatrix} \sigma^+(x_s + x(1-x_s)) & 0 \\ 0 & \sigma^-(x_s(1-x)) \end{bmatrix} \tag{A.17a}$$

$$\Sigma^{-+}(x) = \begin{bmatrix} \sigma_{11}^{-+}(x) & \sigma_{12}^{-+}(x) \\ \sigma_{21}^{-+}(x) & \sigma_{22}^{-+}(x) \end{bmatrix} = \begin{bmatrix} \sigma^{-}(x_s + x(1-x_s)) & 0 \\ 0 & \sigma^{+}(x_s(1-x)) \end{bmatrix} \tag{A.17b}$$

$$Q_0 = \begin{bmatrix} Q_{11} & Q_{12} \\ Q_{21} & Q_{22} \end{bmatrix} = \begin{bmatrix} 0 & 1 \\ 1 & 0 \end{bmatrix} \tag{A.18a}$$

$$R_1 = \begin{bmatrix} R_{11} & R_{12} \\ R_{21} & R_{22} \end{bmatrix} = \begin{bmatrix} R & 0 \\ 0 & Q \end{bmatrix} \tag{A.18b}$$

$$U(t) = \begin{bmatrix} \bar{U}_1(t) \\ \bar{U}_2(t) \end{bmatrix} = \begin{bmatrix} U_2(t) \\ U_1(t) \end{bmatrix} \tag{A.19}$$

$$y(t) = \begin{bmatrix} \bar{y}_1(t) \\ \bar{y}_2(t) \end{bmatrix} = \begin{bmatrix} y_1(t) \\ y_2(t) \end{bmatrix} \tag{A.20}$$

$$P^{+}(x) = \begin{bmatrix} P_{11}^{+}(x) & P_{12}^{+}(x) \\ P_{21}^{+}(x) & P_{22}^{+}(x) \end{bmatrix} = \begin{bmatrix} P^{++}(x_s + x(1-x_s)) & P^{+-}(x_s + x(1-x_s)) \\ P^{-+}(x_s(1-x)) & P^{--}(x_s(1-x)) \end{bmatrix} \tag{A.21a}$$

$$P^{-}(x) = \begin{bmatrix} P_{11}^{-}(x) & P_{12}^{-}(x) \\ P_{21}^{-}(x) & P_{22}^{-}(x) \end{bmatrix} = \begin{bmatrix} P^{-+}(x_s + x(1-x_s)) & P^{--}(x_s + x(1-x_s)) \\ P^{++}(x_s(1-x)) & P^{+-}(x_s(1-x)) \end{bmatrix} \tag{A.21b}$$

A.4 Case IV

The invertible changes of coordinates

$$\begin{aligned} (\bar{u}(x,t), \bar{v}(x,t)) &= \mathscr{T}_{4,x_s}[u,v](x,t), \\ (\check{u}(x,t), \check{v}(x,t)) &= \mathscr{T}_{4,x_s}[\hat{u},\hat{v}](x,t), \end{aligned} \tag{A.22}$$

with $\mathscr{T}_{4,x_s}$ defined in (4.15d), are applied to map (4.1)–(4.2) into (3.1)–(3.2) and (4.30) into (3.83), respectively. We can then make coefficient assignments as follows:

$$\Lambda^{+}(x) = \begin{bmatrix} \lambda_1(x) & 0 \\ 0 & \lambda_2(x) \end{bmatrix} = \begin{bmatrix} \frac{\mu(x_s(1-x))}{x_s} & 0 \\ 0 & \frac{\lambda(x_s + x(1-x_s))}{1-x_s} \end{bmatrix} \tag{A.23a}$$

$$\Lambda^{-}(x) = \begin{bmatrix} \mu_1(x) & 0 \\ 0 & \mu_2(x) \end{bmatrix} = \begin{bmatrix} \frac{\mu(x_s + x(1-x_s))}{1-x_s} & 0 \\ 0 & \frac{\lambda(x_s(1-x))}{x_s} \end{bmatrix} \tag{A.23b}$$

$$\Sigma^{+-}(x) = \begin{bmatrix} \sigma_{11}^{+-}(x) & \sigma_{12}^{+-}(x) \\ \sigma_{21}^{+-}(x) & \sigma_{22}^{+-}(x) \end{bmatrix} = \begin{bmatrix} 0 & \sigma^{-}(x_s(1-x)) \\ \sigma^{+}(x_s + x(1-x_s)) & 0 \end{bmatrix} \tag{A.24a}$$

$$\Sigma^{-+}(x) = \begin{bmatrix} \sigma_{11}^{-+}(x) & \sigma_{12}^{-+}(x) \\ \sigma_{21}^{-+}(x) & \sigma_{22}^{-+}(x) \end{bmatrix} = \begin{bmatrix} 0 & \sigma^{-}(x_s + x(1-x_s)) \\ \sigma^{+}(x_s(1-x)) & 0 \end{bmatrix} \tag{A.24b}$$

$$Q_0 = \begin{bmatrix} Q_{11} & Q_{12} \\ Q_{21} & Q_{22} \end{bmatrix} = \begin{bmatrix} 1 & 0 \\ 0 & 1 \end{bmatrix} \tag{A.25a}$$

$$R_1 = \begin{bmatrix} R_{11} & R_{12} \\ R_{21} & R_{22} \end{bmatrix} = \begin{bmatrix} 0 & R \\ Q & 0 \end{bmatrix} \tag{A.25b}$$

$$U(t) = \begin{bmatrix} \bar{U}_1(t) \\ \bar{U}_2(t) \end{bmatrix} = \begin{bmatrix} U_2(t) \\ U_1(t) \end{bmatrix} \tag{A.26}$$

$$y(t) = \begin{bmatrix} \bar{y}_1(t) \\ \bar{y}_2(t) \end{bmatrix} = \begin{bmatrix} y_2(t) \\ y_1(t) \end{bmatrix} \tag{A.27}$$

$$P^{+}(x) = \begin{bmatrix} P_{11}^{+}(x) & P_{12}^{+}(x) \\ P_{21}^{+}(x) & P_{22}^{+}(x) \end{bmatrix} = \begin{bmatrix} P^{--}(x_s(1-x)) & P^{-+}(x_s(1-x)) \\ P^{+-}(x_s + x(1-x_s)) & P^{++}(x_s + x(1-x_s)) \end{bmatrix} \tag{A.28a}$$

$$P^{-}(x) = \begin{bmatrix} P_{11}^{-}(x) & P_{12}^{-}(x) \\ P_{21}^{-}(x) & P_{22}^{-}(x) \end{bmatrix} = \begin{bmatrix} P^{--}(x_s + x(1-x_s)) & P^{-+}(x_s + x(1-x_s)) \\ P^{+-}(x_s(1-x)) & P^{++}(x_s(1-x)) \end{bmatrix} \tag{A.28b}$$

Appendix B

Additional Material

B.1 Lemma 2 from Coron et al. (2017)

The following Lemma and its proof, were first stated in Coron et al. (2017) and are stated here almost verbatim.

Lemma B.1. *For any given $K \in L_2((0,1)\times(0,1))^{n\times n}$ with the cascade structure*

$$K = \begin{bmatrix} K_1 & 0 \\ 0 & 0 \end{bmatrix}, \tag{B.1}$$

where $K_1 \in L_2((0,1)\times(0,1))^{m\times m}$ is the strictly lower triangular matrix

$$K_1 = \begin{bmatrix} 0 & \dots & \dots & 0 \\ k_{21} & \ddots & \ddots & \vdots \\ \vdots & \ddots & \ddots & \vdots \\ k_{m1} & \dots & k_{mm-1} & 0 \end{bmatrix} \tag{B.2}$$

and $\forall i \in \{2,\dots,m\}$, $\forall j \in \{1,\dots,i-1\}$, $k_{ij} \in L_2((0,1)\times(0,1))$, the Fredholm transformation $\mathcal{F} : L_2(0,1)^n \to L_2(0,1)^n$ defined $\forall x \in (0,1)$ and $\forall z \in L_2(0,1)^n$ by

$$\mathcal{F}[z](x) = z(x) + \int_0^1 K(x,\xi)z(\xi)d\xi, \tag{B.3}$$

is invertible. Moreover, its inverse has the same form, defined $\forall x \in (0,1)$ and $\forall \varpi \in L_2(0,1)^n$ as

$$\mathcal{F}^{-1}[\varpi](x) = \varpi(x) + \int_0^1 \Gamma(x,\xi)\varpi(\xi)d\xi, \tag{B.4}$$

for some $\Gamma \in L_2((0,1)\times(0,1))^{n\times n}$ with the same structure as K, that is

$$\Gamma = \begin{bmatrix} \Gamma_1 & 0 \\ 0 & 0 \end{bmatrix} \tag{B.5}$$

in which $\Gamma_1 \in L_2((0,1)\times(0,1))^{n\times n}$ *is a strictly lower triangular matrix defined as*

$$\Gamma_1 = \begin{bmatrix} 0 & \dots & \dots & 0 \\ \gamma_{21} & \ddots & \ddots & \vdots \\ \vdots & \ddots & \ddots & \vdots \\ \gamma_{m1} & \dots & \gamma_{mm-1} & 0 \end{bmatrix} \tag{B.6}$$

for some $\gamma_{ij} \in L_2((0,1)\times(0,1))$, $\forall i \in \{2,\dots,m\}$, $\forall j \in \{1,\dots,i-1\}$.

Proof. Let $\varpi = \mathcal{F}[z]$, where $z \in L_2(0,1)$ is given. Due to (B.1) and (B.3), we have

$$z_i = \varpi_i, \forall i \in \{m+1,\dots,n\}. \tag{B.7}$$

Additionally, due to (B.2) and (B.3), we have

$$\begin{cases} \varpi_1 = z_1 \\ \varpi_i = z_i + \sum_{j=1}^{i-1} \int_0^1 k_{ij}(\cdot,\xi) z_j(\xi) d\xi, \forall i \in \{2,\dots,m\}. \end{cases} \tag{B.8}$$

It can then be seen by induction that

$$\begin{cases} z_1 = \varpi_1 \\ z_i = \varpi_i + \sum_{j=1}^{i-1} \int_0^1 \gamma_{ij}(\cdot,\xi) \varpi(\xi) d\xi, \forall i \in \{2,\dots,m\} \end{cases} \tag{B.9}$$

for some $\gamma_{ij} \in L_2(0,1)$ which only depends on k_{pq} for $p \in \{1,\dots,i\}$ and $q \in \{1,\dots,j\}$. □

B.2 Integral Equations

In Khvedelidze (2013), an integral equation is defined as any equation containing the unknwon under the integral sign. An integral equation defined over a $1D$ domain $[a,b] \ni x$ can in general be stated as

$$A(x)\phi(x) + \int_a^b K(x,\xi)\phi(\xi) d\xi = d(x) \tag{B.10}$$

Integral equations can be classified according to the parameters which define it. Depending on the definition of $d(x)$, integral equations can be classified as follows:

1. If $\forall x \in [a,b]$ we have $d(x) = 0$, the integral equation (B.10) is referred to as *homogeneous*.
2. Otherwise the integral equation is *inhomogeneous*.

Depending on the behaviour of $A(x)$ across the interval $x \in [a, b]$, the integral equation can be classified as one of three types:

1. If $\forall x \in [a, b]$ we have $A(x) = 0$, (B.10) is an integral equation of the *first kind*.
2. If $\forall x \in [a, b]$ we have $A(x) \neq 0$, (B.10) is an integral equation of the *second kind*.
3. If $A(x) = 0$, $\forall x \in I$, where $\neq I \subset [a, b]$, then (B.10) is an integral equation of the *third kind*.

Depending on whether the interval limits a and b are fixed or not, we can further classify integral equations as follows:

1. If $a = x$ or $b = x$, implying the limits are variable, (B.10) is a *Volterra* integral equation.
2. If a and b are fixed constants, (B.10) is a *Fredholm* integral equation.

Therefore, in this thesis we have primarily considered Fredholm and Volterra integral equations of the second kind, with $A(x) = 1$.

B.3 Numerical Integration

The trapezoidal rule was used for calculating integrals in the simulations. Given a function $f(x)$, with $x \in [a, b]$, the trapezoidal rule attempts to approximate the integral $\int_a^b f(x)dx$ by splitting the area under the integral into N trapezoids(MathWorks (2018)). Let the interval $[a, b]$ be split into $N + 1$ points so that $a = x_1 < x_2 < \cdots < x_N < x_{N+1} = b$. Then, from the formula of the area of a trapezoid, we have that the integral between point x_i and x_{i+1}, $i \in \{1, \dots N\}$ can be found to be

$$A_i = \frac{1}{2}(x_{i+1} - x_i)[f(x_i) + f(x_{i+1}] \tag{B.11}$$

Summing all these across the interval $[a, b]$, we see the integral can be approximated by

$$\int_a^b f(x)dx \approx \sum_{i=1}^{N} A_i = \frac{1}{2}\sum_{i=1}^{N}(x_{i+1} - x_i)[f(x_i) + f(x_{i+1})] \tag{B.12}$$

If equal spacing is used, we have $\forall i \in \{1, \dots, N\}$ that $x_{i+1} - x_i = \frac{b-a}{N}$, so we get

$$\begin{aligned} \int_a^b f(x)dx &\approx \frac{b-a}{2N}\sum_{i=1}^{N}[f(x_i) + f(x_{i+1})] \\ &= \frac{b-a}{2N}[f(x_1) + 2f(x_2) + \cdots + 2f(x_N) + f(x_{N+1})] \end{aligned} \tag{B.13}$$

Appendix C

Folder Structure

The MATLAB code that was written for this thesis and used to generate the simulation results is handed in as a folder organized in the following way. It has been tested, and verified to run using MATLAB R2017a on a computer with the operating system Ubuntu 16.04.3 LTS.

Directory tree

- *simulations* — Top level directory containing all simulation files.
  - `path_config.m` — MATLAB source code called by simulation files for adding the necessary folders to their path.
  - *toy_simulations* — Directory containing main simulation files for the toy simulations shown in Chapter 6.
    - `toy_case_1.m` — MATLAB main file for running first toy simulation shown in Section 6.2.
    - `toy_case_2.m` — MATLAB main file for running second toy simulation shown in Section 6.3.
  - *drilling_simulations* — Directory containing main simulation files for the drilling simulations shown in Chapter 7.
    - `drilling_case_1.m` — MATLAB main file for running. drilling simulation shown in Section 8.2.
  - *src* — Directory containing all the. source files used to run the simulations.
    - *observer_gain_calcs* — Directory containing source. files used to calculate observer gains.

- `bilateral_2t2_obs_gain_case_1.m` .. `MATLAB` source code file for calculating observer gains for the 2×2 bilateral observer when $2+2$ coefficients are assigned according to Case I in Appendix A.
- `bilateral_2t2_obs_gain_case_2.m` .. `MATLAB` source code file for calculating observer gains for the 2×2 bilateral observer when $2+2$ coefficients are assigned according to Case II in Appendix A.
- `bilateral_2t2_obs_gain_case_3.m` .. `MATLAB` source code file for calculating observer gains for the 2×2 bilateral observer when $2 + 2$ coefficients are assigned according to Case III in Appendix A.
- `bilateral_2t2_obs_gain_case_4.m` .. `MATLAB` source code file for calculating observer gains for the 2×2 bilateral observer when $2 + 2$ coefficients are assigned according to Case IV in Appendix A.
- `right_2p2_obs_gain_case_1_4.m` .... `MATLAB` source code file for calculating observer gains for the $2 + 2$ collocated observer when $2 + 2$ coefficients are assigned according to Case I or IV in Appendix A.
- `right_2p2_obs_gain_case_2_3.m` .... `MATLAB` source code file for calculating observer gains for the $2 + 2$ collocated observer when $2 + 2$ coefficients are assigned according to Case II or III in Appendix A.
- `right_2t2_obs_gain.m` ..... `MATLAB` source code file for calculating observer gains for the 2×2 unilateral observer.

plotting ..... Directory containing source files defining enumerations used for plotting.

- `toy_plot_enums.m` ..... Enumeration definitions for plotting in the toy simulations shown in Chapter 6.

- `drill_plot_enums.m` — Enumeration definitions for plotting in the drilling simulation shown in Chapter 8.
- *solvers* — Directory containing all the PDE solvers used in the simulations.
  - *general_solvers* — Directory containing solvers used for calculating solutions to the kernel PDEs in their general form.
    - `solver_advection.m` — MATLAB source code with subroutine for numerically solving the advection equation (2.22).
    - `solver_n1.m` — MATLAB source code with subroutine for numerically solving the general $2 + 1$ kernel equations (5.10)–(5.11)(written by Henrik Anfinsen).
    - `solver_nm.m` — MATLAB source code with subroutine for numerically solving the general $2 + 2$ kernel equations (5.21) with boundary conditions (5.24).
    - `solver_nm_mod.m` — MATLAB source code with subroutine for numerically solving the general $2 + 2$ kernel equations (5.21) with boundary conditions (5.44).
  - *kernel_solvers* — Directory containing solvers used for calculating solutions to the specific kernel PDEs used in this thesis by performing coordinate transformations, as was explained in Chapter 5, and calling the solvers in the `general_solvers` directory.
    - `first_solver_case_1_4.m` — Calls the subroutine defined in `solver_nm_mod.m` with the coefficient assignments (5.38) and (5.45).
    - `first_solver_case_2_3.m` — Calls the subroutine defined in `solver_nm_mod.m` with the coefficient assignments (5.41) and (5.46).

- `second_solver_case_1_4.m` ..... Calls the subroutine defined. in `solver_nm.m` with the coefficient assignments (5.23) and (5.25), for case I and IV in Appendix A.
- `second_solver_case_2_3.m` ..... Calls the subroutine defined. in `solver_nm.m` with the coefficient assignments (5.23) and (5.25), for case II and III in Appendix A.
- `third_solver.m` ..... Solves the kernel PDE (5.47)–. (5.48) by calling the subroutine in `solver_advection.m` with the appropriate coefficient definitions..
- `fourth_solver.m` ..... Solves the kernel PDEs (5.3)–. (5.4).
- *simulation_loops* ..... Directory containing time. marching finite difference simulation loop used in the simulation.
  - `sim_loop_u_v.m` ..... `MATLAB` source code for time. marching finite difference simulation loop used in the simulation.

Appendix D

Conference Paper

The following conference paper will be submitted to the *European Control Conference(ECC)*, that will be held from 25^{th}–28^{th} June 2019 in Naples, Italy, after the submission opens on 5^{th} September 2018.

Minimum Time Bilateral Observer Design for 2×2 Linear Hyperbolic Systems

Nils Christian A. Wilhelmsen, Henrik Anfinsen, Ole Morten Aamo

***Abstract*— In this paper we derive a minimum time convergent bilateral observer for a 2×2 system of linear coupled first-order 1-D hyperbolic PDEs. First, a Volterra integral transformation is combined with a Fredholm integral transformation to derive a minimum time collocated observer for a class of $2+2$ systems (four coupled PDEs). Then, it is shown that the 2×2 system (two coupled PDEs) can be transformed to a $2+2$ system via an invertible coordinate transformation. The 2×2 bilateral observer is subsequently obtained from the $2+2$ minimum time collocated observer, and it is shown that it has convergence time equal to the theoretical minimum time for bilateral sensing. The performance of the 2×2 bilateral observer is demonstrated in a simulation and compared to a previously derived observer using only unilateral sensing.**

I. INTRODUCTION

A. Problem statement

We are interested in systems with dynamics, in terms of the state (u,v), given by

$$u_t(x,t) + \lambda(x)u_x(x,t) = \sigma^+(x)v(x,t), \tag{1a}$$
$$v_t(x,t) - \mu(x)v_x(x,t) = \sigma^-(x)u(x,t), \tag{1b}$$
$$u(0,t) = qv(0,t) + U_1(t), \tag{1c}$$
$$v(1,t) = \rho v(1,t) + U_2(t), \tag{1d}$$

defined over $x \in [0,1]$ and $t \in [0,\infty)$, where

$$\lambda, \mu \in C^1([0,1]), \lambda(x), \mu(x) > 0, \forall x \in (0,1), \tag{2}$$

$$\sigma^+, \sigma^- \in C^0(0,1), \tag{3}$$

$$q, \rho \in \mathbb{R}, \tag{4}$$

and $U_1(t)$ and $U_2(t)$ are boundary control inputs. We assume that the initial conditions $u(x,0) = u_0(x)$ and $v(x,0) = v_0(x)$ satisfy $u_0, v_0 \in L_2(0,1)$.

System (1) is referred to as a 2×2 hyperbolic system, and u and v are scalar values that carry information in opposite directions on $(0,1)$. More generally, u and v may be vector-valued with n and m components, respectively, in which case the system is referred to an $n+m$ hyperbolic system. Notice that 2×2 systems and $1 + 1$ systems are the same.

We assume that measurements from (1) are taken at the boundaries, only, defined as

The authors are with the Department of Engineering Cybernetics, Norwegian University of Science and Technology, Trondheim N-7491, Norway. (e-mail: nilscw@stud.ntnu.no, henrik.anfinsen@ntnu.no, aamo@ntnu.no)

$$y_1(t) = u(1,t), \tag{5a}$$
$$y_2(t) = v(0,t). \tag{5b}$$

The goal of the paper is to design an observer for (1), using the measurements (5), only, that provides state estimates $\hat{u}$, $\hat{v}$ which converge to the correct system states in the minimum time for bilateral sensing, defined in [1] as

$$t_{2,min} = \max\left\{\int_0^1 \frac{dx}{\lambda(x)}, \int_0^1 \frac{dx}{\mu(x)}\right\}, \tag{6}$$

which is strictly smaller than the theoretical lower boundary $t_{1,min}$ when only measuring a single boundary, also defined in [1] as

$$t_{1,min} = \int_0^1 \frac{dx}{\lambda(x)} + \int_0^1 \frac{dx}{\mu(x)}. \tag{7}$$

In [2], the problem is solved for a general $n+m$ system, and the bilateral minimum time observer for (1), that is the $n = m = 1$ case, takes the form

$$\begin{aligned}\hat{u}_t(x,t) + \lambda(x)\hat{u}_x(x,t) &= \sigma^+(x)\hat{v}(x,t) \\ &\quad + P^{++}(x)(y_1(t) - \hat{u}(1,t)) \\ &\quad + P^{+-}(x)(y_2(t) - \hat{v}(0,t))\end{aligned} \tag{8a}$$
$$\begin{aligned}\hat{v}_t(x,t) - \mu(x)\hat{v}_x(x,t) &= \sigma^-(x)\hat{u}(x,t) \\ &\quad + P^{-+}(x)(y_1(t) - \hat{u}(1,t)) \\ &\quad + P^{--}(x)(y_2(t) - \hat{v}(0,t))\end{aligned} \tag{8b}$$
$$\hat{u}(0,t) = qy_2(t) + U_1(t) \tag{8c}$$
$$\hat{v}(1,t) = \rho y_1(t) + U_2(t) \tag{8d}$$

where P^{++}, P^{+-}, P^{-+} and P^{--} are observer gains tailored to achieve convergence in finite time given by (6). The contribution of the present paper is twofold: First, we design a minimum time convergent observer for a class of $2 + 2$ systems using a single measurement taken at one boundary. This problem has to the best of the authors' knowledge not been solved before. Second, we show that the $2 + 2$ system can be transformed by an invertible change of coordinates into the 2×2 system (1), thereby obtaining the observer gains in (8) by an alternative route.

To facilitate the design of the observer for the $2+2$ system, we impose the following assumption on the transport speeds

of (1), in addition to (2):

$$\mu(x) \leq \overline{\mu} \leq \underline{\lambda} \leq \lambda(x), \forall x \in (0,1). \tag{9}$$

Notice that the direction of the inequality signs in (9) is chosen without loss of generality in view of the symmetry in (1). In [2], constant transport speeds are considered, so there (9) holds trivially. One immediate consequence of (9) is that

$$t_{2,min} = \int_0^1 \frac{dx}{\mu(x)}. \tag{10}$$

B. Background

Systems of coupled first-order linear hyperbolic PDEs, along with their observation and control problems, have been subject to research recently due to their application in modeling various physical scenarios. Applications include heat exchangers [3], gas pipelines [4] and oil well drilling [5], to name a few.

A gradually more common method for observer and controller design for this type of systems is the infinite dimensional backstepping method, initially pioneered for parabolic PDE control design in [6], and subsequently appearing in its fully infinite dimensional form in [7]. Applying the backstepping method for observer design was first seen for parabolic PDEs in [8].

In [9], the first observer for 2×2 systems (1) relying on the single boundary measurement (5a), only, was presented. An observer with single boundary sensing for the more general class of $n+m$ hyperbolic systems was achieved in [10], albeit converging in non-minimum time. The $2+2$ system observer designed in the present paper builds on the $n+m$ system observer from [10] by modifying the non-minimum time target system used there with the help of a Fredholm integral transformation, following ideas from [11], [12]. We find expressions for the 2×2 bilateral observer gains using a domain folding trick similar to the one suggested in [13] for stabilization of systems of reaction-diffusion equations, and demonstrate in simulations that our 2×2 bilateral observer converges within (10), which is quicker than (7) achieved by the observer from [9].

This paper is organized as follows. Section II presents the minimum time collocated observer design for the $2+2$ system, and the result is applied in Section III to obtain the minimum time 2×2 bilateral observer. Results from a simulation are given in Section IV before some concluding remarks are offered in Section V.

II. MINIMUM-TIME COLLOCATED OBSERVER FOR $2+2$ SYSTEMS

A. Class of $2+2$ systems

Consider now the $2+2$ system defined as

$$\bar{u}_t(x,t) + \Lambda^+(x)\bar{u}_x(x,t) = \Sigma^{+-}(x)\bar{v}(x,t) \tag{11a}$$
$$\bar{v}_t(x,t) - \Lambda^-(x)\bar{v}_x(x,t) = \Sigma^{-+}(x)\bar{u}(x,t) \tag{11b}$$
$$\bar{u}(0,t) = Q_0\bar{v}(0,t) \tag{11c}$$
$$\bar{v}(1,t) = R_1\bar{u}(1,t) + U(t) \tag{11d}$$

evolving over $x\in[0,1]$ and $t\in[0,\infty)$, where

$$\bar{u}(x,t) = [u_1(x,t), u_2(x,t)]^T \tag{12a}$$
$$\bar{v}(x,t) = [v_1(x,t), v_2(x,t)]^T \tag{12b}$$

are the states. We assume that initial conditions, defined as $\bar{u}(x,0) = [u_{1,0}(x), u_{2,0}(x)]^T$ and $\bar{v}(x,0) = [v_{1,0}(x), v_{2,0}(x)]^T$ satisfy $u_{1,0}, u_{2,0}, v_{1,0}, v_{2,0} \in L_2(0,1)$.

The transport speed matrices, which are defined as

$$\Lambda^+(x) = diag\{\lambda_1(x), \lambda_2(x)\} \tag{13a}$$
$$\Lambda^-(x) = diag\{\mu_1(x), \mu_2(x)\} \tag{13b}$$

have components satisfying

$$\lambda_1, \lambda_2, \mu_1, \mu_2 \in C^1(0,1) \tag{14}$$

and are subject to the restriction

$$\lambda_2(x) \geq \lambda_1(x) > 0 > -\mu_1(x) \geq -\mu_2(x), \forall x \in (0,1) \tag{15}$$

The two coupling coefficient matrices

$$\Sigma^{+-}(\bar{x}) = \{\sigma_{ij}^{+-}(\bar{x})\}_{1\leq i,j\leq 2} \tag{16a}$$
$$\Sigma^{-+}(\bar{x}) = \{\sigma_{ij}^{-+}(\bar{x})\}_{1\leq i,j\leq 2} \tag{16b}$$

have components satisfying $\forall i,j \in \{1,2\}$

$$\sigma_{ij}^{+-}, \sigma_{ij}^{-+} \in C^0([0,1]), \tag{17}$$

whereas the reflection coefficients

$$Q_0 = \{q_{ij}\}_{1\leq i,j\leq 2} \tag{18a}$$
$$R_1 = \{\rho_{ij}\}_{1\leq i,j\leq 2}, \tag{18b}$$

have components satisfying $\forall i,j \in \{1,2\}$

$$q_{ij}, \rho_{ij} \in \mathbb{R}. \tag{19}$$

The term $U(t) = [U_1(t), U_2(t)]^T$ is a boundary control input for (11), entering at $x=1$. In addition to right boundary actuation, it is assumed that the collocated boundary measurement vector $y = [y_1, y_2]^T$ with components

$$y_1(t) = u_1(1,t) \tag{20a}$$
$$y_2(t) = u_2(1,t) \tag{20b}$$

is available.

B. Collocated observer for the $2+2$ system

We consider here the observer

$$\begin{aligned}\check{u}_t(x,t)+\Lambda^+(x)\check{u}_x(x,t)&=\Sigma^{+-}(x)\check{v}(x,t)\\&\quad+P^+(x)(y(t)-\check{u}(1,t))\quad(21a)\\ \check{v}_t(x,t)-\Lambda^-(x)\check{v}_x(x,t)&=\Sigma^{-+}(x)\check{u}(x,t)\\&\quad+P^-(x)(y(t)-\check{u}(1,t)\quad(21b)\\ \check{u}(0,t)&=Q_1\check{v}(0,t)\quad(21c)\\ \check{v}(1,t)&=R_1y(t)+U(t)\quad(21d)\end{aligned}$$

providing state estimates $\check{u}=[\check{u}_1,\check{u}_2]^T$ and $\check{v}=[\check{v}_1,\check{v}_2]^T$, where

$$\begin{aligned}P^+(x)&=M(x,1)\Lambda^+(1)+T^+(x)\\&\quad+\int_x^1 M(x,\xi)T^+(\xi)d\xi\quad(22a)\end{aligned}$$

$$P^-(x)=N(x,1)\Lambda^+(1)+\int_x^1 N(x,\xi)T^+(\xi)d\xi\quad(22b)$$

are the observer gains. M and N in (22) are 2×2 matrix-valued functions

$$\begin{aligned}M(x,\xi)&=\{M_{ij}(x,\xi)\}_{1\le i,j\le 2}\quad(23a)\\ N(x,\xi)&=\{N_{ij}(x,\xi)\}_{1\le i,j\le 2}\quad(23b)\end{aligned}$$

which are solutions to the kernel PDE

$$\begin{aligned}\Lambda^+(x)M_x(x,\xi)+M_\xi(x,\xi)\Lambda^+(\xi)&=-M(x,\xi)\Lambda^+_\xi(\xi)\\&\quad+\Sigma^{+-}(x)N(x,\xi)\quad(24a)\\ -\Lambda^-(x)N_x(x,\xi)+N_\xi(x,\xi)\Lambda^+(\xi)&=-N(x,\xi)\Lambda^+_\xi(\xi)\\&\quad+\Sigma^{-+}(x)M(x,\xi)\quad(24b)\\ \Lambda^-(x)N(x,x)+N(x,x)\Lambda^+(x)&=\Sigma^{-+}(x)\quad(24c)\\ Q_0N(0,\xi)-M(0,\xi)&=H(\xi)\quad(24d)\\ M_{12}(x,x)=M_{21}(x,x)&=0\quad(24e)\\ M_{21}(x,1)&=0\quad(24f)\end{aligned}$$

defined over the triangular domain $\mathcal{T}_u=\{(x,\xi)\mid 0\le x\le\xi\le 1\}$. In (24d), $H=\{h_{ij}\}_{1\le i,j\le 2}$ is a strictly lower triangular 2×2 matrix, and its only non-zero component h_{21} is defined as

$$h_{21}(\xi)=\sum_{k=1}^{2}q_{2k}N_{k1}(0,\xi)-M_{21}(0,\xi).\quad(25)$$

The term $T^+=\{T^+_{ij}\}_{1\le i,j\le 2}$ appearing in (22) is a strictly lower triangular 2×2 matrix, and its only non-zero term T^+_{21} is defined as

$$T^+_{21}(x)=k_{21}(x,1)\lambda_1(1),\quad(26)$$

where k_{21} is the solution to the PDE

$$\begin{aligned}k_{21,x}(x,\xi)\lambda_2(x)+k_{21,\xi}(x,\xi)\lambda_1(\xi)&=-k_{21}(x,\xi)\lambda_{1,\xi}(\xi)\quad(27a)\\ k_{21}(0,\xi)&=h_{21}(\xi)\quad(27b)\\ k_{21}(x,0)&=0.\quad(27c)\end{aligned}$$

Provided that (15) holds, well-posedness of (24)–(25) is ensured by Theorem 3.2 in [14] whereas in [11] the explicit solution to an equation of the form (27) is given. Note that in [14] the well-posedness proof is given for the case of constant transport velocities, but it is claimed that the proof extends to cases involving spatially varying transport speeds with little effort. Next, we present a convergence result for the observer (21).

Theorem 2.1: Consider system (11) with outputs (20) and the observer (21). If the output injection gains are selected as (22)–(27), then $\check{u}(x,t)$ and $\check{v}(x,t)$ converge to $\bar{u}(x,t)$ and $\bar{v}(x,t)$, respectively, in finite time given by

$$t_{min}=\int_0^1\frac{dx}{\mu_1(x)}+\int_0^1\frac{dx}{\lambda_1(x)}.\quad(28)$$

Subsections II-C and II-D are devoted to proving Theorem 2.1.

C. Volterra backstepping transformation

Define the estimation errors $\tilde{u}=\bar{u}-\check{u}$ and $\tilde{v}=\bar{v}-\check{v}$. The error dynamics can then be found from (11) and (21) as

$$\begin{aligned}\tilde{u}_t(x,t)+\Lambda^+(x)\tilde{u}_x(x,t)&=\Sigma^{+-}(x)\tilde{v}(x,t)\\&\quad-P^+(x)\tilde{u}(1,t)\quad(29a)\\ \tilde{v}_t(x,t)-\Lambda^-(x)\tilde{v}_x(x,t)&=\Sigma^{-+}(x)\tilde{u}(x,t)\\&\quad-P^-(x)\tilde{v}(1,t)\quad(29b)\\ \tilde{u}(0,t)&=Q_0\tilde{v}(0,t)\quad(29c)\\ \tilde{v}(1,t)&=0.\quad(29d)\end{aligned}$$

The proof of the following Lemma follows similar steps as the proof of Lemma 10 in [10], but is included here to show the details behind the new observer gains (22), which are different from those in [10] to accommodate minimum time convergence.

Lemma 2.2: The invertible Volterra integral transformation

$$\begin{aligned}\tilde{u}(x,t)&=\tilde{\alpha}(x,t)+\int_x^1 M(x,\xi)\tilde{\alpha}(\xi,t)d\xi\quad(30a)\\ \tilde{v}(x,t)&=\tilde{\beta}(x,t)+\int_x^1 N(x,\xi)\tilde{\alpha}(\xi,t)d\xi\quad(30b)\end{aligned}$$

maps

$$\tilde{\alpha}_t(x,t)+\Lambda^+(x)\tilde{\alpha}_x(x,t)=\Sigma^{+-}(x)\tilde{\beta}(x,t) - \int_x^1 D^+(x,\xi)\tilde{\beta}(\xi,t)d\xi - T^+(x)\tilde{\alpha}(1,t) \tag{31a}$$

$$\tilde{\beta}_t(x,t)-\Lambda^-(x)\tilde{\beta}_x(x,t)=-\int_x^1 D^-(x,\xi)\tilde{\beta}(\xi,t)d\xi \tag{31b}$$

$$\tilde{\alpha}(0,t)=Q_0\tilde{\beta}(0,t) + \int_0^1 H(\xi)\tilde{\alpha}(\xi,t)d\xi \tag{31c}$$

$$\tilde{\beta}(1,t)=0 \tag{31d}$$

into (29), where M and N satisfy (24)–(25). $D^+ = \{d^+_{ij}\}_{i,j\in\{1,2\}}$, $D^- = \{d^-_{ij}\}_{i,j\in\{1,2\}}$ are the solutions to the integral equations

$$D^+(x,\xi)=M(x,\xi)\Sigma^{+-}(\xi) - \int_\xi^x M(\xi,s)D^+(s,\xi)ds, \tag{32a}$$

$$D^-(x,\xi)=N(x,\xi)\Sigma^{+-}(\xi) - \int_\xi^x N(\xi,s)D^+(s,\xi)ds, \tag{32b}$$

respectively.

Proof: Differentiating (30) with respect to time and space, substituting in the target error system (31), integrating by parts and combining with (29) we find

$$\begin{aligned}&\tilde{u}_t(x,t)+\Lambda^+(x)\tilde{u}_x(x,t)-\Sigma^{+-}(x)\tilde{v}(x,t)+P^+(x)\tilde{u}(1,t)\\ &\quad=[M(x,x)\Lambda^+(x)-\Lambda^+(x)M(x,x)]\tilde{\alpha}(x,t)\\ &\quad+\int_x^1[M_\xi(x,\xi)\Lambda^+(\xi)+M(x,\xi)\Lambda^+_\xi(\xi)+\Lambda^+(x)M_x(x,\xi)\\ &\qquad-\Sigma^{+-}(x)N(x,\xi)]\tilde{\alpha}(\xi,t)d\xi+\int_x^1[M(x,\xi)\Sigma^{+-}(\xi)\\ &\qquad-D^+(x,\xi)-\int_\xi^x M(\xi,s)D^+(s,\xi)ds]\tilde{\beta}(\xi,t)d\xi\\ &\qquad+[P^+(x)-M(x,1)\Lambda^+(1)-T^+(x)\\ &\qquad-\int_x^1 M(x,\xi)T^+(\xi)d\xi]\tilde{\alpha}(1,t)=0\end{aligned} \tag{33}$$

and

$$\begin{aligned}&\tilde{v}_t(x,t)-\Lambda^-(x)\tilde{v}_x(x,t)-\Sigma^{-+}(x)\tilde{u}(x,t)+P^-(x)\tilde{u}(1,t)\\ &\quad=[N(x,x)\Lambda^+(x)+\Lambda^-(x)N(x,x)-\Sigma^{-+}(x)]\tilde{\alpha}(x,t)\\ &\quad+\int_x^1[N_\xi(x,\xi)\Lambda^+(\xi)+N(x,\xi)\Lambda^+_\xi(\xi)-\Lambda^-(x)N_x(x,\xi)\\ &\qquad-\Sigma^{-+}(x)M(x,\xi)]\tilde{\alpha}(\xi,t)d\xi+\int_x^1[N(x,\xi)\Sigma^{+-}(\xi)\\ &\qquad-D^-(x,\xi)-\int_\xi^x N(\xi,s)D^+(s,\xi)ds]\tilde{\beta}(\xi,t)d\xi\\ &\qquad+[P^-(x)-N(x,1)\Lambda^+(1)\\ &\qquad-\int_x^1 N(x,\xi)T^+(\xi)d\xi]\tilde{\alpha}(1,t)=0\end{aligned} \tag{34}$$

From (33) and (34) we obtain P^+ and P^- (22), the definitions of D^+ and D^- (32), the PDE (24b) and the first two boundary conditions (24e) and (24c). For the third boundary condition (24d), set $x=0$ in (30) and substitute this into (29c), and then apply (31c) to obtain

$$\int_0^1 H(\xi)\tilde{\alpha}(\xi,t)d\xi=\int_0^1[Q_0N(0,\xi)-M(0,\xi)]\tilde{\alpha}(\xi,t)d\xi \tag{35}$$

from which the required boundary condition trivially follows. Finally, (24f) is an additional boundary condition required for well-posedness, as was done in [14] for equations in the same form. ■

D. Fredholm integral transformation

Now a target system which converges in minimum time (28) is introduced, and proved to be equivalent with (31). The proof of the following Lemma relies on similar steps as in the proof of Lemma 11 in [10] together with straightforward application of the method of characteristics, but is included here for completeness.

Lemma 2.3: Consider the error system with states $\tilde{\gamma} = [\tilde{\gamma}_1, \tilde{\gamma}_2]^T$ and $\tilde{\nu} = [\tilde{\nu}_1, \tilde{\nu}_2]^T$, governed by the dynamics

$$\tilde{\gamma}_t(x,t)+\Lambda^+(x)\tilde{\gamma}_x(x,t)=\Sigma^{+-}(x)\tilde{\nu}(x,t) - \int_x^1 D^+(x,\xi)\tilde{\nu}(\xi,t)d\xi - \int_0^1 \check{K}_1(x,\xi)[\check{\Sigma}^{+-}(\xi)\tilde{\nu}(\xi,t) - \int_\xi^1 \check{D}^+(\xi,s)\tilde{\nu}(s,t)ds]d\xi \tag{36a}$$

$$\tilde{\nu}_t(x,t) - \Lambda^-(x,t)\tilde{\nu}_x(x,t) = -\int_x^1 D^-(x,\xi)\tilde{\nu}(\xi,t)d\xi \tag{36b}$$

$$\tilde{\gamma}(0,t) = Q_0\tilde{\nu}(0,t) \tag{36c}$$

$$\tilde{\nu}(1,t) = 0. \tag{36d}$$

where $\breve{K}_1$, $\breve{\Sigma}^{+-}$ and $\breve{D}^+$ in (36a) are defined as

$$\breve{K}_1(x,\xi) = \begin{bmatrix} 0 & 0 \\ 0 & k_{21}(x,\xi) \end{bmatrix}, \tag{37a}$$

$$\breve{\Sigma}^{+-}(x) = \begin{bmatrix} 0 & 0 \\ \sigma_{11}^{+-}(x) & \sigma_{12}^{+-}(x) \end{bmatrix}, \tag{37b}$$

$$\breve{D}^{+}(x,\xi) = \begin{bmatrix} 0 & 0 \\ d_{11}^{+}(x,\xi) & d_{12}^{+}(x,\xi) \end{bmatrix} \tag{37c}$$

Then $\tilde{\gamma}(x,t), \tilde{\nu}(x,t)$ converge to zero in finite time given by (28).

Proof: By the method of characteristics and cascade structure of (36), we see from (36b) with boundary (36d) that $\tilde{\nu}(t) = 0 \ \forall t \geq \int_0^1 \frac{dx}{\mu_1(x)}$. (36a) reduces after this to $\tilde{\gamma}_t + \Lambda^+\tilde{\gamma}_x = 0$ with left boundary condition $\tilde{\gamma}(0,t) = 0$, which vanishes after another $\int_0^1 \frac{dx}{\lambda_1(x)}$ time steps. ■

We will now consider the Fredholm integral transformation

$$\tilde{\alpha}(x,t) = \tilde{\gamma}(x,t) + \int_0^1 K_1(x,\xi)\tilde{\gamma}(\xi,t)d\xi \tag{38a}$$

$$\tilde{\beta}(x,t) = \tilde{\nu}(x,t) \tag{38b}$$

with $K_1 = \{k_{ij}\}_{i,j\in\{1,2\}}$ being a strictly lower triangular 2×2 matrix, with k_{21} being the only nonzero element. We know from [11] that since K_1 is strictly lower triangular, the Fredholm integral transformation (38) is invertible.

Lemma 2.4: If k_{21} satisfies (27), then the invertible Fredholm integral transformation (38) maps the error system (36) into (31).

Proof: Noticing that (38b) is the identity, and that the first component of $\tilde{\alpha}$ equals the first component of $\tilde{\gamma}$ due to the structure of K_1, we only need to deal with the second component of $\tilde{\alpha}$, $\tilde{\alpha}_2$. Differentiating $\tilde{\alpha}_2$ in (38a) with respect to time and space, substituting in (36a), integrating by parts and combining with (31a) we find that

$$\begin{aligned} &\tilde{\alpha}_{2,t}(x,t) + \lambda_2(x)\tilde{\alpha}_{2,x}(x,t) - \sigma_{21}^{+-}(x)\tilde{\beta}_1(x,t) \\ &-\sigma_{22}^{+-}(x)\tilde{\beta}_2(x,t) = [T_{21}^{+}(x) - k_{21}(x,1)\lambda_1(1)]\tilde{\gamma}_1(1,t) \\ &+\int_0^1 [k_{21,x}(x,\xi)\lambda_2(x) + k_{21,\xi}(x,\xi)\lambda_1(\xi) \\ &+k_{21}(x,\xi)\lambda_{1,\xi}(\xi)]\tilde{\gamma}_1(\xi,t)d\xi + k_{21}(x,0)\lambda_1(0)\tilde{\gamma}_1(0,t) = 0, \end{aligned} \tag{39}$$

where (26)–(27) were used in the last step. Setting $x = 0$ into (38a), and comparing with (31c) we find

$$\int_0^1 K_1(0,\xi)\tilde{\gamma}(\xi,t)d\xi = \int_0^1 H(\xi)\tilde{\alpha}(\xi,t)d\xi \tag{40}$$

due to the boundary condition (27b), and the fact that $\tilde{\alpha}_1 = \tilde{\gamma}_1$.

■

We can now prove Theorem 2.1 by combining the Lemmas.

Proof: [Proof of Theorem 2.1] By Lemma 2.2 and Lemma 2.4, the dynamics of (29) and (36) are equivalent. Since by Lemma 2.3, $(\tilde{\gamma}, \tilde{\beta}) = 0$ in finite time given by (28), it follows (see (38) and (30)), that $(\tilde{u}, \tilde{v}) = 0$ in finite time given by (28). ■

III. MINIMUM-TIME BILATERAL OBSERVER FOR 2×2 SYSTEMS

A. Folding the 2×2 system into the $2+2$ system

Lemma 3.1: Let the transformation $T : (L_2([0,1]))^2 \to (L_2([0,1]))^4$ be defined by

$$T[u,v](x) = (\begin{bmatrix} v(\frac{1}{2}(1-x)) \\ u(\frac{1}{2}(1+x)) \end{bmatrix}, \begin{bmatrix} v(\frac{1}{2}(1+x)) \\ u(\frac{1}{2}(1-x)) \end{bmatrix}) \tag{41}$$

with inverse $T^{-1} : (L_2([0,1]))^4 \to (L_2([0,1]))^2$ given by

$$T^{-1}[\bar{u},\bar{v}](x) = \begin{cases} (v_2(1-2x), u_1(1-2x)), & x\in[0,\frac{1}{2}] \\ (u_2(2x-1), v_1(2x-1)), & x\in[\frac{1}{2},1] \end{cases} \tag{42}$$

The invertible change of coordinates $(\bar{u}(x,t), \bar{v}(x,t)) = T[u,v](x,t)$ maps (1) into (11), with coefficients given by

$$\Lambda^+(x) = \begin{bmatrix} 2\mu(\frac{1}{2}(1-x)) & 0 \\ 0 & 2\lambda(\frac{1}{2}(1+x)) \end{bmatrix} \tag{43a}$$

$$\Lambda^-(x) = \begin{bmatrix} 2\mu(\frac{1}{2}(1+x)) & 0 \\ 0 & 2\lambda(\frac{1}{2}(1-x)) \end{bmatrix} \tag{43b}$$

$$\Sigma^{+-}(x) = \begin{bmatrix} 0 & \sigma^-(\frac{1}{2}(1-x)) \\ \sigma^+(\frac{1}{2}(1+x)) & 0 \end{bmatrix} \tag{43c}$$

$$\Sigma^{-+}(x) = \begin{bmatrix} 0 & \sigma^-(\frac{1}{2}(1+x)) \\ \sigma^+(\frac{1}{2}(1-x)) & 0 \end{bmatrix} \tag{43d}$$

$$Q_0 = \begin{bmatrix} 1 & 0 \\ 0 & 1 \end{bmatrix} \qquad R_1 = \begin{bmatrix} 0 & \rho \\ q & 0 \end{bmatrix} \tag{44a}$$

$$U(t) = \begin{bmatrix} U_2(t) \\ U_1(t) \end{bmatrix} \qquad y(t) = \begin{bmatrix} y_2(t) \\ y_1(t) \end{bmatrix}. \tag{44b}$$

Proof: Differentiating (41) with respect to x and applying the chain rule we can express $\bar{u}_x$ and $\bar{v}_x$ in terms of u_x and v_x as

$$\bar{u}_x(x,t) = \begin{bmatrix} -\frac{1}{2}v_x(\frac{1}{2}(1-x),t) \\ \frac{1}{2}u_x(\frac{1}{2}(1+x),t) \end{bmatrix} \tag{45a}$$

$$\bar{v}_x(x,t) = \begin{bmatrix} \frac{1}{2}v_x(\frac{1}{2}(1+x),t) \\ -\frac{1}{2}u_x(\frac{1}{2}(1-x),t) \end{bmatrix}. \tag{45b}$$

Also, differentiating (41) with respect to time, we find

$$\bar{u}_t(x,t) = \begin{bmatrix} v_t(\frac{1}{2}(1-x),t) \\ u_t(\frac{1}{2}(1+x),t) \end{bmatrix} \tag{46a}$$

$$\bar{v}_t(x,t) = \begin{bmatrix} v_t(\frac{1}{2}(1+x),t) \\ u_t(\frac{1}{2}(1-x),t) \end{bmatrix}. \tag{46b}$$

Inserting (45) and (46) into (11) and comparing to (1) we find that the transport speeds can be assigned as (43a)–(43b) and the coupling coefficients become (43c)–(43d). In order to obey the restriction (15) which is a prerequisite for well-posedness of (24), we must have

$$\lambda(\frac{1}{2}(1+x)) \geq \mu(\frac{1}{2}(1-x)), \tag{47a}$$

$$\lambda(\frac{1}{2}(1-x)) \geq \mu(\frac{1}{2}(1+x)) \tag{47b}$$

which trivially satisfies (9) $\forall x \in [0,1]$. Applying (41) for $x = 0$ and $x = 1$ we find

$$\bar{u}(0,t) = \begin{bmatrix} v(\frac{1}{2},t) \\ u(\frac{1}{2},t) \end{bmatrix}, \qquad \bar{v}(0,t) = \begin{bmatrix} v(\frac{1}{2},t) \\ u(\frac{1}{2},t) \end{bmatrix} \tag{48a}$$

$$\bar{u}(1,t) = \begin{bmatrix} v(0,t) \\ u(1,t) \end{bmatrix}, \qquad \bar{v}(1,t) = \begin{bmatrix} v(1,t) \\ u(0,t) \end{bmatrix} \tag{48b}$$

which confirms that the inverse transform (42) is well-defined and the boundary condition matrices along with boundary measurement and control assignments can be found as (44). ∎

B. 2×2 bilateral observer with minimum time convergence

Now we find the observer gains for (8), and prove that using these it converges within time $t_{2,min}$ given by (10).

Lemma 3.2: The invertible change of coordinates $(\hat{u}(x,t), \hat{v}(x,t)) = T^{-1}[\check{u}_1, \check{u}_2, \check{v}_1, \check{v}_2](x)$, maps (21) into (8) with observer gains given in terms of (22) as

$$P^{++}(x) = \begin{cases} P^-_{22}(1-2x), & x \in [0, \frac{1}{2}] \\ P^+_{22}(2x-1), & x \in (\frac{1}{2}, 1] \end{cases}, \tag{49a}$$

$$P^{+-}(x) = \begin{cases} P^-_{21}(1-2x), & x \in [0, \frac{1}{2}] \\ P^+_{21}(2x-1), & x \in (\frac{1}{2}, 1] \end{cases}, \tag{49b}$$

$$P^{-+}(x) = \begin{cases} P^+_{12}(1-2x), & x \in [0, \frac{1}{2}] \\ P^-_{12}(2x-1), & x \in (\frac{1}{2}, 1] \end{cases}, \tag{49c}$$

$$P^{--}(x) = \begin{cases} P^+_{11}(1-2x), & x \in [0, \frac{1}{2}] \\ P^-_{11}(2x-1), & x \in (\frac{1}{2}, 1] \end{cases}. \tag{49d}$$

Proof: Consider first the left half-interval $x \in [0, \frac{1}{2}]$. From (42) we have $\hat{u}(x,t) = \check{v}_2(1-2x,t)$ and $\hat{v}(x,t) = \check{u}_1(1-2x,t)$. Taking the terms for $\check{v}_2(x,t)$ and $\check{u}_1(x,t)$ from (21), applying the coefficient assignments (43)–(44), recognizing that $x \equiv 1-2x$ for the left half-interval and substituting in $\hat{u}(x,t)$ and $\hat{v}(x,t)$ along with their respective partial derivatives, which are equivalent to the ones from (45)–(46), we find

$$\begin{aligned} \hat{u}_t(x,t) - 2\lambda(x)(-\frac{1}{2}\hat{u}_x(x,t)) = \sigma^+(x)\hat{v}(x,t) \\ + P^-_{21}(1-2x)(y_2(t) \\ - \hat{v}(0,t)) \\ + P^-_{22}(1-2x)(y_1(t) \\ - \hat{u}(1,t)) \end{aligned} \tag{50a}$$

$$\begin{aligned} \hat{v}_t(x,t) + 2\mu(x)(-\frac{1}{2}\hat{v}_x(x,t)) = \sigma^-(x)\hat{v}(x,t) \\ + P^+_{11}(1-2x)(y_2(t) \\ - \hat{v}(0,t)) \\ + P^+_{12}(1-2x)(y_1(t) \\ - \hat{u}(1,t)) \end{aligned} \tag{50b}$$

Comparing (50) to (8), we obtain the observer gains in (49) valid $\forall x \in [0, \frac{1}{2}]$. Applying the same steps for the right half-interval $x \in (\frac{1}{2}, 1]$, the observer gain assignments in (49) valid $\forall x \in (\frac{1}{2}, 1]$ are obtained. ∎

Theorem 3.3: Consider system (1) with outputs (5) and the observer (8). If the output injection gains are selected as (49), then $\hat{u}(x,t)$ and $\hat{v}(x,t)$ converge to $u(x,t)$ and $v(x,t)$, respectively, in finite time given by (10).

Proof: From Lemma 3.2 we know that (8) is mapped into (21) using the invertible transform (41). Hence the convergence time of (8) can be expressed as (28) using the relevant transport speeds from (43a)–(43b) as

$$t_{min} = \int_0^1 \frac{d\bar{x}}{2\mu(\frac{1}{2}(1+\bar{x}))} + \int_0^1 \frac{d\bar{x}}{2\mu(\frac{1}{2}(1-\bar{x}))}. \tag{51}$$

Applying the change of variables $\bar{x} = 2x - 1$ to the first integral and $\bar{x} = 1 - 2x$ to the second integral, we find

$$\begin{aligned} t_{min} &= \int_{\frac{1}{2}}^1 \frac{2dx}{2\mu(x)} + \int_{\frac{1}{2}}^0 \frac{-2dx}{2\mu(x)} = \int_{\frac{1}{2}}^1 \frac{dx}{\mu(x)} + \int_0^{\frac{1}{2}} \frac{dx}{\mu(x)} \\ &= \int_0^1 \frac{dx}{\mu(x)} \end{aligned} \tag{52}$$

which is (10). ∎

IV. SIMULATION

The 2×2 system (1) is implemented along with the bilateral observer (8) in `MATLAB` using the method presented in [15] for solving the kernel equations. The right boundary observer from [9] is also implemented for comparison. The system and observers are implemented with coefficients

$$\lambda(x) = 1, \qquad \mu(x) = \frac{1}{2}, \tag{53a}$$

$$\sigma^+(x) = x^2, \qquad \sigma^-(x) = -\sin(3x), \tag{53b}$$

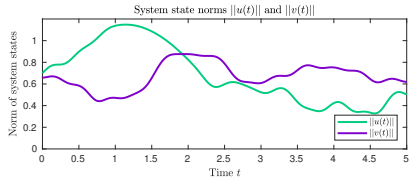

Fig. 1. Time evolution of the L_2 norms $||u(t)||$ and $||v(t)||$ of respective system states $u(x,t)$ and $v(x,t)$.

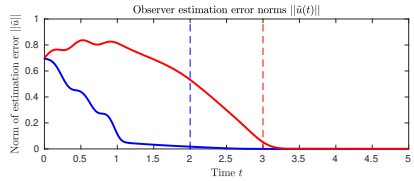

Fig. 2. Time evolution of the L_2 norms $||\tilde{u}(t)||$ of estimation error $\tilde{u}(x,t)$.

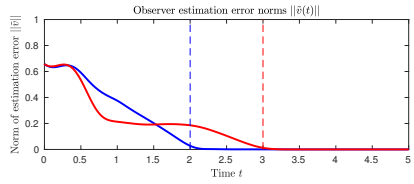

Fig. 3. Time evolution of the L_2 norms $||\tilde{v}(t)||$ of estimation error $\tilde{v}(x,t)$.

$$q = 1, \qquad \rho = \frac{1}{2} \tag{53c}$$

and initial conditions and inputs

$$u_0(x) = \cos(8x), \qquad v_0(x) = e^{-x}, \tag{54a}$$
$$U_1(t) = \sin(t), \qquad U_2(t) = \cos(8t). \tag{54b}$$

The unilateral observer only uses the right boundary measurement $y_1(t) = u(1,t)$, whereas the bilateral observer additionally uses the left boundary measurement $y_2(t) = v(0,t)$.

To show that the system states $u(x,t)$ and $v(x,t)$ do not go to zero during the simulation, in Fig. 1 we see the L_2 norms $||u(t)||$ and $||v(t)||$ of the states of (1) with parameters specified in (54).

Fig. 2 shows $||\tilde{u}(t)||$ for both observers, whereas Fig. 3 shows $||\tilde{v}(t)||$ for both observers. The blue line in both plots shows the error norm from the bilateral observer (8), whereas the red line is the error norm from the unilateral observer. The dashed blue line shows $t_{2,min}$ defined in (10), whereas the dashed red line is $t_{1,min}$ defined in (7).

V. CONCLUSIONS

We have shown an alternative way of deriving a 2×2 minimum time bilateral observer than the one presented in [2]. An observer for (1) utilizing measurements from both boundaries was derived, going via the derivation of a minimum time collocated observer for the $2+2$ system (11), which was done by making the target system converge in minimum time with the help of a Fredholm transformation. The bilateral observer was shown to converge within the theoretical lower convergence bound from [1] for observers using both boundary measurements.

As was noted in [13], some of the ideas considered there for control design could be applied to the design of bilateral observers. Indeed, this paper demonstrates that the trick of domain folding is also applicable within the venue of observation problems, and it would therefore be interesting to investigate its applicability to the design of observers for systems different from the hyperbolic ones considered here.

REFERENCES

[1] T. Li and B. Rao, "Strong (weak) exact controllability and strong (weak) exact observability for quasilinear hyperbolic systems," *Chinese Annals of Mathematics, Series B*, vol. 31, no. 5, pp. 723–742, 2010.

[2] J. Auriol and F. Di Meglio, "Two sided boundary stabilization of heterodirectional linear coupled hyperbolic PDEs," *IEEE Transactions on Automatic Control*, 2017.

[3] C.-Z. Xu and G. Sallet, "Exponential stability and transfer functions of processes governed by symmetric hyperbolic systems," *ESAIM: Control, Optimisation and Calculus of Variations*, vol. 7, pp. 421–442, 2002.

[4] M. Gugat, M. Dick, and G. Leugering, "Gas flow in fan-shaped networks: Classical solutions and feedback stabilization," *SIAM Journal on Control and Optimization*, vol. 49, no. 5, pp. 2101–2117, 2011.

[5] F. Di Meglio and U. J. F. Aarsnes, "A distributed parameter systems view of control problems in drilling," *IFAC-PapersOnLine*, vol. 48, no. 6, pp. 272–278, 2015.

[6] D. M. Boskovic, M. Krstic, and W. Liu, "Boundary control of an unstable heat equation via measurement of domain-averaged temperature," *IEEE Transactions on Automatic Control*, vol. 46, no. 12, pp. 2022–2028, 2001.

[7] W. Liu, "Boundary feedback stabilization of an unstable heat equation," *SIAM journal on control and optimization*, vol. 42, no. 3, pp. 1033–1043, 2003.

[8] A. Smyshlyaev and M. Krstic, "Backstepping observers for a class of parabolic PDEs," *Systems & Control Letters*, vol. 54, no. 7, pp. 613–625, 2005.

[9] R. Vazquez, M. Krstic, and J.-M. Coron, "Backstepping boundary stabilization and state estimation of a $2\times$ 2 linear hyperbolic system," in *Decision and Control and European Control Conference (CDC-ECC), 2011 50th IEEE Conference on*. IEEE, 2011, pp. 4937–4942.

[10] H. Anfinsen and O. M. Aamo, "Disturbance rejection in general heterodirectional 1-D linear hyperbolic systems using collocated sensing and control," *Automatica*, vol. 76, pp. 230–242, 2017.

[11] J.-M. Coron, L. Hu, and G. Olive, "Finite-time boundary stabilization of general linear hyperbolic balance laws via fredholm backstepping transformation," *Automatica*, vol. 84, pp. 95–100, 2017.

[12] J. Auriol and F. Di Meglio, "Minimum time control of heterodirectional linear coupled hyperbolic PDEs," *Automatica*, vol. 71, pp. 300–307, 2016.

[13] R. Vazquez and M. Krstic, "Bilateral boundary control of one-dimensional first-and second-order pdes using infinite-dimensional backstepping," in *Decision and Control (CDC), 2016 IEEE 55th Conference on*. IEEE, 2016, pp. 537–542.

[14] L. Hu, F. Di Meglio, R. Vazquez, and M. Krstic, "Control of homodirectional and general heterodirectional linear coupled hyperbolic pdes," *IEEE Transactions on Automatic Control*, vol. 61, no. 11, pp. 3301–3314, 2016.

[15] H. Anfinsen and O. M. Aamo, "Adaptive stabilization of 2×2 linear hyperbolic systems with an unknown boundary parameter from collocated sensing and control," *Automatic Control, IEEE Transactions on*, vol. 62, no. 12, pp. 6237–6249, December 2017.

Bibliography

Aadnoy, B. S. et al. (2011). *Fundamentals of drilling engineering*, Society of Petroleum Engineers.

Aamo, O. M. (2013). Disturbance rejection in 2 x 2 linear hyperbolic systems, *IEEE Transactions on Automatic Control* **58**(5): 1095–1106.

Aarsnes, U. J. F., Flåtten, T. and Aamo, O. M. (2016). Review of two-phase flow models for control and estimation, *Annual Reviews in Control* **42**: 50–62.

Ahmed, M. A., Hegab, O. A. and Sabry, A. (2016). Early detection enhancement of the kick and near-balance drilling using mud logging warning sign, *Egyptian Journal of Basic and Applied Sciences* **3**(1): 85–93.

Alsaba, M., Nygaard, R., Hareland, G. and Contreras, O. (2014). Review of lost circulation materials and treatments with an updated classification, *AADE National Technical Conference and Exhibition, Houston, TX, Apr*, pp. 15–16.

Anfinsen, H. (2013). *Disturbance attenuation in linear 2 x 2 hyperbolic systems: With application to the heave problem in managed pressure drilling*, Master's thesis, Institutt for teknisk kybernetikk.

Anfinsen, H. (2018). Adaptive control of linear hyperbolic pdes.

Anfinsen, H. and Aamo, O. M. (2016). Disturbance rejection in n+ 1 coupled 1-d linear hyperbolic pdes using collocated sensing and control, *IFAC-PapersOnLine* **49**(8): 192–198.

Anfinsen, H. and Aamo, O. M. (2017a). Adaptive stabilization of 2×2 linear hyperbolic systems with an unknown boundary parameter from collocated sensing and control, *Automatic Control, IEEE Transactions on* **62**(12): 6237–6249.

Anfinsen, H. and Aamo, O. M. (2017b). Disturbance rejection in general heterodirectional 1-d linear hyperbolic systems using collocated sensing and control, *Automatica* **76**: 230–242.

Auriol, J. and Di Meglio, F. (2016). Minimum time control of heterodirectional linear coupled hyperbolic pdes, *Automatica* **71**: 300–307.

Auriol, J. and Di Meglio, F. (in press). Two sided boundary stabilization of heterodirectional linear coupled hyperbolic pdes, *Accepted for publication in IEEE Transactions on Automatic Control. Available as an early access paper* .

Balas, M. J. (1983). The galerkin method and feedback control of linear distributed parameter systems, *Journal of Mathematical Analysis and Applications* **91**(2): 527–546.

Balogh, A. and Krstic, M. (2001). Infinite-step backstepping for a heat equation-like pde with arbitrarily many unstable eigenvalues, *American Control Conference, 2001. Proceedings of the 2001*, Vol. 3, IEEE, pp. 2480–2485.

Balogh, A. and Krstic, M. (2002). Infinite dimensional backstepping-style feedback transformations for a heat equation with an arbitrary level of instability, *European journal of control* **8**(2): 165–175.

Bartecki, K. (2015). Transfer function–based impulse response analysis for a class of hyperbolic systems of balance laws, *Control and Cybernetics* **44**(3): 327–356.

Bastin, G. and Coron, J.-M. (2011). On boundary feedback stabilization of non-uniform linear 2× 2 hyperbolic systems over a bounded interval, *Systems & Control Letters* **60**(11): 900–906.

Borthwick, D. (2016). Introduction to partial differential equations.

Boskovic, D. M., Krstic, M. and Liu, W. (2001). Boundary control of an unstable heat equation via measurement of domain-averaged temperature, *IEEE Transactions on Automatic Control* **46**(12): 2022–2028.

Canuto, C. and Quarteroni, A. (1987). On the boundary treatment in spectral methods for hyperbolic systems, *Journal of Computational Physics* **71**(1): 100–110.

Chapra, S. C. and Canale, R. P. (1998). *Numerical methods for engineers*, Vol. 2, McGraw-Hill New York.

Chen, C.-T. (1998). *Linear system theory and design*, Oxford University Press, Inc.

Chen, Z. et al. (2003). Bayesian filtering: From kalman filters to particle filters, and beyond, *Statistics* **182**(1): 1–69.

Clarke, B. (1983). Eigenvalue assignment of an augmented hyperbolic system by linear feedback, *Journal of mathematical analysis and applications* **97**(2): 417–440.

Colombo, R. M. (2002). A 2× 2 hyperbolic traffic flow model, *Mathematical and computer modelling* **35**(5-6): 683–688.

Coron, J.-M., d'Andrea Novel, B. and Bastia, G. (1999). A lyapunov approach to control irrigation canals modeled by saint-venant equations, *Control Conference (ECC), 1999 European*, IEEE, pp. 3178–3183.

Coron, J.-M., Hu, L. and Olive, G. (2017). Finite-time boundary stabilization of general linear hyperbolic balance laws via fredholm backstepping transformation, *Automatica* **84**: 95–100.

Coron, J.-M., Vazquez, R., Krstic, M. and Bastin, G. (2013). Local exponential h^2 stabilization of a 2×2 quasilinear hyperbolic system using backstepping, *SIAM Journal on Control and Optimization* **51**(3): 2005–2035.

Curro, C., Fusco, D. and Manganaro, N. (2011). A reduction procedure for generalized riemann problems with application to nonlinear transmission lines, *Journal of Physics A: Mathematical and Theoretical* **44**(33): 335205.

Di Meglio, F. and Aarsnes, U. J. F. (2015). A distributed parameter systems view of control problems in drilling, *IFAC-PapersOnLine* **48**(6): 272–278.

Di Meglio, F., Vazquez, R. and Krstic, M. (2013). Stabilization of a system of $n+1$ coupled first-order hyperbolic linear pdes with a single boundary input, *IEEE Transactions on Automatic Control* **58**(12): 3097–3111.

Farlow, S. J. (1993). *Partial differential equations for scientists and engineers*, Courier Corporation.

Fosse, M. (2015). *Wired drill pipe technology: technical and economic overview*, Master's thesis, University of Stavanger, Norway.

Fujii, N. (1980). Feedback stabilization of distributed parameter systems by a functional observer, *SIAM Journal on Control and Optimization* **18**(2): 108–120.

Goatin, P. (2006). The aw–rascle vehicular traffic flow model with phase transitions, *Mathematical and computer modelling* **44**(3-4): 287–303.

Grace, R. D. (2017). *Blowout and well control handbook*, Gulf Professional Publishing.

Gravdal, A. E., Lorentzen, R. J., Time, R. W. et al. (2010). Wired drill pipe telemetry enables real-time evaluation of kick during managed pressure drilling, *SPE Asia Pacific Oil and Gas Conference and Exhibition*, Society of Petroleum Engineers.

Griffiths, D. F., Dold, J. W. and Silvester, D. J. (2015). *Essential partial differential equations*, Springer.

Gugat, M., Dick, M. and Leugering, G. (2011). Gas flow in fan-shaped networks: Classical solutions and feedback stabilization, *SIAM Journal on Control and Optimization* **49**(5): 2101–2117.

Hauge, E., Aamo, O. M. and Godhavn, J.-M. (2013). Application of an infinite-dimensional observer for drilling systems incorporating kick and loss detection, *Control Conference (ECC), 2013 European*, IEEE, pp. 1065–1070.

Holta, H., Anfinsen, H. and Aamo, O. M. (2017). Estimation of an uncertain bilinear boundary condition in linear 2× 2 hyperbolic systems with application to drilling, pp. 188–193.

Hu, L. and Di Meglio, F. (2015). Finite-time backstepping boundary stabilization of 3× 3 hyperbolic systems, *Control Conference (ECC), 2015 European*, IEEE, pp. 67–72.

Hu, L., Di Meglio, F., Vazquez, R. and Krstic, M. (2016). Control of homodirectional and general heterodirectional linear coupled hyperbolic pdes, *IEEE Transactions on Automatic Control* **61**(11): 3301–3314.

Hu, L., Vazquez, R., Di Meglio, F. and Krstic, M. (2015). Boundary exponential stabilization of 1-d inhomogeneous quasilinear hyperbolic systems, *arXiv preprint arXiv:1512.03539* .

Hutton, D. V. and Wu, J. (2004). *Fundamentals of finite element analysis*, Vol. 1, McGraw-hill New York.

Johnson, R. W. (2016). *Handbook of fluid dynamics*, Crc Press.

Khalil, H. K. (2002). Nonlinear systems, 3rd, *New Jewsey, Prentice Hall* **9**(4.2).

Khvedelidze, B. (2013). Integral equation, *Encyclopedia of Mathematics*. **URL:** *http://www.encyclopediaofmath.org/index.php?title=Integral*$_e$*quationoldid* = 30324

Komarla, S. (2016). How do i classify first order pde (elliptic, hyperbolic or parabolic) using method of characteristics?(quora post). Accessed: 2018-05-07. **URL:** *https://www.quora.com/How-do-I-classify-first-order-PDE-elliptic-hyperbolic-or-parabolic-using-method-of-characteristics*

Krener, A. J. and Kang, W. (2003). Locally convergent nonlinear observers, *SIAM Journal on Control and Optimization* **42**(1): 155–177.

Kreyszig, E. (2010). *Advanced engineering mathematics*, John Wiley & Sons.

Krstic, M. and Bekiaris-Liberis, N. (2013). Nonlinear stabilization in infinite dimension, *Annual Reviews in Control* **37**(2): 220–231.

Krstic, M., Guo, B.-Z., Balogh, A. and Smyshlyaev, A. (2008). Output-feedback stabilization of an unstable wave equation, *Automatica* **44**(1): 63–74.

Krstic, M. and Smyshlyaev, A. (2008a). Backstepping boundary control for first-order hyperbolic pdes and application to systems with actuator and sensor delays, *Systems & Control Letters* **57**(9): 750–758.

Krstic, M. and Smyshlyaev, A. (2008b). *Boundary control of PDEs: A course on backstepping designs*, Vol. 16, Siam.

Landet, I. S., Pavlov, A. and Aamo, O. M. (2013). Modeling and control of heave-induced pressure fluctuations in managed pressure drilling, *IEEE Transactions on Control Systems Technology* **21**(4): 1340–1351.

Li, T. and Rao, B. (2010). Strong (weak) exact controllability and strong (weak) exact observability for quasilinear hyperbolic systems, *Chinese Annals of Mathematics, Series B* **31**(5): 723–742.

Li, X. and Liu, J. (2012). Collocated observer design based on continuum backstepping for a class of hyperbolic pdes., *JCP* **7**(12): 2955–2961.

Liu, W. (2003). Boundary feedback stabilization of an unstable heat equation, *SIAM journal on control and optimization* **42**(3): 1033–1043.

Logemann, H. (1993). Stabilization and regulation of infinite-dimensional systems using coprime factorizations, *Analysis and optimization of systems: state and frequency domain approaches for infinite-dimensional systems*, Springer, pp. 102–139.

Luenberger, D. (1966). Observers for multivariable systems, *IEEE Transactions on Automatic Control* **11**(2): 190–197.

Malloy, K. P., Stone, R., Medley, G. H., Hannegan, D. M., Coker, O. D., Reitsma, D., Santos, H. M., Kinder, J. I., Eck-Olsen, J., McCaskill, J. W. et al. (2009). Managed-pressure drilling: What it is and what it is not, *IADC/SPE Managed Pressure Drilling and Underbalanced Operations Conference & Exhibition*, Society of Petroleum Engineers.

MathWorks (2018). `MATLAB trapz` - trapezoidal method. Accessed: 2018-06-21. **URL:** *https://se.mathworks.com/help/matlab/ref/trapz.htmlbua4lsr*

Myint-U, T. and Debnath, L. (2007). *Linear partial differential equations for scientists and engineers*, Springer Science & Business Media.

Nambu, T. (1984). On the stabilization of diffusion equations: boundary observation and feedback, *Journal of differential equations* **52**(2): 204–233.

Nayeem, A. A., Venkatesan, R. and Khan, F. (2016). Monitoring of down-hole parameters for early kick detection, *Journal of Loss Prevention in the Process Industries* **40**: 43–54.

NORSOK (2004). Well integrity in drilling and well operations, *D-010, rev* **3**.

Otto, A. (2011). Methods of numerical simulation in fluids and plasmas, *Lecture notes, University of Alaska* .

Pavlov, A., Kaasa, G.-O. and Imsland, L. (2010). Experimental disturbance rejection on a full-scale drilling rig, *IFAC Proceedings Volumes* **43**(14): 1338–1343.

Radke, A. and Gao, Z. (2006). A survey of state and disturbance observers for practitioners, *American Control Conference, 2006*, IEEE, pp. 6–pp.

Rehm, B., Haghshenas, A., Paknejad, A. S., Al-Yami, A. and Hughes, J. (2013). *Underbalanced drilling: limits and extremes*, Elsevier.

Schiesser, W. E. (2012). *The numerical method of lines: integration of partial differential equations*, Elsevier.

Smyshlyaev, A. and Krstic, M. (2005). Backstepping observers for a class of parabolic pdes, *Systems & Control Letters* **54**(7): 613–625.

Stamnes, Ø. N., Kaasa, G.-O. and Aamo, O. M. (2011). Adaptive estimation of downhole pressure for managed pressure drilling operations, *Intelligent Control (ISIC), 2011 IEEE International Symposium on*, IEEE, pp. 989–995.

Strauss, W. A. (1992). *Partial differential equations*, John Wiley & Sons New York, NY, USA.

Strikwerda, J. C. (2004). *Finite difference schemes and partial differential equations*, Vol. 88, Siam.

Sui, D., Sukhoboka, O. and Aadnøy, B. S. (2017). Improvement of wired drill pipe data quality via data validation and reconciliation, *International Journal of Automation and Computing* pp. 1–12.

Suslick, S. B., Schiozer, D. and Rodriguez, M. R. (2009). Uncertainty and risk analysis in petroleum exploration and production, *Terrae* **6**(1): 2009.

Tamim, N., Laboureur, D. M., Mentzer, R. A., Hasan, A. R. and Mannan, M. S. (2017). A framework for developing leading indicators for offshore drillwell blowout incidents, *Process Safety and Environmental Protection* **106**: 256–262.

Tricomi, F. G. (1985). *Integral equations*, Vol. 5, Courier Corporation.

Vazquez, R. and Krstic, M. (2016). Bilateral boundary control of one-dimensional first-and second-order pdes using infinite-dimensional backstepping, *Decision and Control (CDC), 2016 IEEE 55th Conference on*, IEEE, pp. 537–542.

Vazquez, R., Krstic, M. and Coron, J.-M. (2011). Backstepping boundary stabilization and state estimation of a 2× 2 linear hyperbolic system, *Decision and Control and European Control Conference (CDC-ECC), 2011 50th IEEE Conference on*, IEEE, pp. 4937–4942.

Wendt, J. F. (2008). *Computational fluid dynamics: an introduction*, Springer Science & Business Media.

Whitham, G. B. (2011). *Linear and nonlinear waves*, Vol. 42, John Wiley & Sons.

Woittennek, F., Rudolph, J. and Knüppel, T. (2009). Flatness based trajectory planning for a semi-linear hyperbolic system of first order pde modeling a tubular reactor, *PAMM* **9**(1): 3–6.

Xu, C.-Z. and Sallet, G. (2002). Exponential stability and transfer functions of processes governed by symmetric hyperbolic systems, *ESAIM: Control, Optimisation and Calculus of Variations* **7**: 421–442.

Zhang, J. (2011). Pore pressure prediction from well logs: Methods, modifications, and new approaches, *Earth-Science Reviews* **108**(1-2): 50–63.

Zhou, J., Nygaard, G., Godhavn, J.-M., Breyholtz, Ø. and Vefring, E. H. (2010). Adaptive observer for kick detection and switched control for bottomhole pressure regulation and kick attenuation during managed pressure drilling, *American Control Conference (ACC), 2010*, IEEE, pp. 3765–3770.

Zhou, J., Stamnes, Ø. N., Aamo, O. M. and Kaasa, G.-O. (2011). Switched control for pressure regulation and kick attenuation in a managed pressure drilling system, *IEEE Transactions on Control Systems Technology* **19**(2): 337–350.